Les environnements sédimentaires profonds

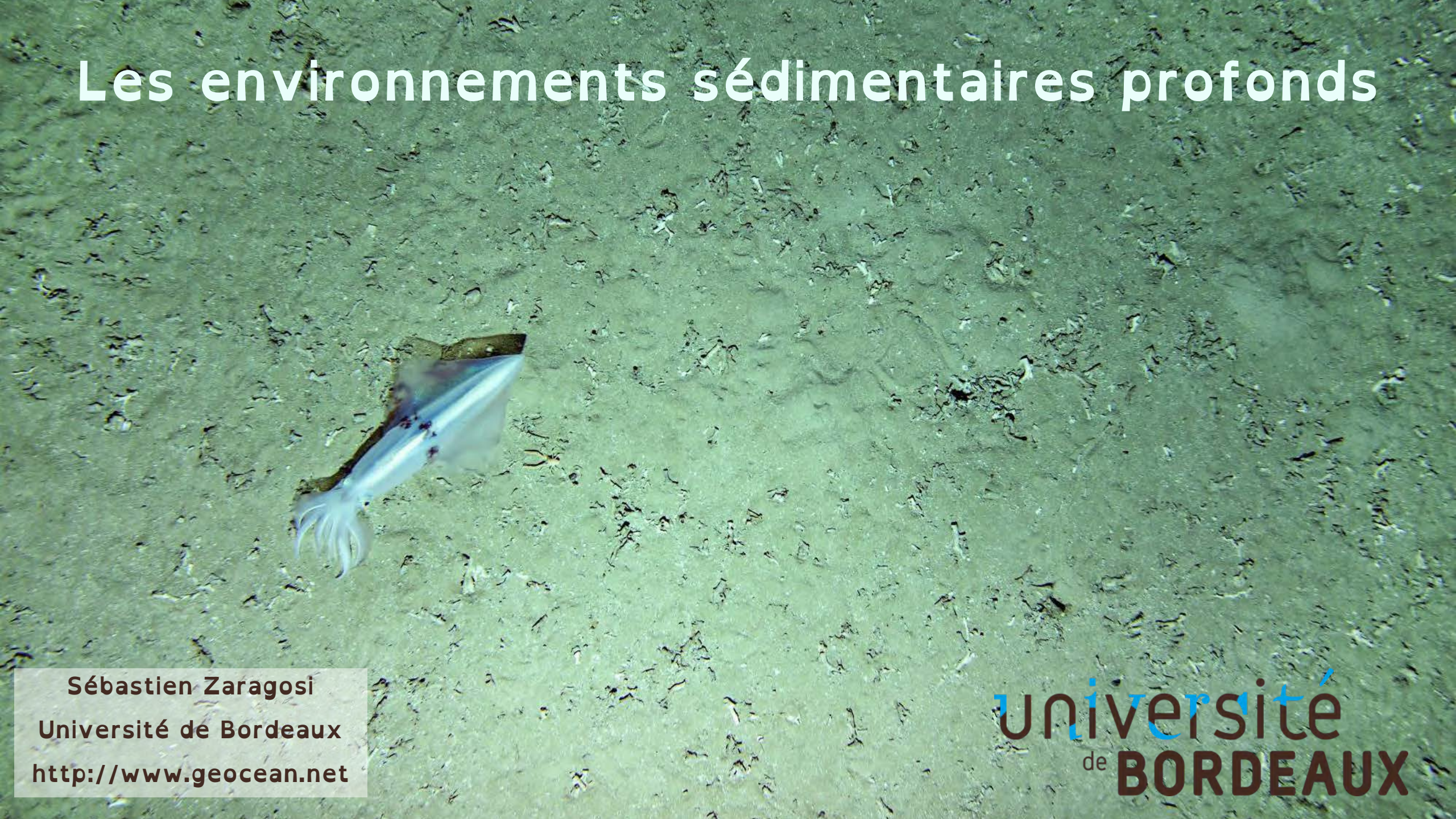

Sébastien Zaragosi
Université de Bordeaux
http://www.geocean.net

université de BORDEAUX

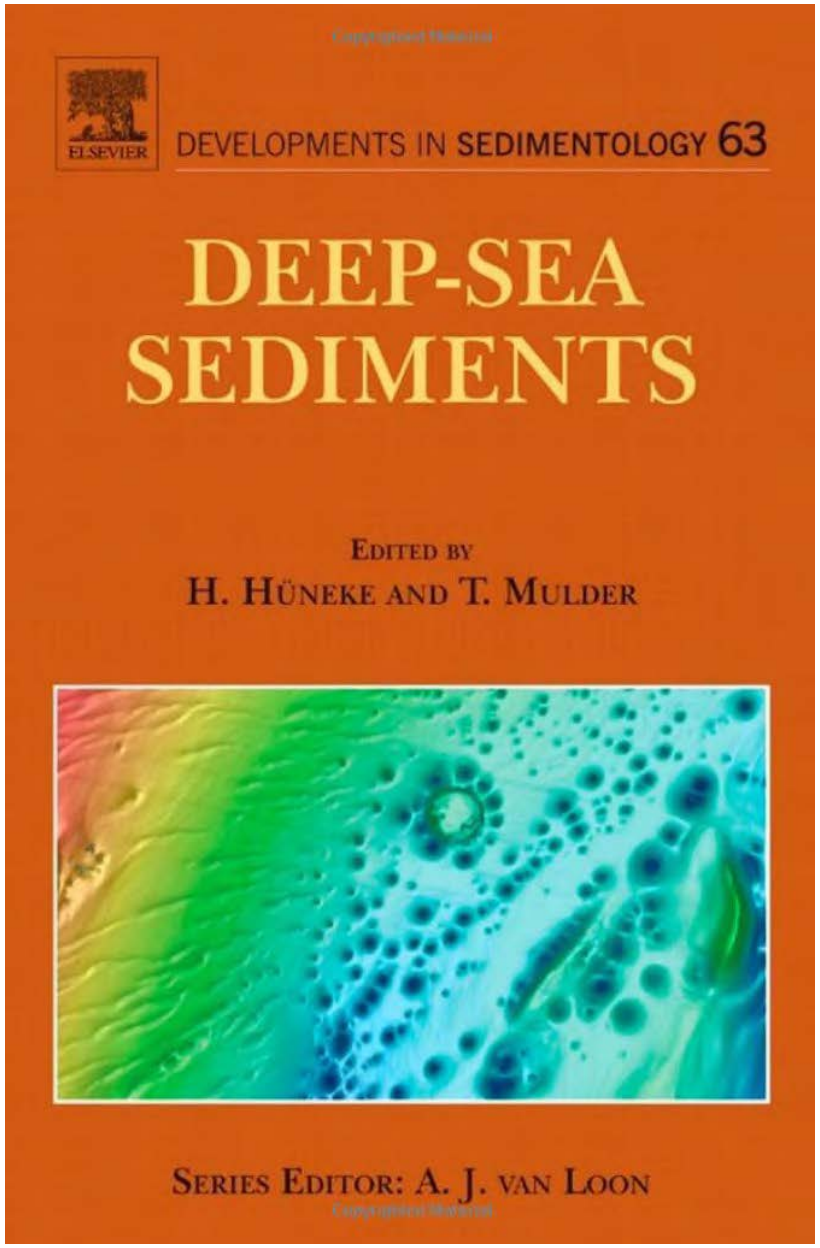
ELSEVIER
DEVELOPMENTS IN SEDIMENTOLOGY 63
DEEP-SEA SEDIMENTS
EDITED BY
H. HÜNEKE AND T. MULDER
SERIES EDITOR: A. J. VAN LOON

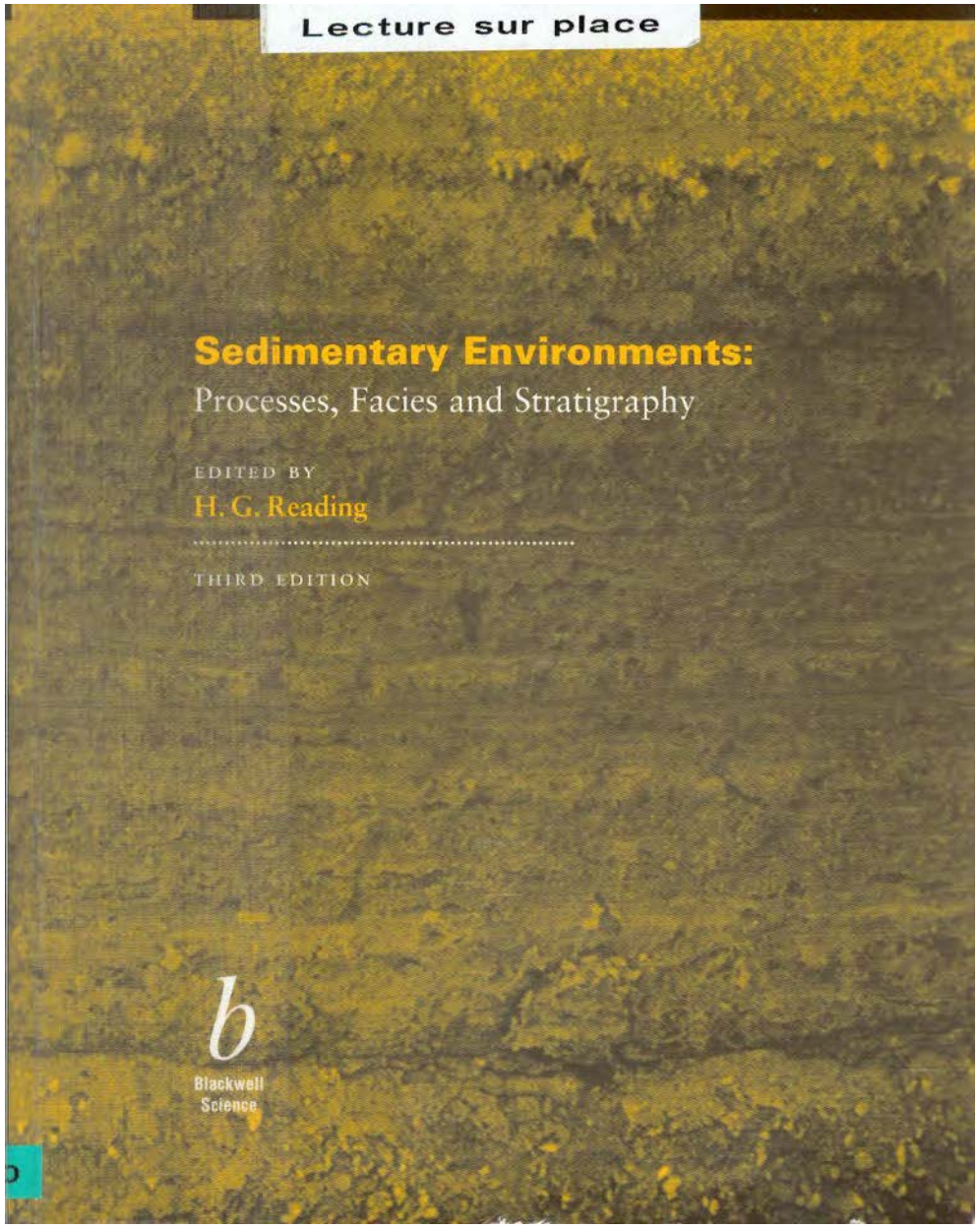
Lecture sur place
Sedimentary Environments:
Processes, Facies and Stratigraphy
EDITED BY
H. G. Reading
THIRD EDITION
Blackwell Science

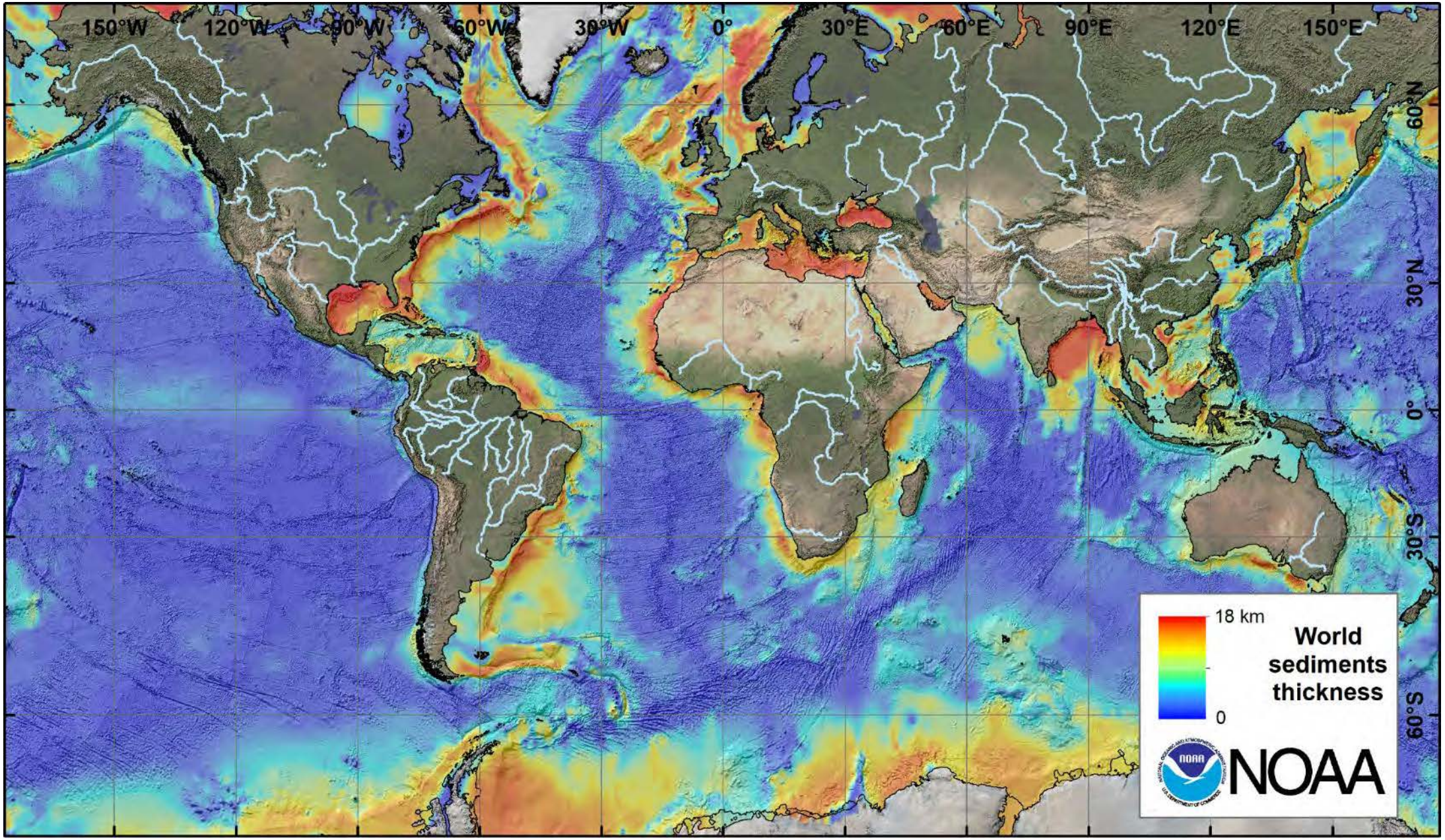

Straume, E.O., et al. 2019. GlobSed: Updated Total Sediment Thickness in the World's Oceans. Geochem. Geophys. Geosyst. 20, 1756–1772.

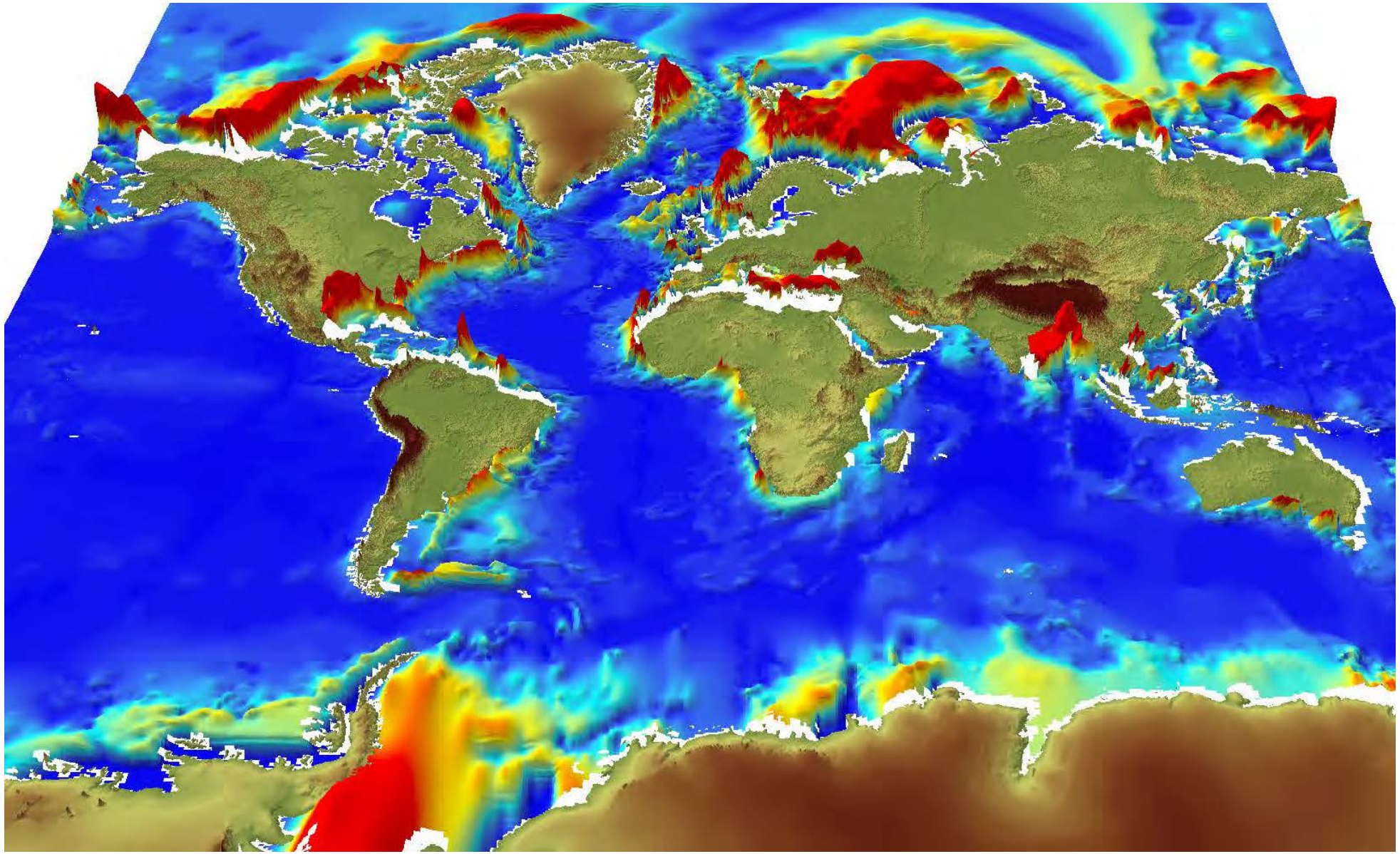

Straume, E.O., et al. 2019

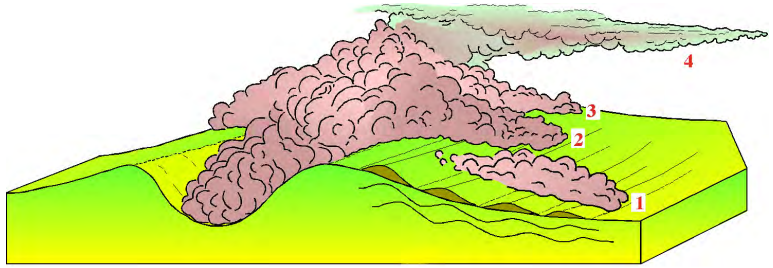

Sédimentation gravitaire – turbiditique

=> Histoire des fleuves

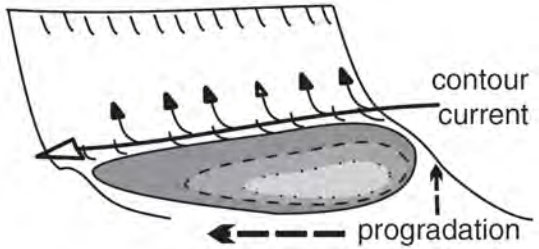

Ex: Faro Drift

Sédimentation contouritique

=> Histoire des courants océaniques

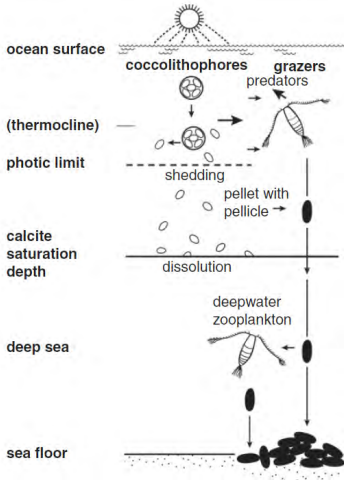

Sédimentation pélagique et hémipélagique

=> Histoire du climat

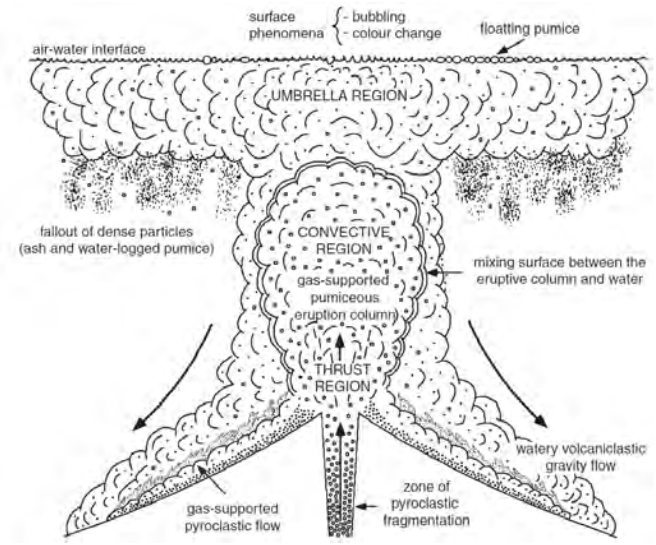

Sédimentation volcanoclastique

=> Histoire du volcanisme

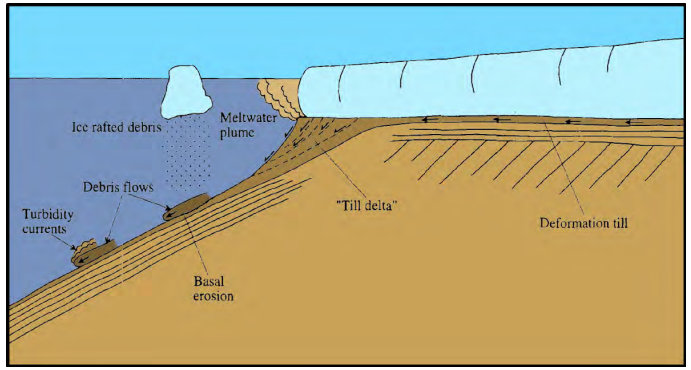

Sédimentation glaci-marine

=> Histoire des calottes et glaciers

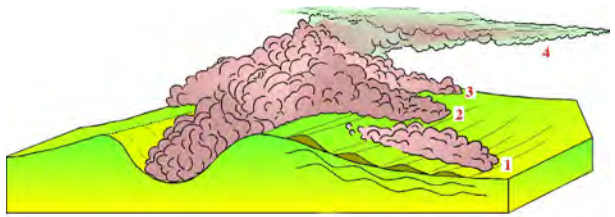

Sédimentation gravitaire – turbiditique

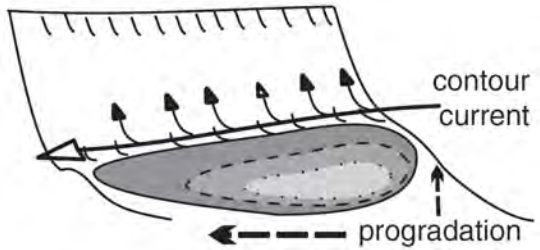

Ex: Faro Drift

Sédimentation contouritique

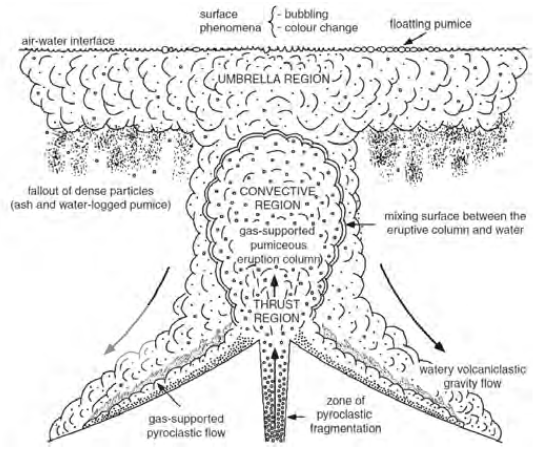

Sédimentation volcanoclastique

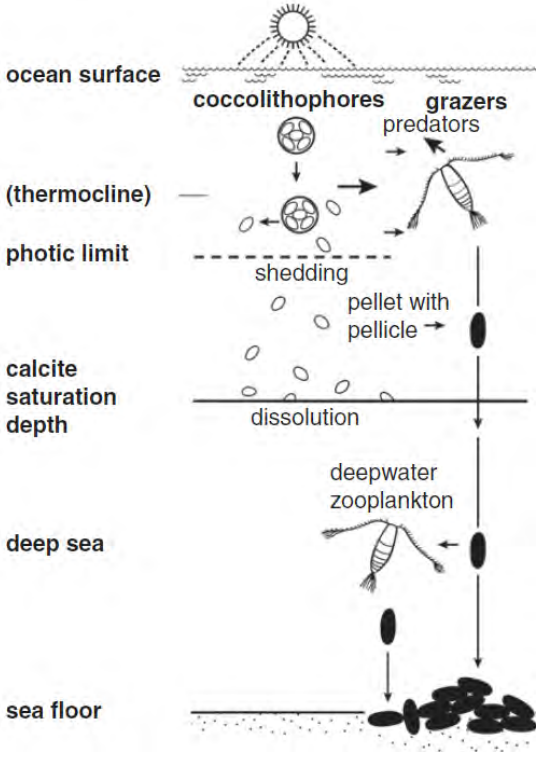

Sédimentation pélagique et hémipélagique

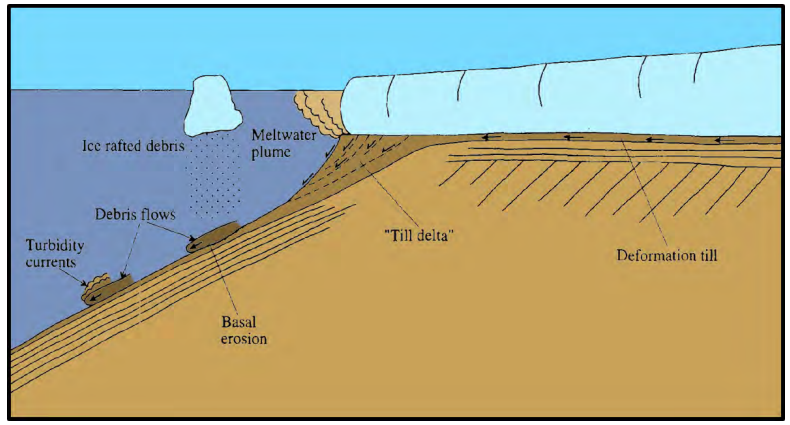

Sédimentation glaci-marine

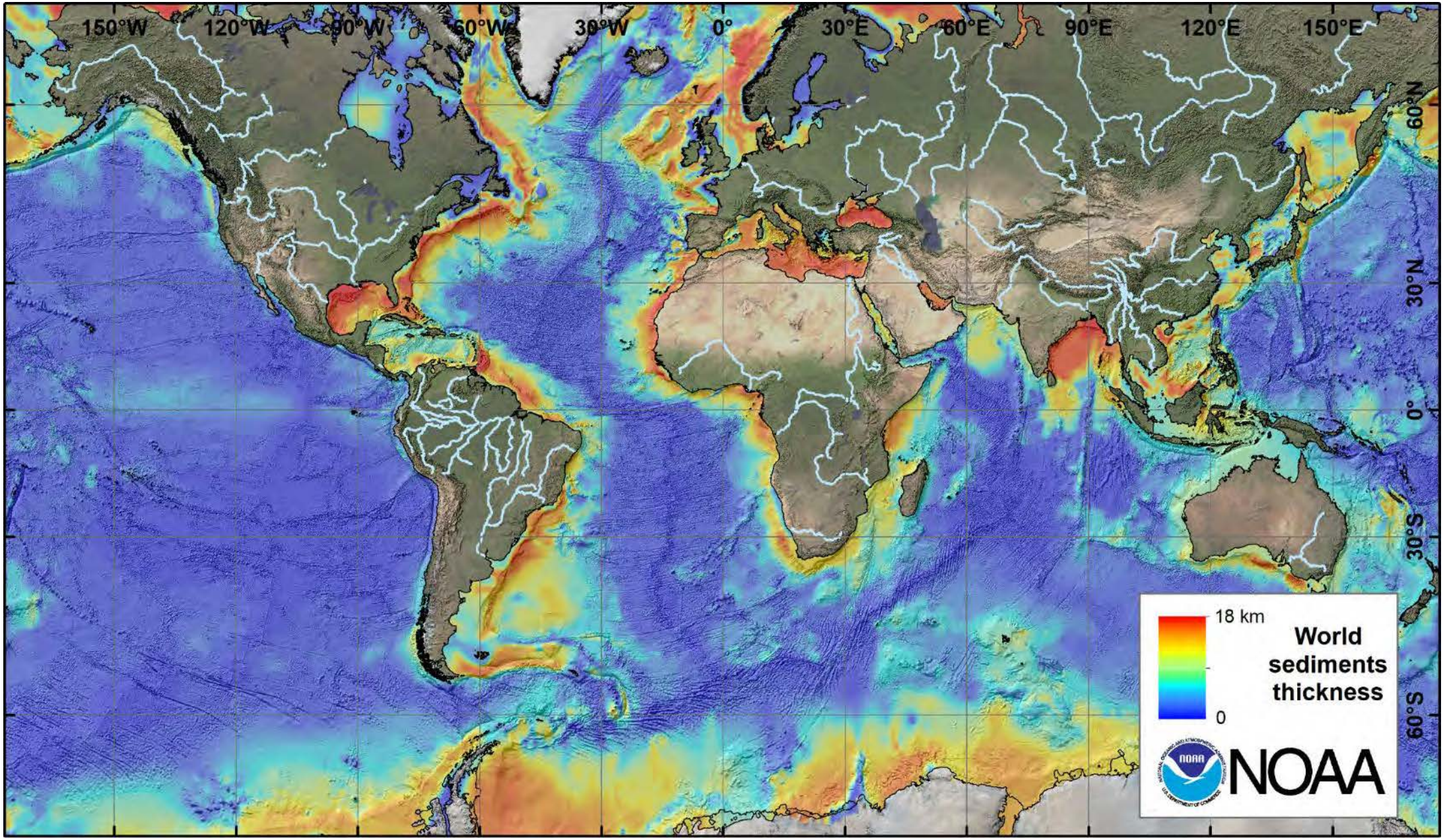

Straume, E.O., et al. 2019. GlobSed: Updated Total Sediment Thickness in the World's Oceans. Geochem. Geophys. Geosyst. 20, 1756–1772.

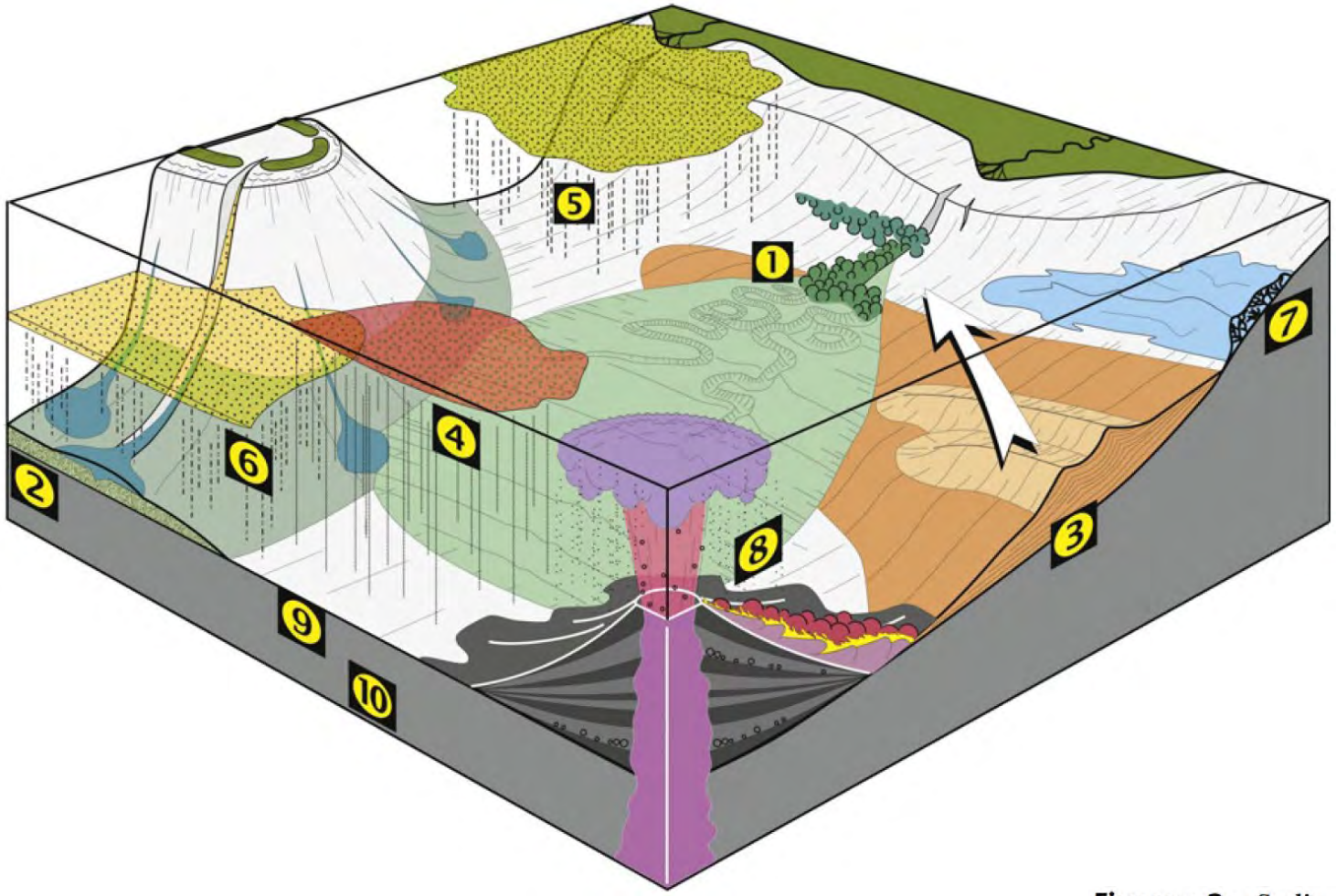

Figure 1.8 Sedimentary processes in the deep-sea (see text for further explanation): 1, gravity-flow processes (deep-sea fan); 2, rock fall and gravity-flow processes (slope-apron); 3, bottom current (contourite drift); 4, pelagic sedimentation; 5, hemipelagic advection; 6, periplatform sedimentation; 7, benthic carbonate production (cool-water coral reefs); 8, volcaniclastic processes (seamounts); 9, bioturbation; and 10, early diagenesis. (A multi-colour version of this figure is on the included CD-ROM.)

Hüneke, H. (Ed.), 2011. Deep-sea sediments, Developments in sedimentology. Elsevier, Amsterdam.

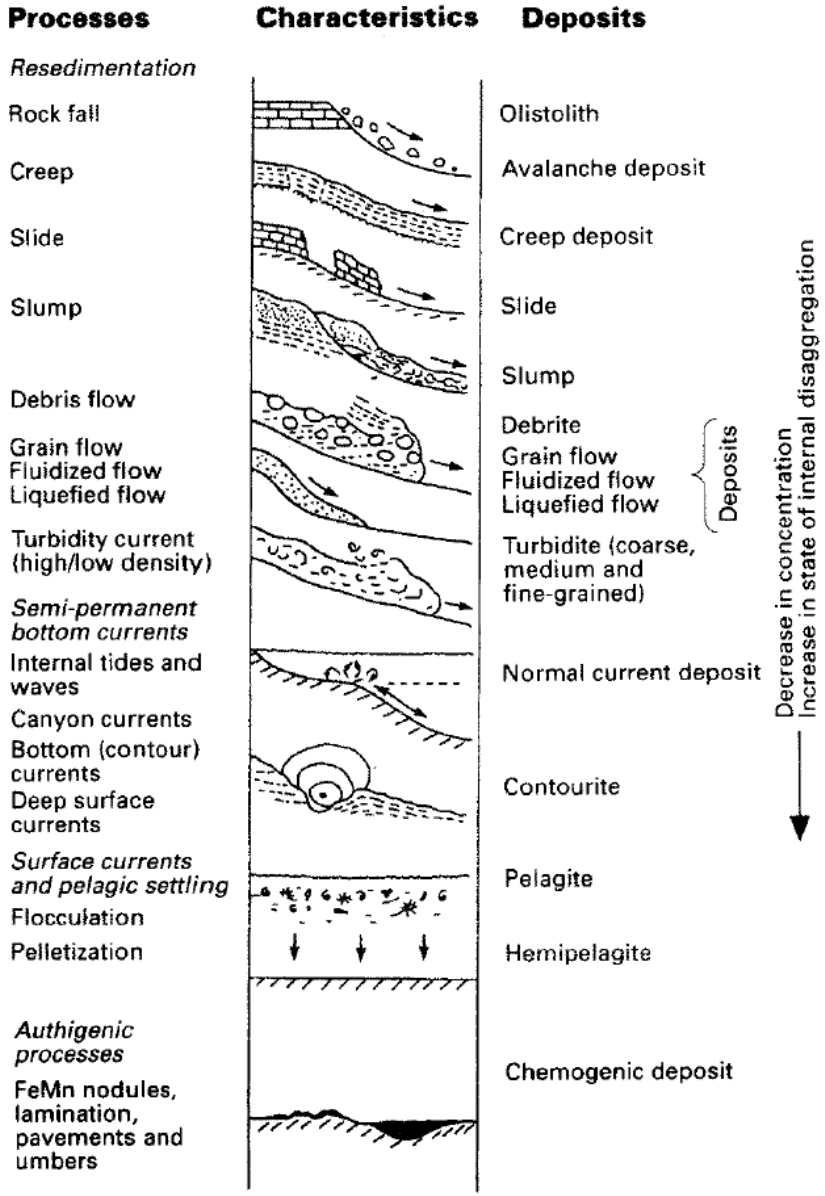

Figure 10.2 The range of processes that operate in the deep sea and their products (from Stow, 1994).

1. Sédimentation gravitaire – turbiditique

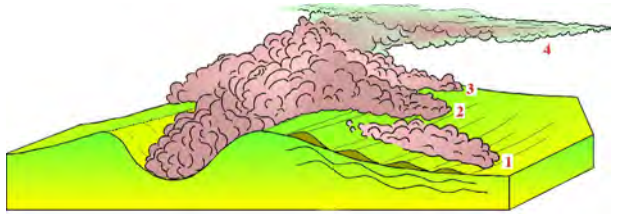

2. Sédimentation volcanoclastique

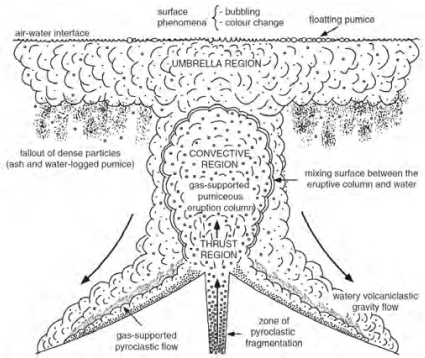

3. Sédimentation pélagique et hémipélagique

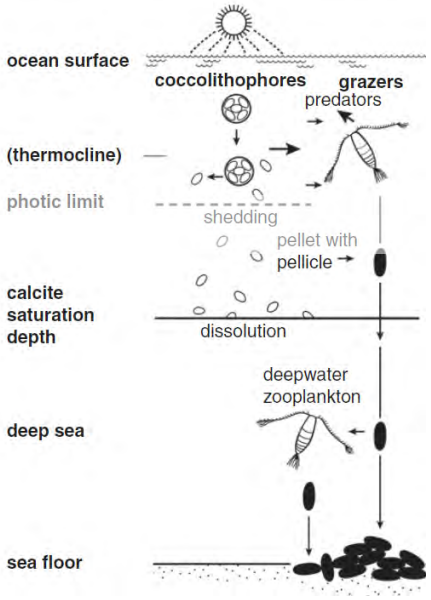

4. Sédimentation glaci-marine

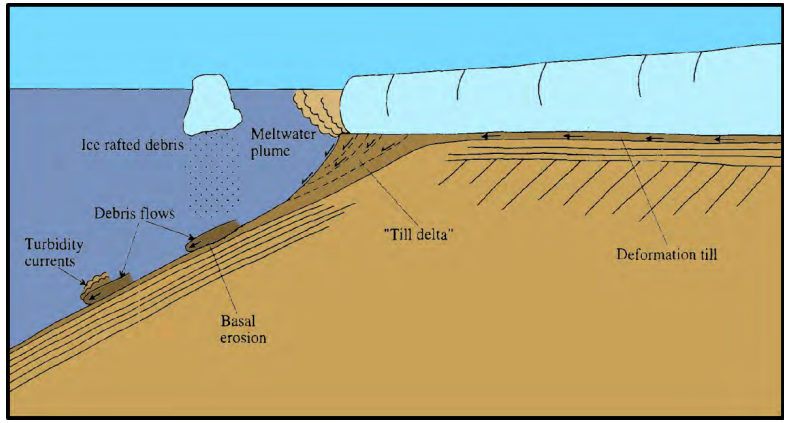

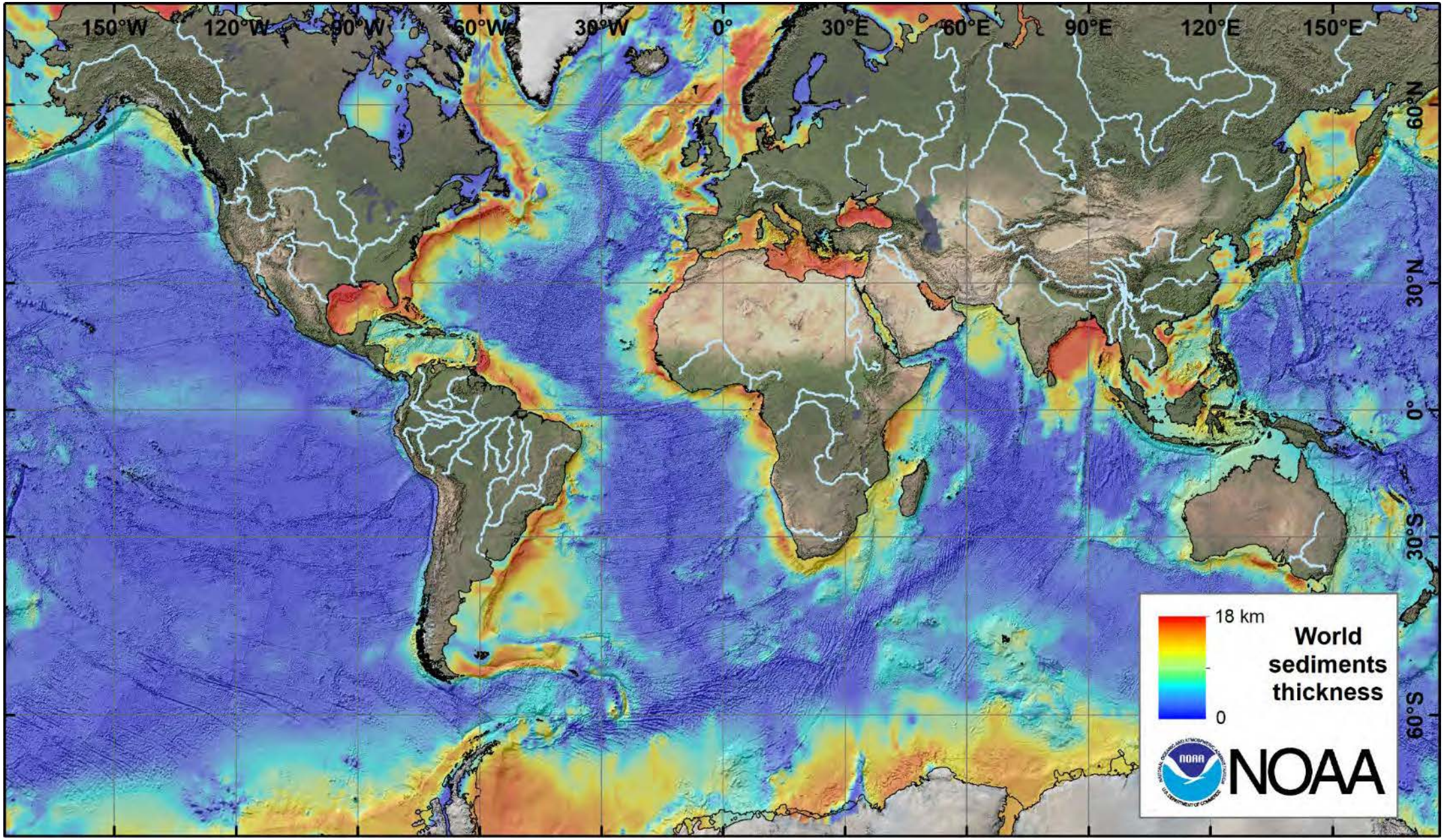

Straume, E.O., et al. 2019. GlobSed: Updated Total Sediment Thickness in the World's Oceans. Geochem. Geophys. Geosyst. 20, 1756–1772.

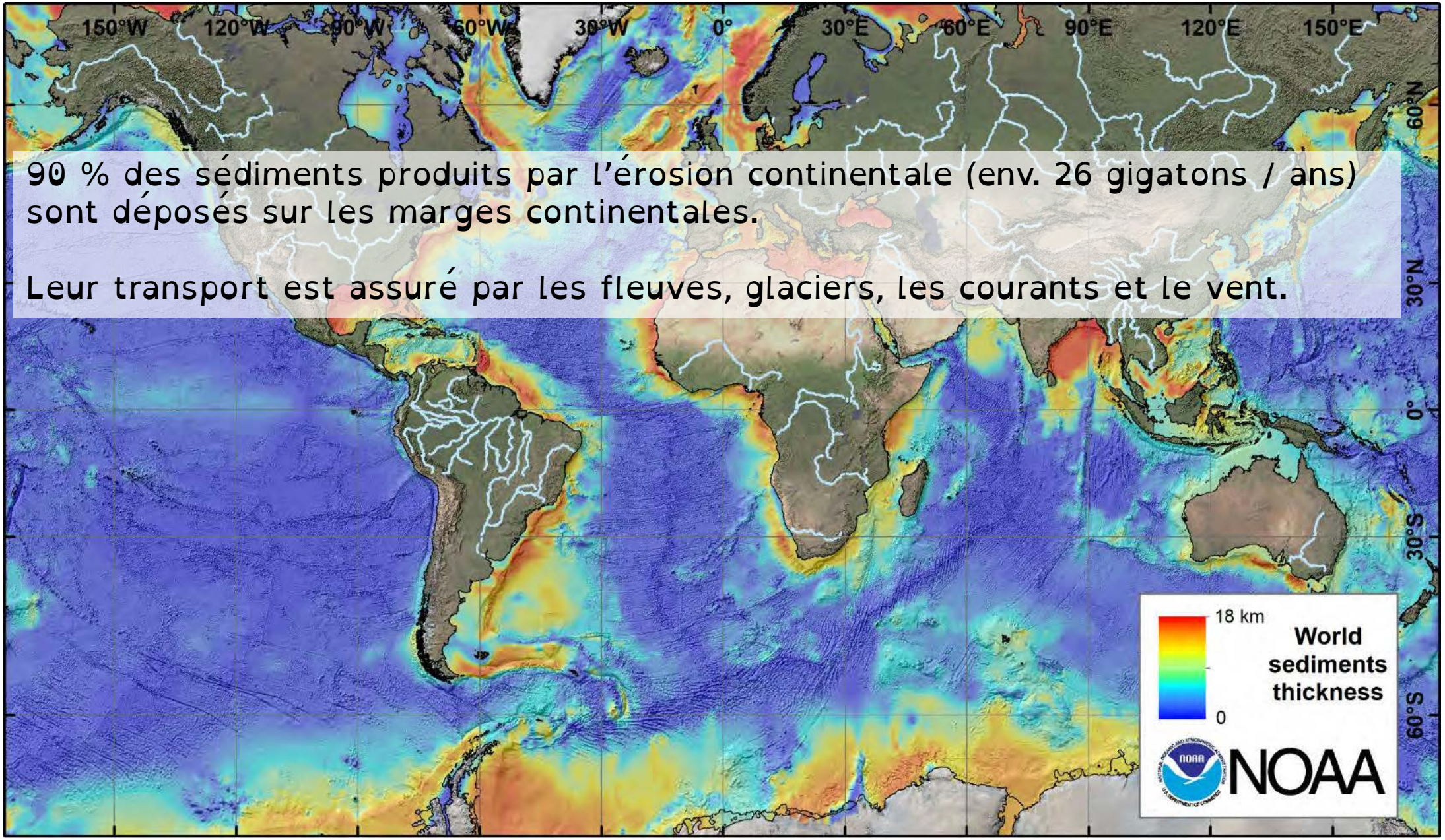

90 % des sédiments produits par l'érosion continentale (env. 26 gigatons / ans) sont déposés sur les marges continentales.

Leur transport est assuré par les fleuves, glaciers, les courants et le vent.

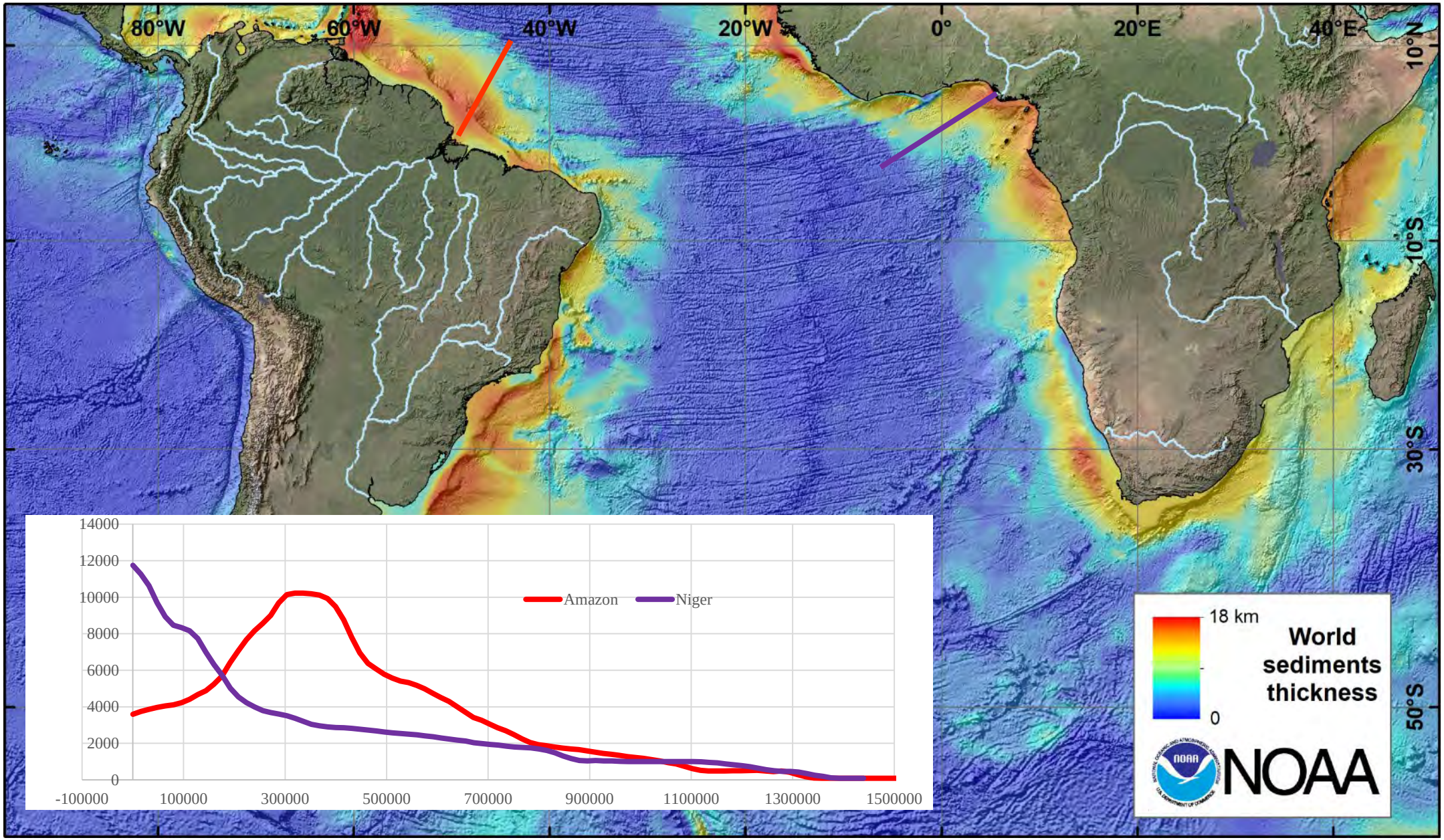
80°W
60°W
40°W
20°W
0°
20°E
40°E
10°N
10°S
30°S
50°S
Amazon
Niger
14000
12000
10000
8000
6000
4000
2000
0
-100000
100000
300000
500000
700000
900000
1100000
1300000
1500000
18 km
0
World sediments thickness
NOAA

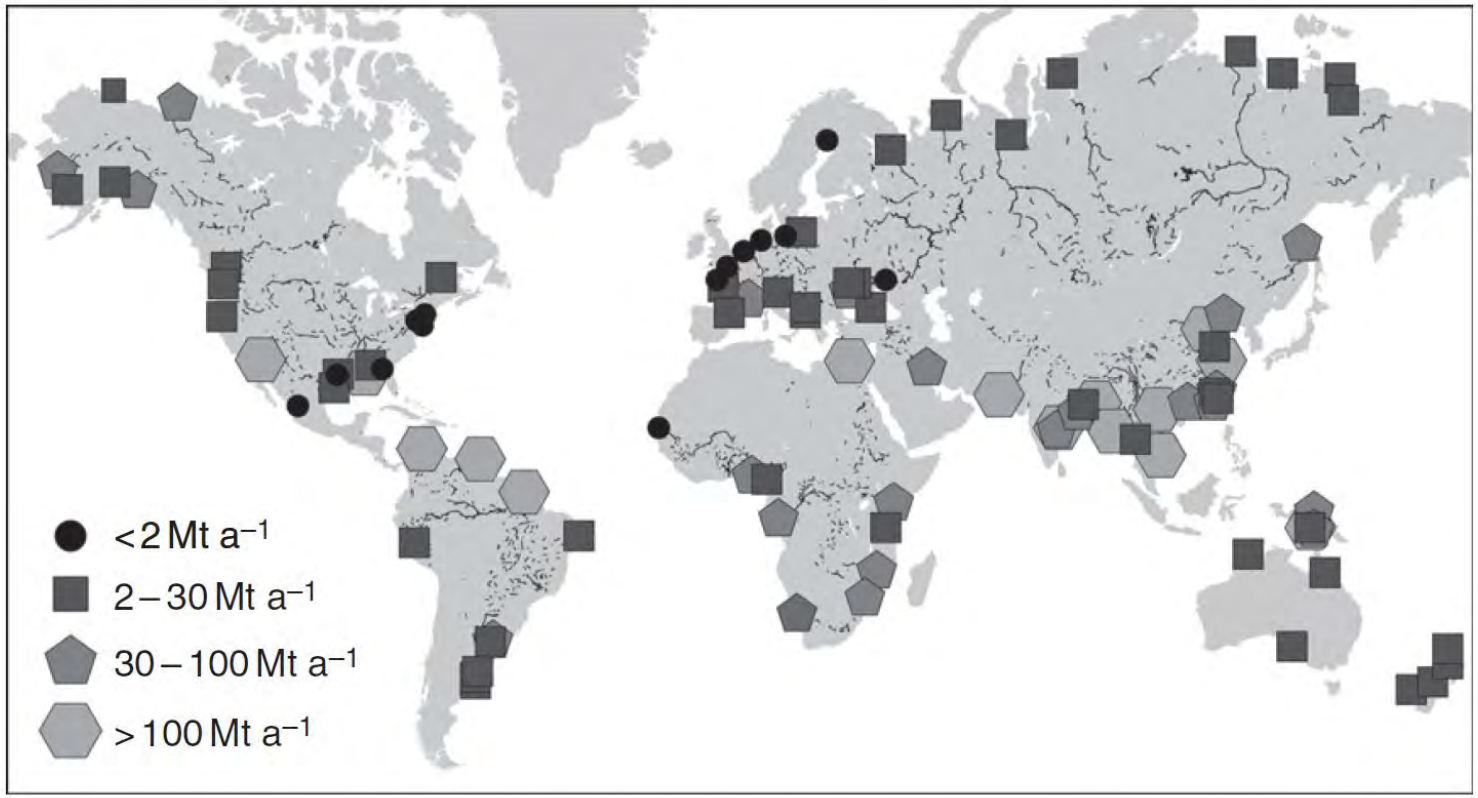

Figure 5.1 Magnitude of sediment discharge at large river mouths. Data are adopted from Milliman and Syvitski (1992) and Hovius (1998) (redrawn and slightly modified after Walsh and Nittrouer, 2009).

Décharges sédimentaires dépendent de :

- **Surface des bassins versants.**
- **Altitude maximale des bassins versants.**
- **Couvert végétal (climat).**
- **Pluviosité (climat).**
- **Taux d'uplift du bassin versant.**

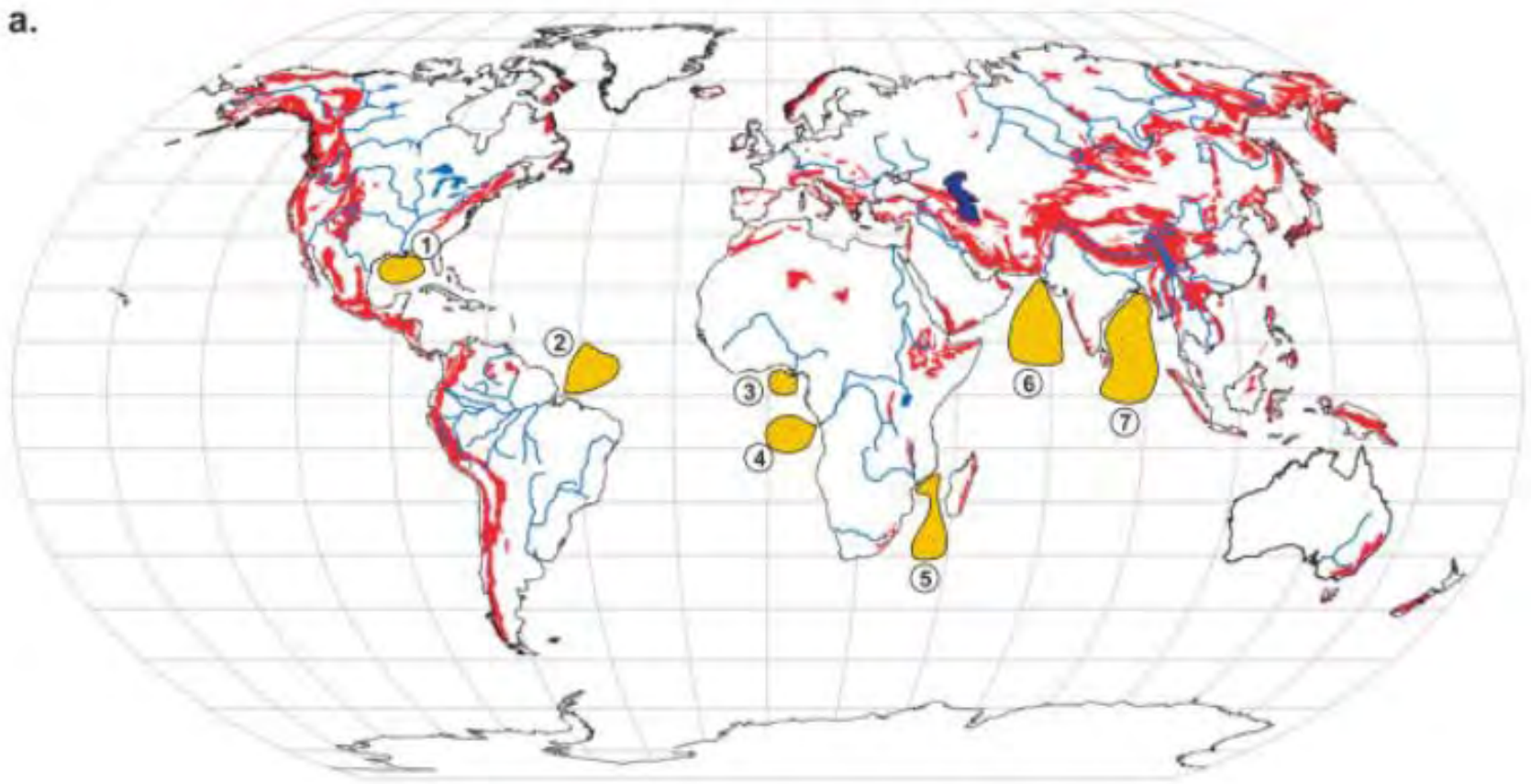

Figure I.4 : a. Distribution globale des terrains montagneux dont l'élévation est supérieure à 1000 m en rouge (Milliman and Farnsworth (2011) et position des 7 plus grands systèmes source-to-sink du monde. b. Distribution globale des précipitations annuelles entre 1901-2000, basée sur une grille de 0.5°(Climate Research Unit, East Anglia University, dans Millliman and Farnsworth, 2013) et position des 7 plus grands systèmes source-to-sink du monde.

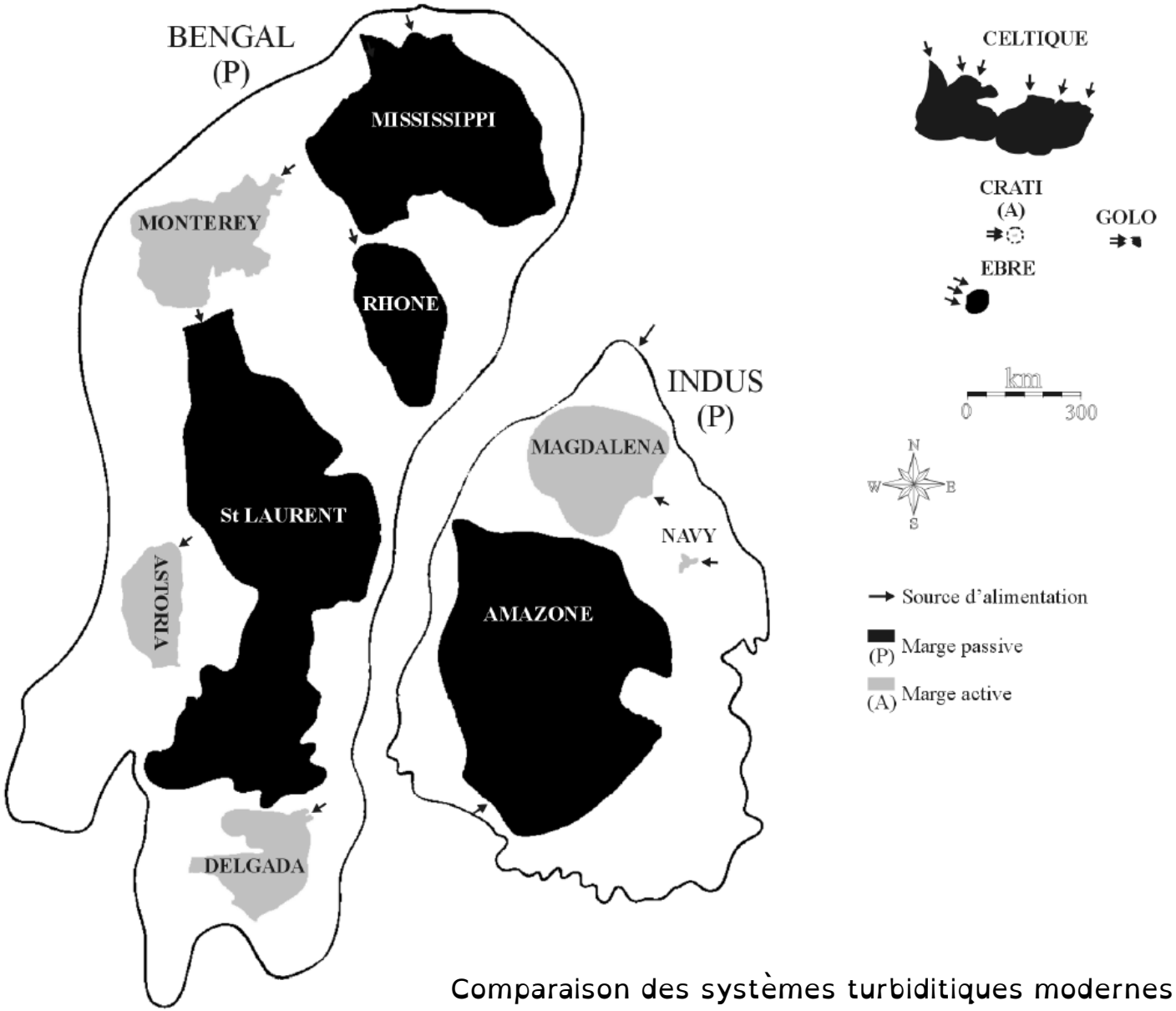

Comparaison des systèmes turbiditiques modernes (modifié d'après Barnes et Normark, 1985).

1. Sédimentation gravitaire – turbiditique : le système turbiditique du Gange - Brahmapoutre

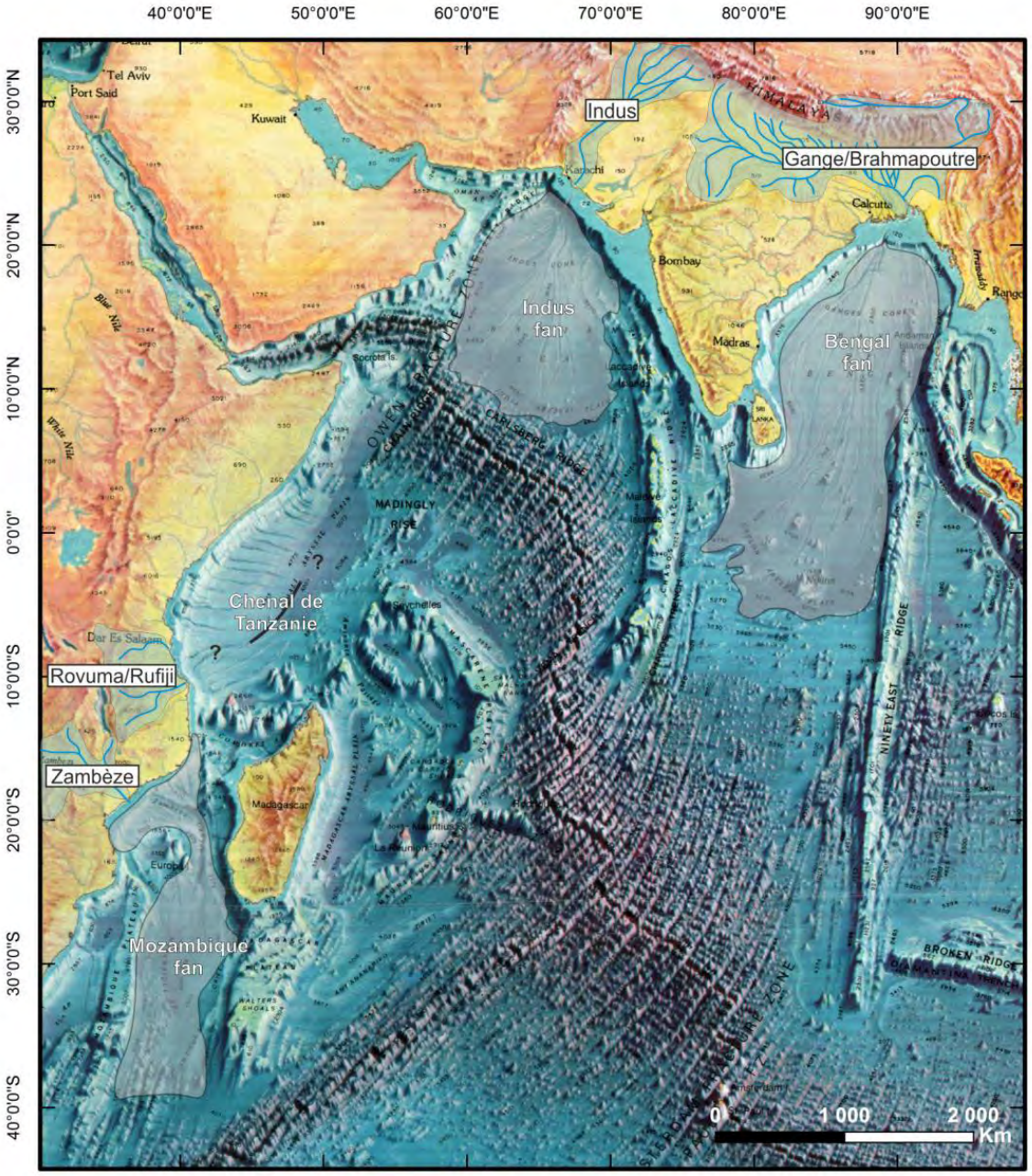

1. Sédimentation gravitaire – turbiditique : le système turbiditique du Gange - Brahmapoutre

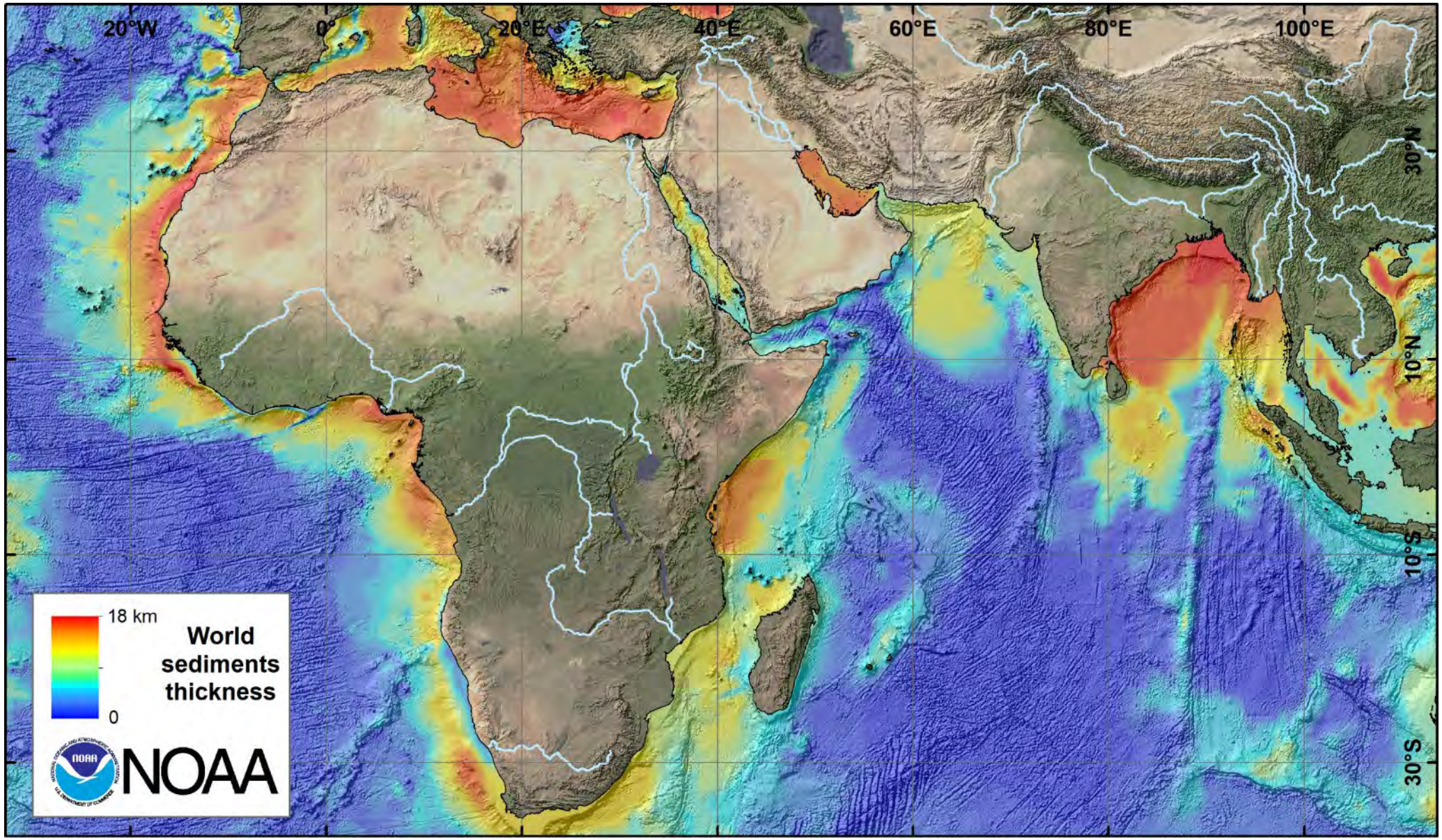

1. Sédimentation gravitaire – turbiditique : le système turbiditique du Gange - Brahmapoutre

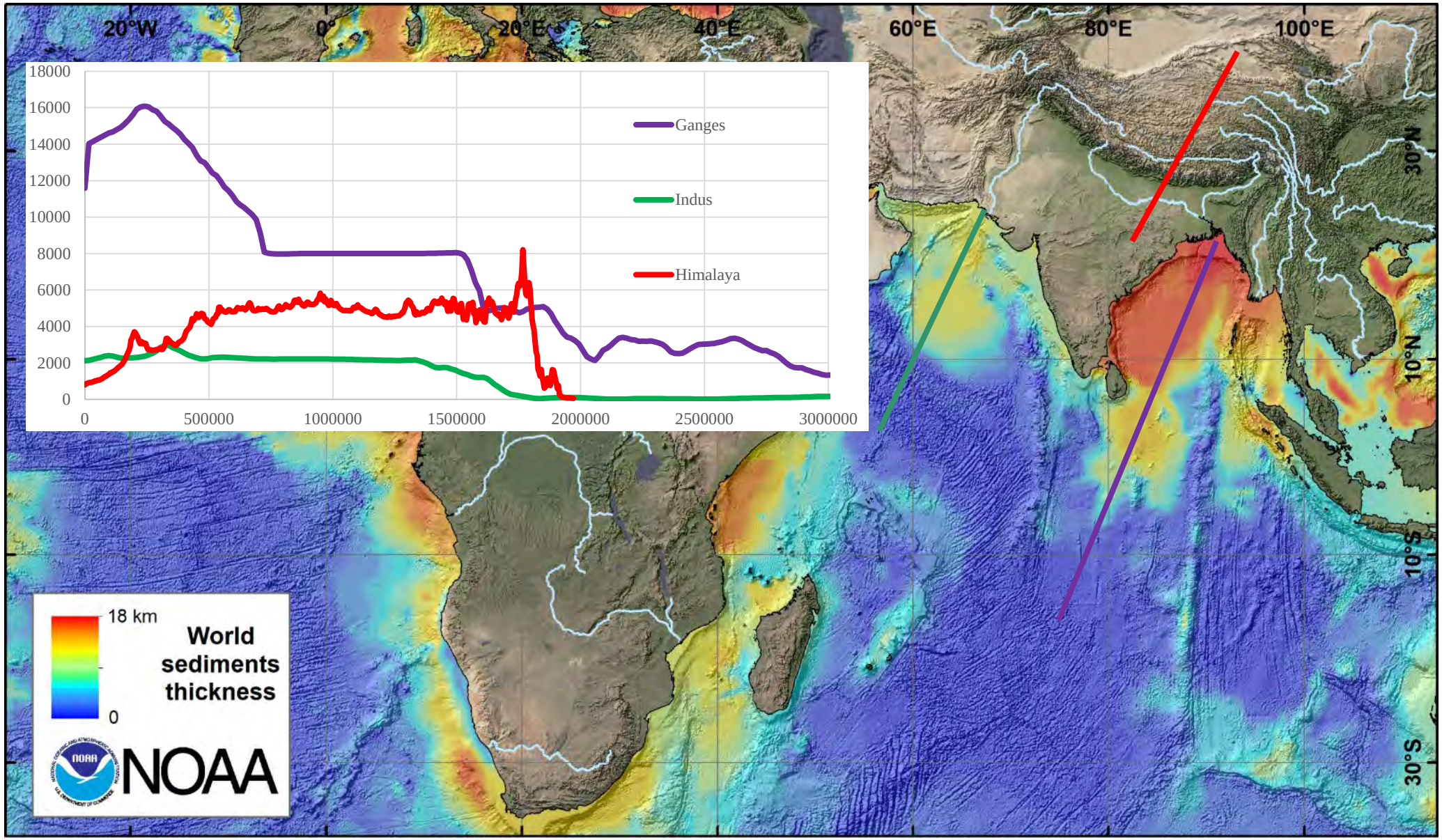

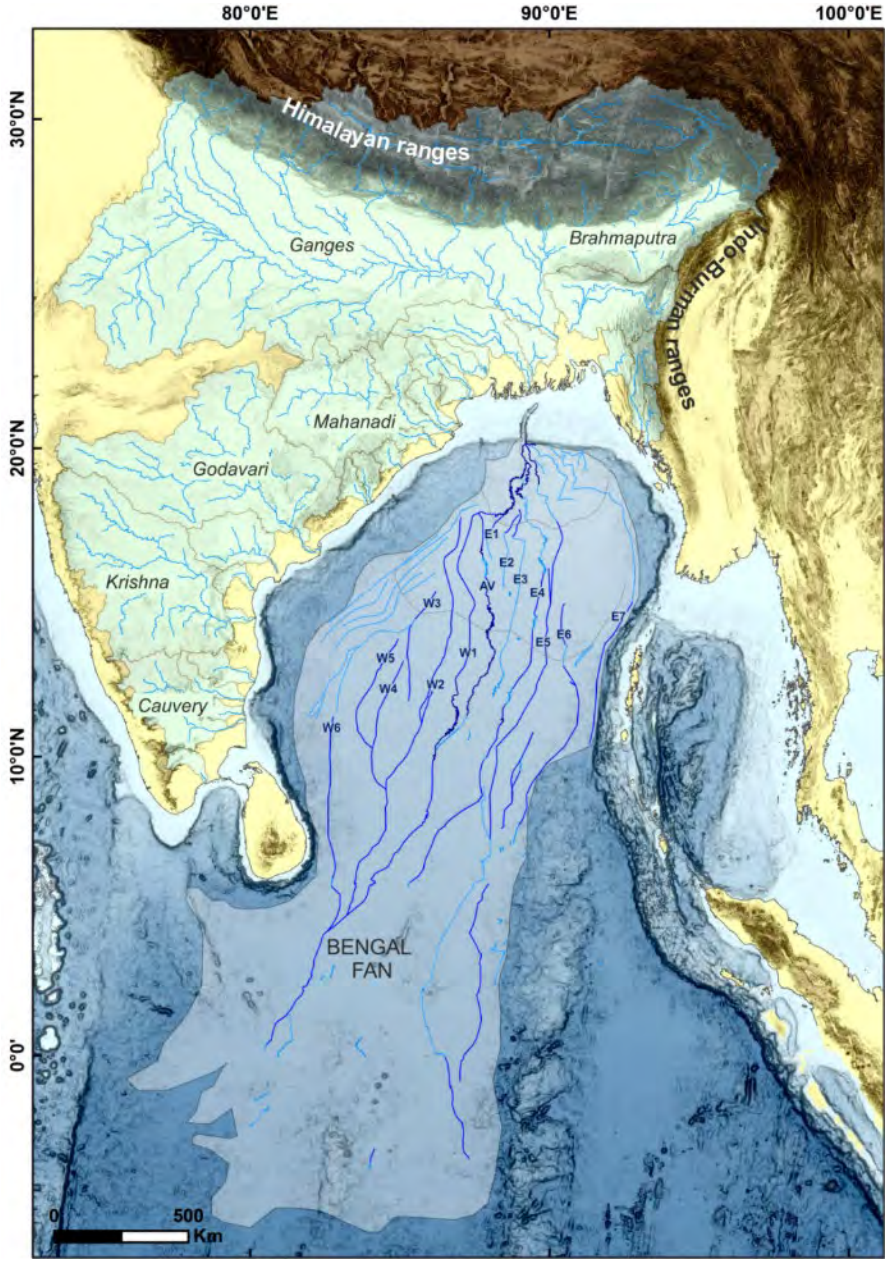

Bassin versant du Gange – Brahmapoutre : 1,830,000 km²

Décharge sédimentaire : 1×10^9 t/an

Surface du système turbiditique : 3×10^6 km²

Epaisseur max. 16.5 km

Fournier, L., et al. 2017. The Bengal fan: External controls on the Holocene Active Channel turbidite activity. The Holocene 27, 900–913.

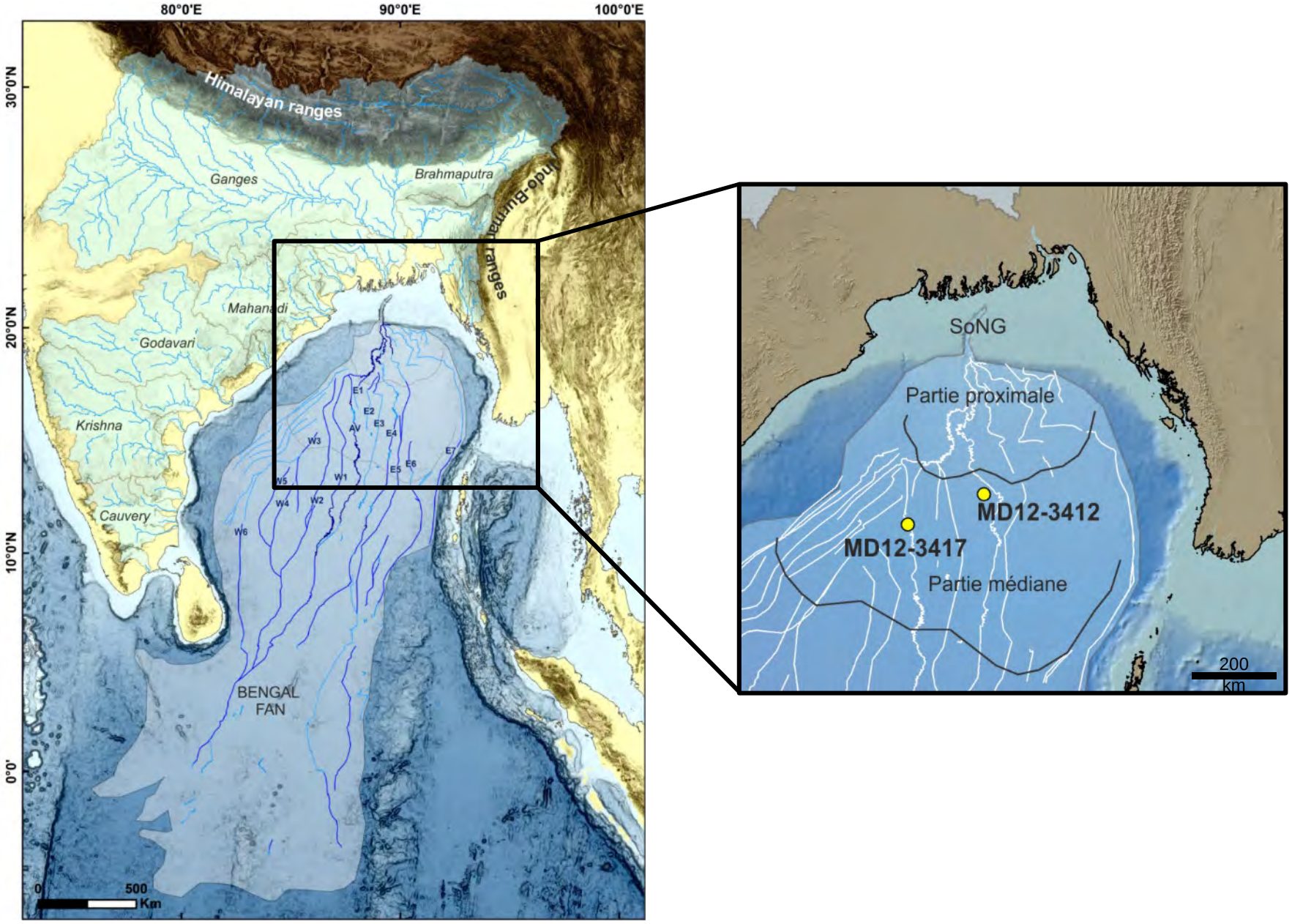

Fournier, L., et al. 2017. The Bengal fan: External controls on the Holocene Active Channel turbidite activity. The Holocene 27, 900–913.

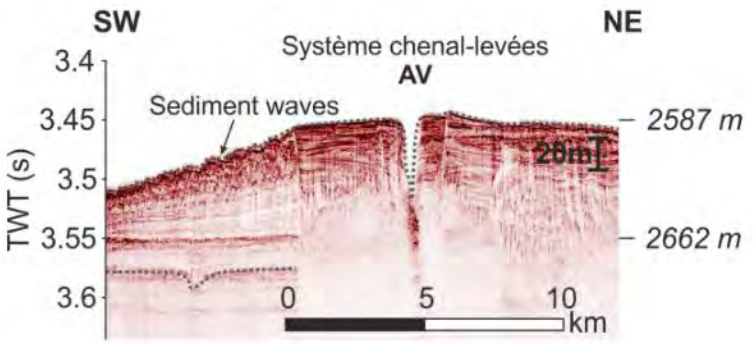

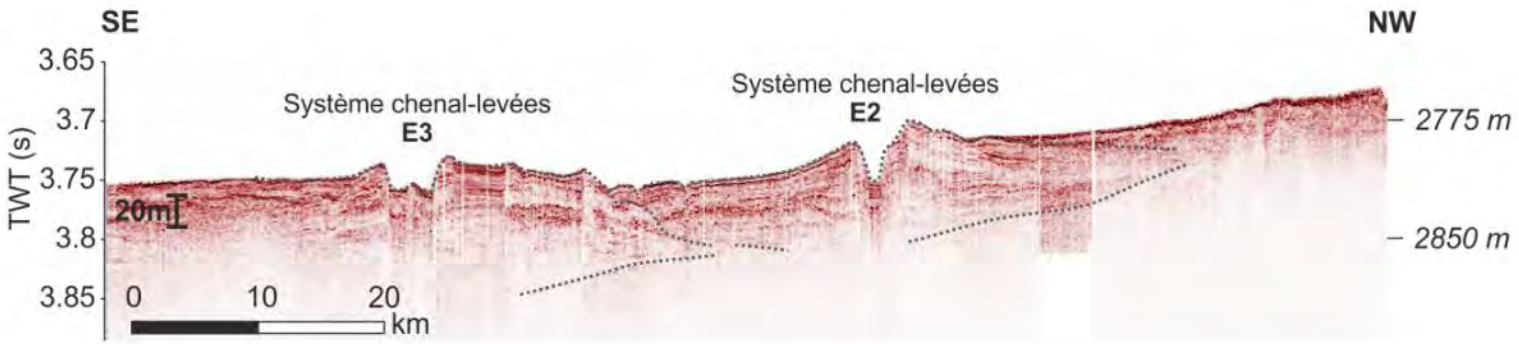

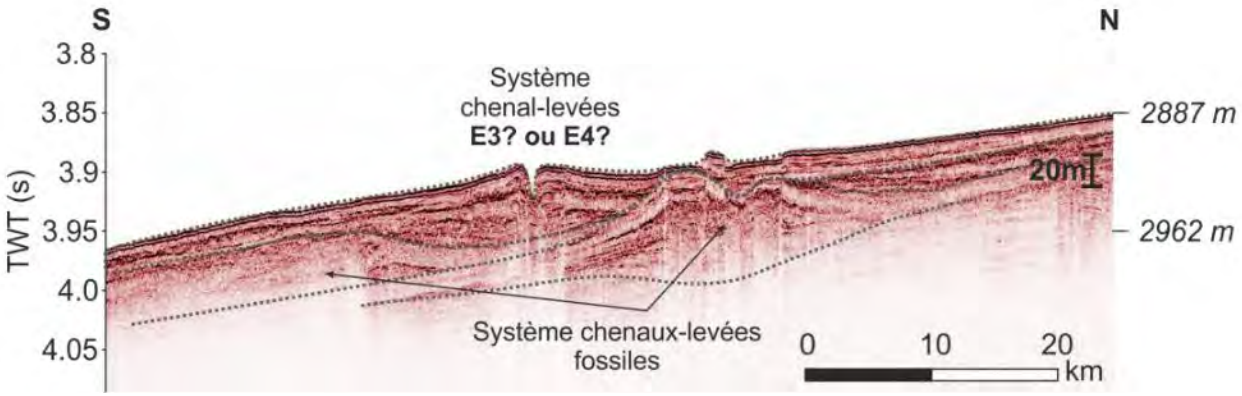

Fournier, L., et al. 2017. The Bengal fan: External controls on the Holocene Active Channel turbidite activity. The Holocene 27, 900–913.

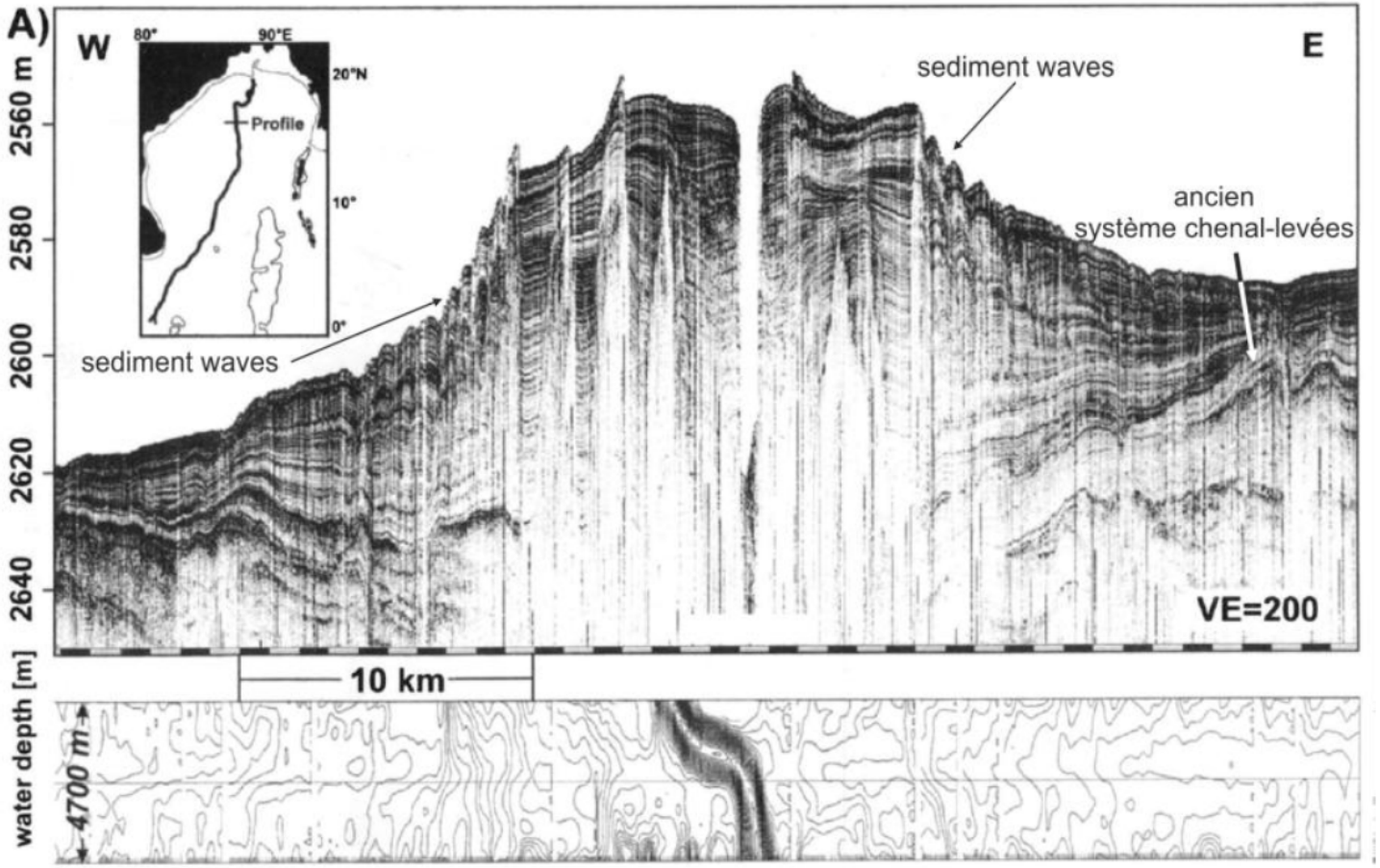

Weber, M.E., et al. 1997. Active growth of the Bengal Fan during sea-level rise and highstand. Geology 25, 315–318.

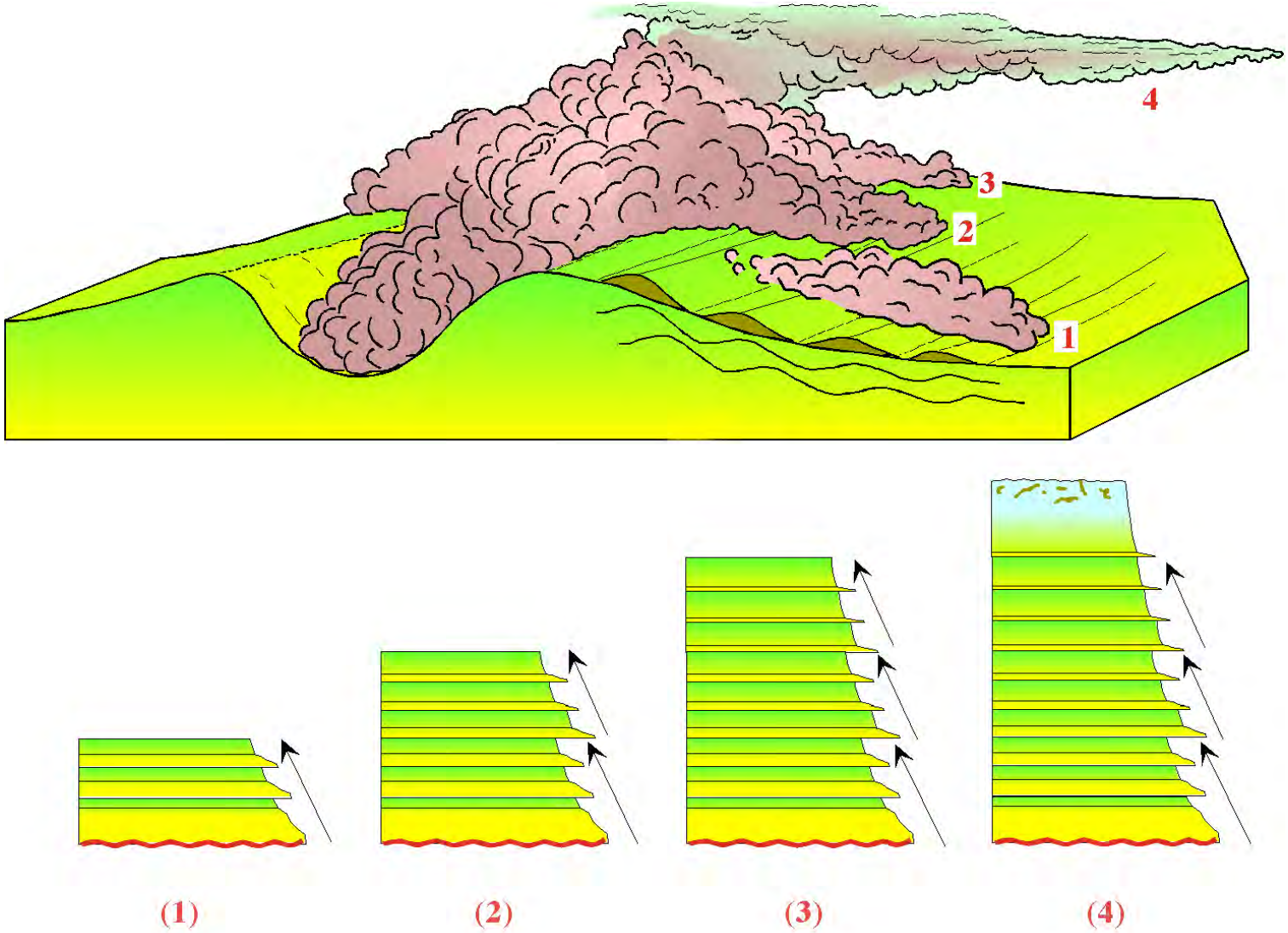

Schéma conceptuel illustrant le processus de débordement permettant la construction des levées (d'après Migeon, 2000). Un même écoulement turbiditique peut générer plusieurs débordements successifs (1, 2, 3). La succession de ces débordements, suivi de la décantation du "nuage turbiditique" (4) provoque la mise en place de séquences argilo-silteuses normalement granoclassées.

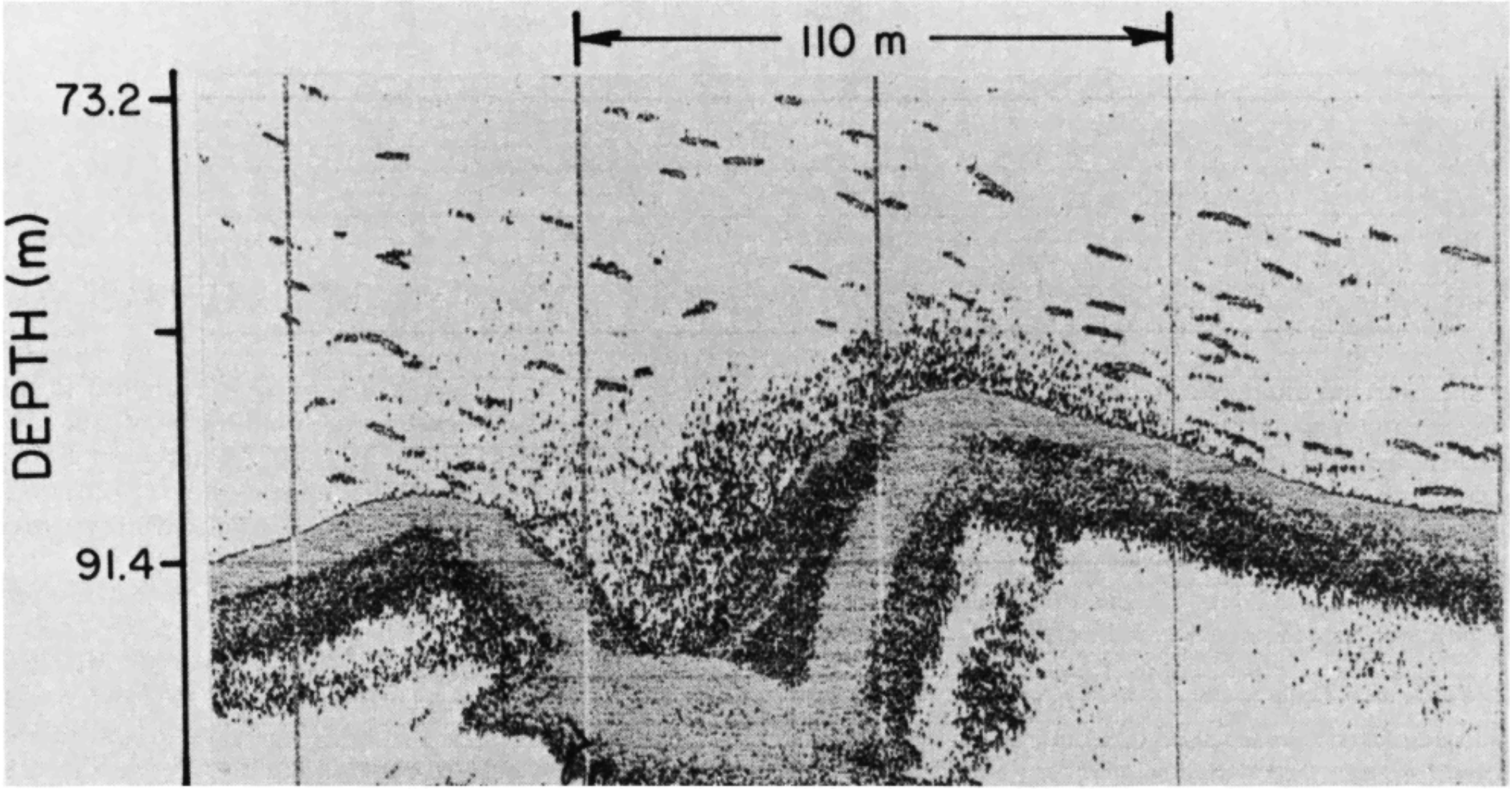

Hay, Alex E. "Turbidity Currents and Submarine Channel Formation in Rupert Inlet, British Columbia: 2. The Roles of Continuous and Surge-Type Flow." *Journal of Geophysical Research: Oceans* 92, no. C3 (1987): 2883–2900.

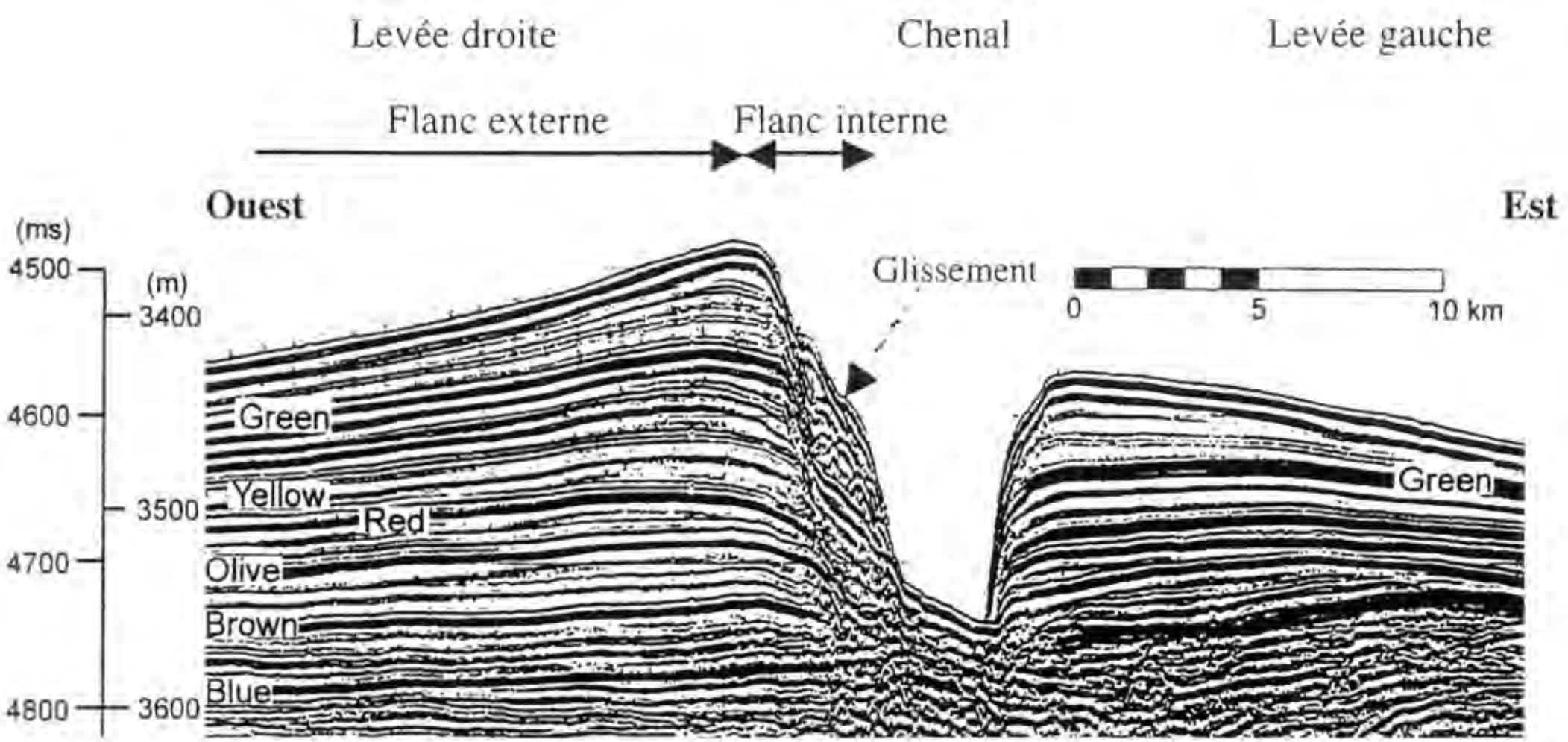

Profil sismique montrant la structure interne des levées du NAMOC (d'après Skene, 1998)

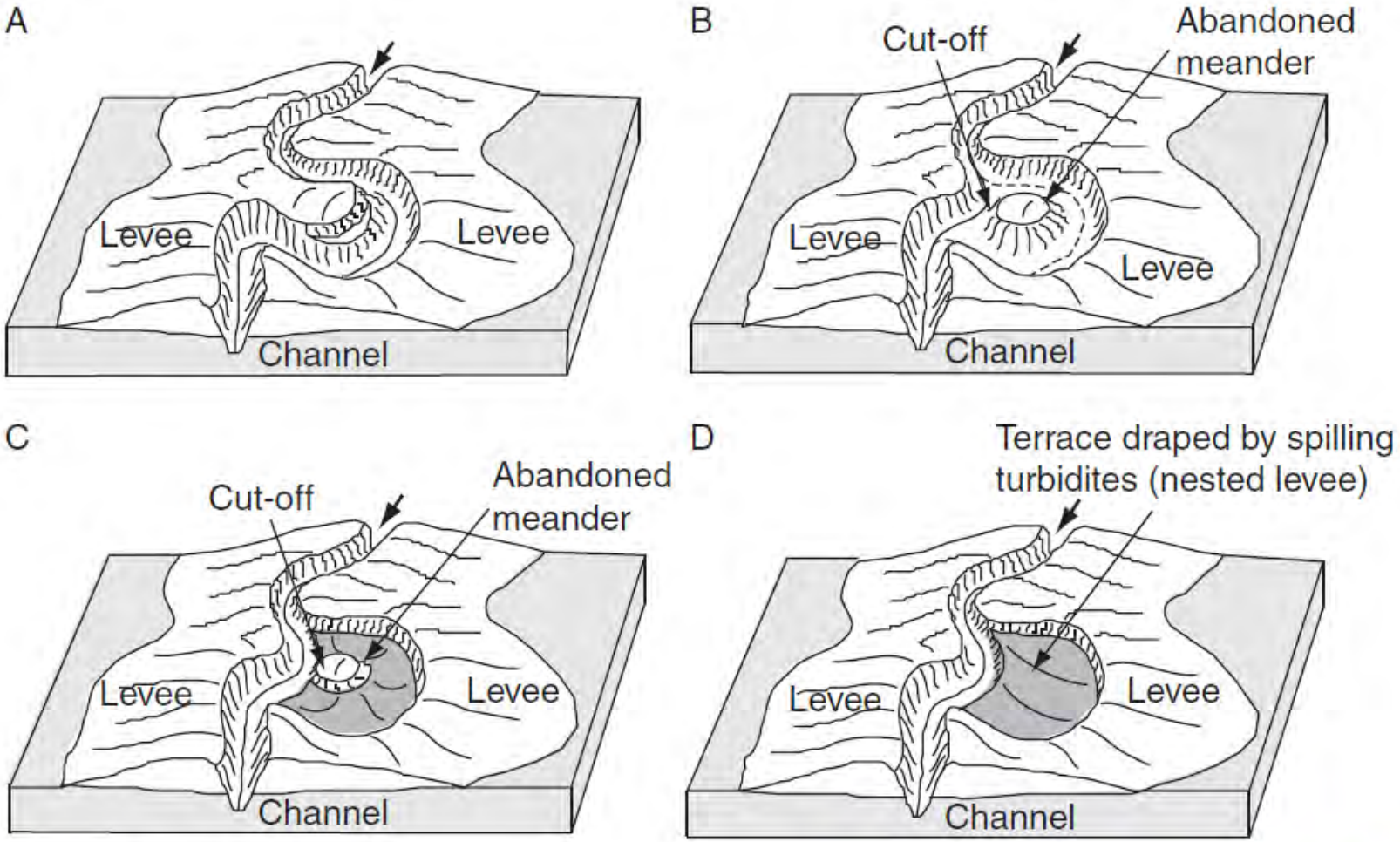

Figure 2.31 Scenario for meander abandonment (Babonneau, 2002; Babonneau et al., 2004). (A) Lateral shift of a talweg. A meander forms. (B) Meander cut-off. (C) Beginning of the filling by spilling of turbidity current in the abandoned meander. (D) Formation of a terrace that acts as a nested levee. Bold arrow indicates direction of the channelized flow. Reproduced with permission from Geological Society, London.

Hüneke, H. (Ed.), 2011. Deep-sea sediments, Developments in sedimentology. Elsevier, Amsterdam.

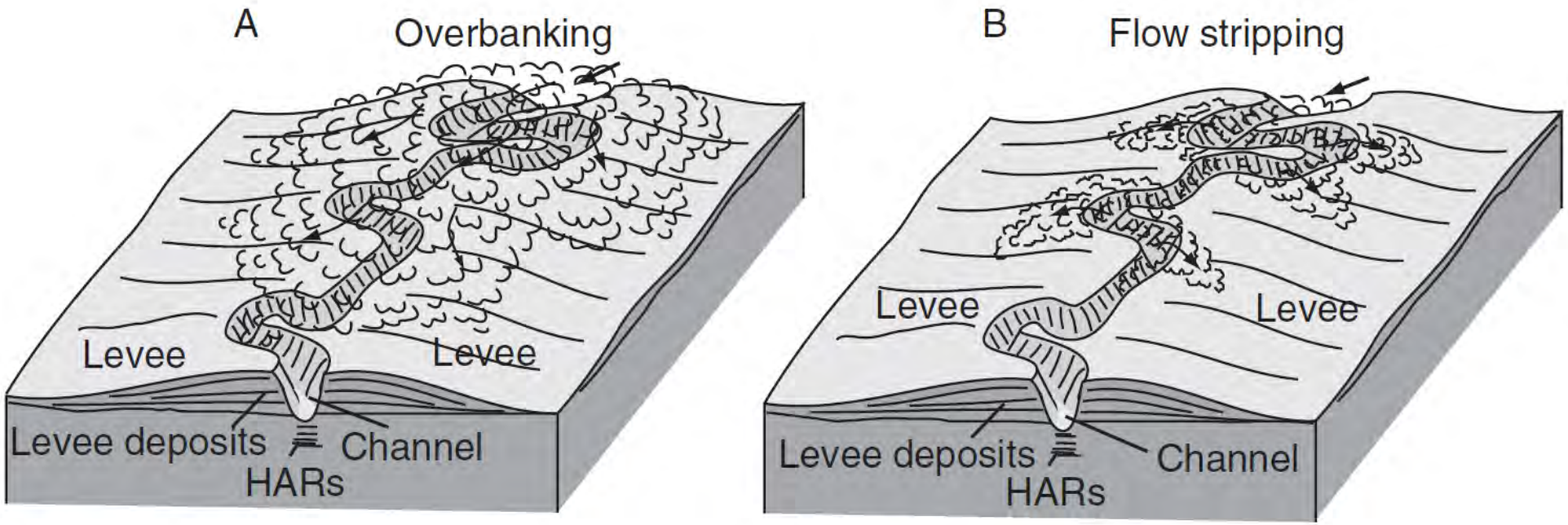

Figure 2.27 (A) Overbanking or overspilling (Hiscott et al., 1997). (B) Flow stripping (Piper and Normark, 1983). Bold arrow indicates direction of the channelized flow (from Babonneau, 2002). Reproduced with permission from N. Babonneau.

Hüneke, H. (Ed.), 2011. Deep-sea sediments, Developments in sedimentology. Elsevier, Amsterdam.

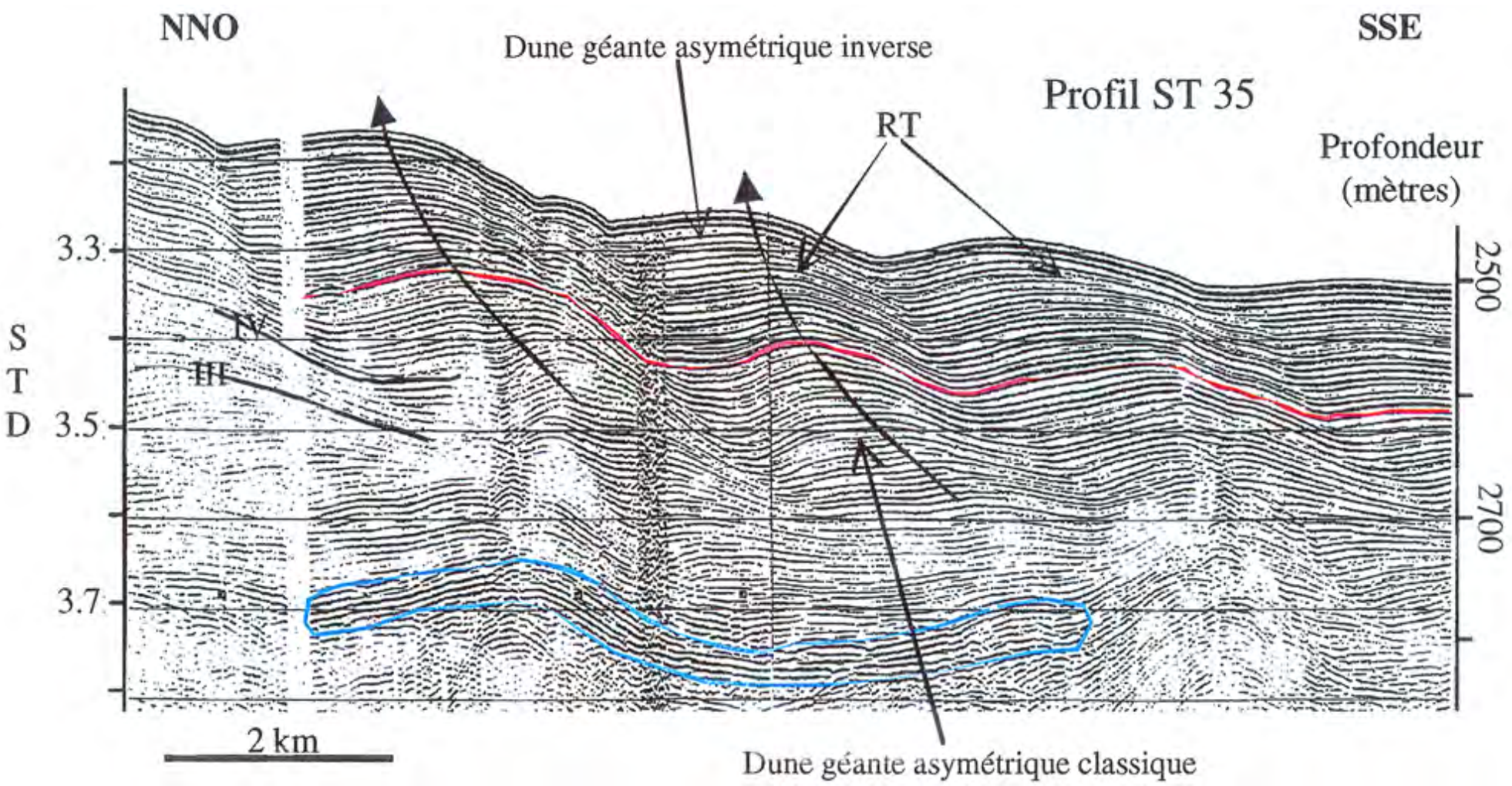

Profil sismique montrant la structure interne des levées de l'éventail du VAR (d'après Migeon, 2000)

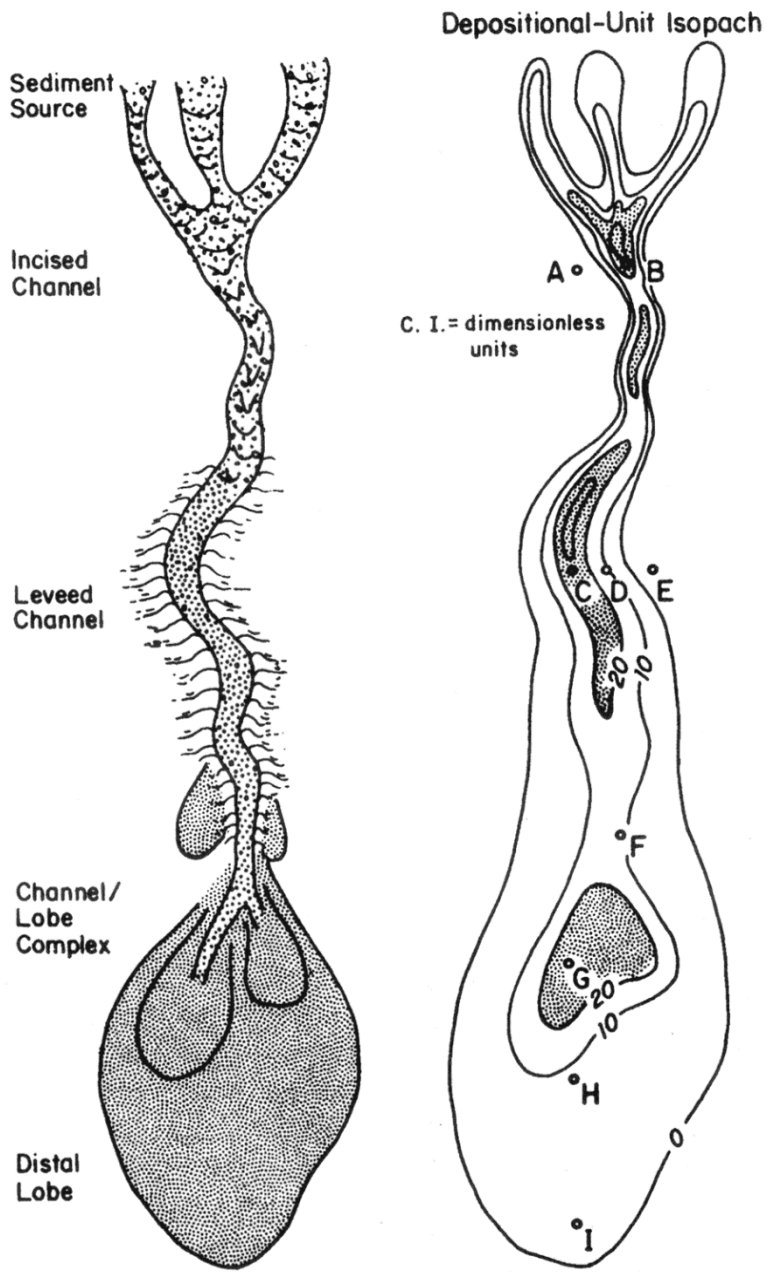

Complexe chenal/lobe synthétique d'après Galloway (1998). (A) *Slump* et *cohesive debris flows*. (B) *Debris flows*. (C) Turbidite de haute densite et *debris flows* sableux. (D) Dépôts de levées hétérolitiques. (E) Turbidite de faible densité, et dépôts hémipélagiques.(F) Turbidites de haute densité. (G) Empilement de turbidites des lobes proximaux. (H) Turbidites hétérolitiques des lobes medians. (I) Turbidites de faible densité des lobes distaux.

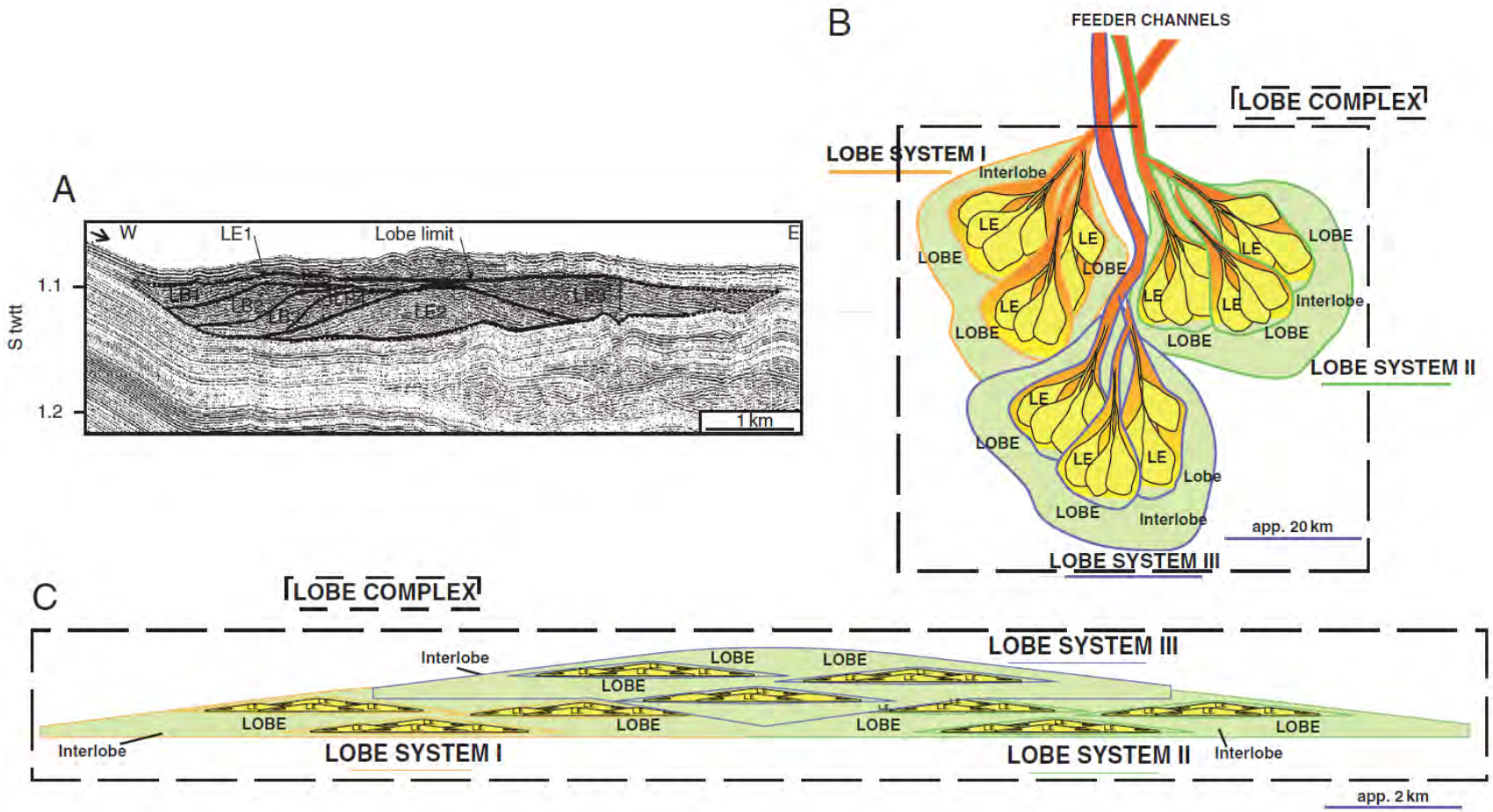

Figure 2.37 Terminology used for lobe geometry. Lobes correspond to nested depositional bodies from lobe complex (basin scale) to lobe bed (depositional process). Modified from Prelat et al. (2009), and Mulder and Etienne (2010). (A) Structure of the South Golo lobe, E. Corsica (Gervais, 2002; Gervais et al., 2005). The lobe is composed of three elements (LE1, LE2 and LE3). LE1 is composed of four lobe beds (LB1, LB2, LB3 and LB4). Reproduced with permission from Elsevier. (B) Plane view of lobe hierarchy in a lobe complex. LE: lobe elements. (C) Transverse view of a lobe complex. (A multi-colour version of this figure is on the included CD-ROM.)

Hüneke, H. (Ed.), 2011. Deep-sea sediments, Developments in sedimentology. Elsevier, Amsterdam.

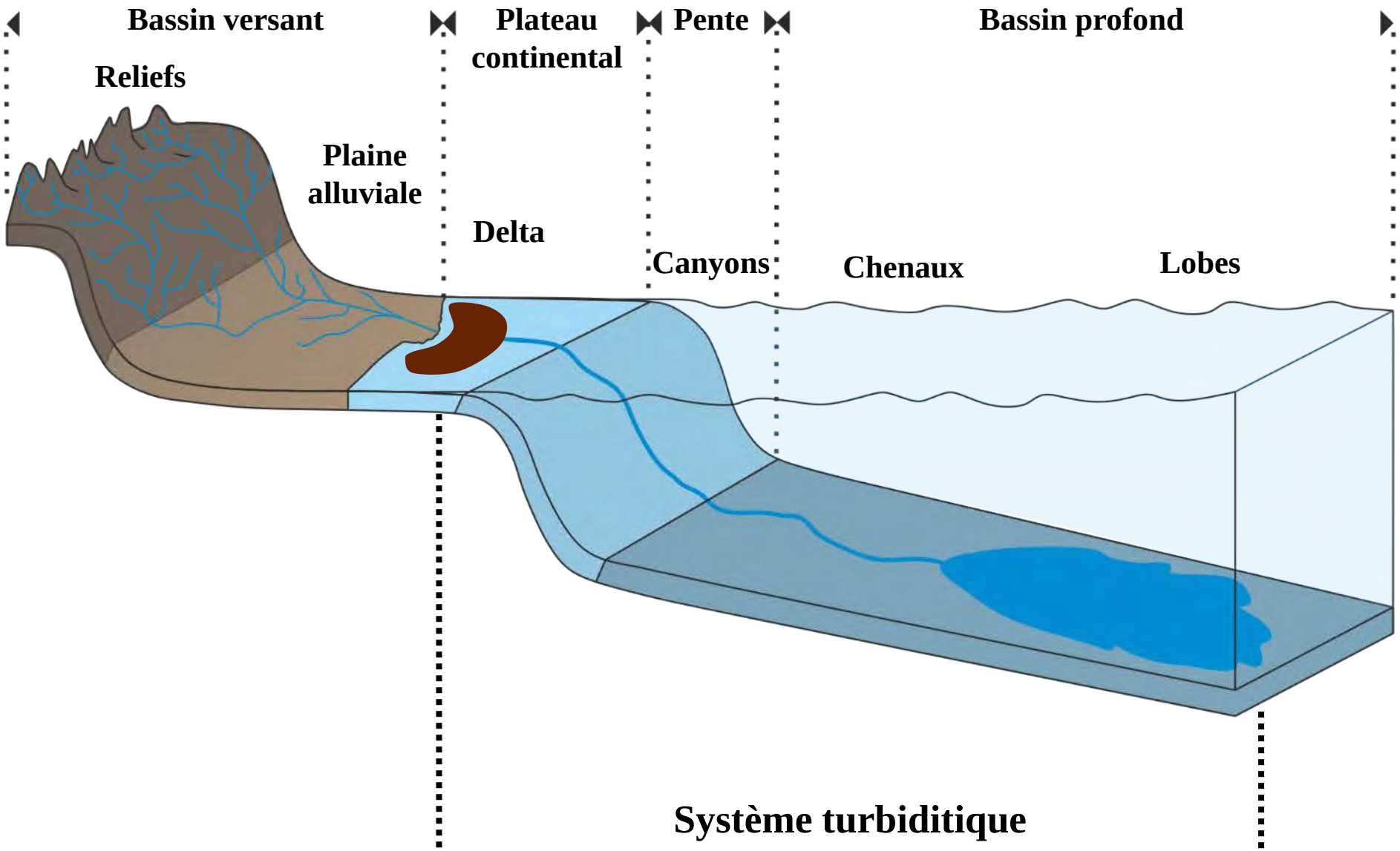
Bassin versant
Plateau continental
Pente
Bassin profond
Reliefs
Plaine alluviale
Delta
Canyons
Chenaux
Lobes
Système turbiditique

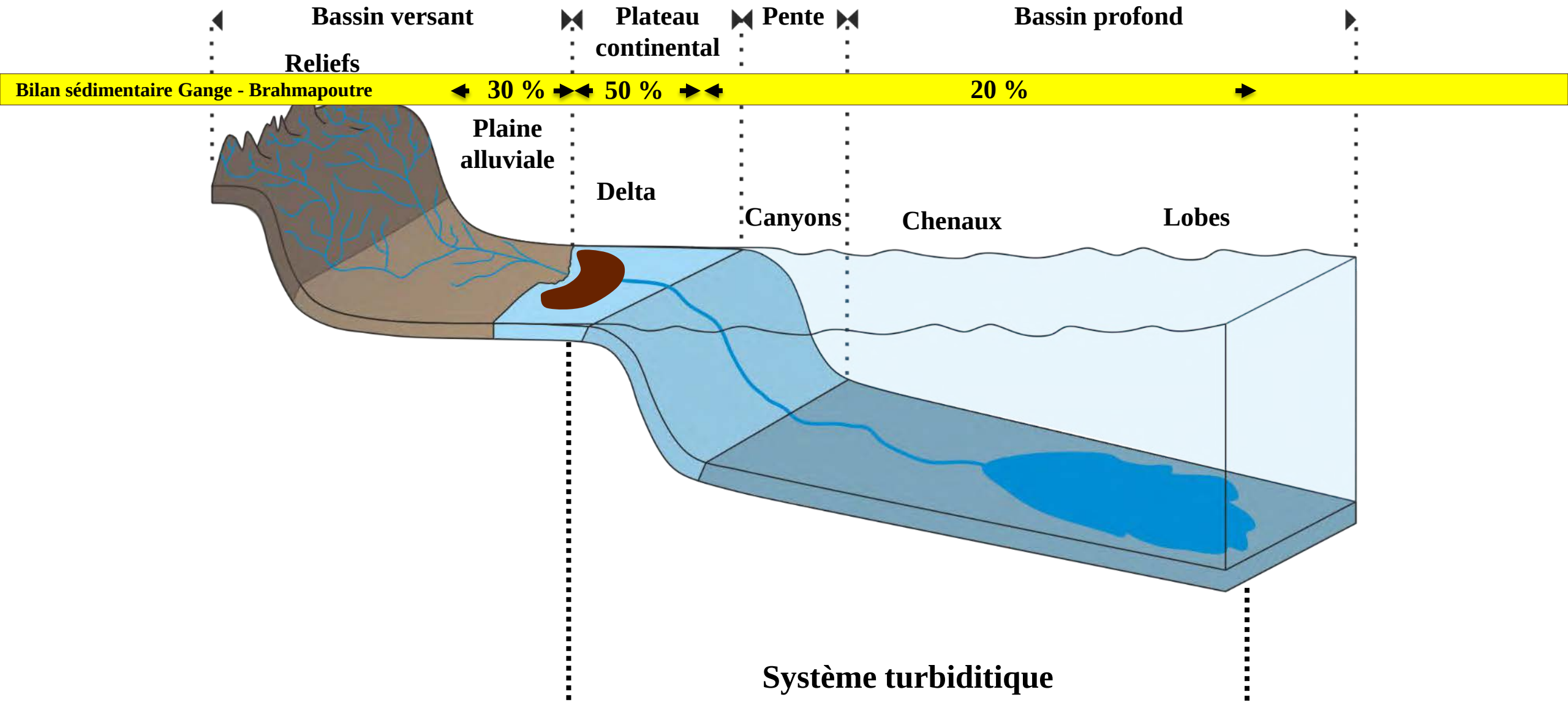
Bassin versant
Plateau continental
Pente
Bassin profond
Reliefs
Bilan sédimentaire Gange - Brahmapoutre
30 %
50 %
20 %
Plaine alluviale
Delta
Canyons
Chenaux
Lobes
Système turbiditique

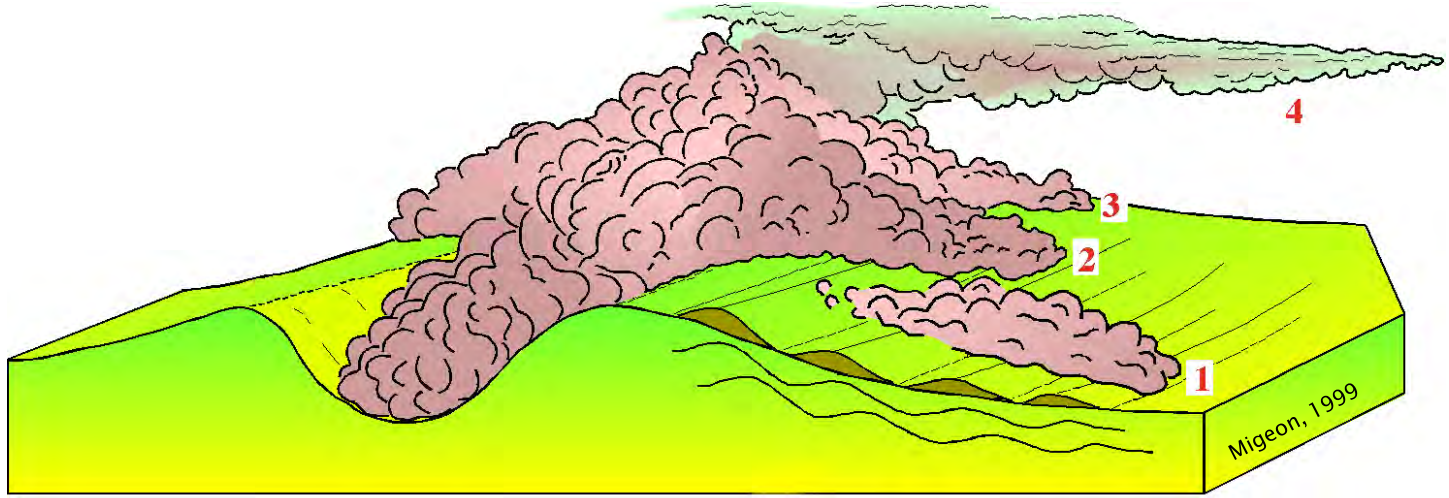

Construction des levées turbiditiques par débordement de nuages turbides

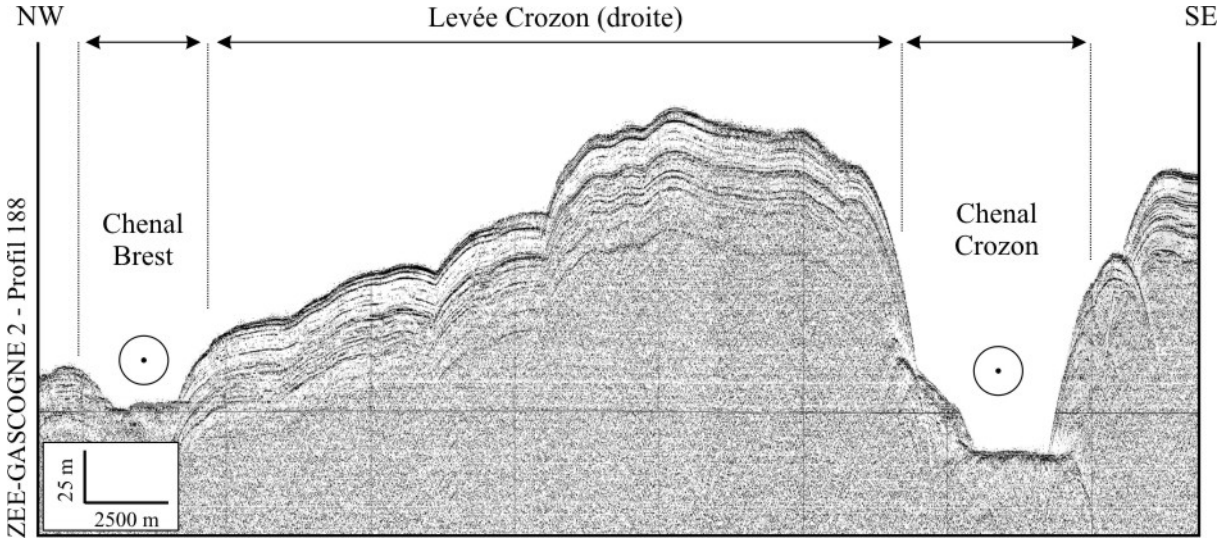

Structure interne de la levée turbiditique de Crozon (3,5 kHz)

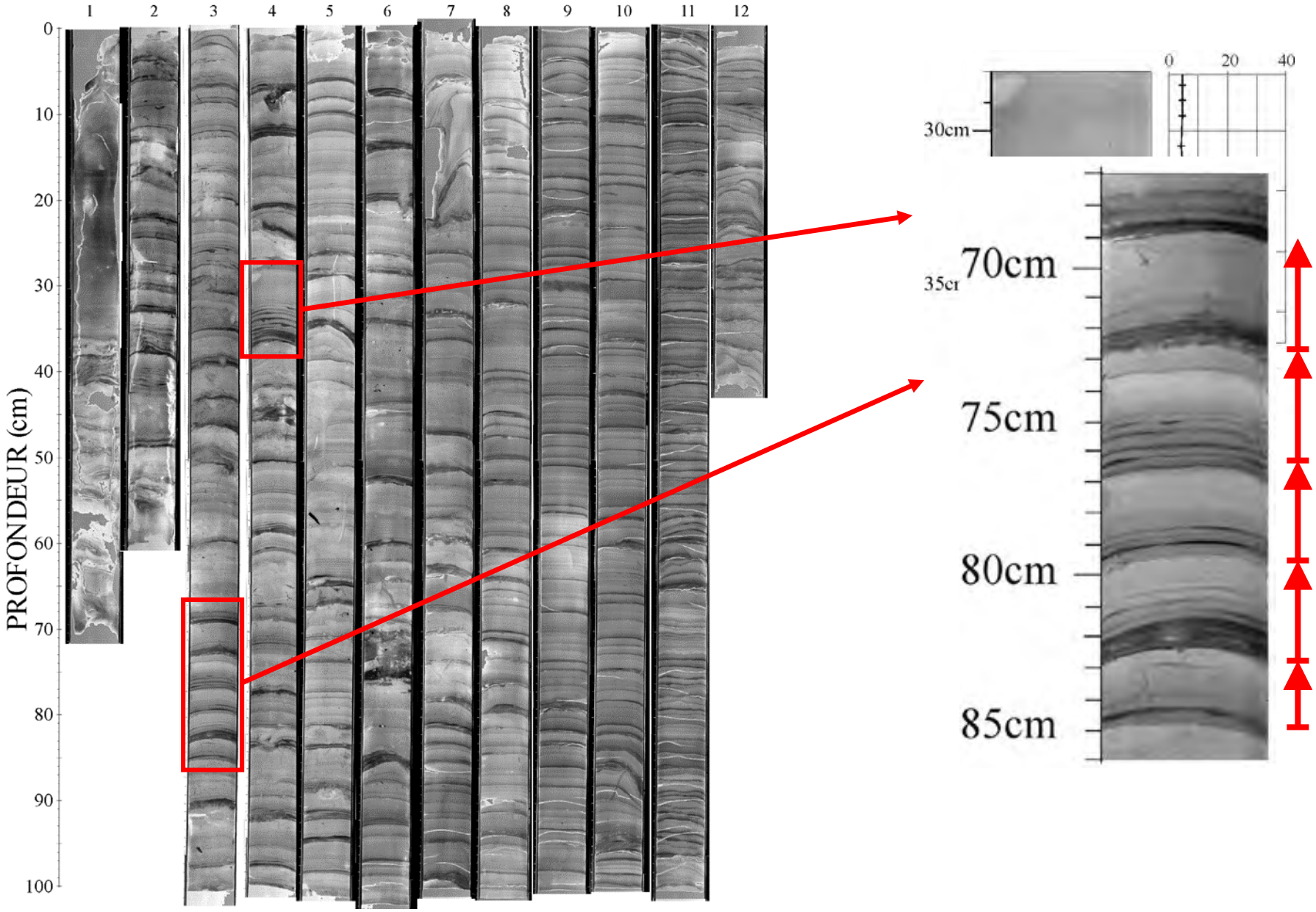
1
2
3
4
5
6
7
8
9
10
11
12
PROFONDEUR (cm)
0
10
20
30
40
50
60
70
80
90
100
0
20
40
30cm
70cm
75cm
80cm
85cm

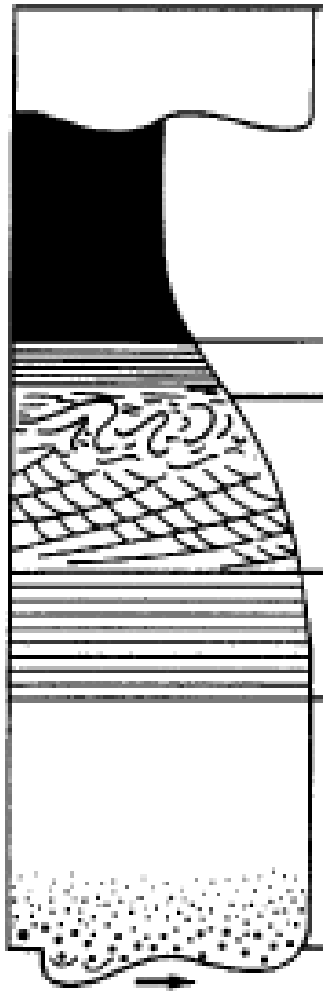

GRAIN SIZE	BOUMA (1962) DIVISIONS	INTERPRETATIONS		
Mud	E Laminated to homogeneous mud	Suspension fallout deposits	Sedimentation dominated by suspension fallout	Turbulent flow regime
Silt	D Upper mud/silt laminae	Low energy planar laminations		
Sand	C Ripples, climbing ripples, wavy or convolute laminae	Ripples with cross-laminations	Sedimentation dominated by traction	
	B Plane laminae	Energy-rich planar laminations		
Coarse Sand	A Structureless or graded sand to granule	Concentrated to hyperconcentrated flow		Laminar flow regime

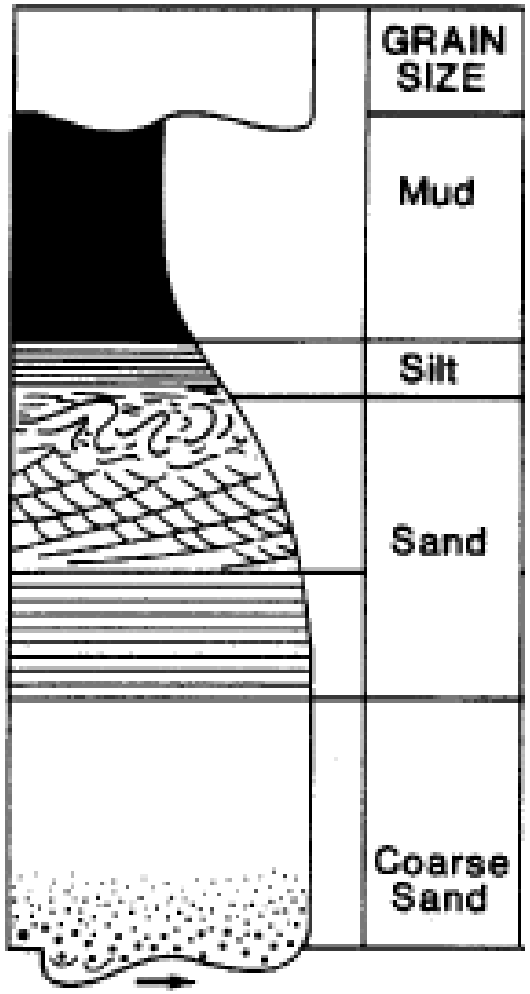

Faciès

Faciès

Faciès

Faciès

Faciès

Succession de faciès génétiquement liés

Séquence

Faciès sédimentaire : ensemble de roches sédimentaires avec des caractéristiques propres (taille de grains, nature des grains, couleur, structures sédimentaires, fossiles…).

Lithofaciès : faciès déterminé sur des caractéristiques sédimentaires (taille de grains, minéralogie).

Biofaciès : faciès déterminé sur le contenu paléontologique.

Ichnofacies : facies déterminé sur l'observation de traces d'organismes

Carotte MD03-2688 (35 mètres – 732 dépôts turbiditiques / 30.000 ans)

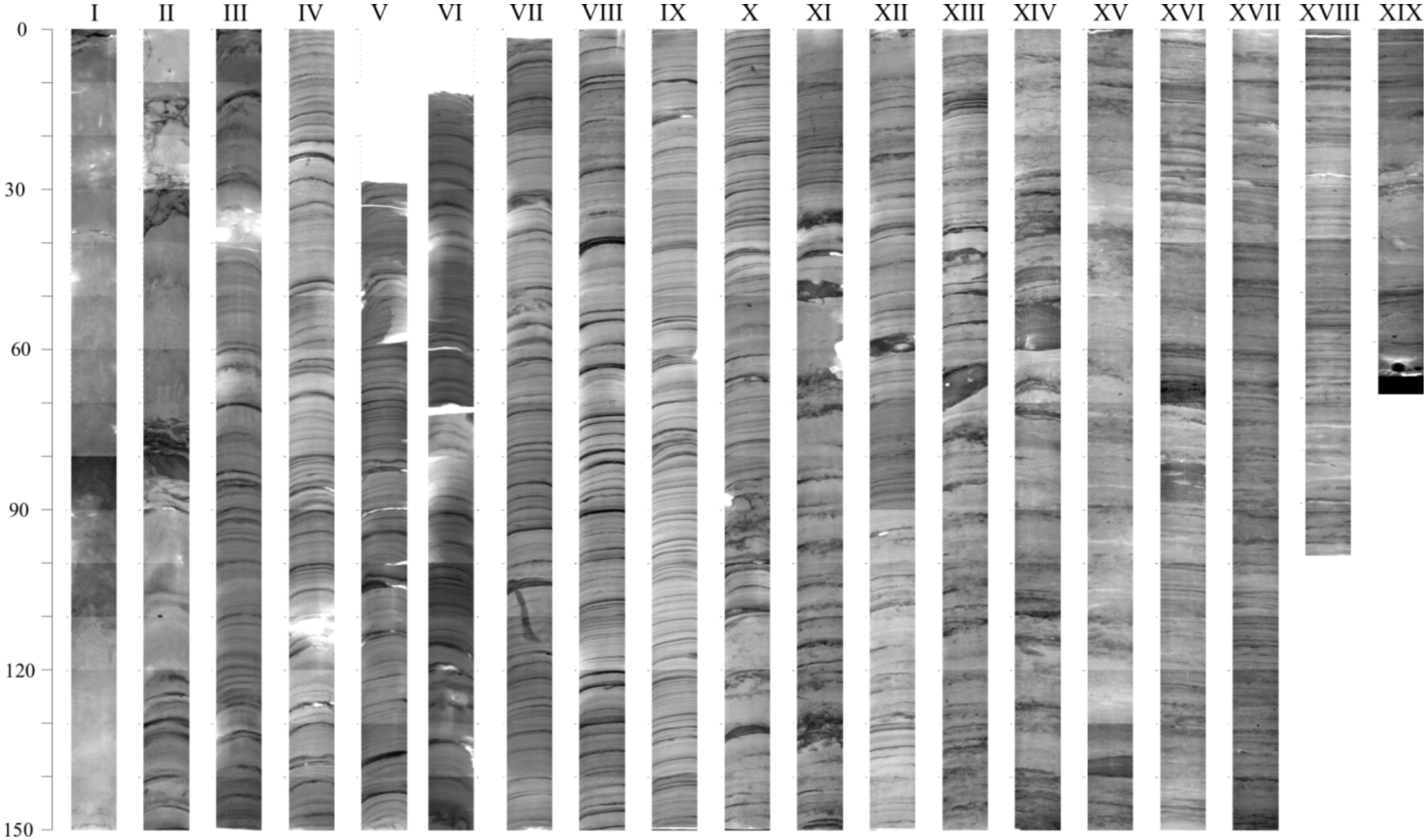

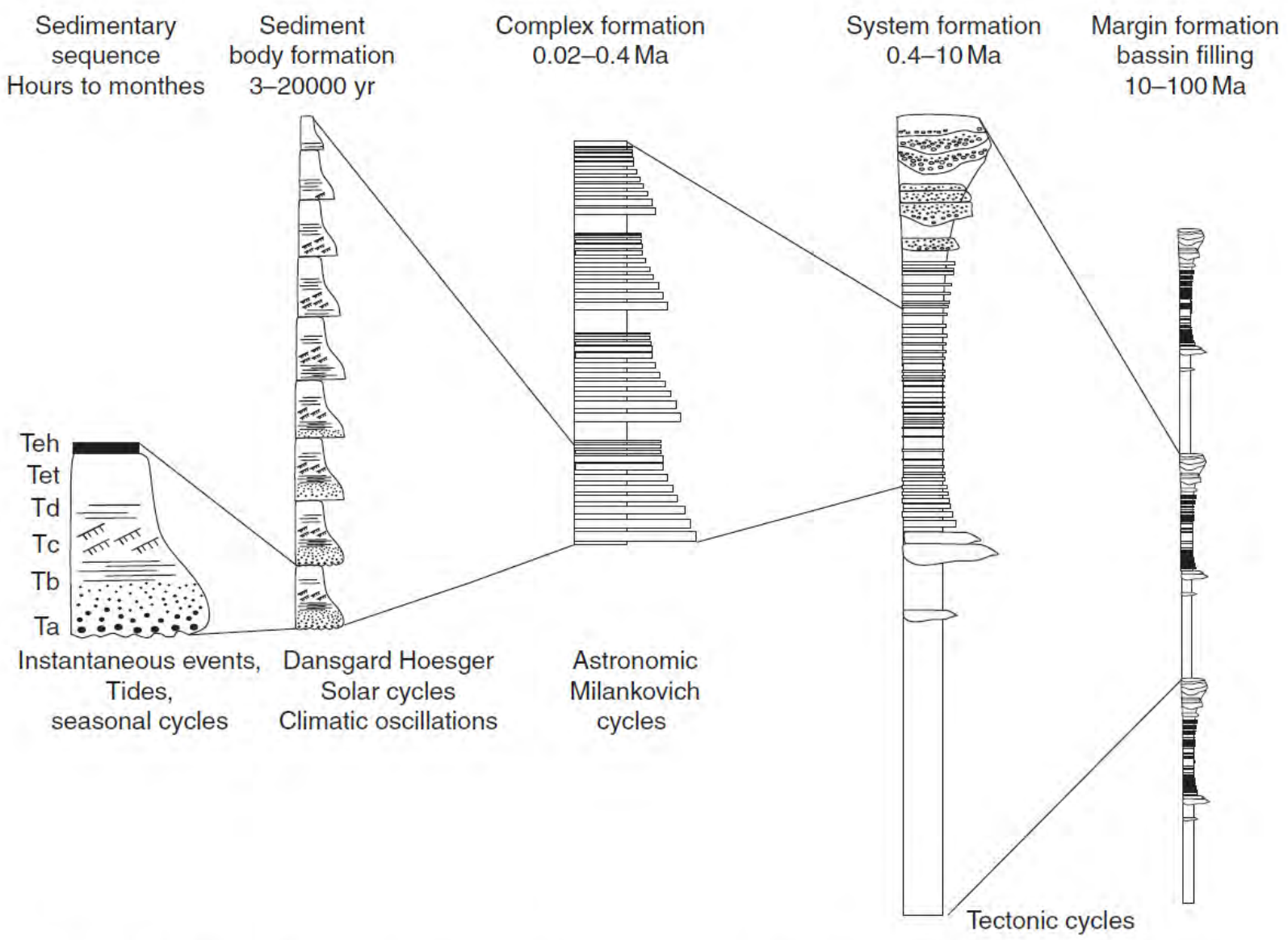

Figure 2.39 Concept of nested sequences and inferred forcing parameters.

Hüneke, H. (Ed.), 2011. Deep-sea sediments, Developments in sedimentology. Elsevier, Amsterdam.

1. Sédimentation gravitaire – turbiditique : la séquence de Bouma

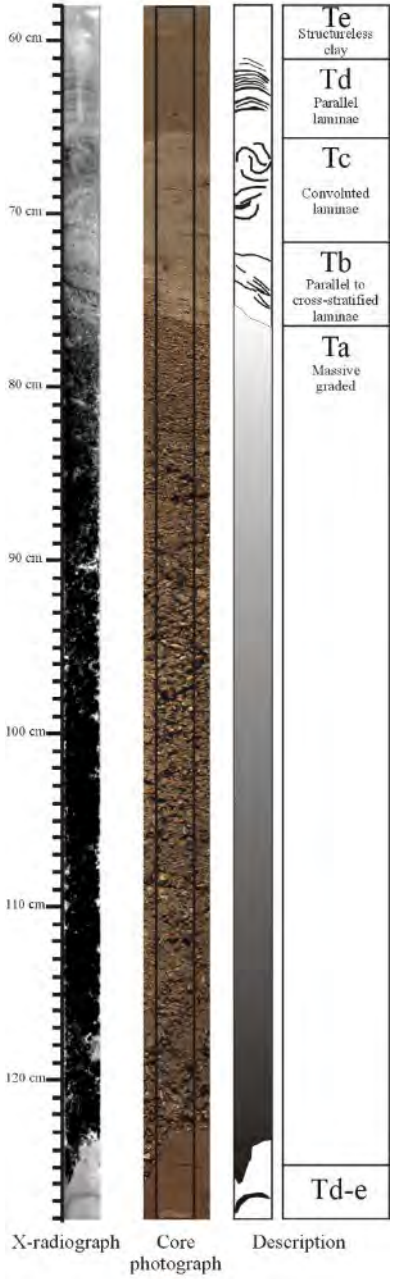

Suspension fallout deposits

Low energy planar laminations

Ripples with cross-laminations

Energy-rich planar laminations

Concentrated flow

hyperconcentrated flow

Sedimentation dominated by suspension fallout	Turbulent flow regime
Sedimentation dominated by traction	
	Laminar flow regime

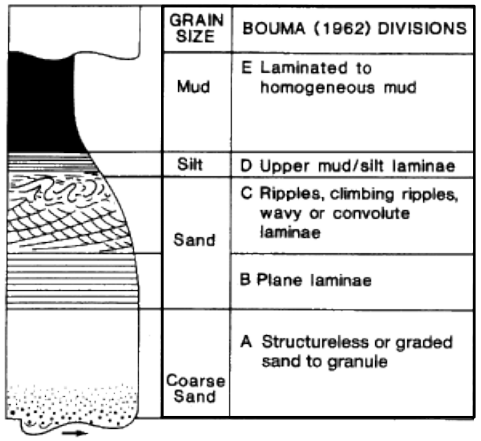

Zaragosi, S., et al. 2001. The deep-sea Armorican depositional system (Bay of Biscay), a multiple source, ramp model. Geo-Mar Lett 20, 219–232.

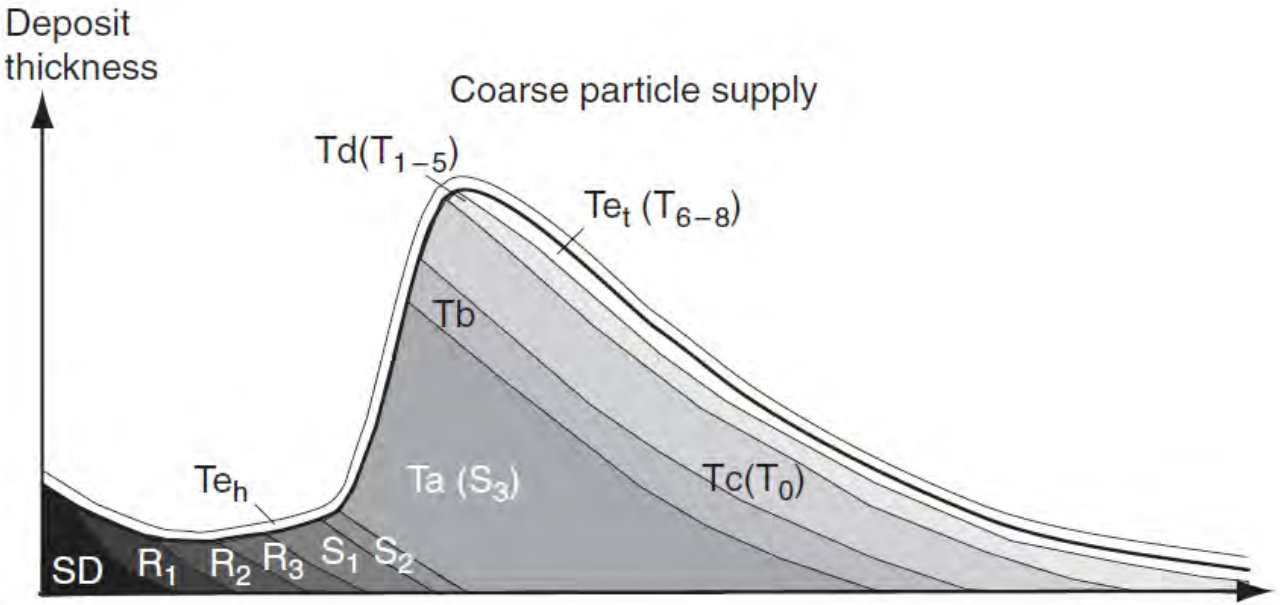

Figure 2.13 Longitudinal evolution of gravity-flow deposits. (A) Depositional setting dominated by coarse-particle supply. (B) Depositional setting dominated by fine particle supply. SD: slump deposits. Facies R, S and T are explained in Fig. 2.11.

Hüneke, H. (Ed.), 2011. Deep-sea sediments, Developments in sedimentology. Elsevier, Amsterdam.

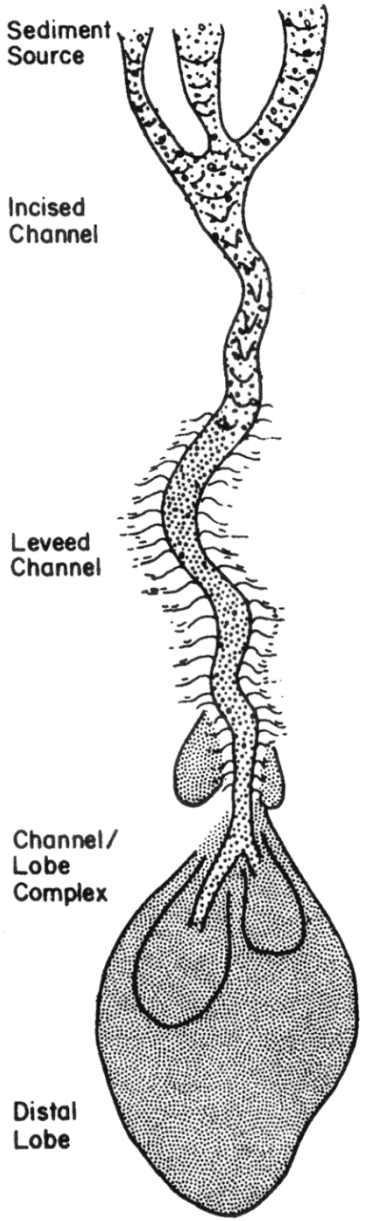

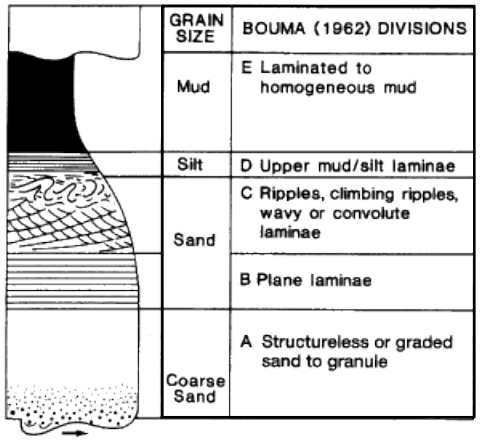

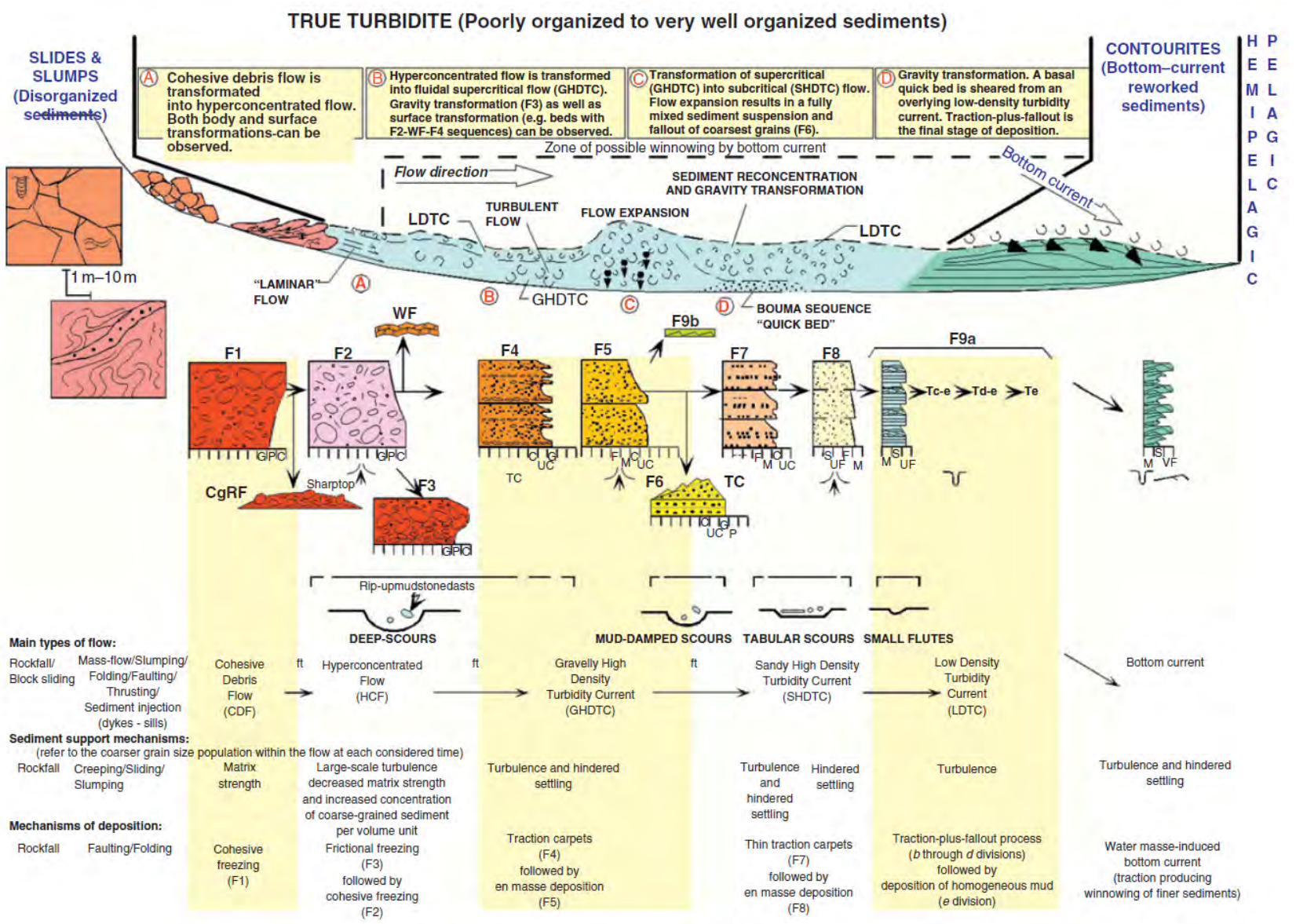

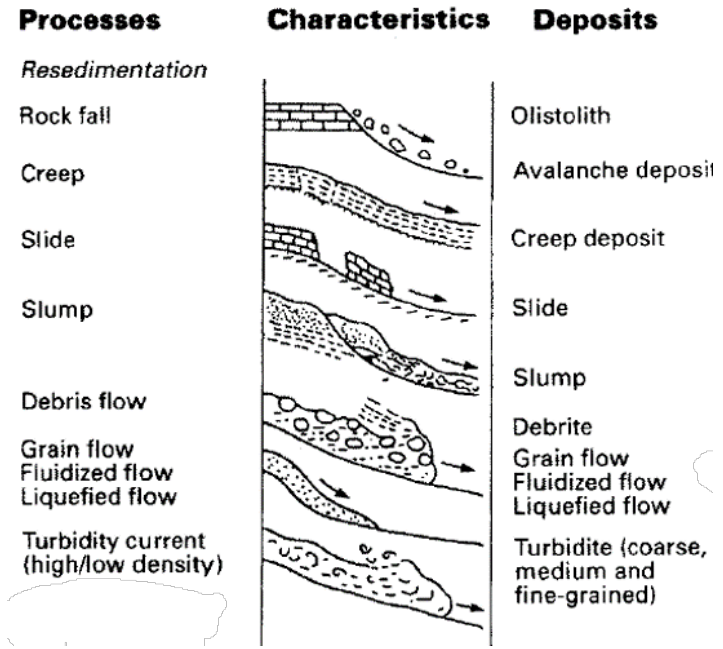

Figure 2.14 Classification of facies evolution (from Gérard et al., 2000; Mutti, 1992; Reproduced with permission from E. Mutti). (A multi-colour version of this figure is on the included CD-ROM.)

 Hüneke, H. (Ed.), 2011. Deep-sea sediments, Developments in sedimentology. Elsevier, Amsterdam.

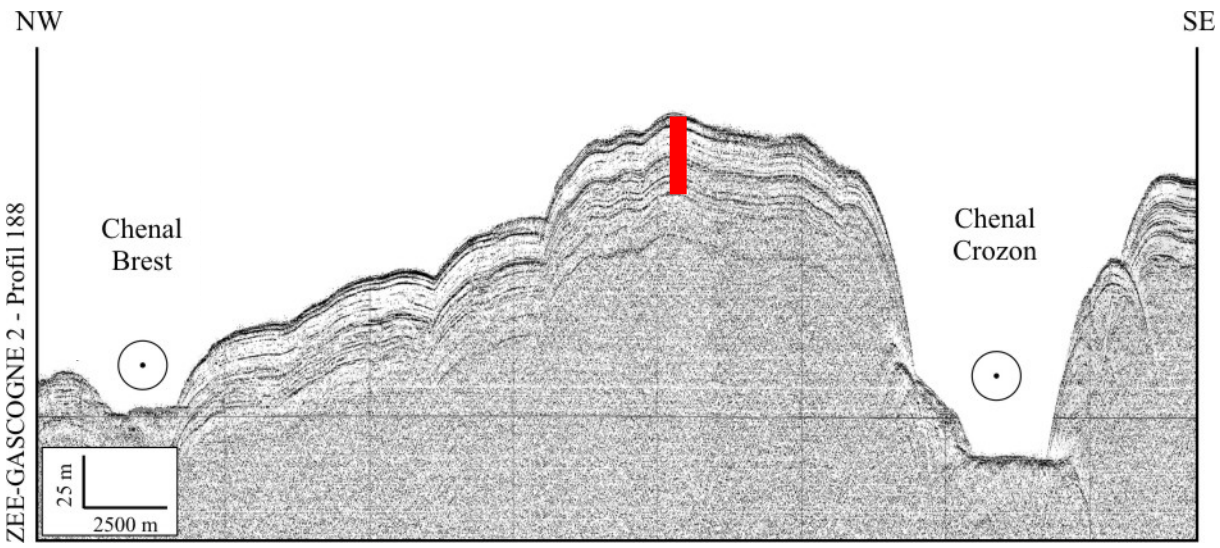

Structure interne de la levée turbiditique de Crozon, golfe de Gascogne. Sismique 3,5 kHz.

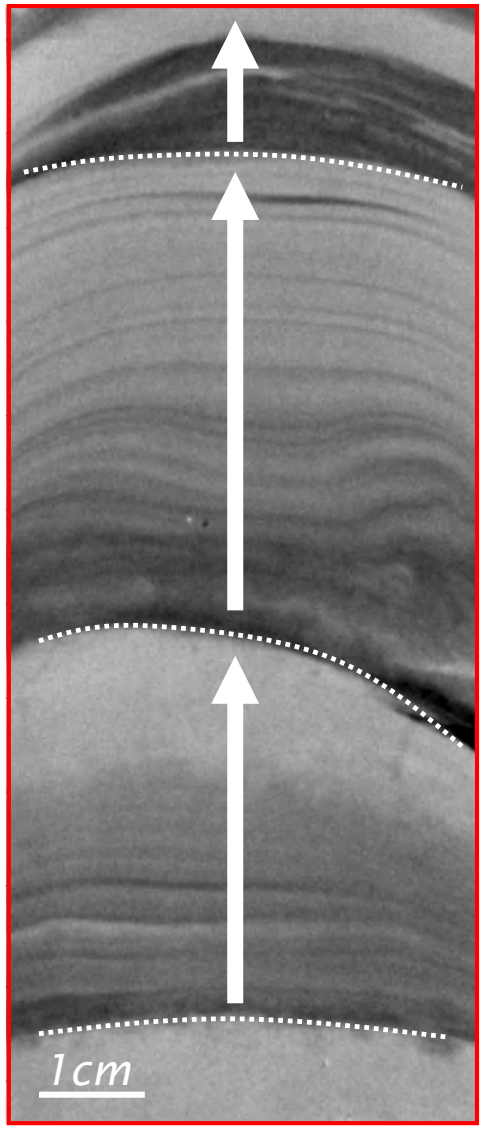

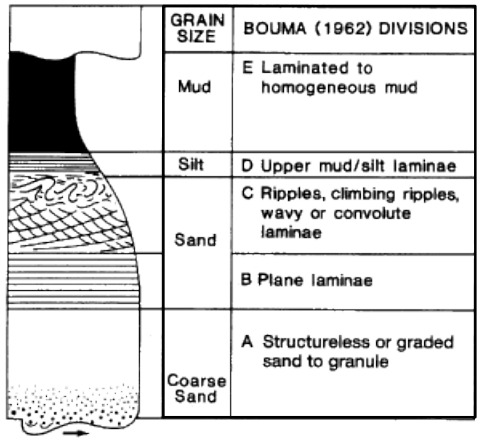

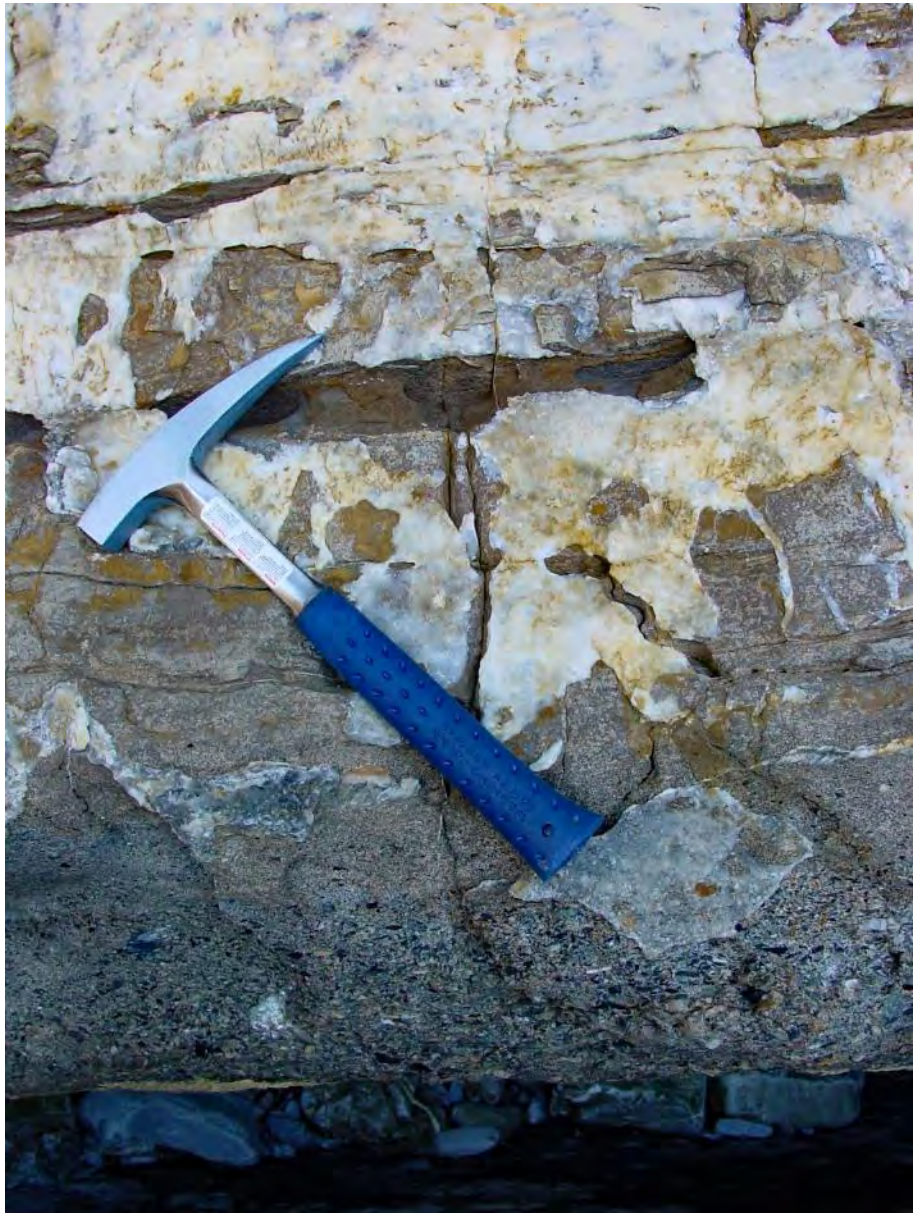

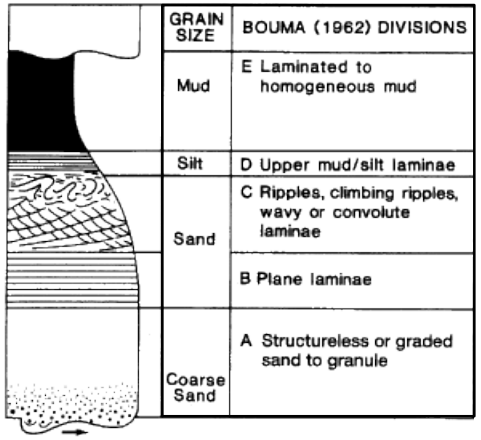

Flysch crétacé du pays Basque

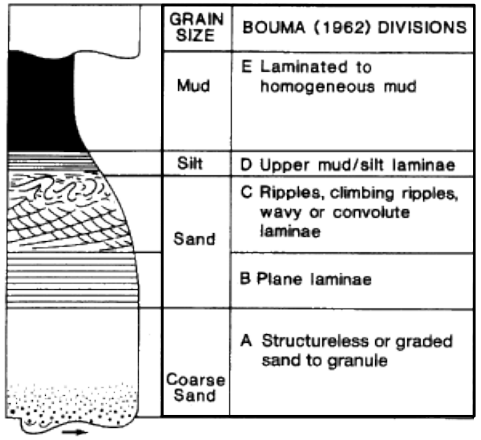

Flysch crétacé du pays Basque

Système turbiditique du Gange - Brahmapoutre

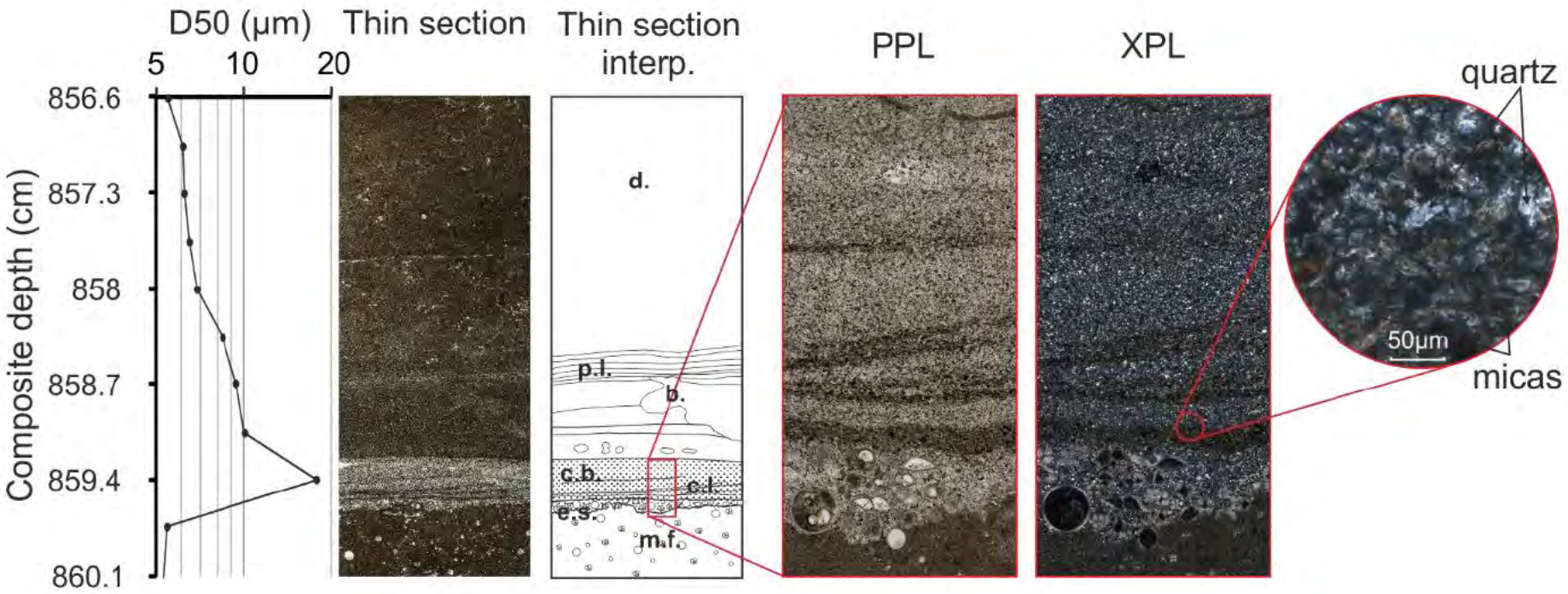

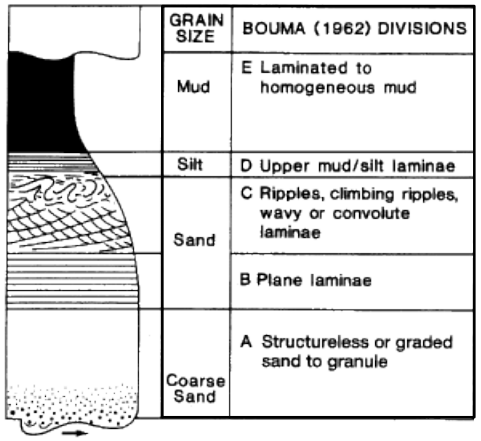

Figure IV.6: Example of grain size excursion and detailed composition of bases in Plane polarised light (PPL) and Cross-polarised light (XPL). d. : decantation, p.l. : planar lamination, b. : bioturbation, c.b. : coarser bed, c.l. : cross lamination, e.s. : erosional surface, m.f. : mud rich in forams. Planar laminations (Td), cross laminations (Tc) and erosional surfaces with decrase in grain size from erosional surface to decantation are typical of Bouma's sequences.

Fournier, L., et al. 2017. The Bengal fan: External controls on the Holocene Active Channel turbidite activity. The Holocene 27, 900–913.

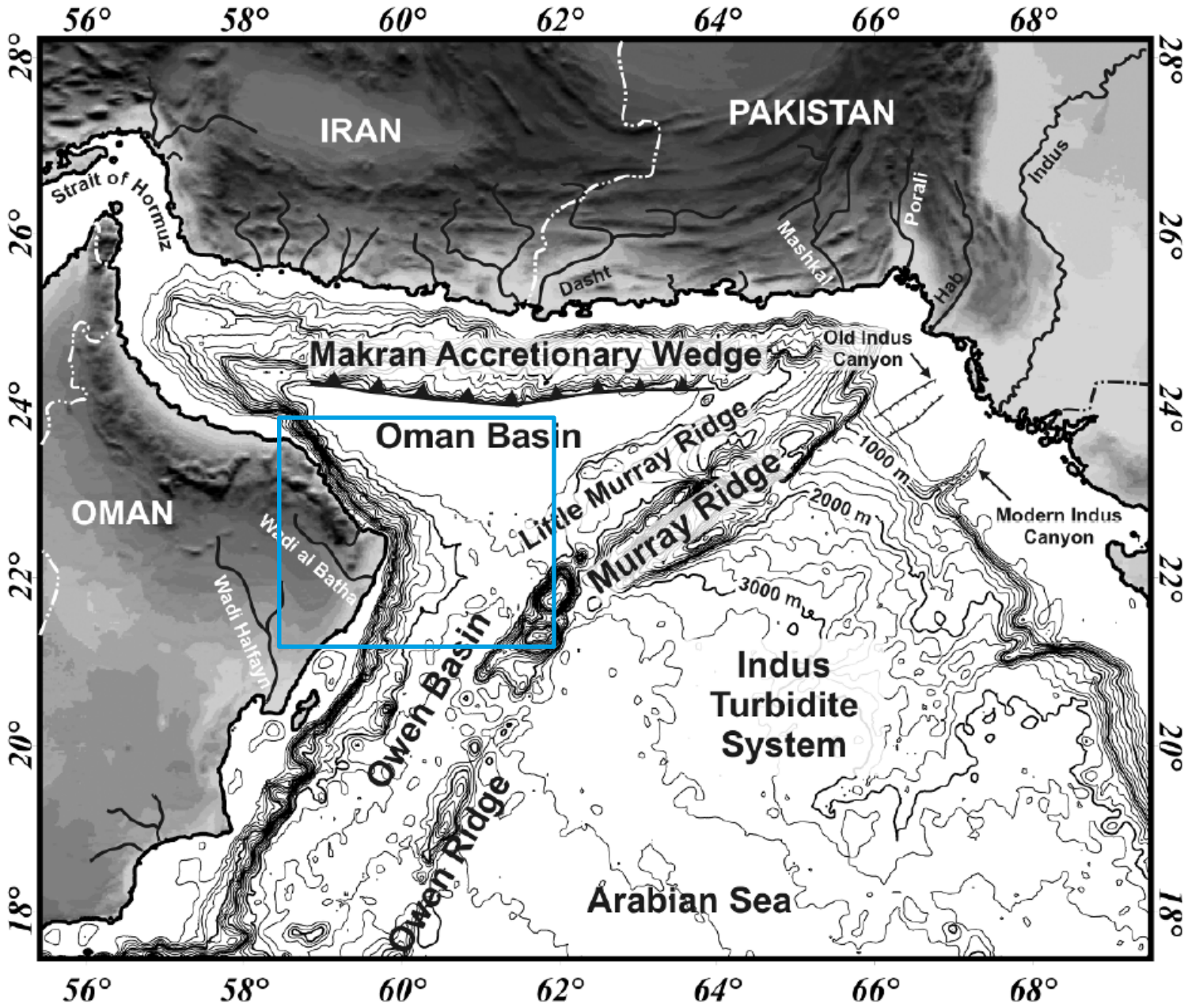
56°
58°
60°
62°
64°
66°
68°
28°
26°
24°
22°
20°
18°
IRAN
PAKISTAN
Strait of Hormuz
Indus
Porali
Mashkai
Hab
Dasht
Makran Accretionary Wedge
Old Indus Canyon
Oman Basin
Little Murray Ridge
Murray Ridge
1000 m
2000 m
3000 m
Modern Indus Canyon
OMAN
Wadi al Batha
Wadi Halfayn
Owen Basin
Owen Ridge
Indus Turbidite System
Arabian Sea

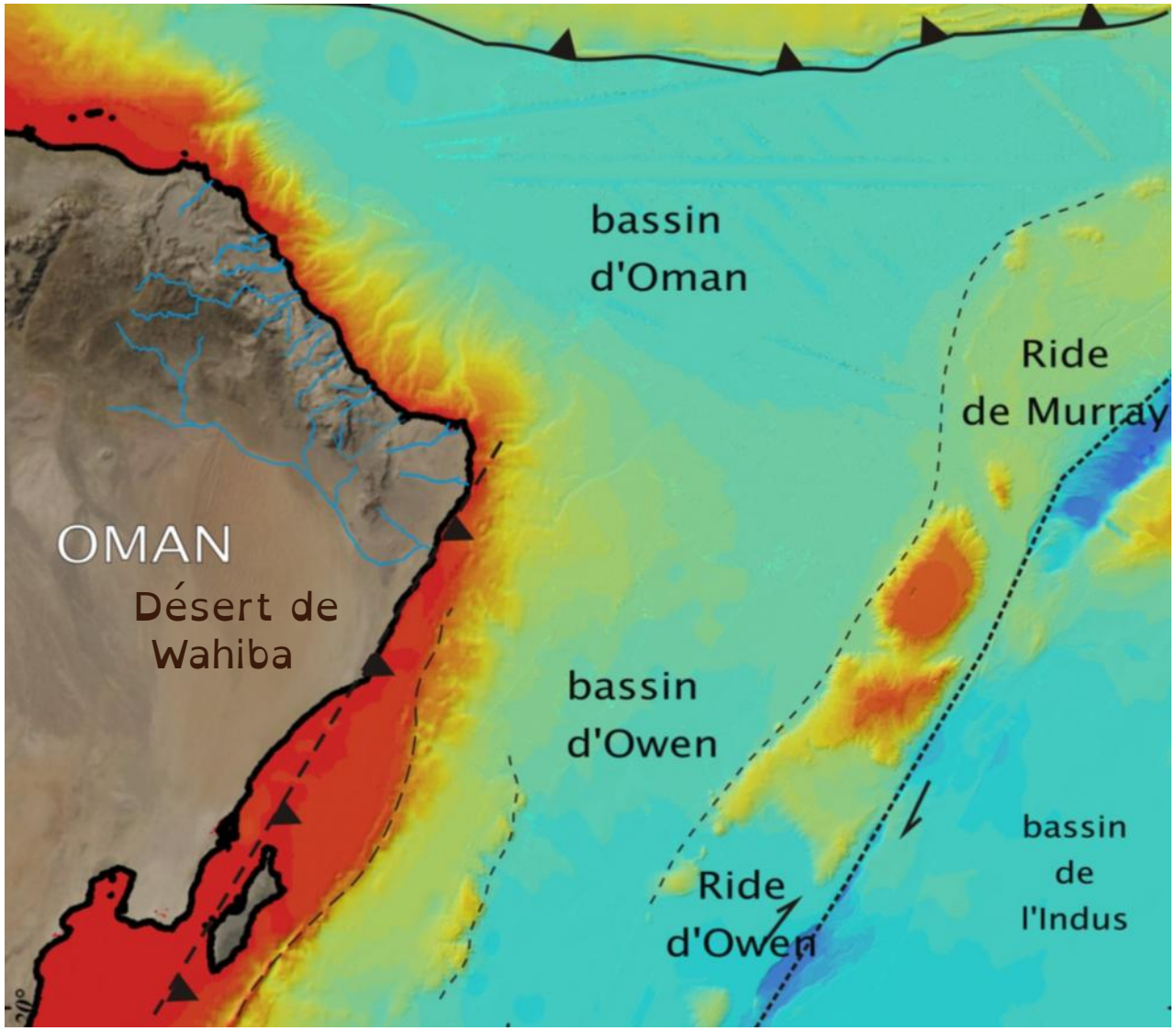

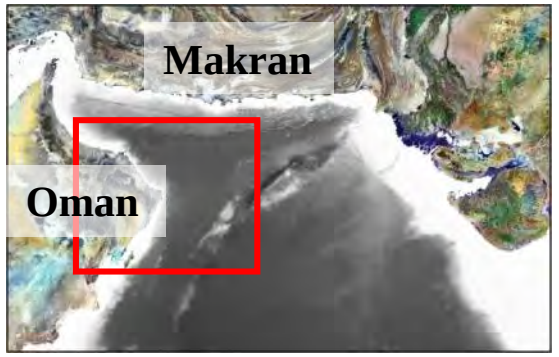

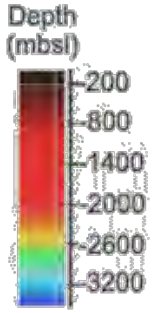

Bourget 2009

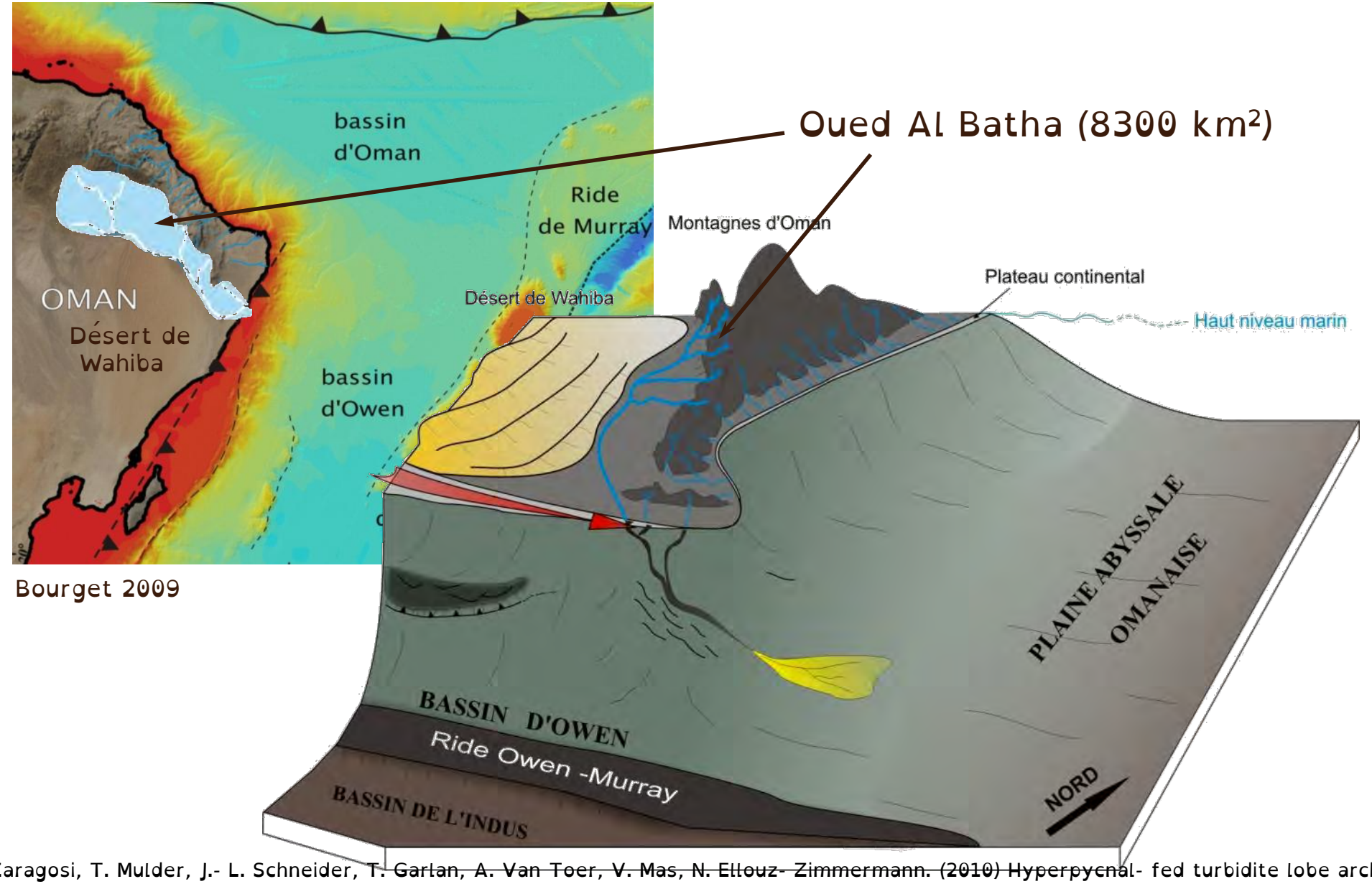

Bourget 2009

J. Bourget, S. Zaragosi, T. Mulder, J.- L. Schneider, T. Garlan, A. Van Toer, V. Mas, N. Ellouz- Zimmermann. (2010) Hyperpycnal- fed turbidite lobe architecture and recent sedimentary processes: A case study from the Al Batha turbidite system, Oman margin **Sedimentary Geology** 229(3), 144-159.

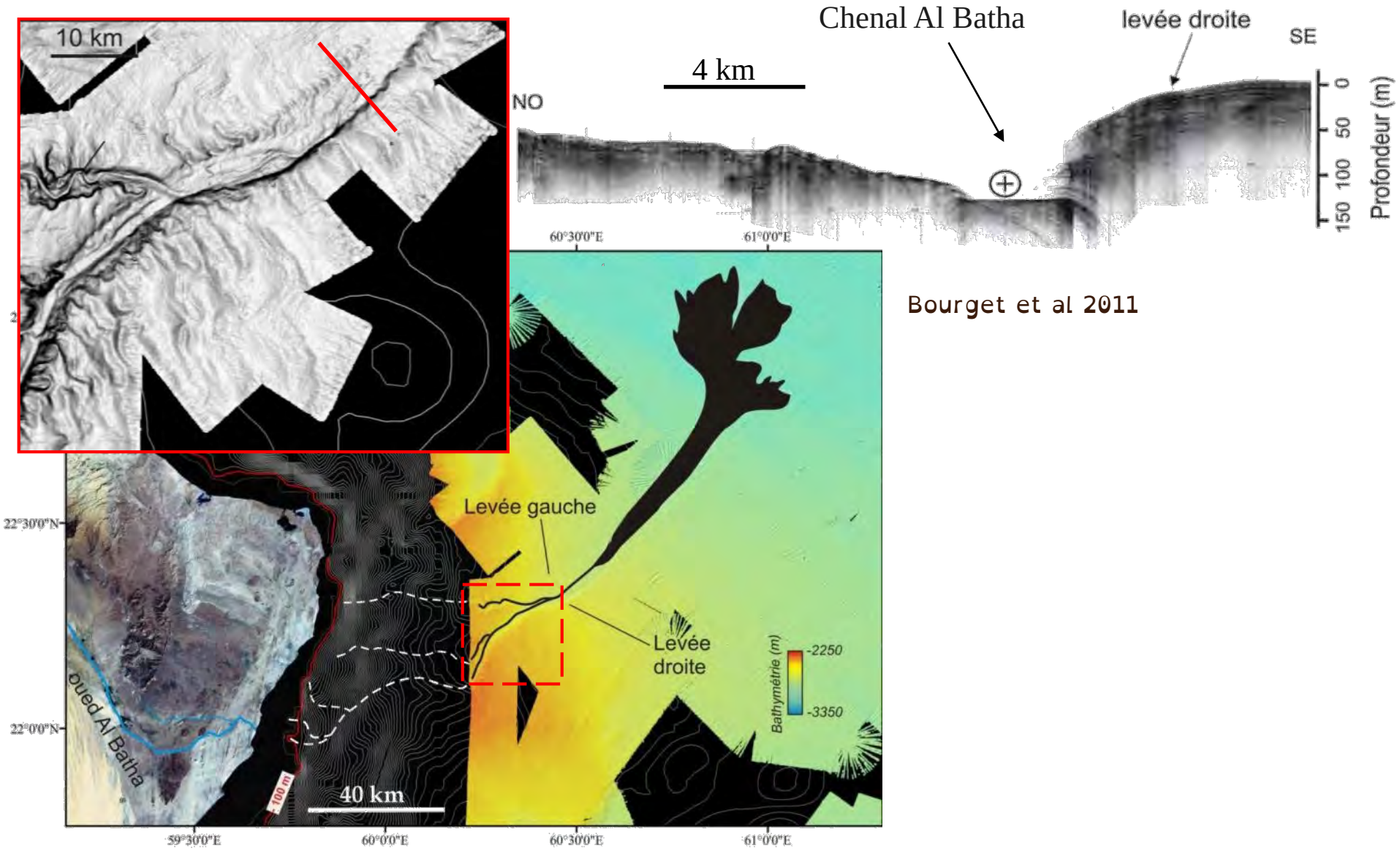

Bourget et al 2011

J. Bourget, S. Zaragosi, T. Mulder, J.- L. Schneider, T. Garlan, A. Van Toer, V. Mas, N. Ellouz- Zimmermann. (2010) Hyperpycnal- fed turbidite lobe architecture and recent sedimentary processes: A case study from the Al Batha turbidite system, Oman margin **Sedimentary Geology** 229(3), 144-159.

Lobe Al Batha (~ 1000 km²)

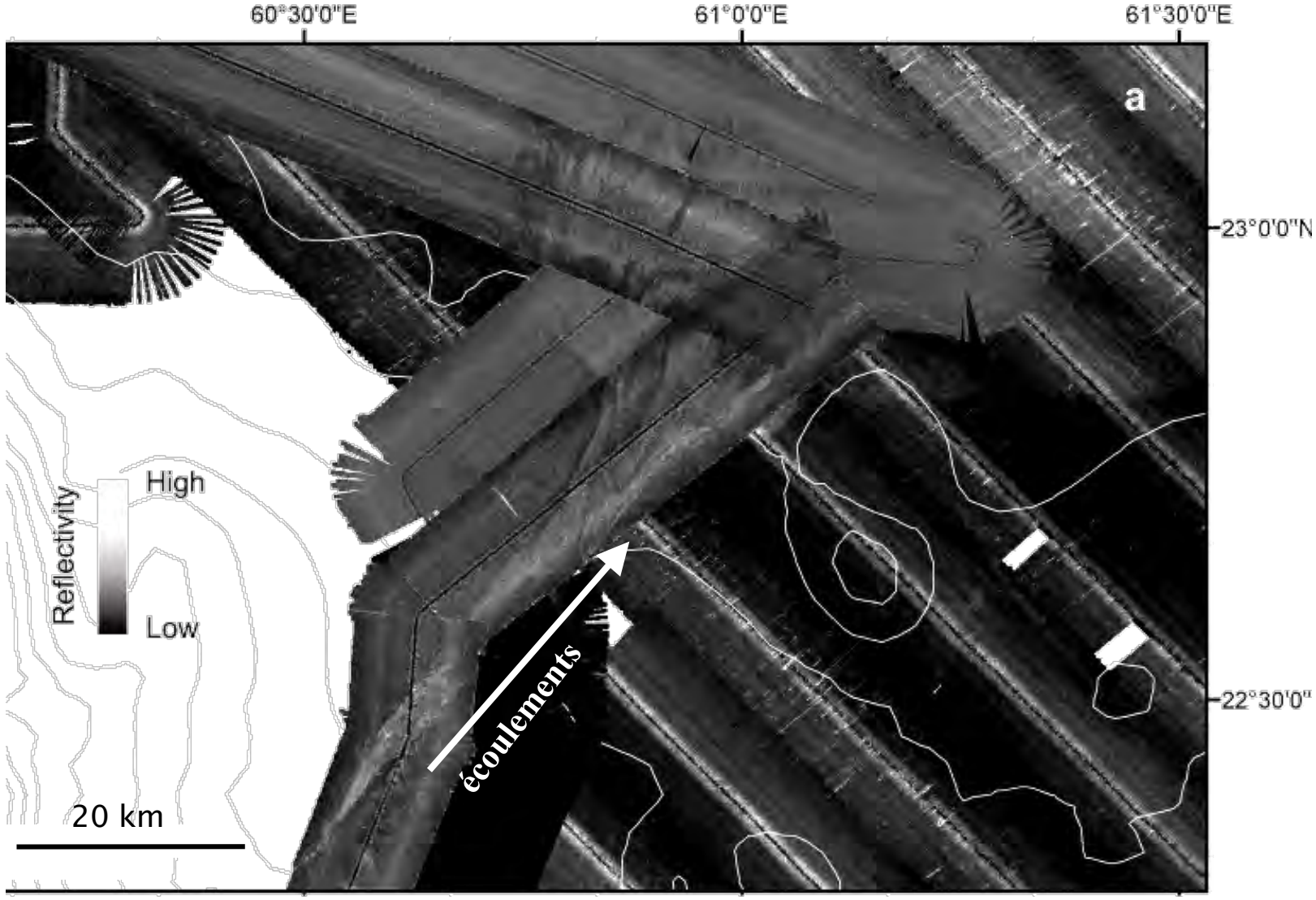

J. Bourget, S. Zaragosi, T. Mulder, J.- L. Schneider, T. Garlan, A. Van Toer, V. Mas, N. Ellouz- Zimmermann. (2010) Hyperpycnal- fed turbidite lobe architecture and recent sedimentary processes: A case study from the Al Batha turbidite system, Oman margin **Sedimentary Geology** 229(3), 144-159.

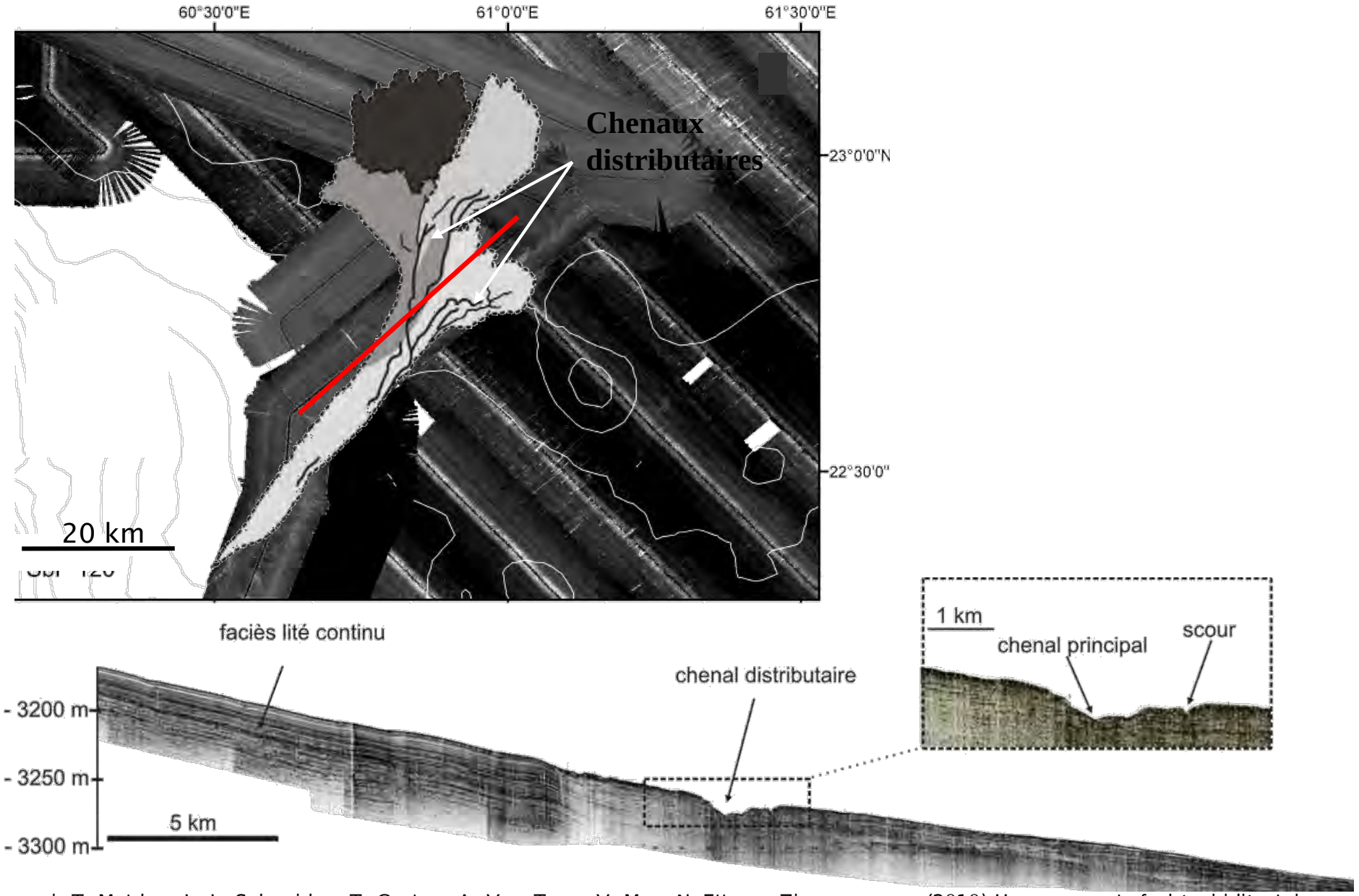

J. Bourget, S. Zaragosi, T. Mulder, J.- L. Schneider, T. Garlan, A. Van Toer, V. Mas, N. Ellouz- Zimmermann. (2010) Hyperpycnal- fed turbidite lobe architecture and recent sedimentary processes: A case study from the Al Batha turbidite system, Oman margin **Sedimentary Geology** 229(3), 144-159.

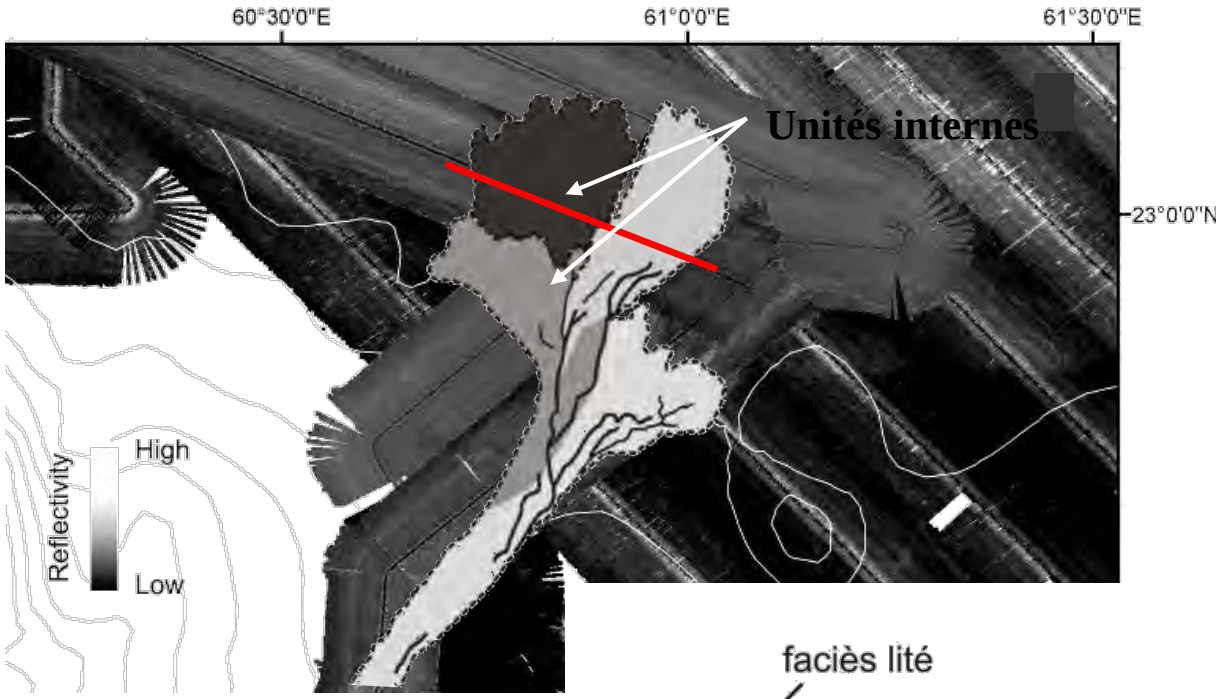

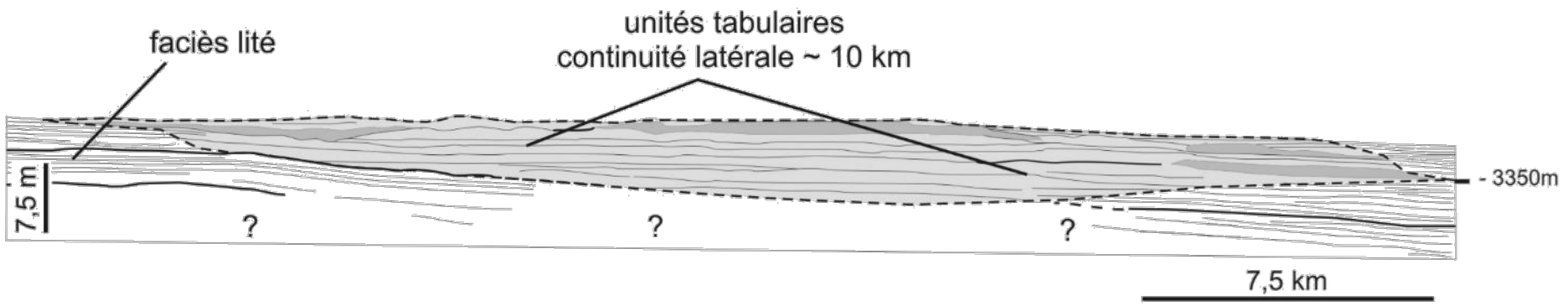

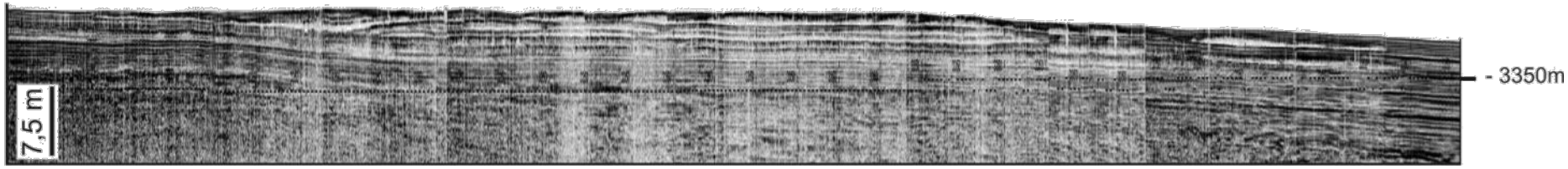

J. Bourget, S. Zaragosi, T. Mulder, J.- L. Schneider, T. Garlan, A. Van Toer, V. Mas, N. Ellouz- Zimmermann. (2010) Hyperpycnal- fed turbidite lobe architecture and recent sedimentary processes: A case study from the Al Batha turbidite system, Oman margin **Sedimentary Geology** 229(3), 144-159.

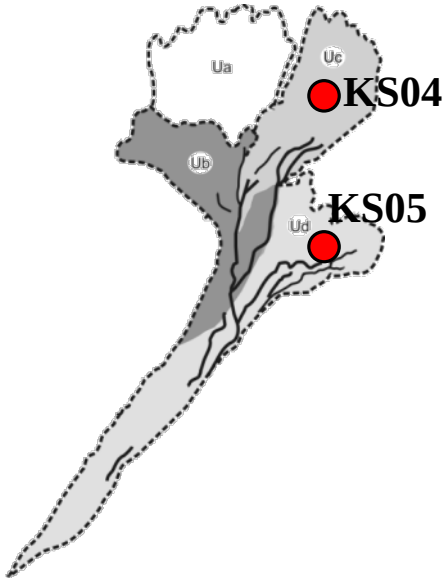

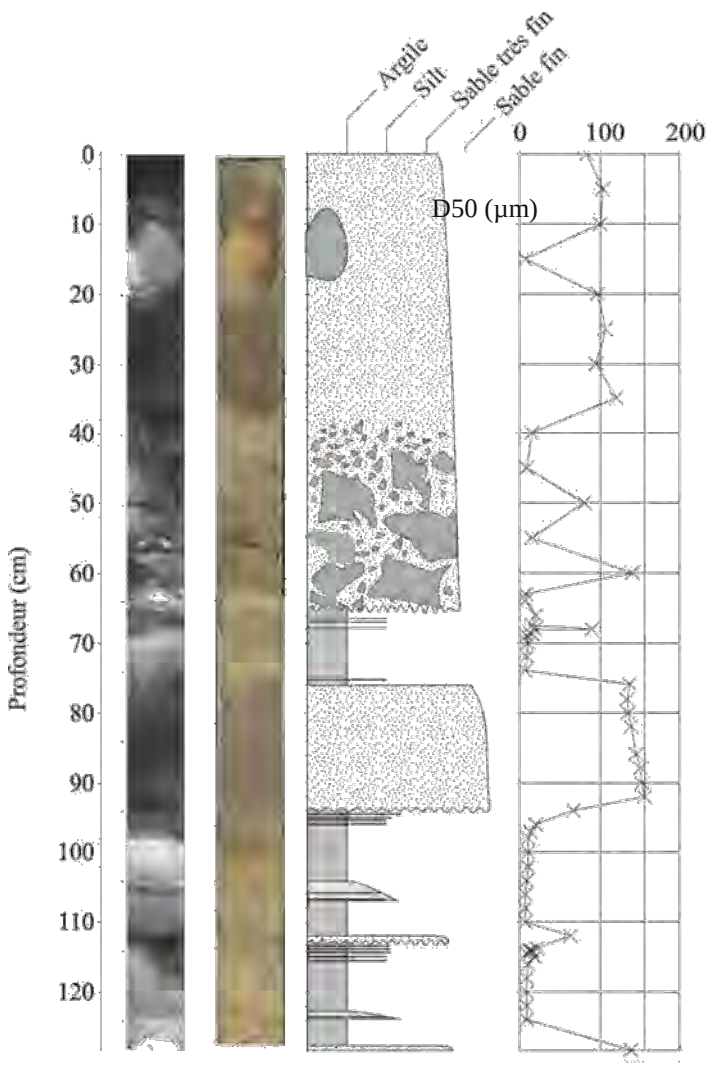

KS04

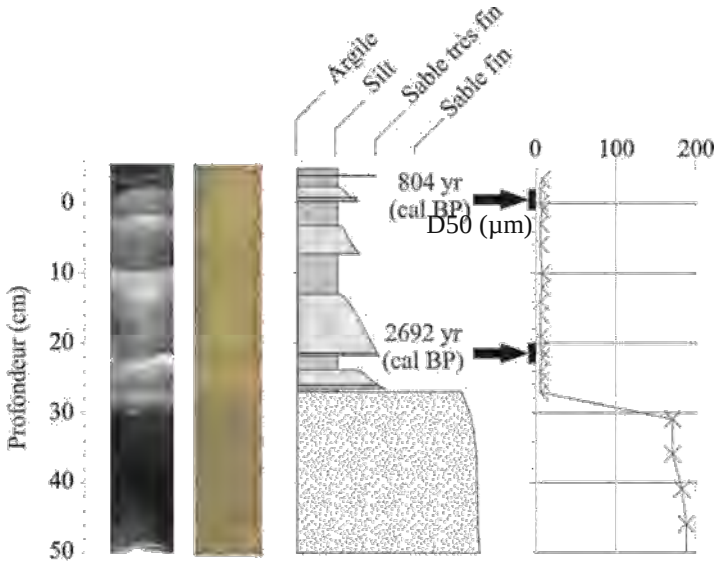

KS05

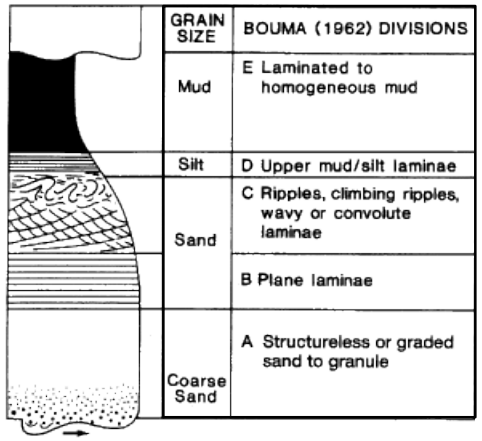

J. Bourget, S. Zaragosi, T. Mulder, J.- L. Schneider, T. Garlan, A. Van Toer, V. Mas, N. Ellouz- Zimmermann. (2010) Hyperpycnal- fed turbidite lobe architecture and recent sedimentary processes: A case study from the Al Batha turbidite system, Oman margin **Sedimentary Geology** 229(3), 144-159.

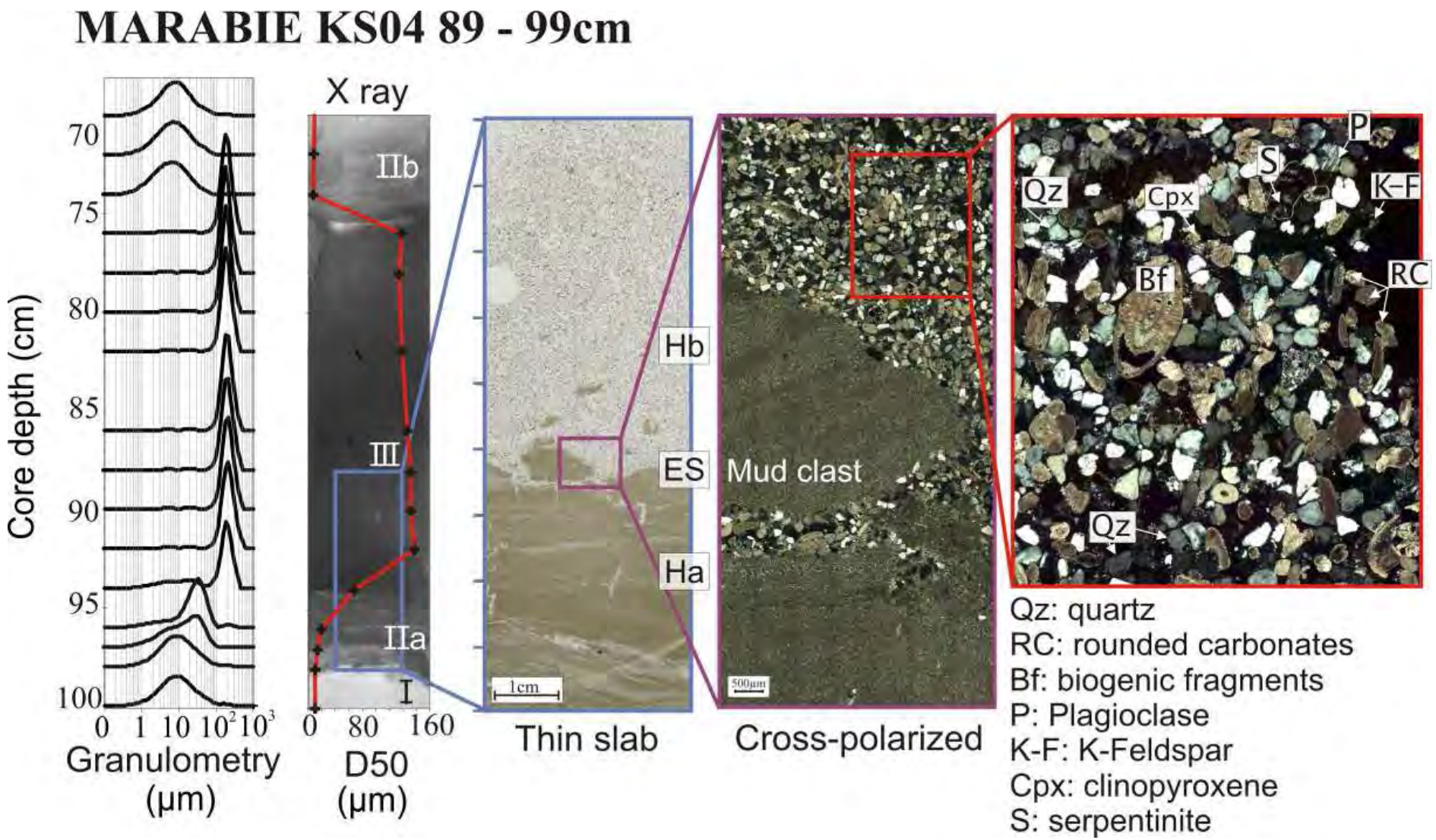

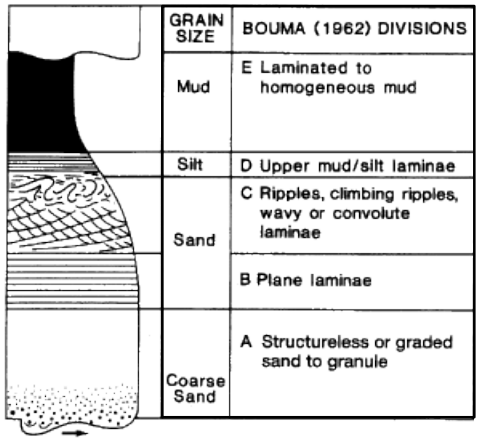

J. Bourget, S. Zaragosi, T. Mulder, J.- L. Schneider, T. Garlan, A. Van Toer, V. Mas, N. Ellouz- Zimmermann. (2010) Hyperpycnal- fed turbidite lobe architecture and recent sedimentary processes: A case study from the Al Batha turbidite system, Oman margin **Sedimentary Geology** 229(3), 144-159.

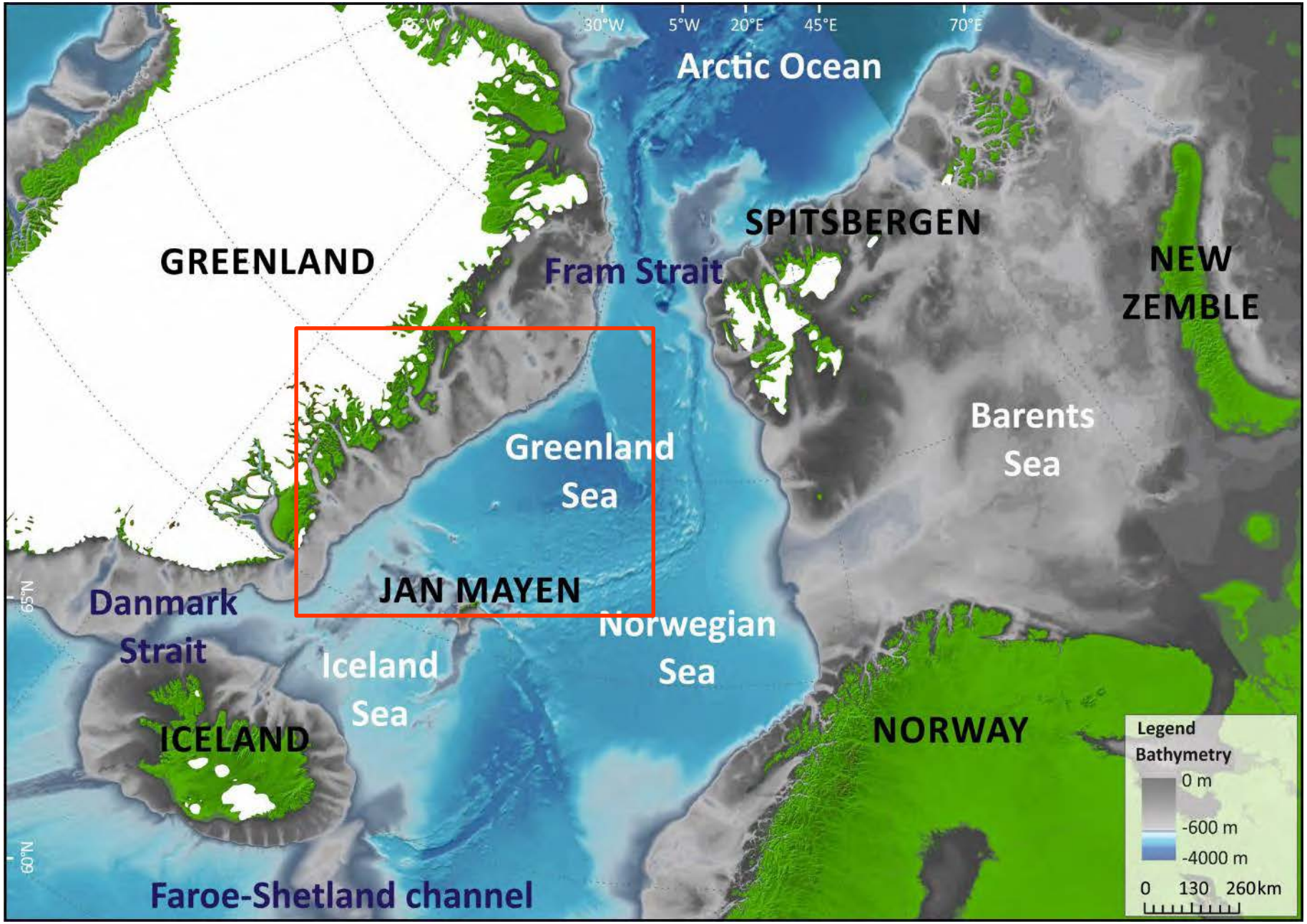
30°W
5°W
20°E
45°E
70°E
Arctic Ocean
GREENLAND
Fram Strait
SPITSBERGEN
NEW ZEMBLE
Barents Sea
Greenland Sea
JAN MAYEN
Danmark Strait
Norwegian Sea
Iceland Sea
ICELAND
NORWAY
65°N
60°N
Faroe-Shetland channel
Legend
Bathymetry
0 m
-600 m
-4000 m
0 130 260km

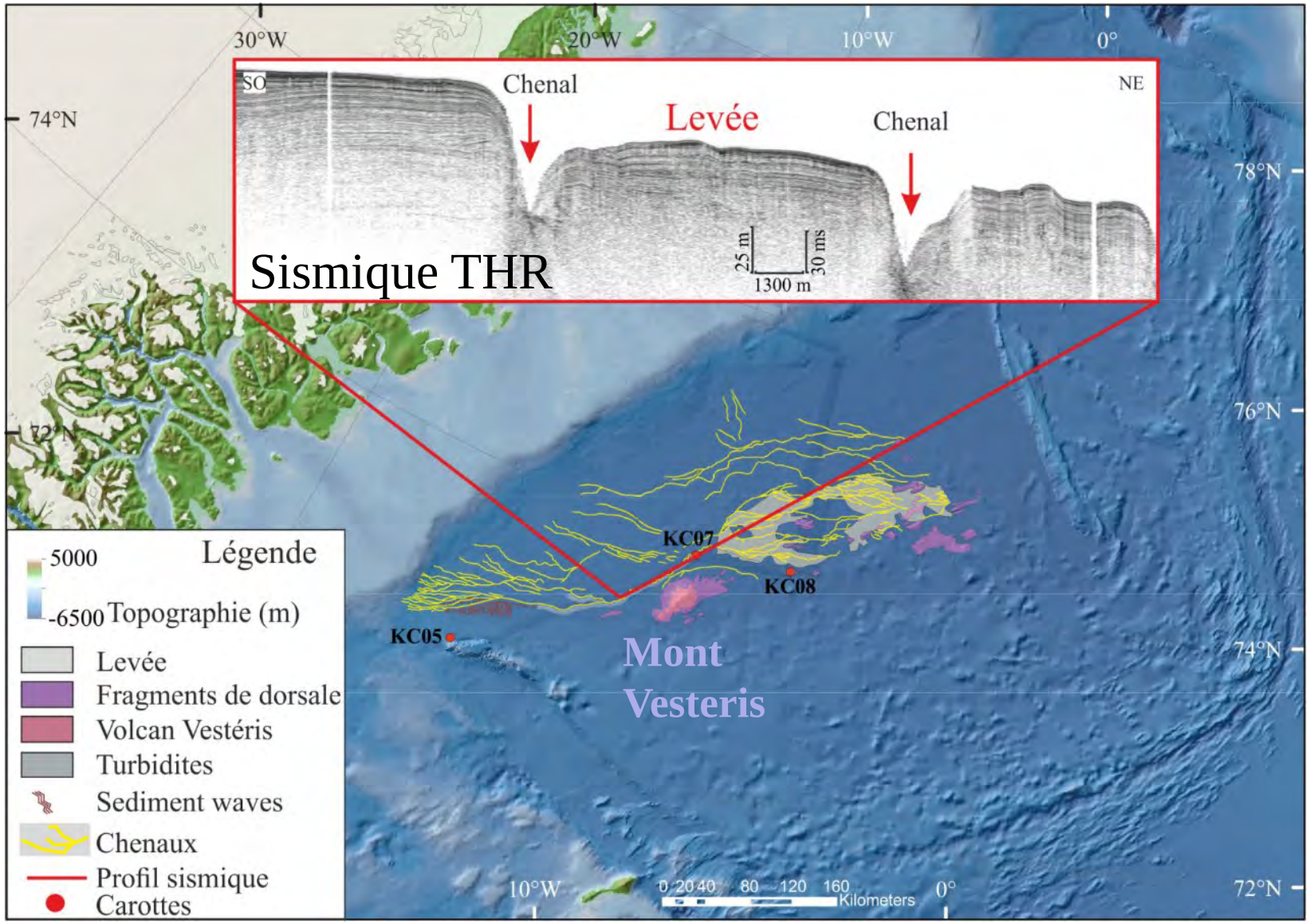

M. Biguenet, (2018) Etude de la sedimentation profonde en mer du Groenland. Master 2 Université de Bordeaux.

Carotte KC07 : Turbidite sableuse

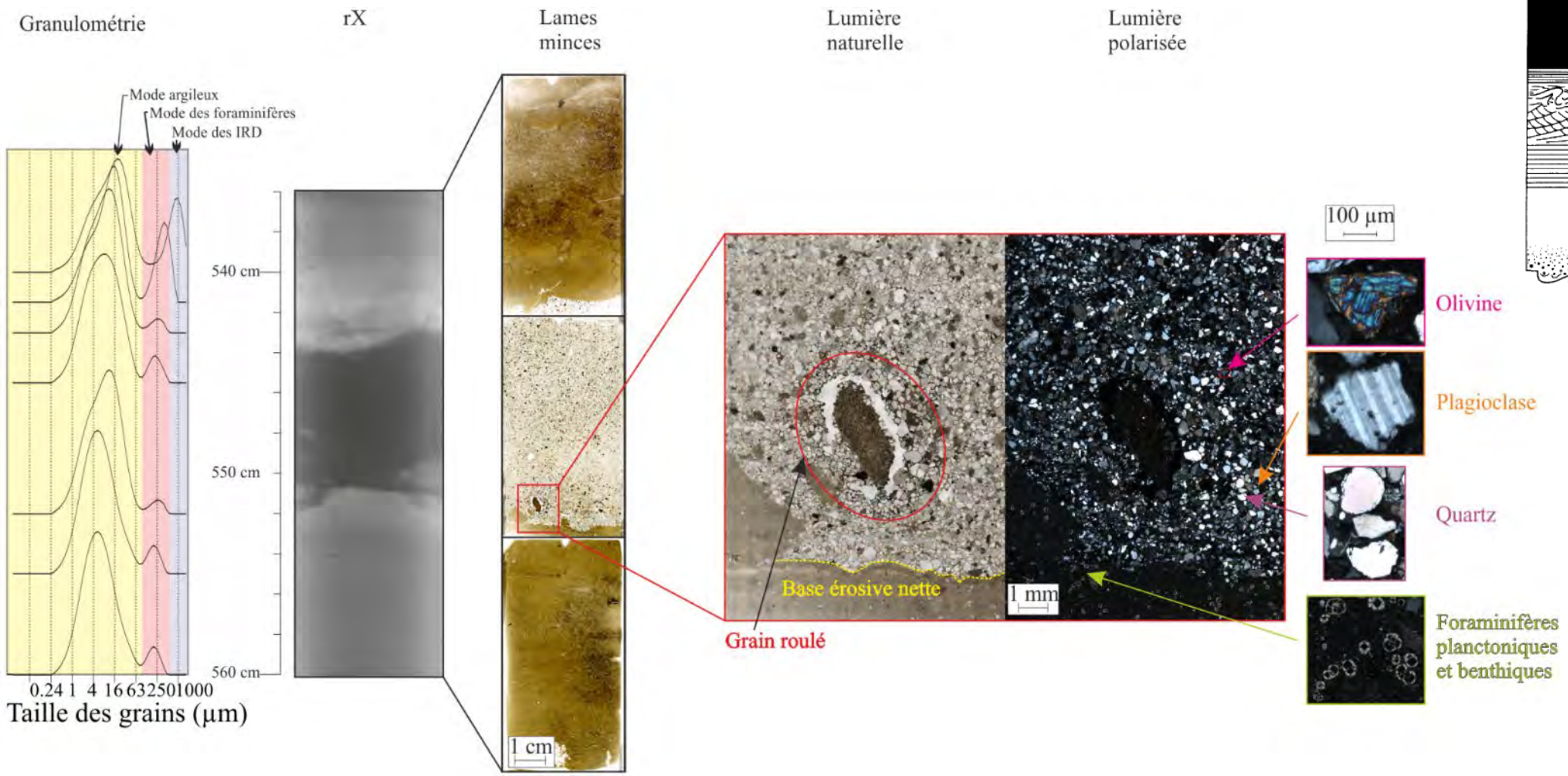

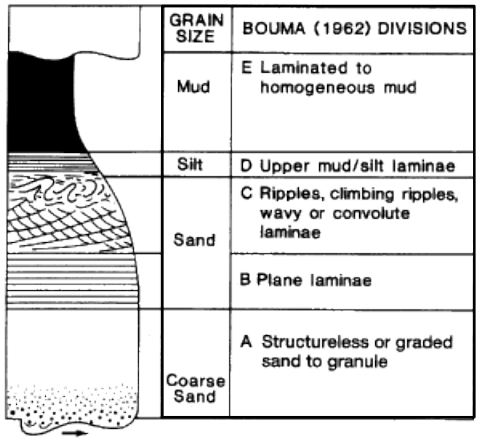

M. Biguenet, (2018) Etude de la sedimentation profonde en mer du Groenland. Master 2 Université de Bordeaux.

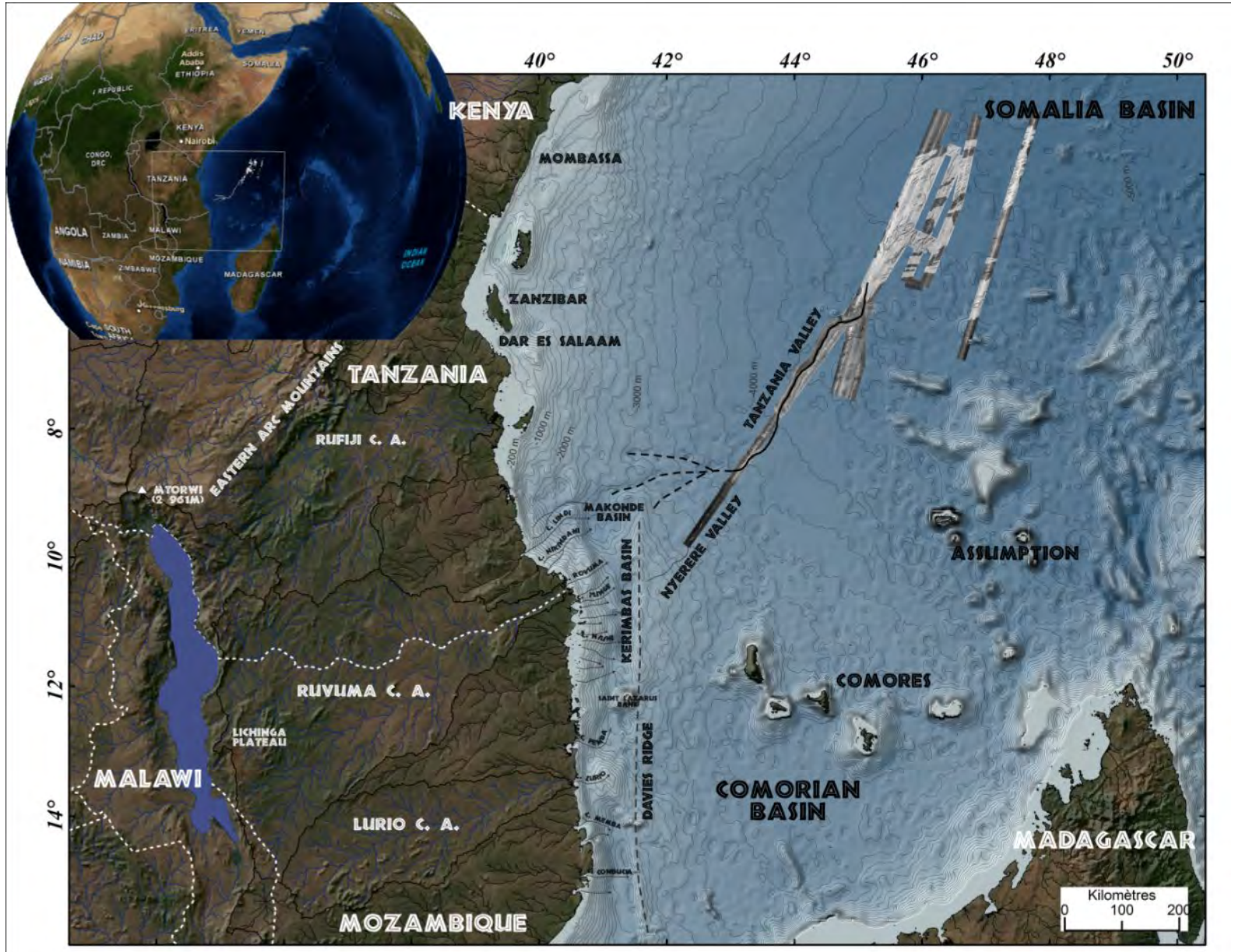

Bourget, J., Zaragosi, S., Garlan, T., Gabelotaud, I., Guyomard, P., Dennielou, B., Ellouz-Zimmermann, N., Schneider, J.L., 2008. Discovery of a giant deep-sea valley in the Indian Ocean, off eastern Africa: The Tanzania channel. Marine Geology 255, 179–185.

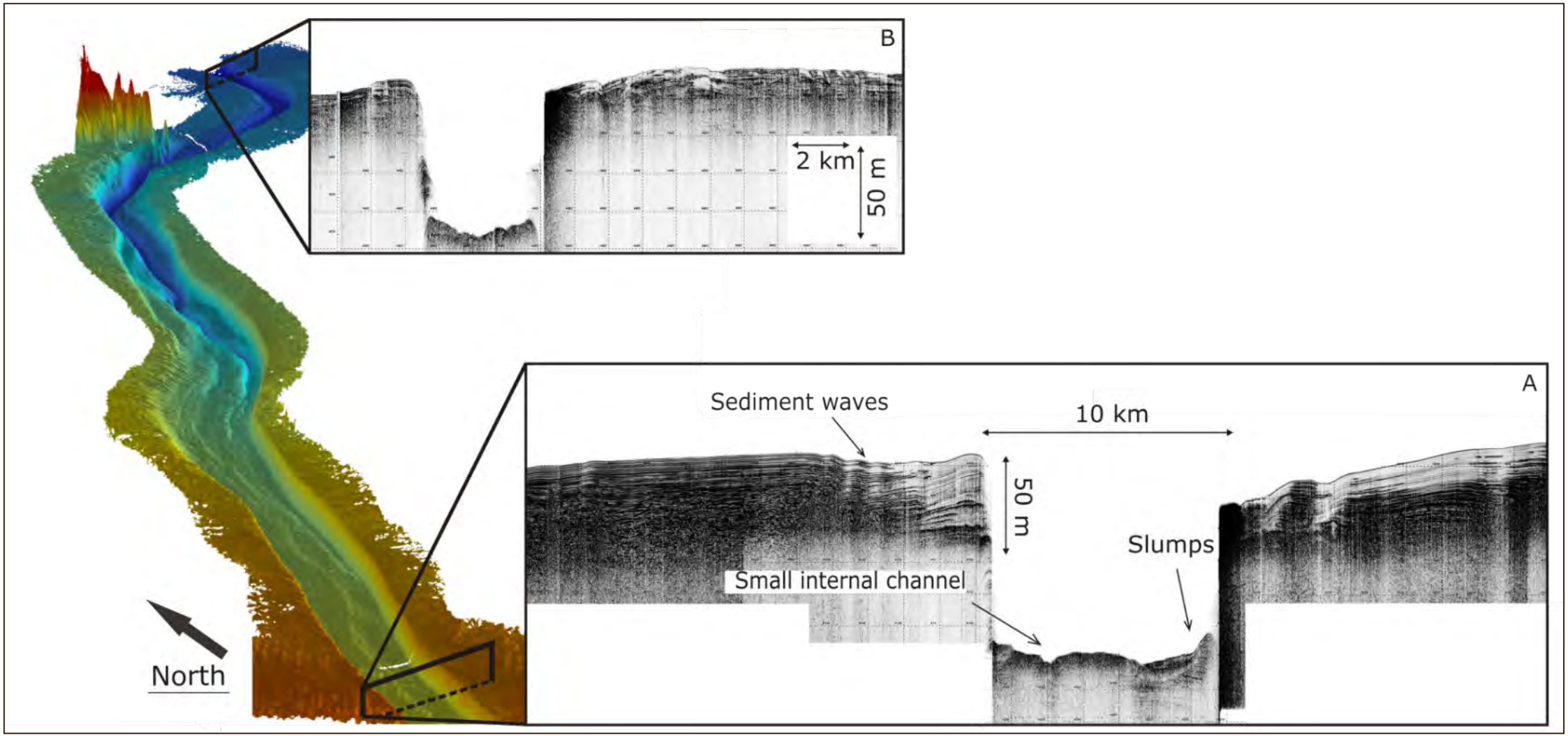

Bourget, J., Zaragosi, S., Garlan, T., Gabelotaud, I., Guyomard, P., Dennielou, B., Ellouz-Zimmermann, N., Schneider, J.L., 2008. Discovery of a giant deep-sea valley in the Indian Ocean, off eastern Africa: The Tanzania channel. Marine Geology 255, 179–185.

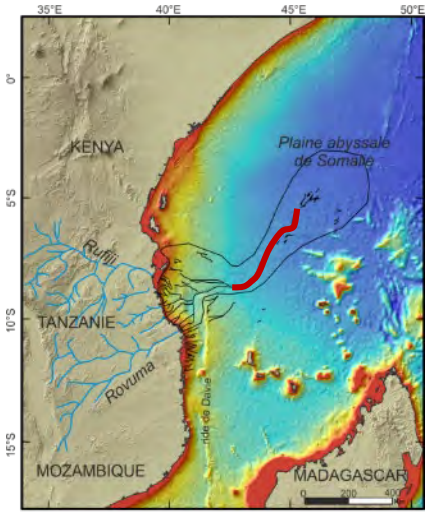

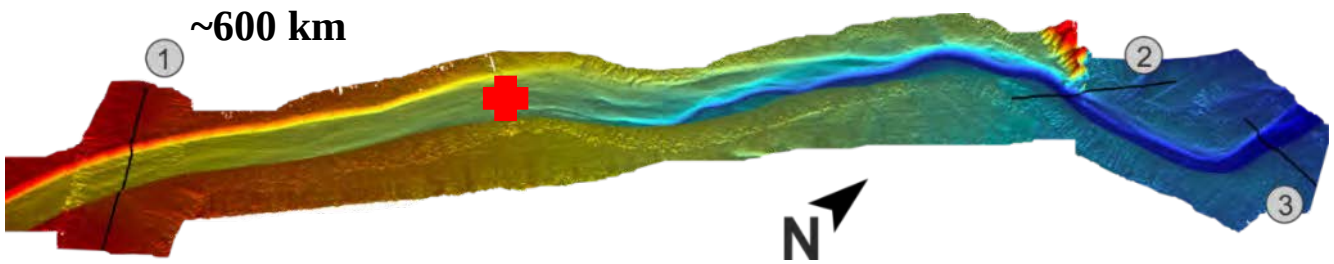

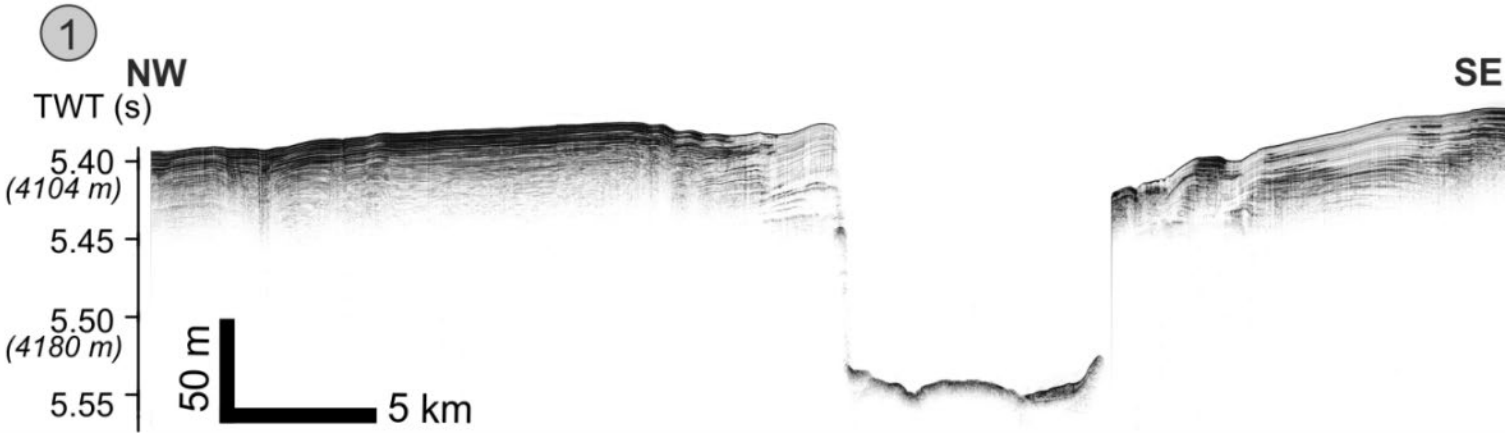

Bourget, J., Zaragosi, S., Garlan, T., Gabelotaud, I., Guyomard, P., Dennielou, B., Ellouz-Zimmermann, N., Schneider, J.L., 2008. Discovery of a giant deep-sea valley in the Indian Ocean, off eastern Africa: The Tanzania channel. Marine Geology 255, 179–185.

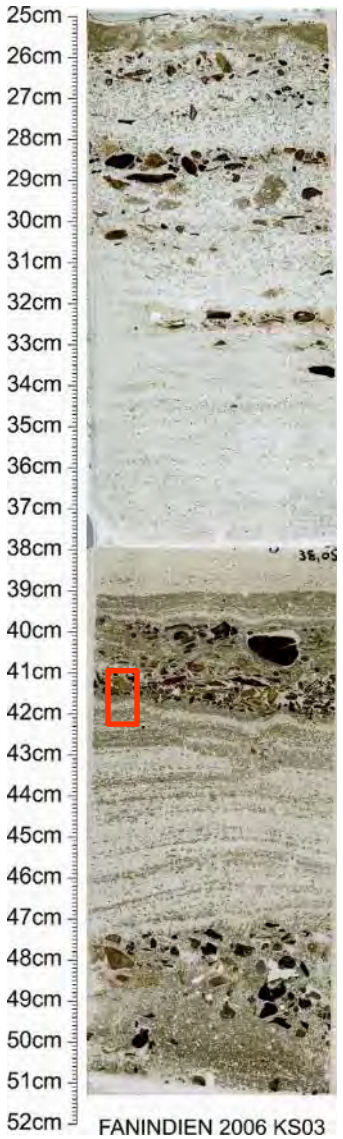
25cm
26cm
27cm
28cm
29cm
30cm
31cm
32cm
33cm
34cm
35cm
36cm
37cm
38cm
39cm
40cm
41cm
42cm
43cm
44cm
45cm
46cm
47cm
48cm
49cm
50cm
51cm
52cm
FANINDIEN 2006 KS03

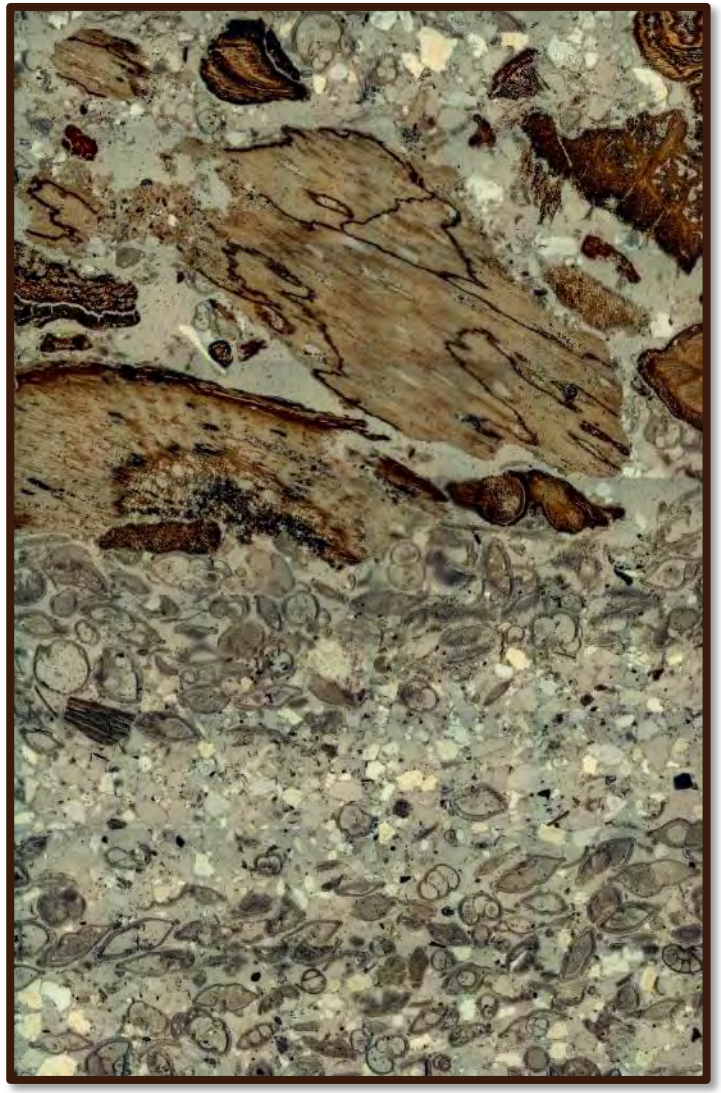

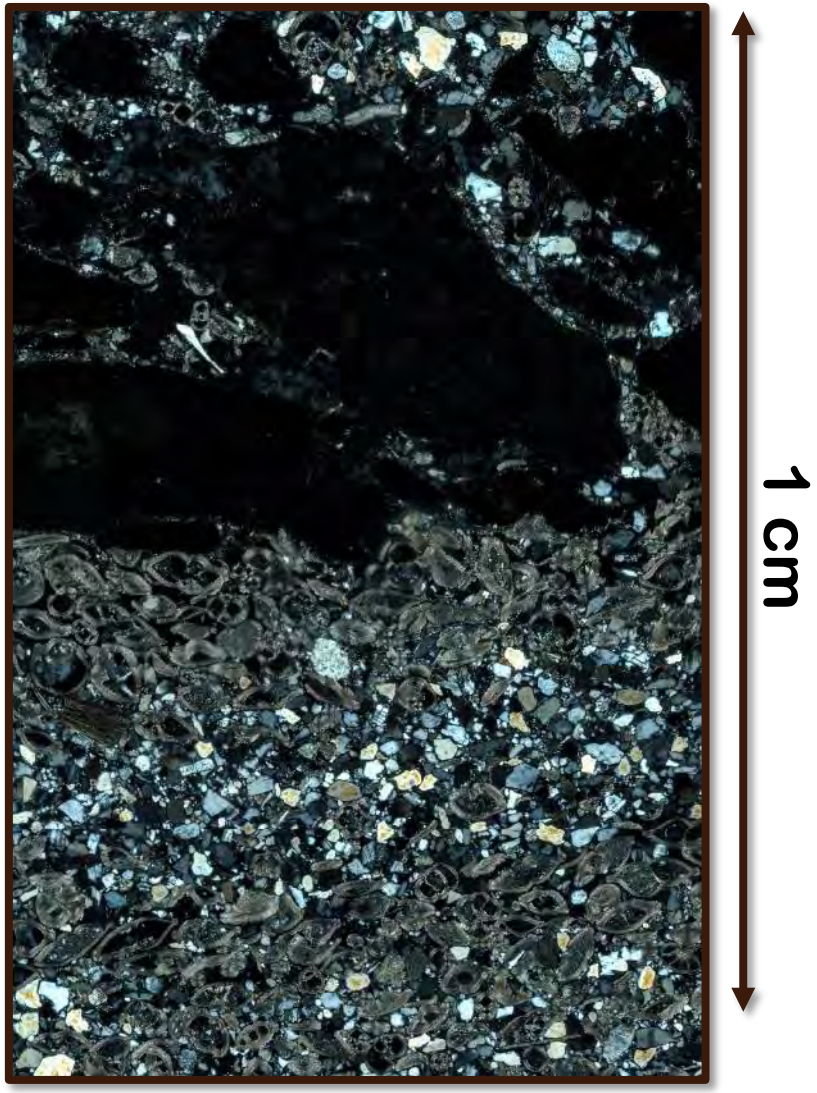
1 cm

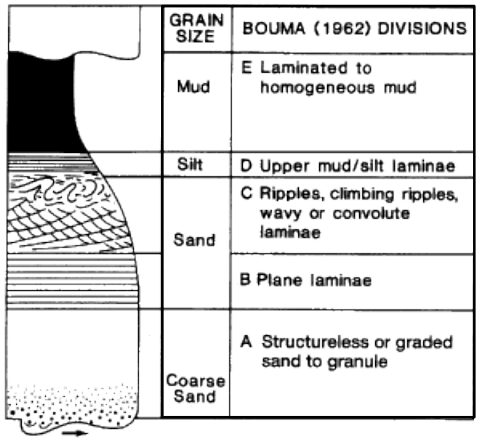
GRAIN SIZE
BOUMA (1962) DIVISIONS
Mud
E Laminated to homogeneous mud
Silt
D Upper mud/silt laminae
Sand
C Ripples, climbing ripples, wavy or convolute laminae
B Plane laminae
Coarse Sand
A Structureless or graded sand to granule

1. Sédimentation gravitaire – turbiditique

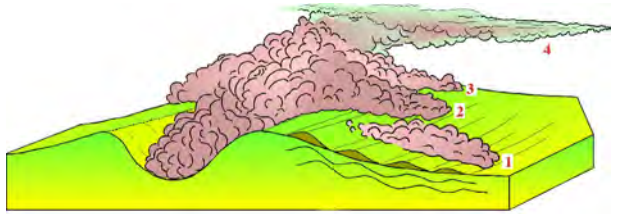

2. Sédimentation volcanoclastique

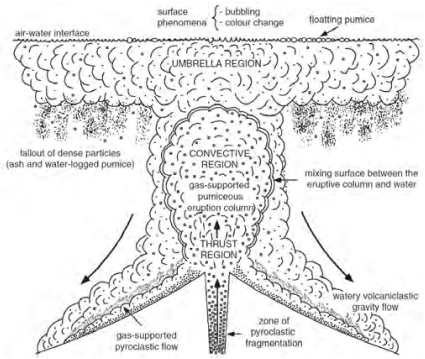

3. Sédimentation pélagique et hémipélagique

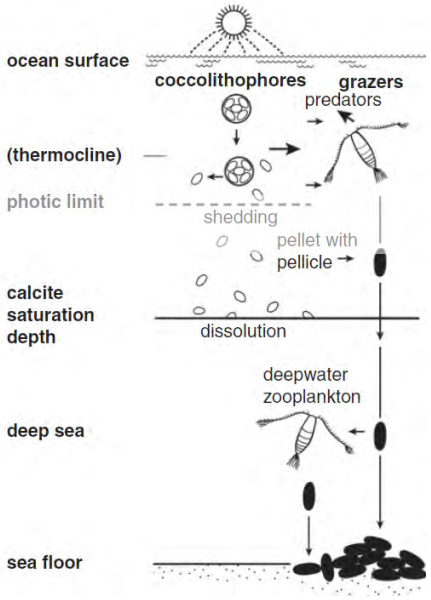

4. Sédimentation glaci-marine

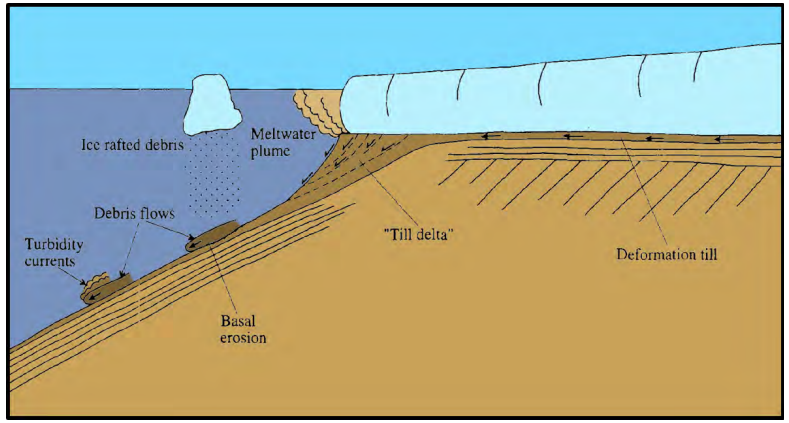

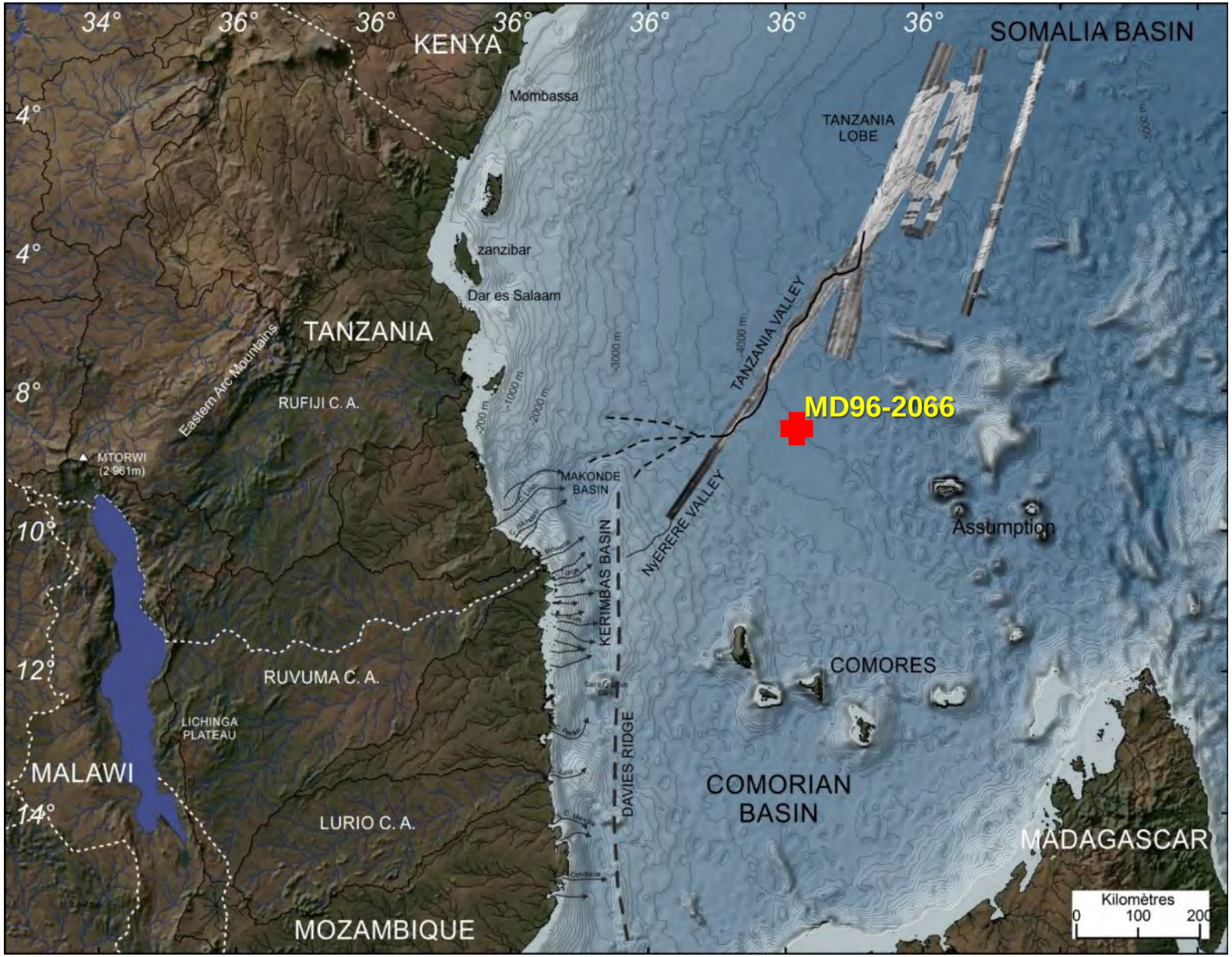
34°
36°
36°
36°
36°
36°
36°
KENYA
SOMALIA BASIN
Mombassa
TANZANIA LOBE
4°
4°
zanzibar
Dar es Salaam
TANZANIA
TANZANIA VALLEY
8°
RUFIJI C. A.
Eastern Arc Mountains
MTORWI (2 961m)
MD96-2066
MAKONDE BASIN
10°
NyERERE VALLEY
KERIMBAS BASIN
Assumption
12°
RUVUMA C. A.
COMORES
LICHINGA PLATEAU
MALAWI
DAVIES RIDGE
COMORIAN BASIN
14°
LURIO C. A.
MADAGASCAR
MOZAMBIQUE
Kilomètres
0
100
200

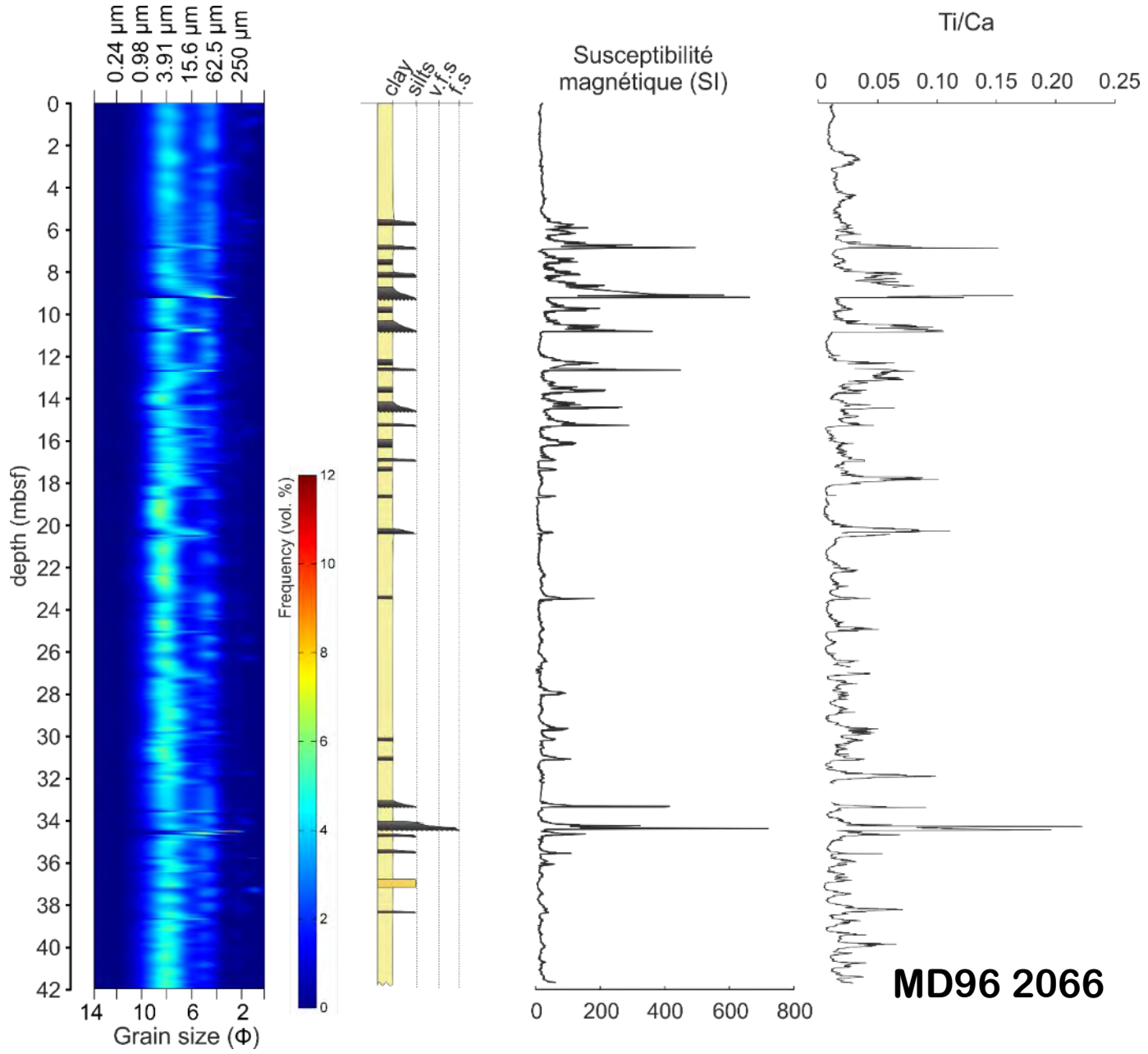
0.24 µm
0.98 µm
3.91 µm
15.6 µm
62.5 µm
250 µm
depth (mbsf)
Grain size (Φ)
Frequency (vol. %)
clay
silts
v.f.s
f.s
Susceptibilité magnétique (SI)
Ti/Ca
MD96 2066

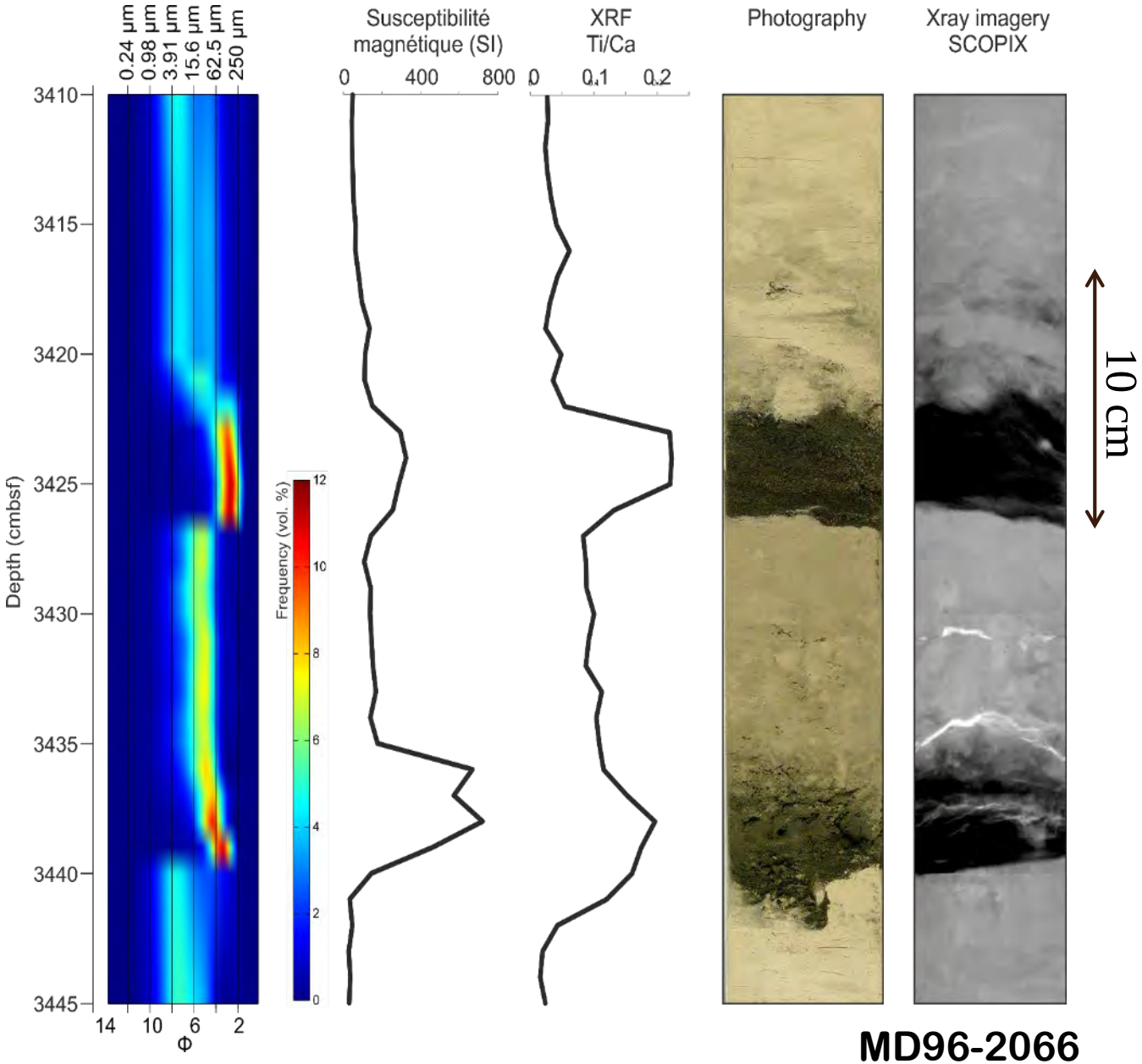
0.24 µm
0.98 µm
3.91 µm
15.6 µm
62.5 µm
250 µm
Depth (cmbsf)
3410
3415
3420
3425
3430
3435
3440
3445
14
10
6
2
Φ
Frequency (vol. %)
12
10
8
6
4
2
0
Susceptibilité magnétique (SI)
0
400
800
XRF Ti/Ca
0
0.1
0.2
Photography
Xray imagery SCOPIX
10 cm

MD96-2066

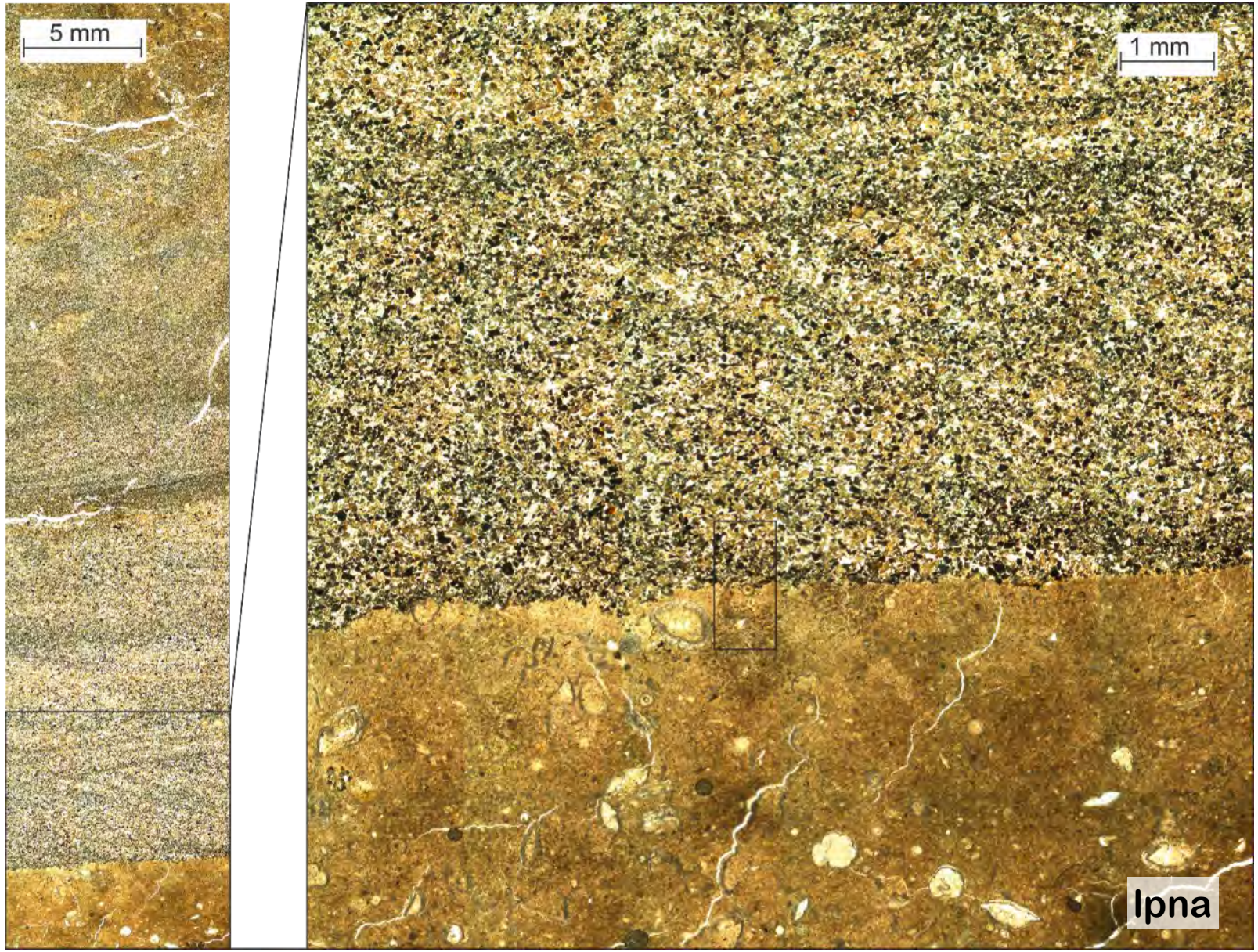

MD96-2066

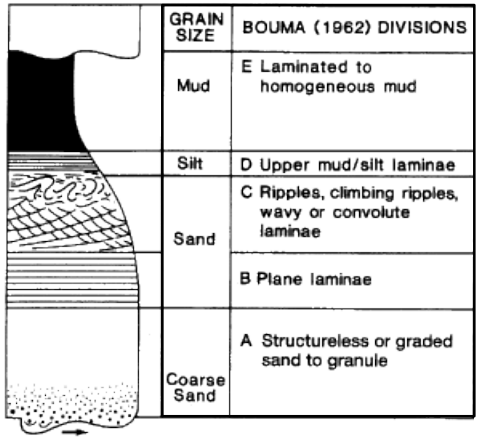

GRAIN SIZE	BOUMA (1962) DIVISIONS
Mud	E Laminated to homogeneous mud
Silt	D Upper mud/silt laminae
Sand	C Ripples, climbing ripples, wavy or convolute laminae
	B Plane laminae
Coarse Sand	A Structureless or graded sand to granule

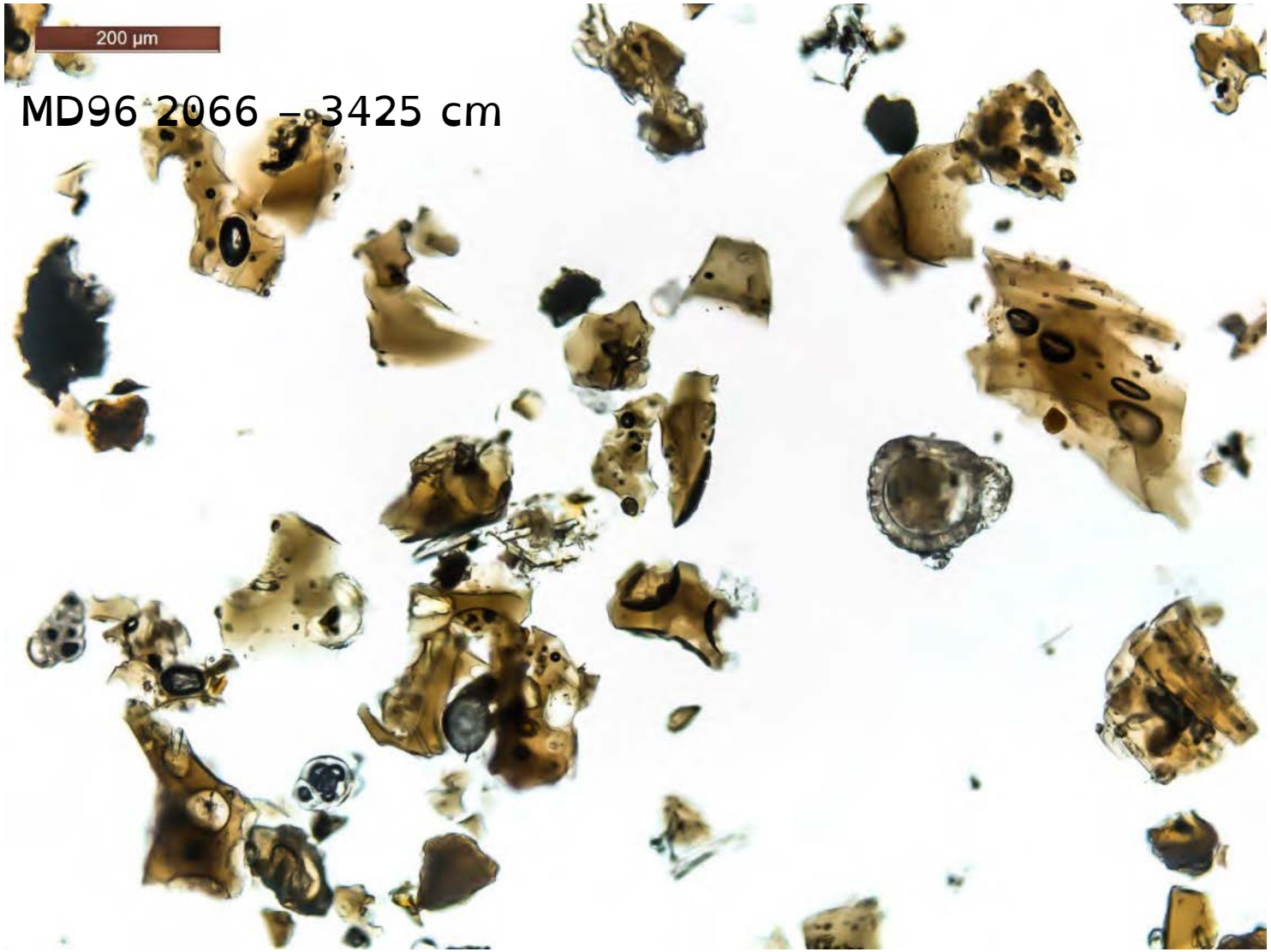

Vesicular basaltic glass from the comorian volcanic archipel

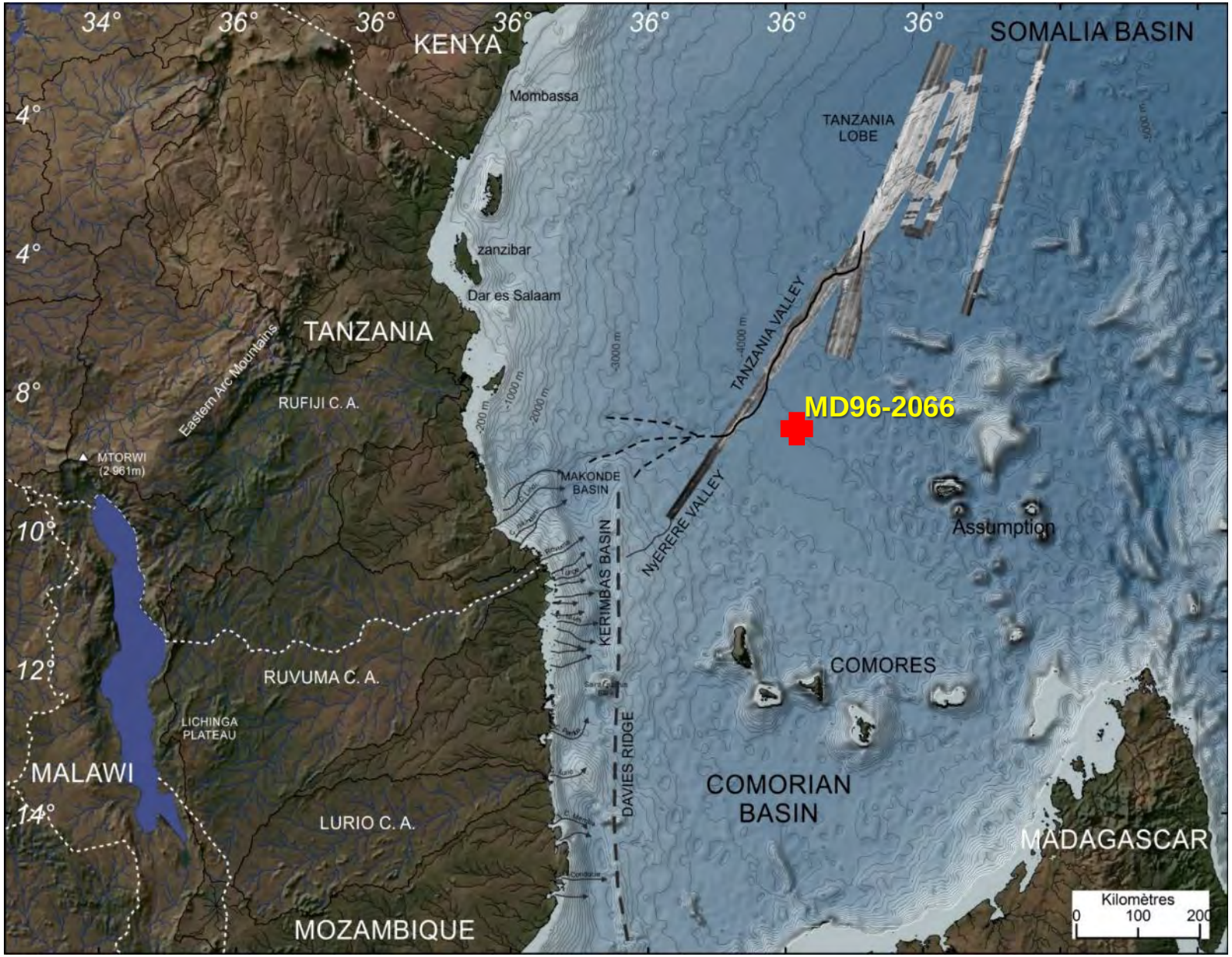
34°
36°
36°
36°
36°
36°
36°
KENYA
SOMALIA BASIN
Mombassa
TANZANIA LOBE
4°
4°
zanzibar
Dar es Salaam
TANZANIA
TANZANIA VALLEY
8°
RUFIJI C. A.
Eastern Arc Mountains
MTORWI (2 961m)
MD96-2066
MAKONDE BASIN
10°
NyERERE VALLEY
KERIMBAS BASIN
Assumption
12°
RUVUMA C. A.
COMORES
LICHINGA PLATEAU
MALAWI
DAVIES RIDGE
COMORIAN BASIN
14°
LURIO C. A.
MADAGASCAR
MOZAMBIQUE
Kilomètres
0
100
200

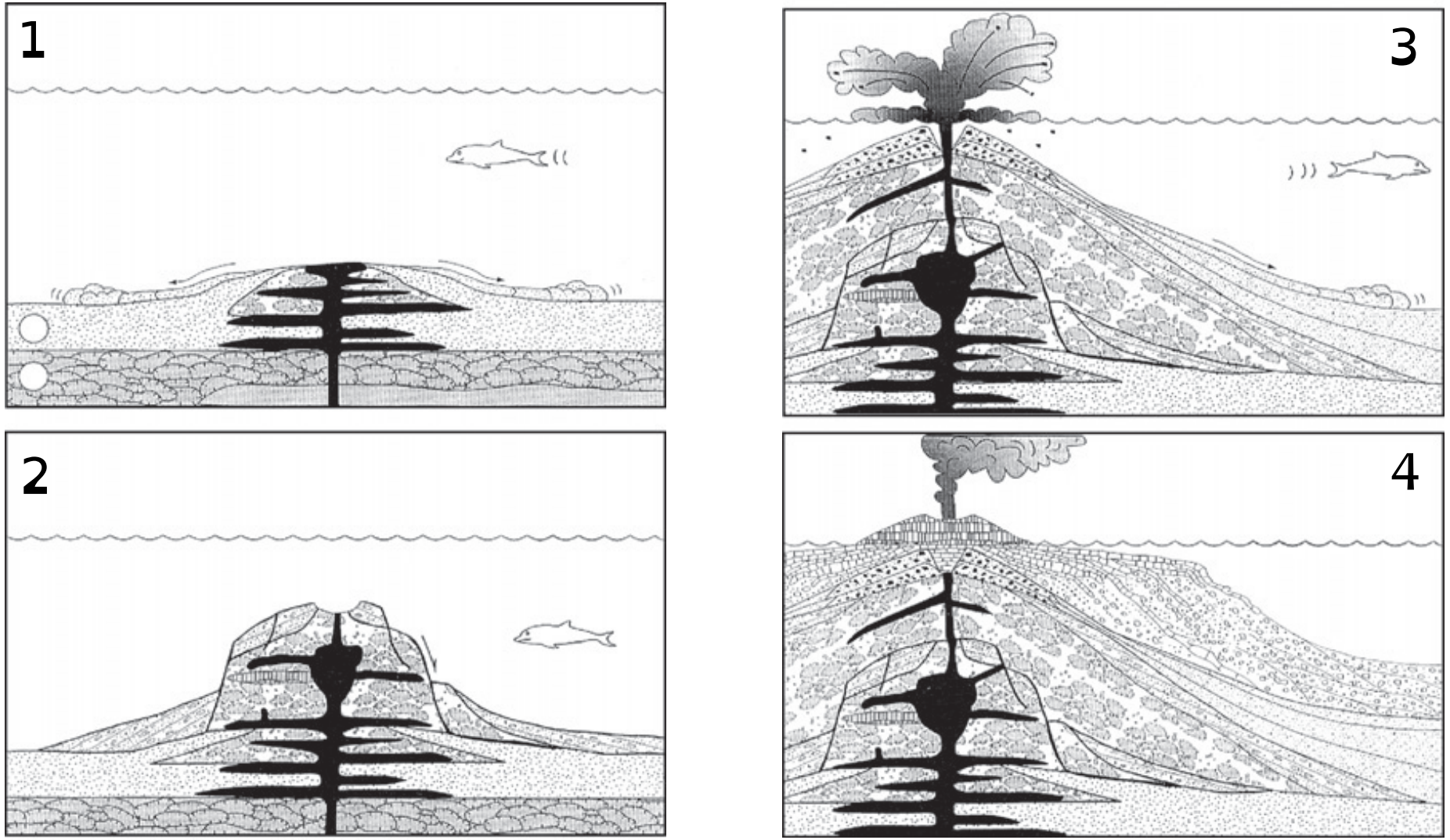

Figure 7.15 Evolution and growth of an oceanic island. Reproduced from Schmidt and Schmincke (2000) with permission from Elsevier. (A) Beginning of island growth, intrusion of dikes and extrusion of pillow lavas; (B) deep-water stage dominated by intrusive and extrusive (pillows and sheet flows); (C) activity become explosive with more fragmental material being produced; (D) sub-aerial emergence of the island and formation of lava deltas.

Hüneke, H. (Ed.), 2011. Deep-sea sediments, Developments in sedimentology. Elsevier, Amsterdam.

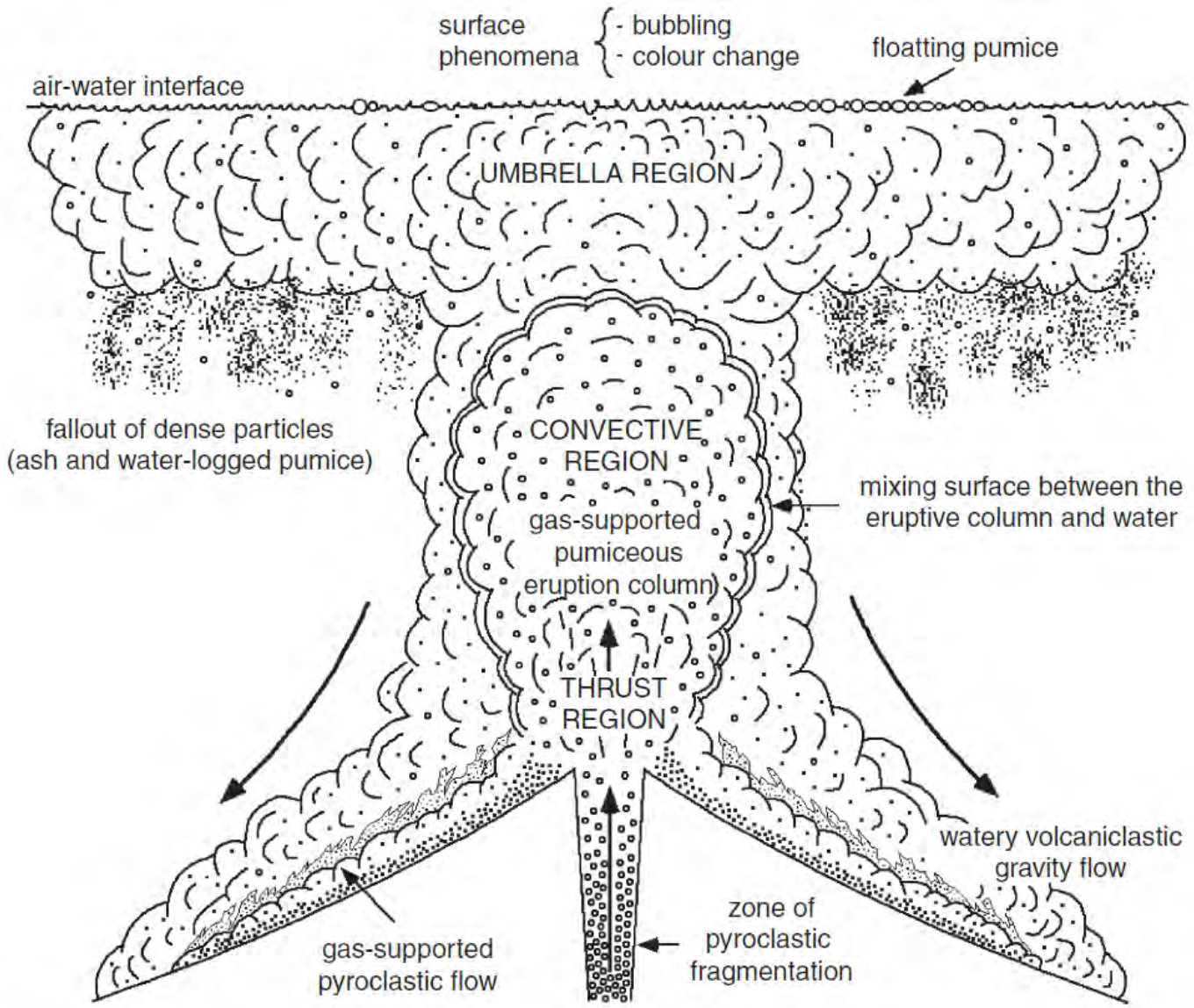

Figure 7.18 Model of a submarine pumice-producing eruption column. Modified from Schneider (2000).

Hüneke, H. (Ed.), 2011. Deep-sea sediments, Developments in sedimentology. Elsevier, Amsterdam.

Primary volcanoclastic deposits

Secondary volcanoclastic deposits

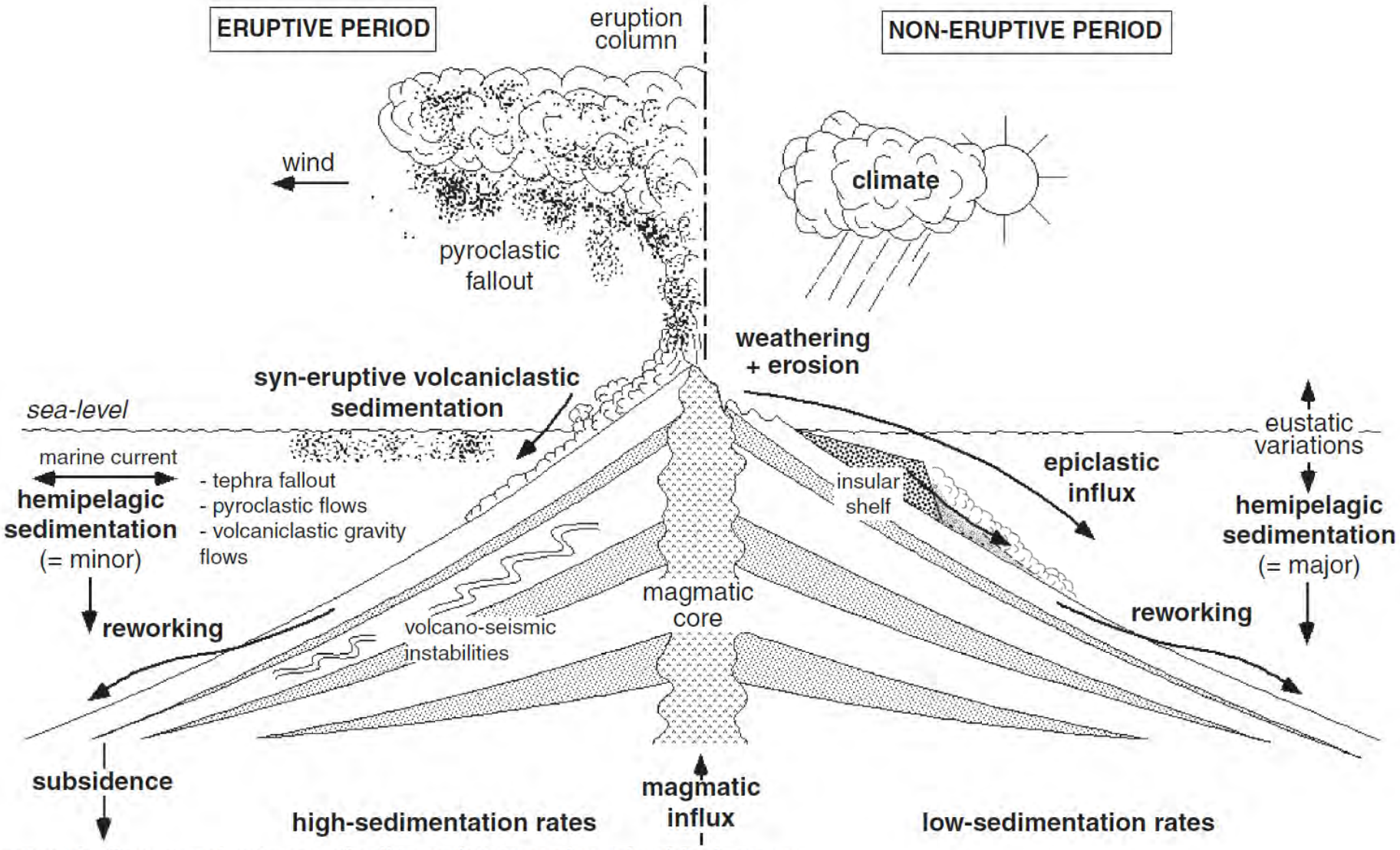

Figure 7.22 Sources and processes of sedimentation on marine volcaniclastic aprons during eruptive and non-eruptive periods. Modified from Schneider (2000).

Hüneke, H. (Ed.), 2011. Deep-sea sediments, Developments in sedimentology. Elsevier, Amsterdam.

The 75,000-year BP eruption of the Toba caldera – Sumatra - Indonesia

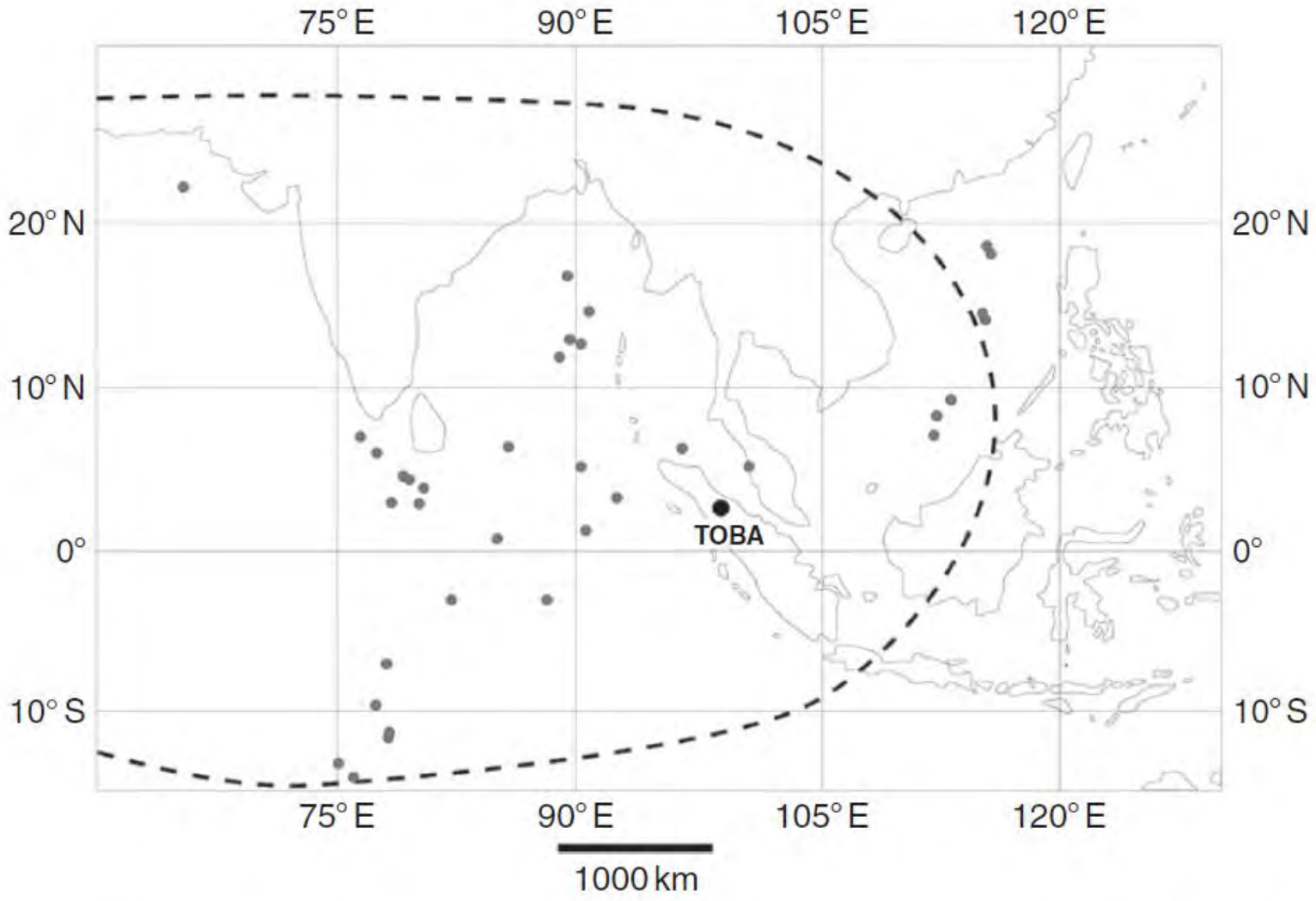

Figure 7.7 Distribution of the Toba ash layer in marine sediments (dashed line) from the Indian Ocean and South China Sea (modified from Buhring et al., 2000).

Primary volcanoclastic deposits

Secondary volcanoclastic deposits

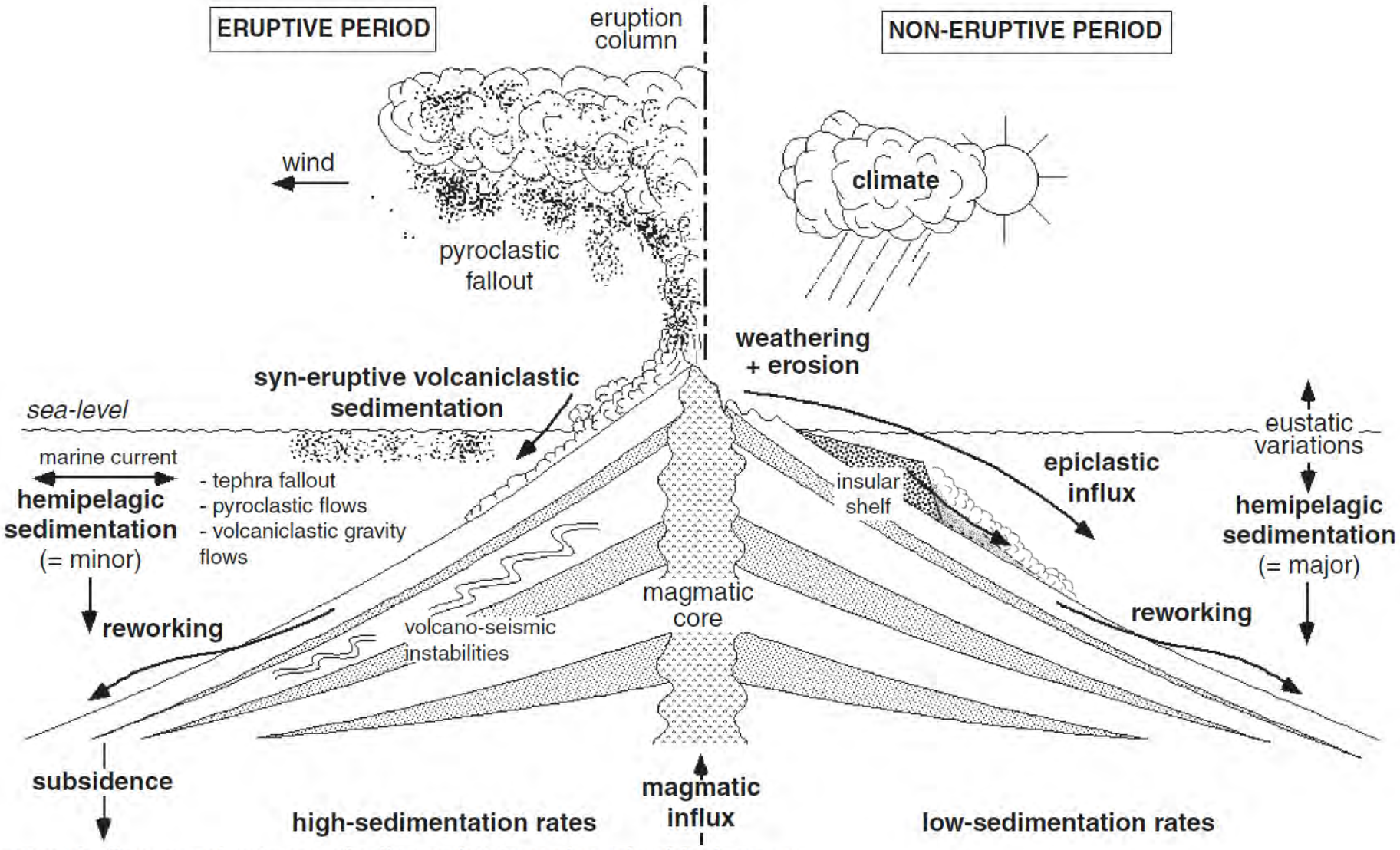

Figure 7.22 Sources and processes of sedimentation on marine volcaniclastic aprons during eruptive and non-eruptive periods. Modified from Schneider (2000).

Hüneke, H. (Ed.), 2011. Deep-sea sediments, Developments in sedimentology. Elsevier, Amsterdam.

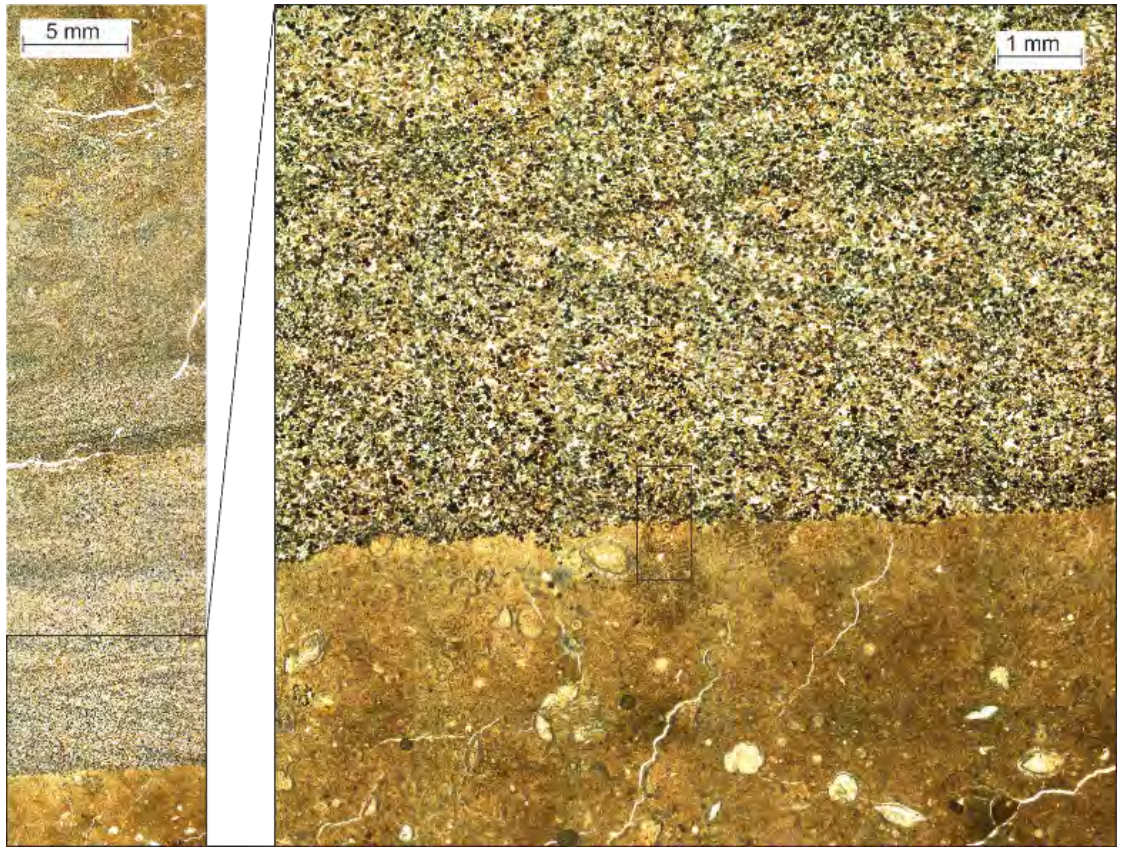

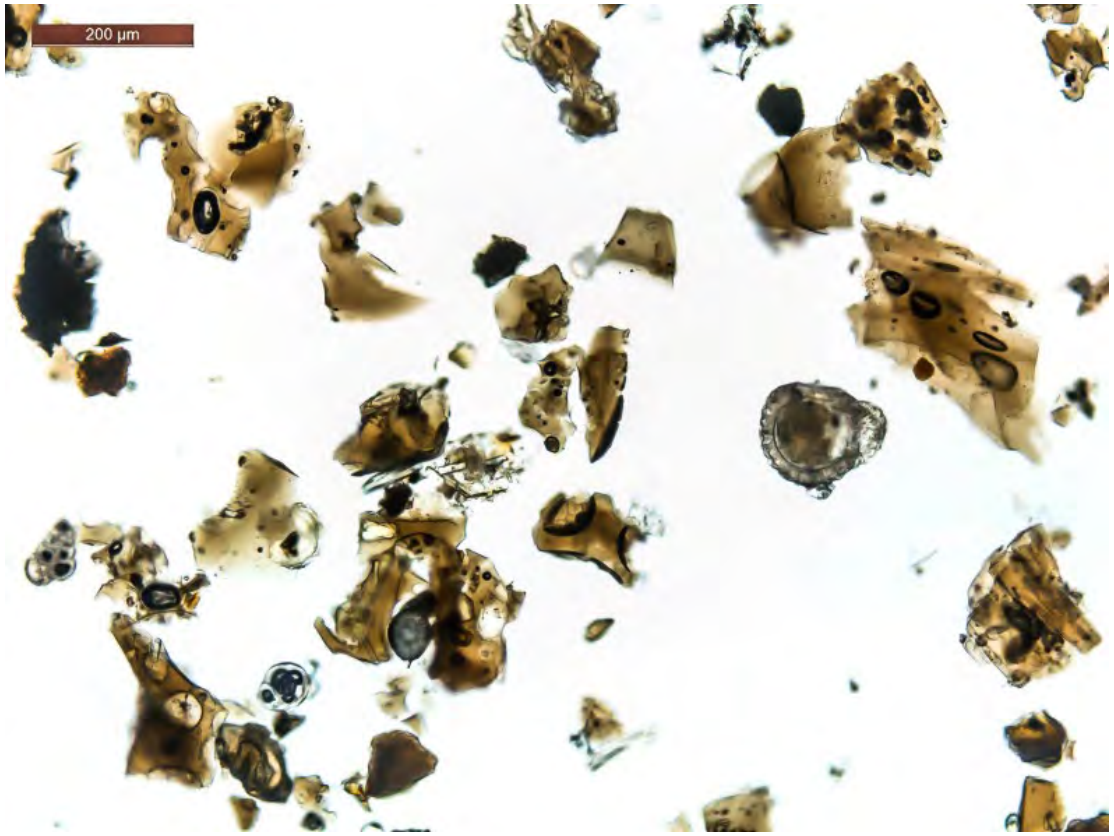

Primary volcanoclastic deposits or Secondary volcanoclastic deposits ?

L'activité volcanique au niveau des dorsales, des îles volcaniques, des zones de subduction génèrent de larges volumes de sédiments volcanoclastiques vers l'océan profond. Ces apports représenteraient 5 à 10 % des flux terrigènes à la surface de la Terre (Fishet and Schmincke, 1994)

1. Sédimentation gravitaire – turbiditique

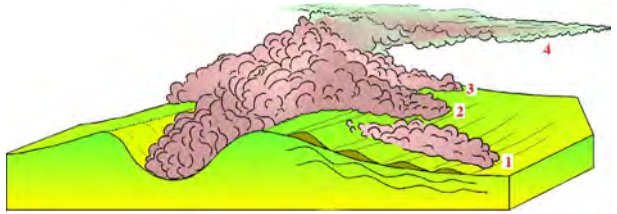

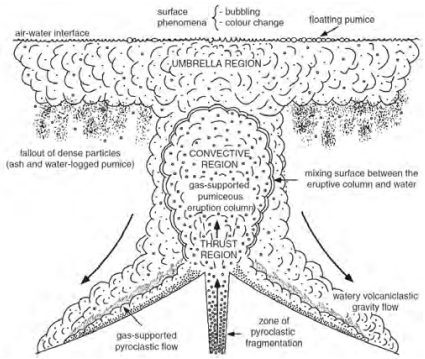

2. Sédimentation volcanoclastique

3. Sédimentation pélagique et hémipélagique

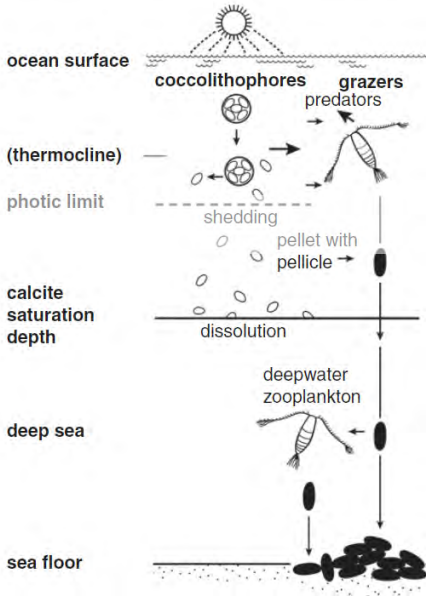

4. Sédimentation glaci-marine

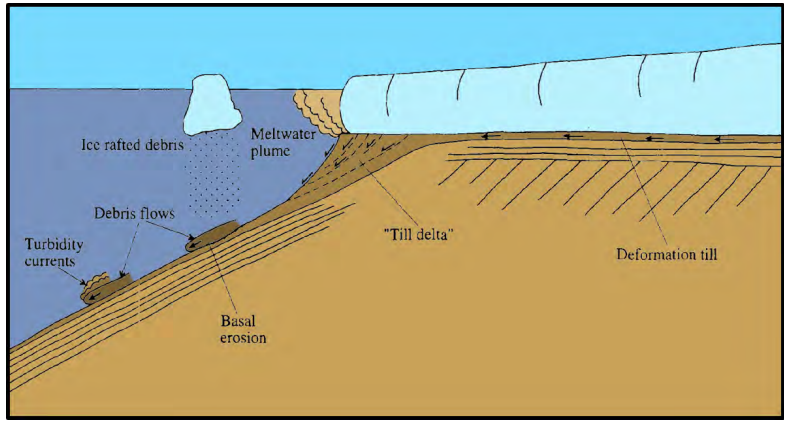

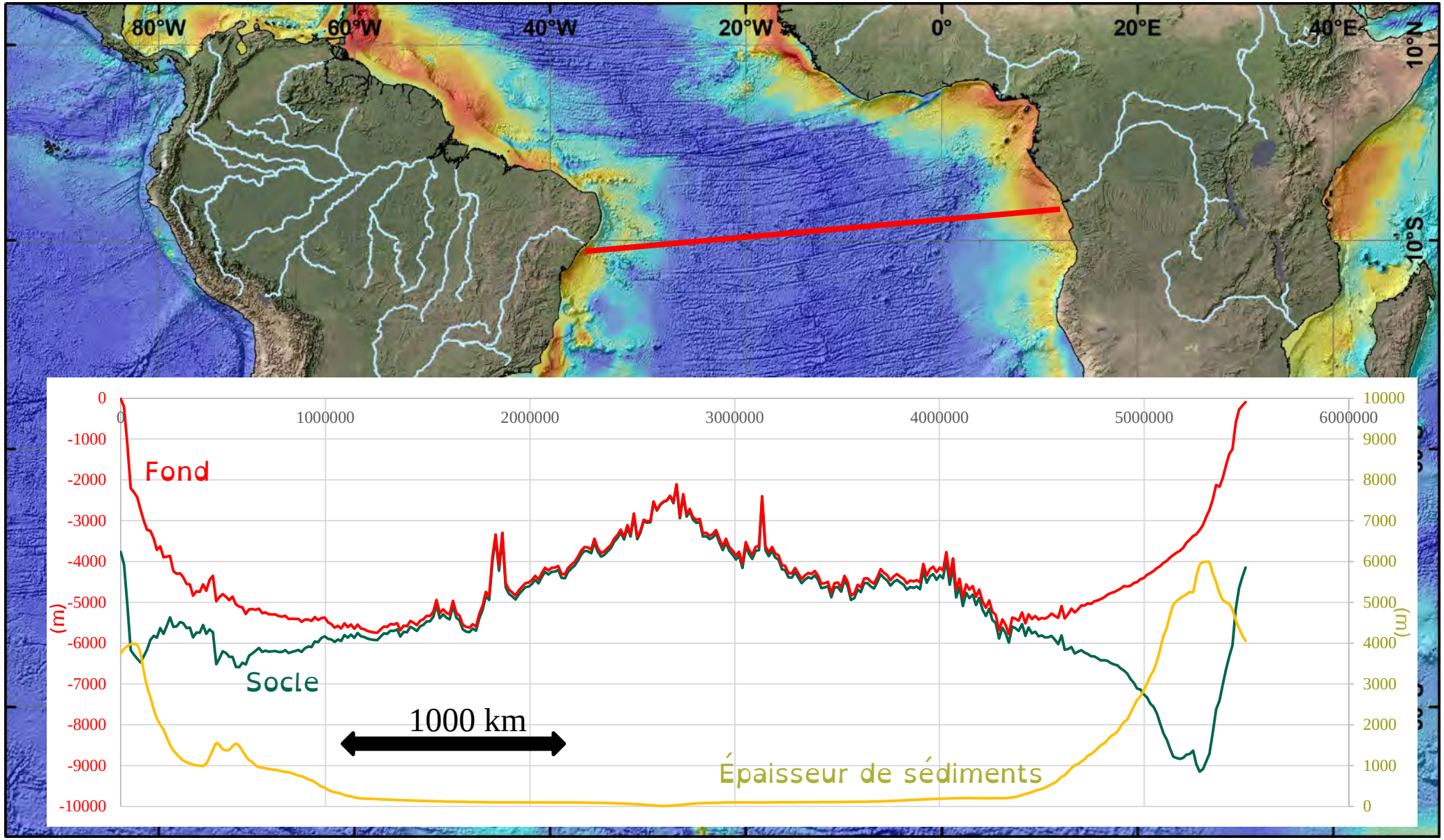
80°W
60°W
40°W
20°W
0°
20°E
40°E
10°N
10°S
0
-1000
-2000
-3000
-4000
-5000
-6000
-7000
-8000
-9000
-10000
(m)
0
1000000
2000000
3000000
4000000
5000000
6000000
10000
9000
8000
7000
6000
5000
4000
3000
2000
1000
0
(m)
Fond
Socle
1000 km
Épaisseur de sédiments

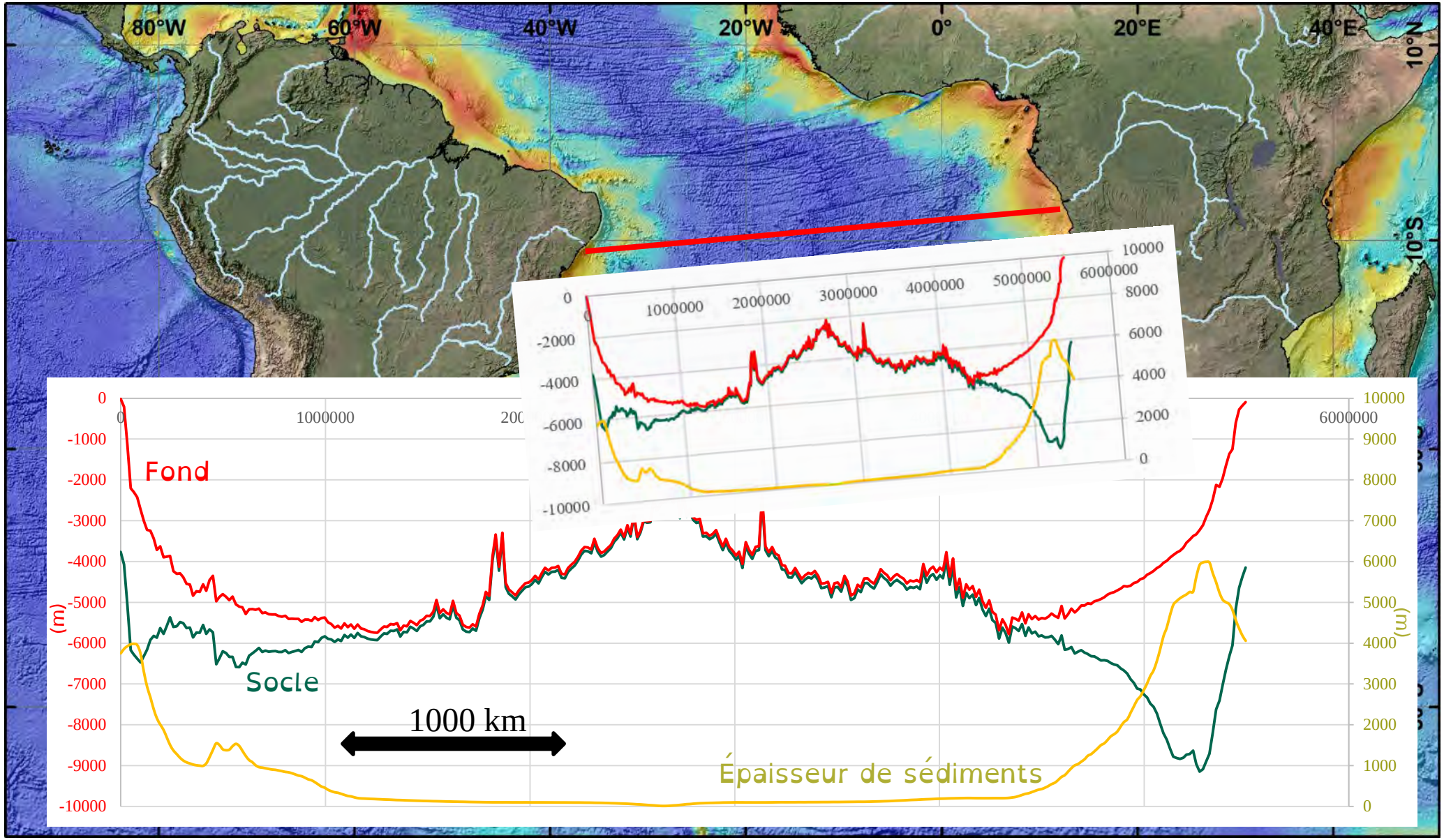
80°W
60°W
40°W
20°W
0°
20°E
40°E
10°N
10°S
Fond
Socle
Épaisseur de sédiments
1000 km
(m)
(m)
0
-1000
-2000
-3000
-4000
-5000
-6000
-7000
-8000
-9000
-10000
1000000
6000000
10000
9000
8000
7000
6000
5000
4000
3000
2000
1000
0

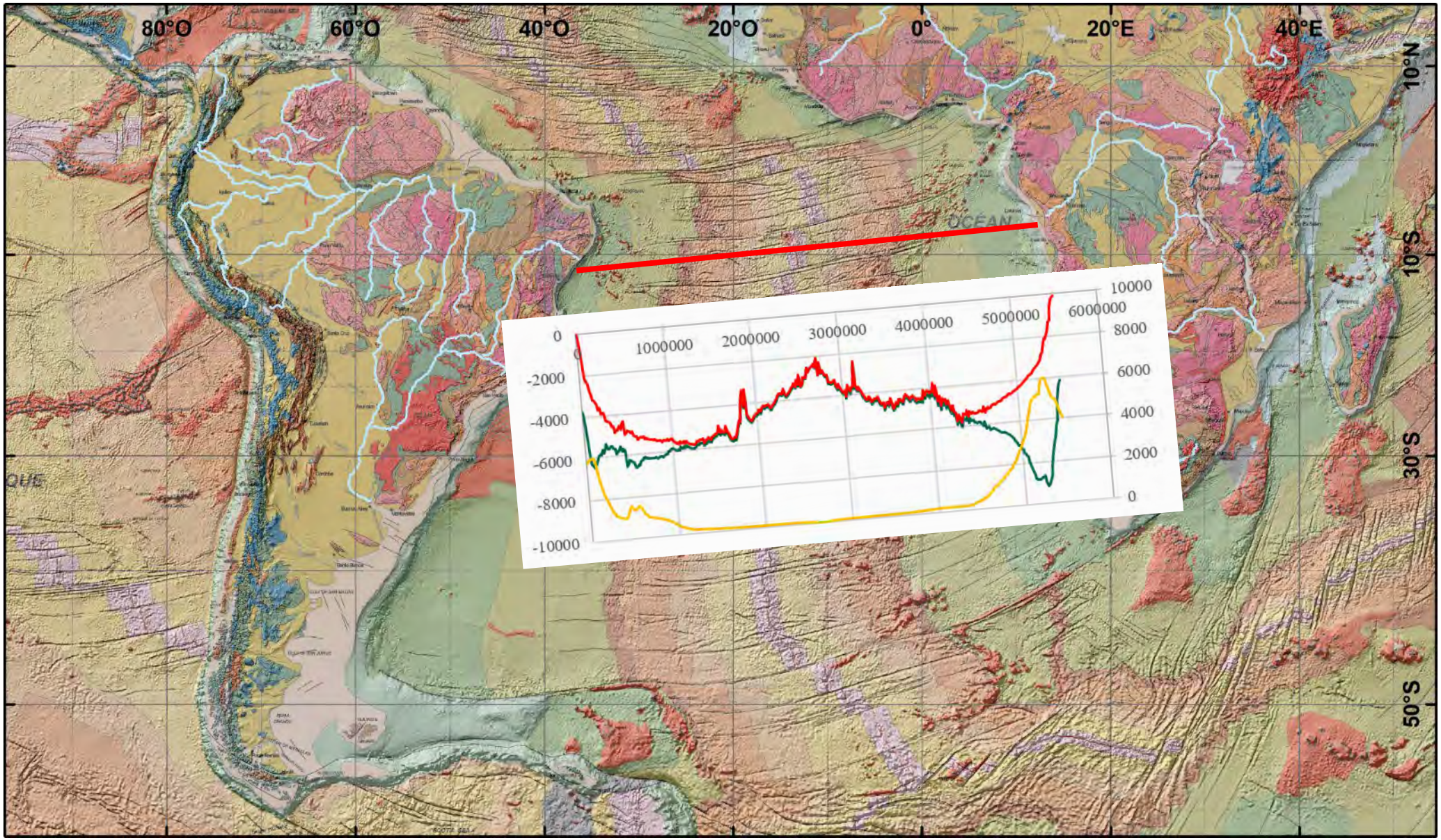
80°O
60°O
40°O
20°O
0°
20°E
40°E
10°N
10°S
30°S
50°S
OCÉAN
0
-2000
-4000
-6000
-8000
-10000
1000000
2000000
3000000
4000000
5000000
6000000
10000
8000
6000
4000
2000
0

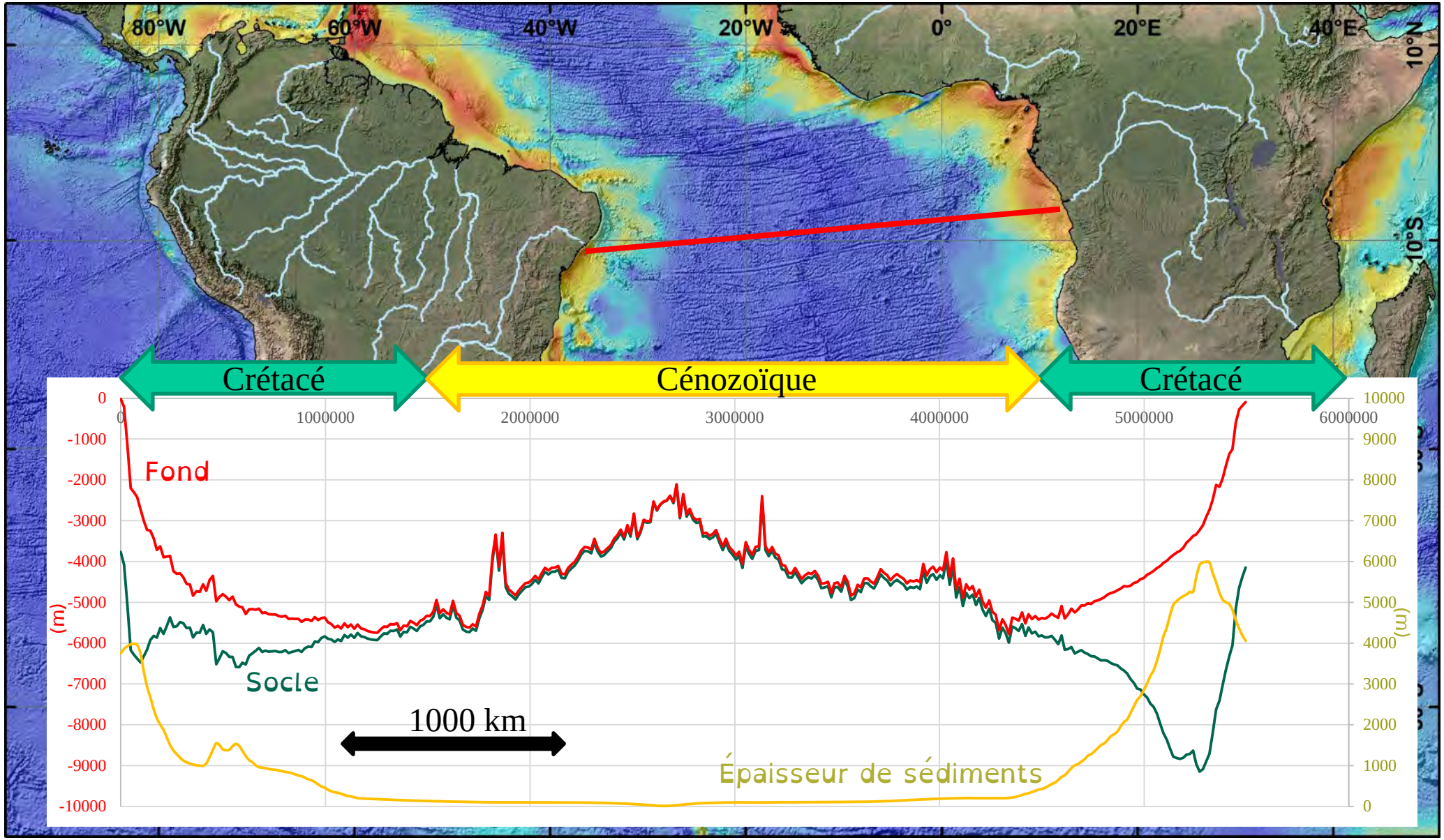
80°W
60°W
40°W
20°W
0°
20°E
40°E
10°N
10°S
Crétacé
Cénozoïque
Crétacé
0
1000000
2000000
3000000
4000000
5000000
6000000
0
-1000
-2000
-3000
-4000
-5000
-6000
-7000
-8000
-9000
-10000
(m)
10000
9000
8000
7000
6000
5000
4000
3000
2000
1000
0
(m)
Fond
Socle
1000 km
Épaisseur de sédiments

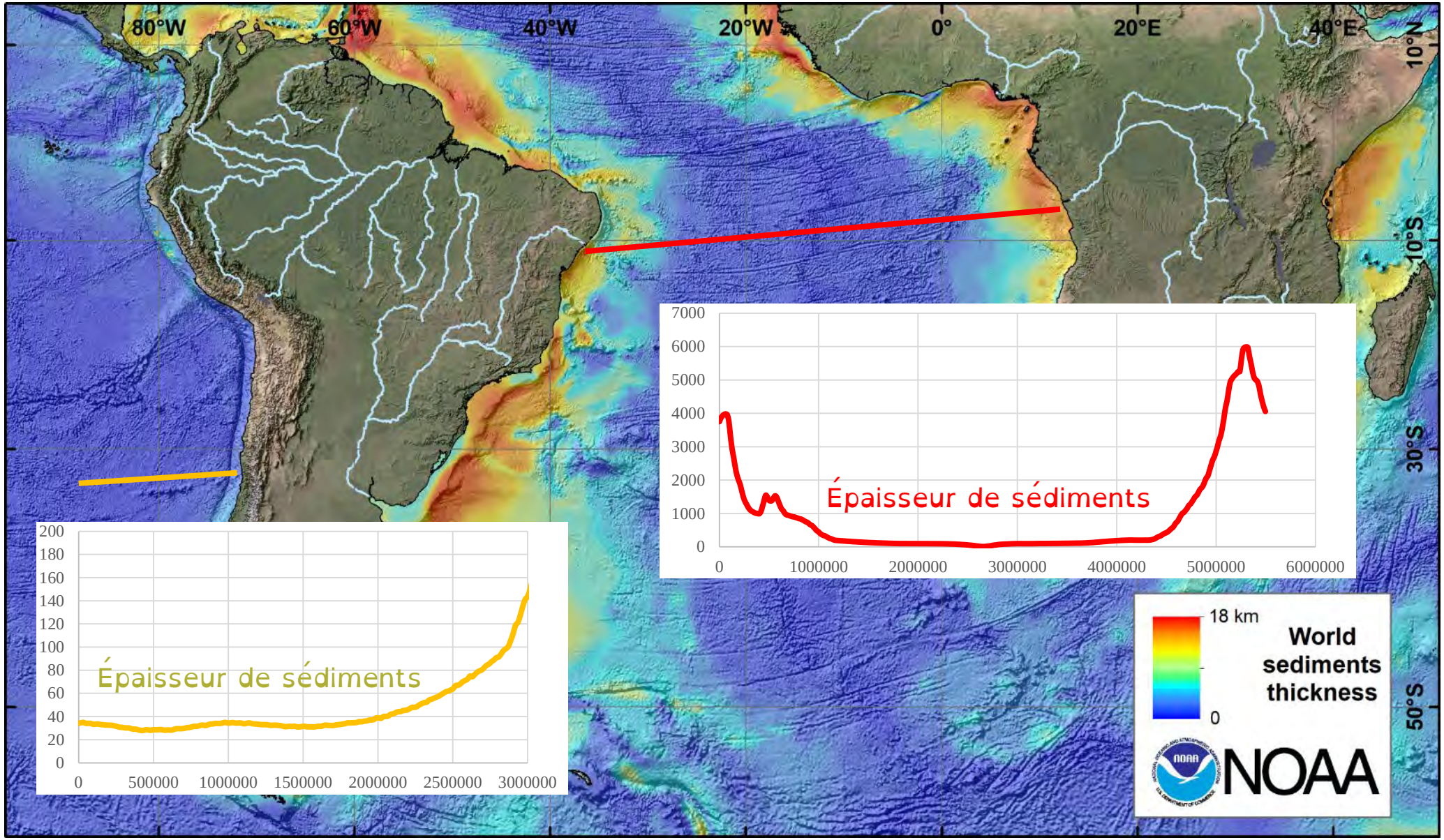
80°W
60°W
40°W
20°W
0°
20°E
40°E
10°N
10°S
30°S
50°S
Épaisseur de sédiments
7000
6000
5000
4000
3000
2000
1000
0
0
1000000
2000000
3000000
4000000
5000000
6000000
Épaisseur de sédiments
200
180
160
140
120
100
80
60
40
20
0
0
500000
1000000
1500000
2000000
2500000
3000000
18 km
0
World sediments thickness
NOAA

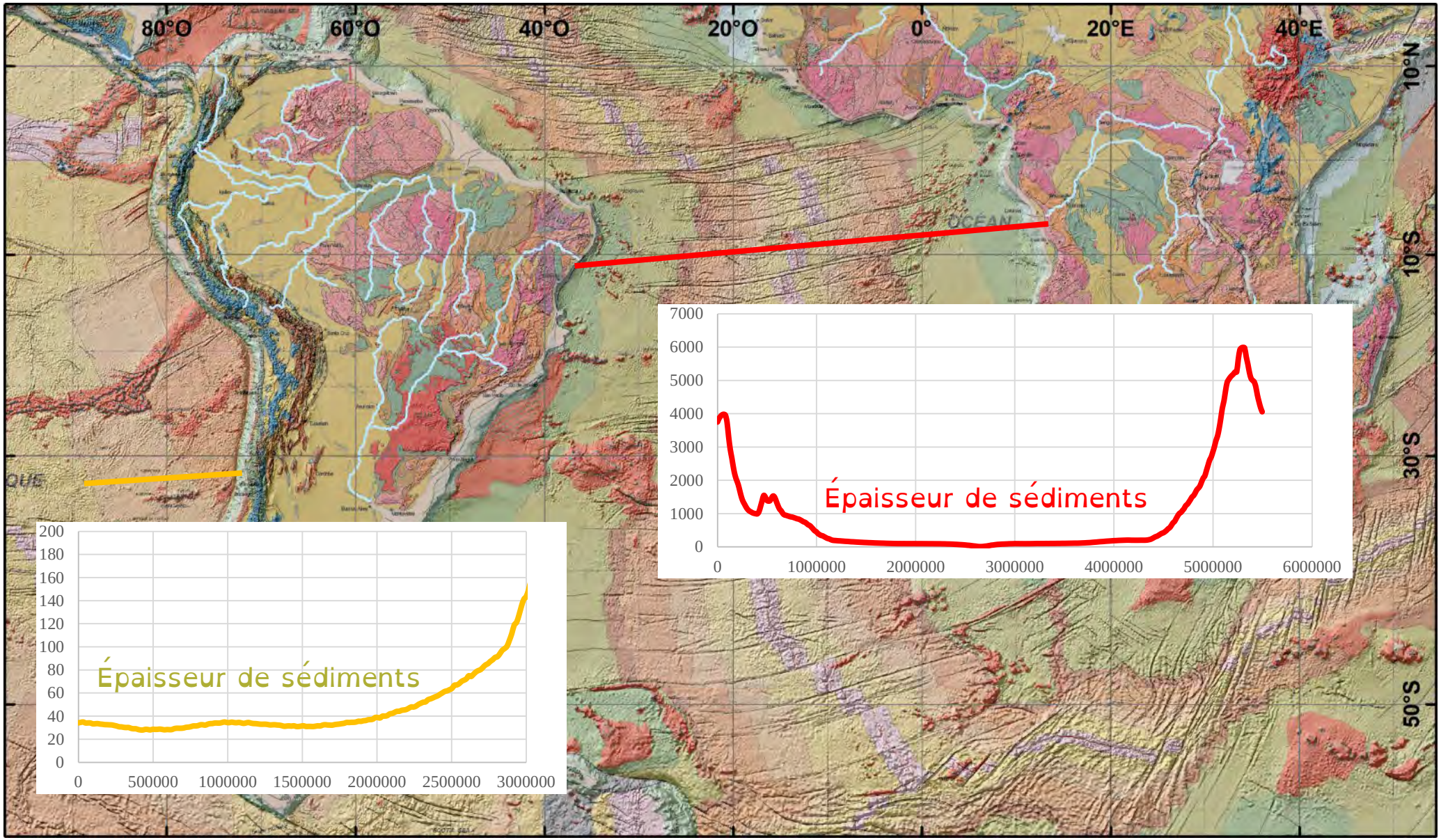
80°O
60°O
40°O
20°O
0°
20°E
40°E
10°N
10°S
30°S
50°S
OCÉAN
7000
6000
5000
4000
3000
2000
1000
0
0
1000000
2000000
3000000
4000000
5000000
6000000
Épaisseur de sédiments
200
180
160
140
120
100
80
60
40
20
0
0
500000
1000000
1500000
2000000
2500000
3000000
Épaisseur de sédiments

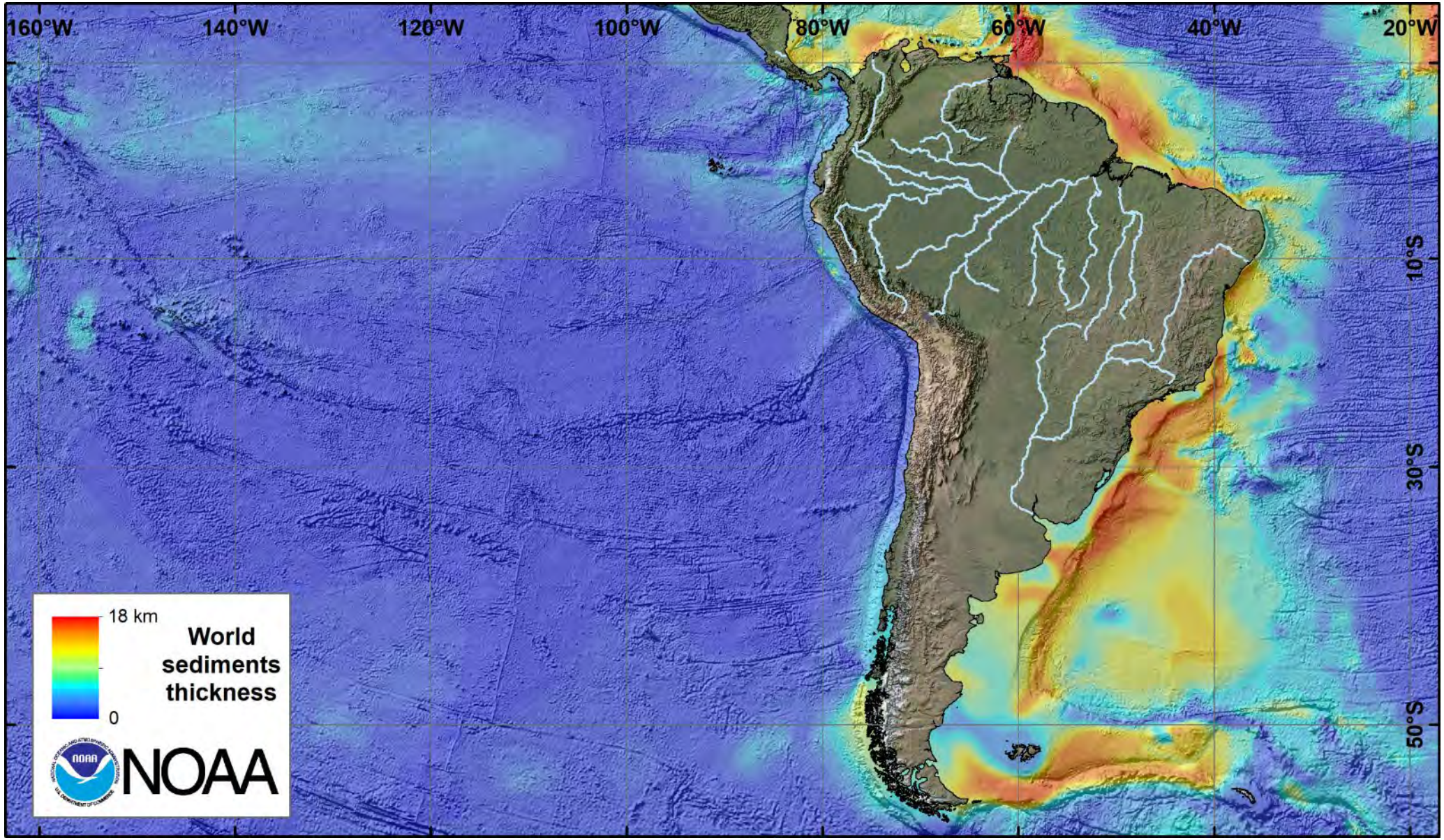
160°W
140°W
120°W
100°W
80°W
60°W
40°W
20°W
10°S
30°S
50°S
18 km
0
World sediments thickness
NOAA

Sédimentation pélagique & hémipélagique : bruit de fond de la sédimentation

Processus dominant : la décantation des particules en provenance de la surface de l'océan

Principalement des organismes planctoniques - > productivité biologique

-> contrôlée par : zone photique, nutriments, température

<u>Phytoplancton</u>

Coccolithophorides (calcaire)
Diatomés (siliceux)

Dinoflagéles (organiques)

<u>Zooplancton</u>

Foraminifères planctoniques (calcaire)
Ptéropodes (calcaires)
Radiolaires (siliceux)

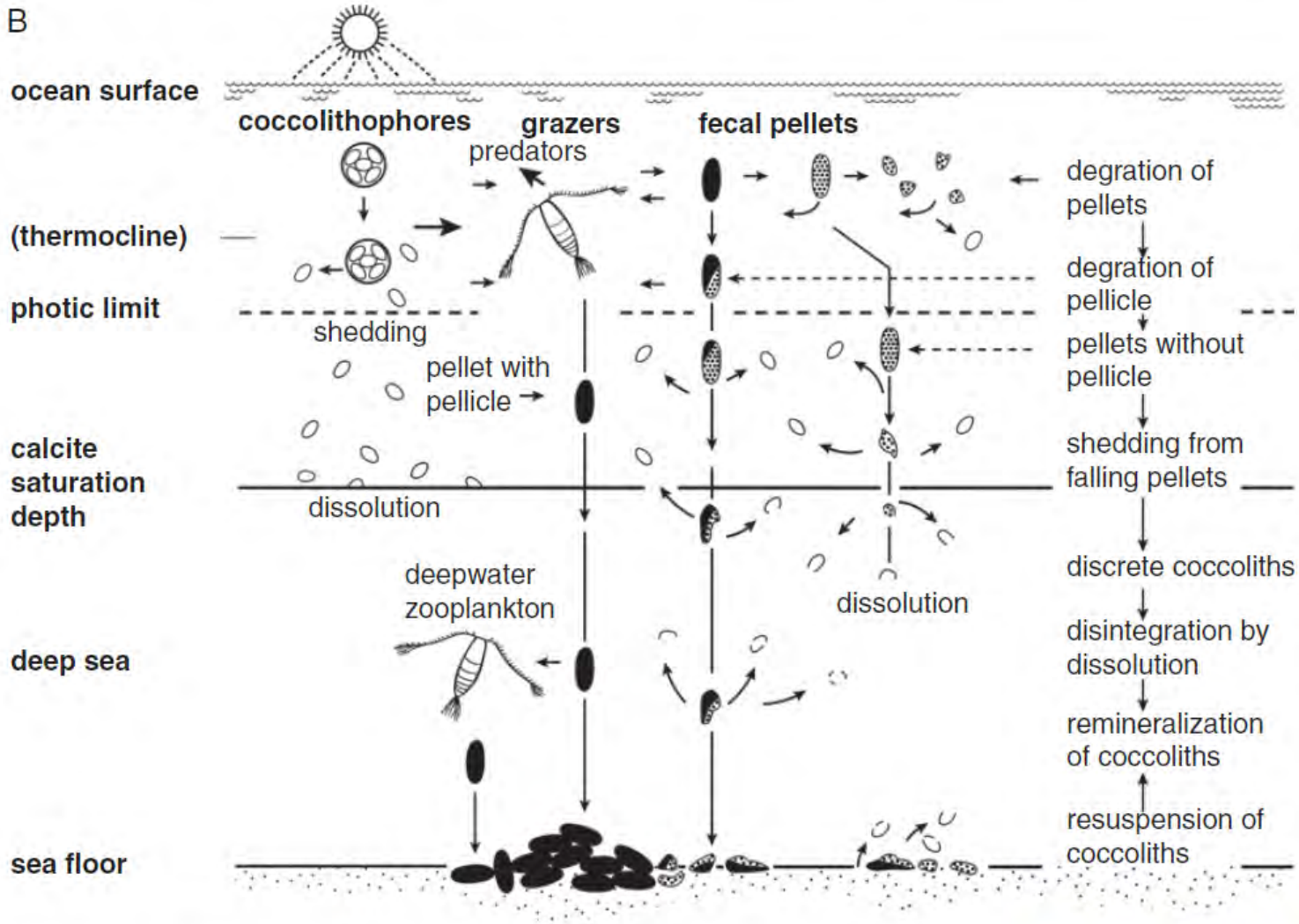

Figure 4.4 Coccoliths. (A) Coccoliths and climate (redrawn after Westbroek et al. (1993)). (B) Schematic cartoon displaying production and flux of coccoliths through the water column (slightly redrawn and modified after Honjo, 1976). Sinking-rate estimates for coccoliths are 160 m per day in a pellet and 0.15 m per day as discrete coccoliths.

Hüneke, H. (Ed.), 2011. Deep-sea sediments, Developments in sedimentology. Elsevier, Amsterdam.

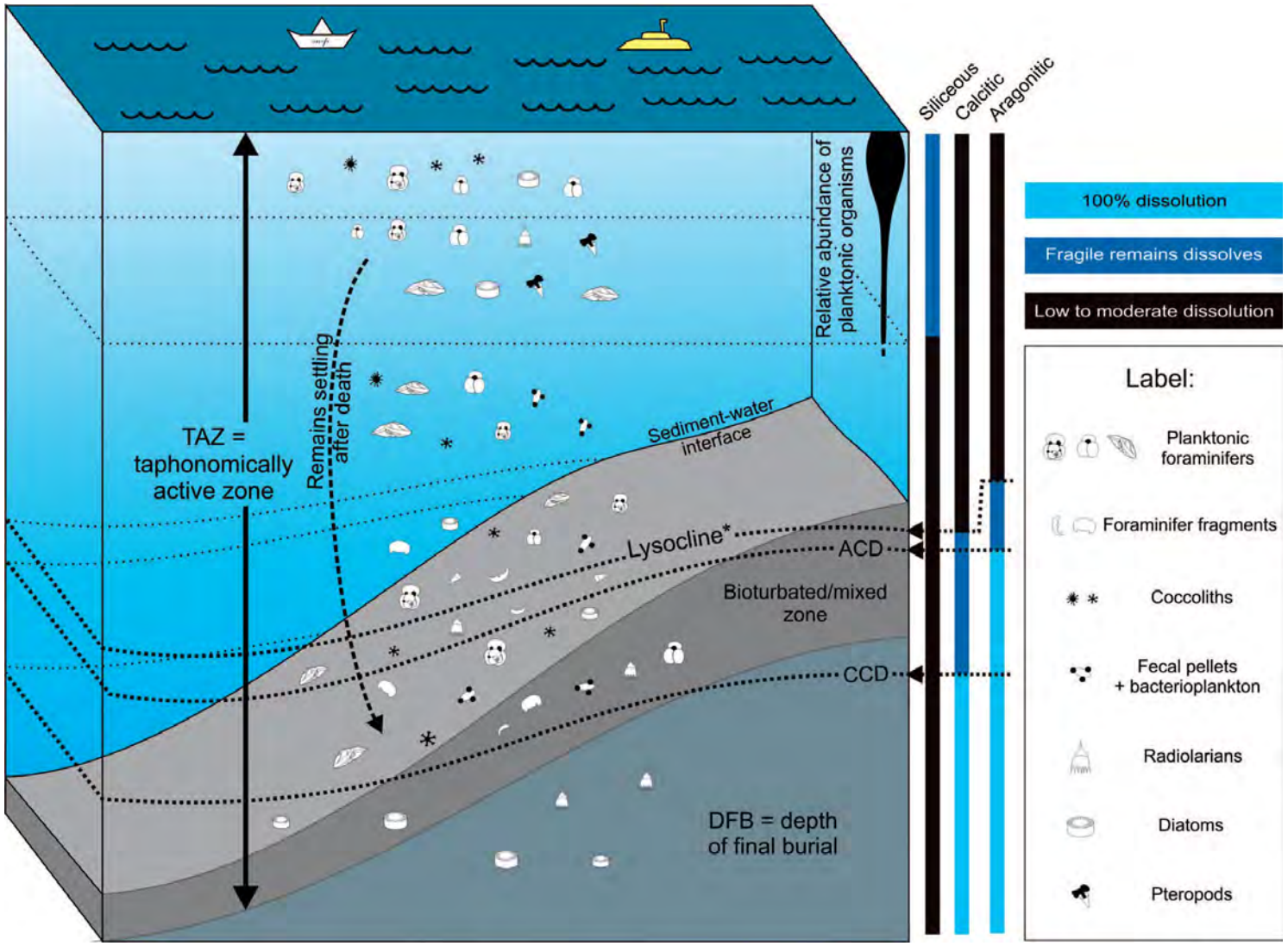

TAZ : Zone taphonomique active. Zone d'altération post-mortem des débris biologiques

Lysocline : profondeur à partir de laquelle la solubilité des carbonates augmente

CCD : Seuil de compensation des carbonates

Petró, S.M., Do Nascimento Ritter, M., Pivel, M.A.G., Coimbra, J.C., 2018. SURVIVING IN THE WATER COLUMN: DEFINING THE TAPHONOMICALLY ACTIVE ZONE IN PELAGIC SYSTEMS. PALAIOS 33, 85–93.

$$CaCO_3 + CO_2 + H_2O \rightleftharpoons Ca^{2+}(aq) + 2\,HCO_3^-(aq)$$

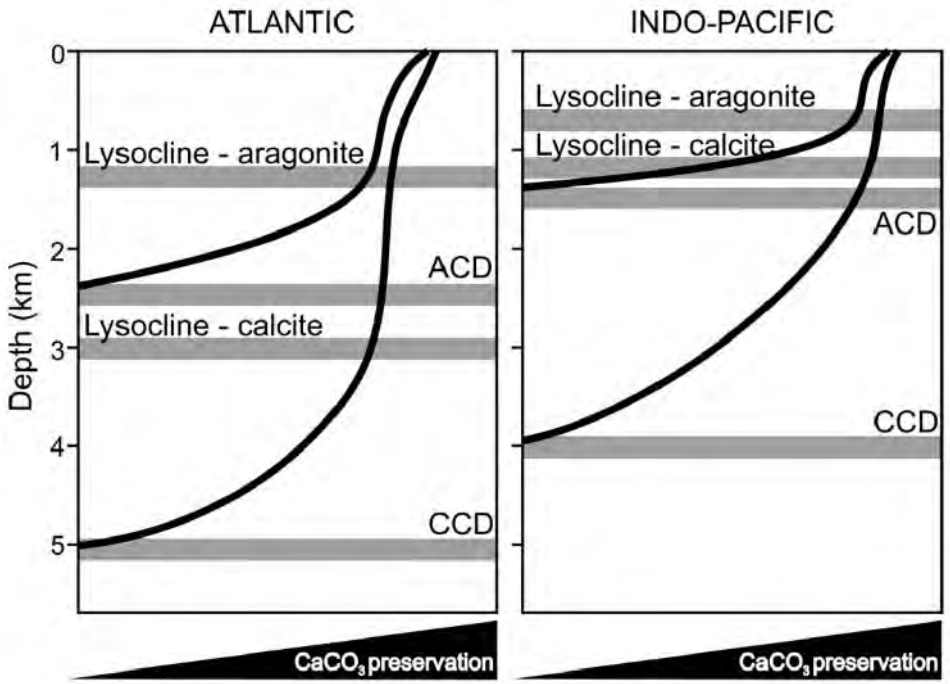

FIG. 4.—Definition of calcium carbonate (calcite and aragonite) dissolution horizons based on $CaCO_3$ preservation within the sediments in low latitudes in the Atlantic and Indo-Pacific oceans. Abbreviations: ACD = aragonite compensation depth; CCD = calcite compensation depth) (modified from Berger 1970).

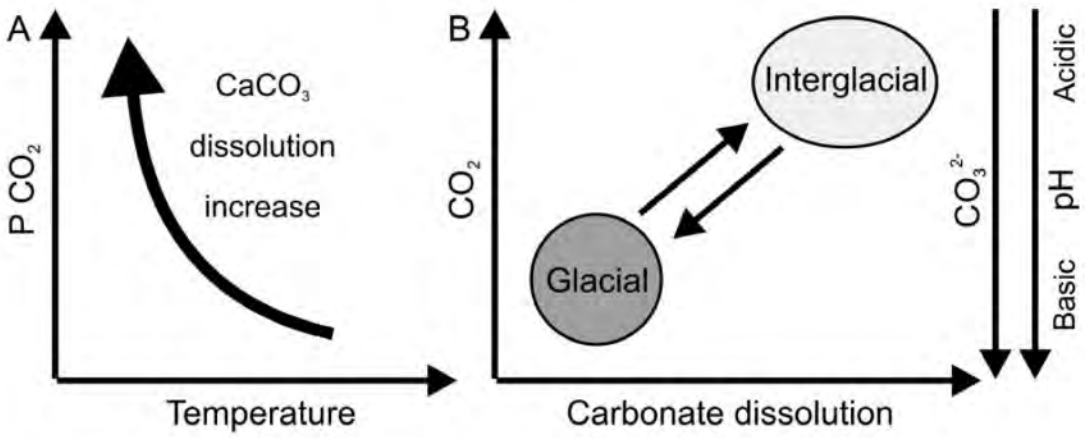

FIG. 3.—Carbonate dissolution and its relation to chemical, physical, and climate variables. **A**) The increase in carbonate dissolution rates with respect to CO_2 pressure and temperature. **B**) The relation between climate changes (interglacial and glacial cycles) and dissolution, CO_2, CO_3^{2-}, and pH in surface waters. Adapted from Petró et al. (2016).

Petró, S.M., Do Nascimento Ritter, M., Pivel, M.A.G., Coimbra, J.C., 2018. SURVIVING IN THE WATER COLUMN: DEFINING THE TAPHONOMICALLY ACTIVE ZONE IN PELAGIC SYSTEMS. PALAIOS 33, 85–93.

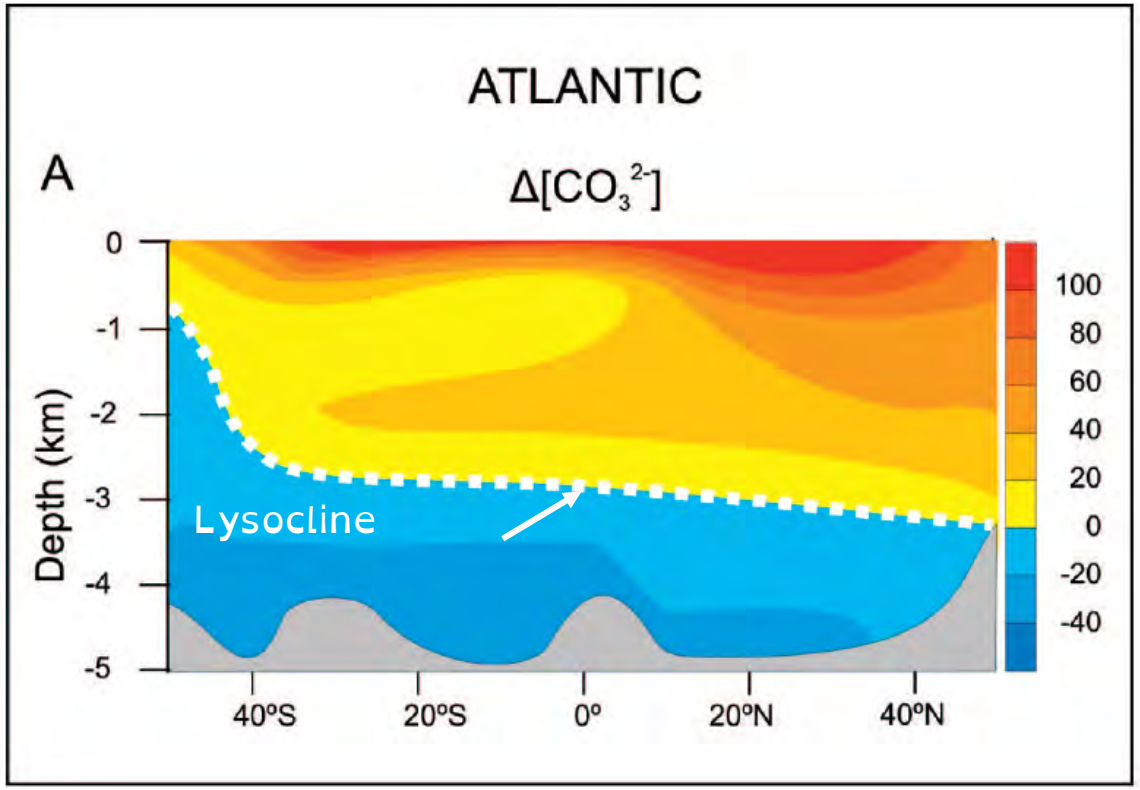

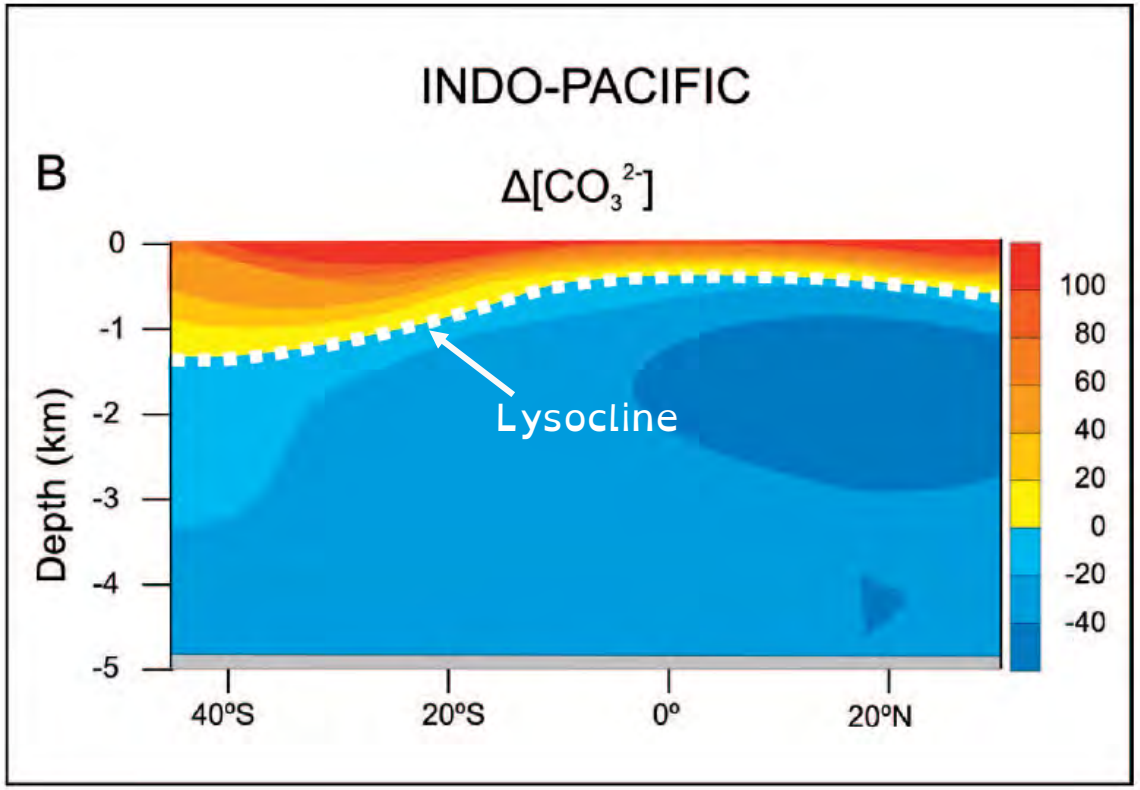

Potential rates of CaCO3 dissolution : $\Delta[CO_3^{2-}] = [CO_3^{2-}]_{seawater} - [CO_3^{2-}]_{calcite/aragonite}$

Petró, S.M., Do Nascimento Ritter, M., Pivel, M.A.G., Coimbra, J.C., 2018. SURVIVING IN THE WATER COLUMN: DEFINING THE TAPHONOMICALLY ACTIVE ZONE IN PELAGIC SYSTEMS. PALAIOS 33, 85–93.

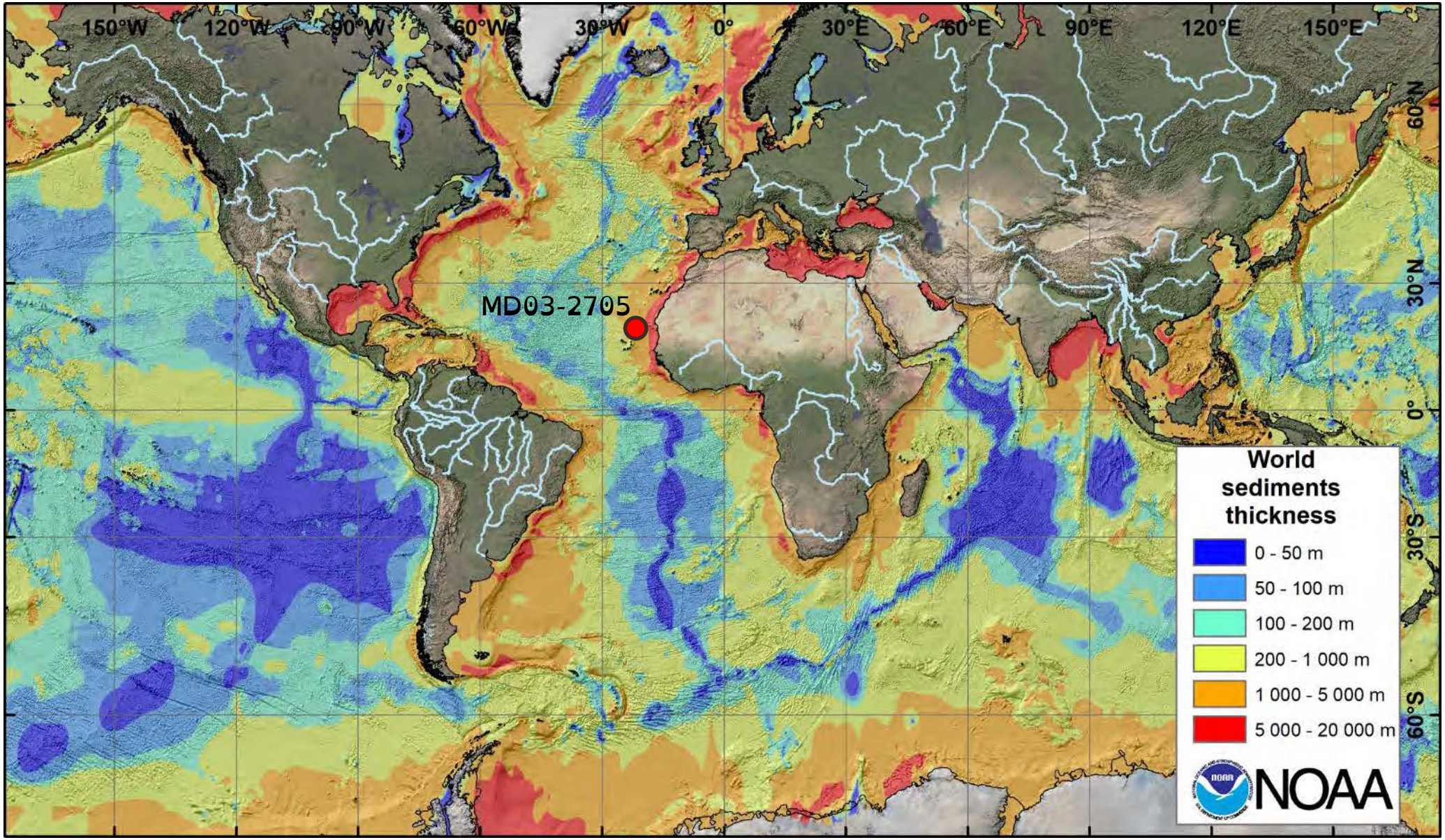
150°W
120°W
90°W
60°W
30°W
0°
30°E
60°E
90°E
120°E
150°E
60°N
30°N
0°
30°S
60°S
MD03-2705
World sediments thickness
0 - 50 m
50 - 100 m
100 - 200 m
200 - 1 000 m
1 000 - 5 000 m
5 000 - 20 000 m
NOAA

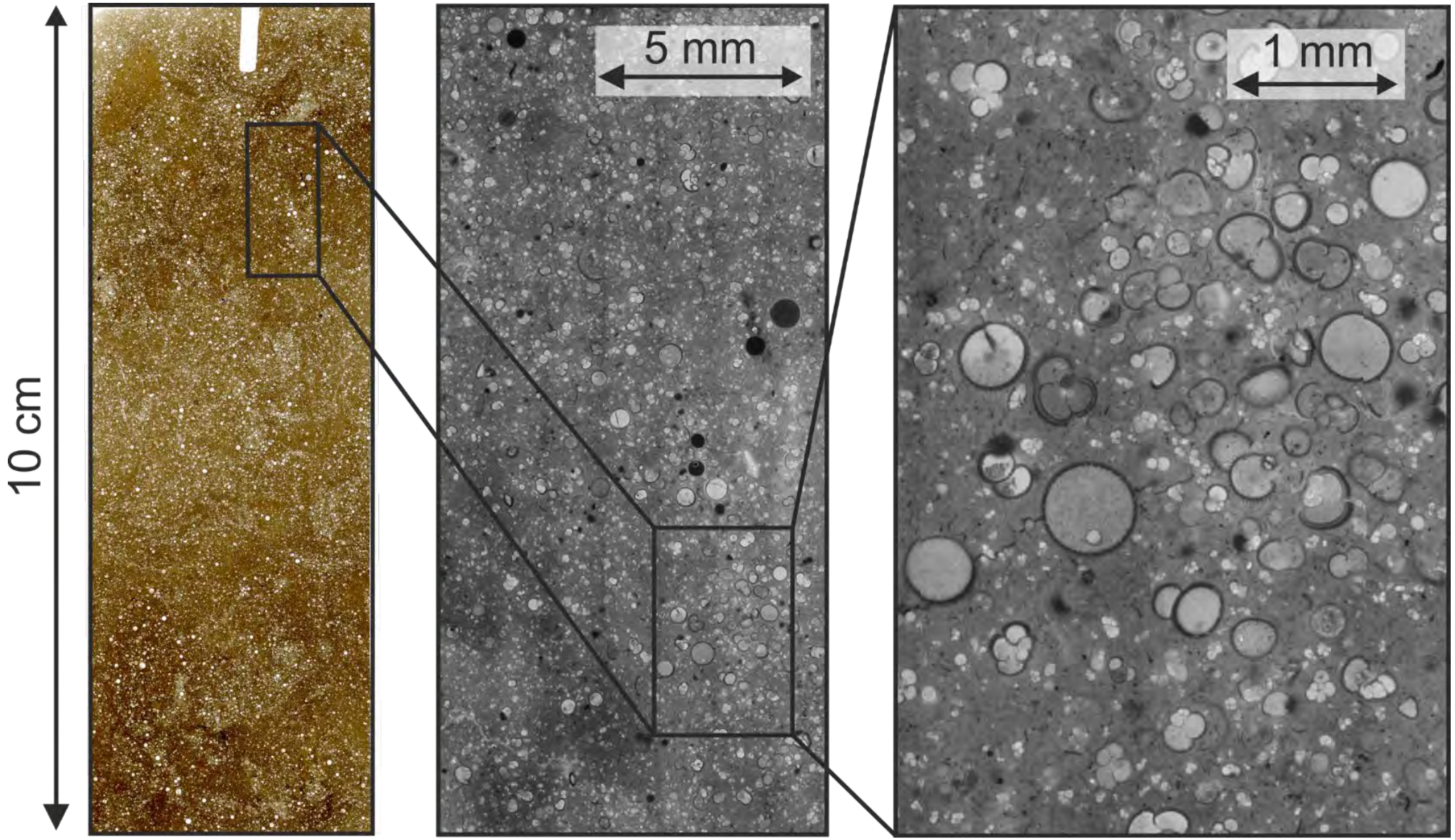

MD 032705 - 930 - 940 cm

Pelagic is used here for sediment which is generated in the open sea. Pelagic sediment is chiefly composed of biogenic material diluted by a proportion (<25%) of non-biogenic components. In areas close to continental margins and in enclosed basins where clastic supply is more abundant, the rain of biogenic debris is further diluted by a silt- and clay-sized terrigenous component. This sediment is regarded as hemipelagic.

Reading, H.G., 1996. Sedimentary Environments: Processes, Facies and Stratigraphy. Wiley.

Boue calcaire :	%CaCO3 > 70 %
Boue marneuse :	30% < %CaCO3 < 70 %
Vase carbonatée :	10%< %CaCO3 < 30 %
Vase :	%CaCO3 < 10 %

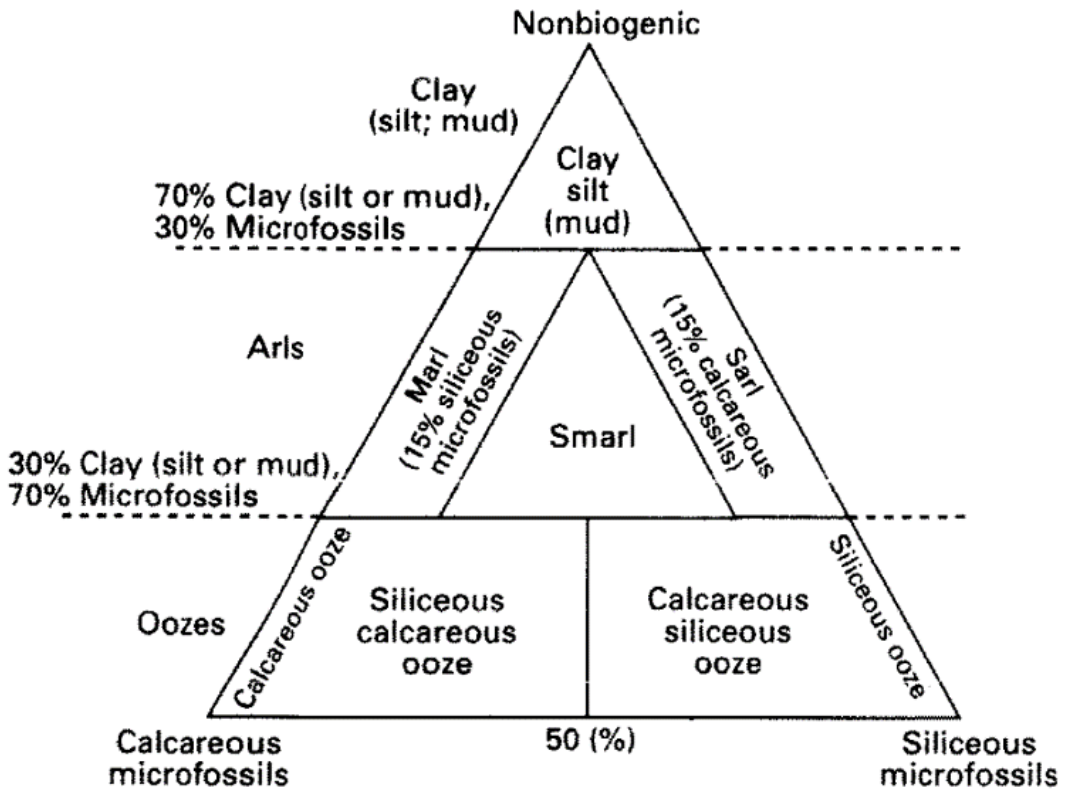

Figure 10.7 Classification of the three-component system (non-biogenic, siliceous biogenic and calcareous biogenic) that makes up pelagic and hemipelagic sediments (after Hay, Sibuet *et al.*, 1984).

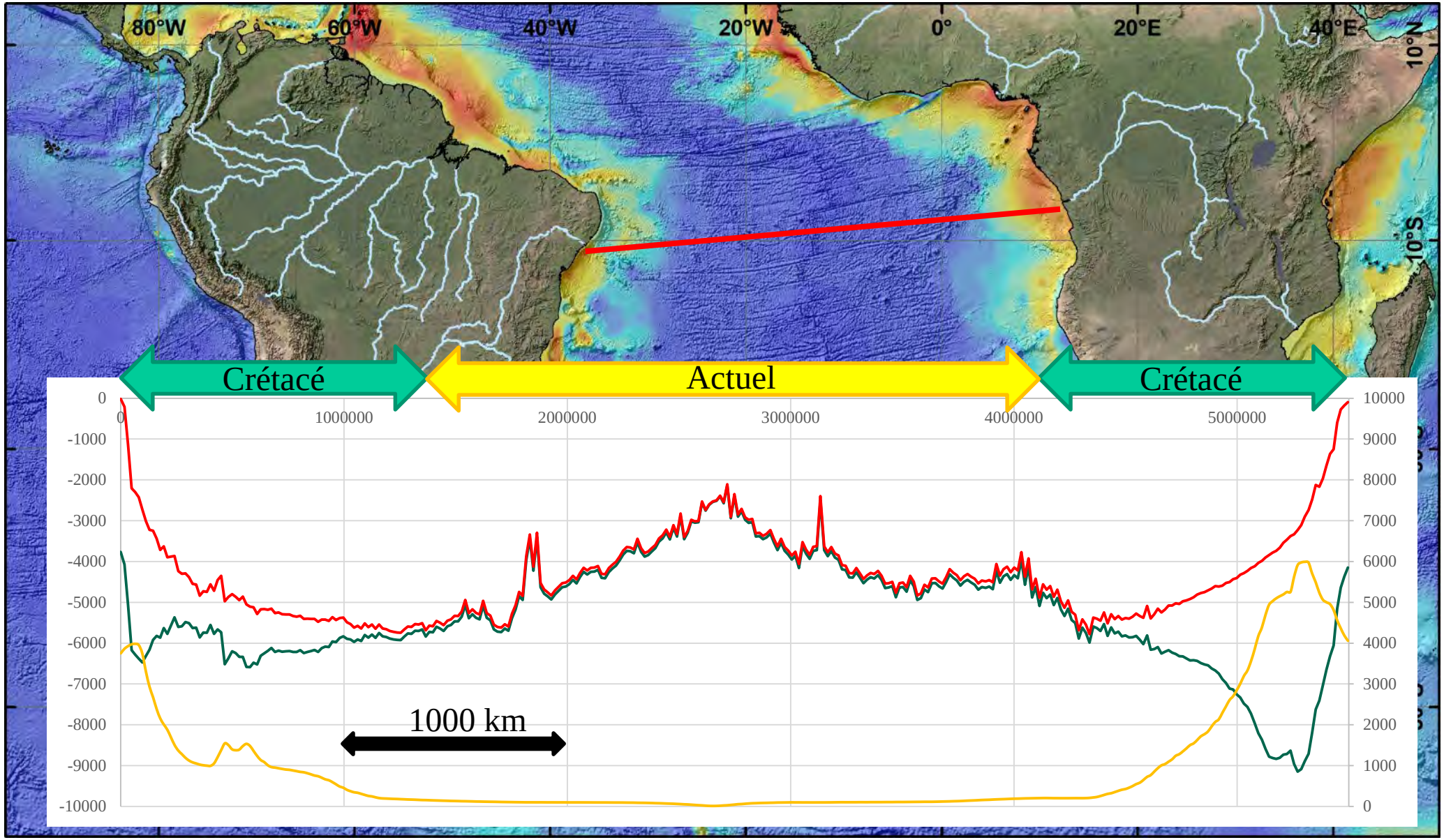
80°W
60°W
40°W
20°W
0°
20°E
40°E
10°N
10°S
Crétacé
Actuel
Crétacé
0
-1000
-2000
-3000
-4000
-5000
-6000
-7000
-8000
-9000
-10000
0
1000000
2000000
3000000
4000000
5000000
10000
9000
8000
7000
6000
5000
4000
3000
2000
1000
0
1000 km

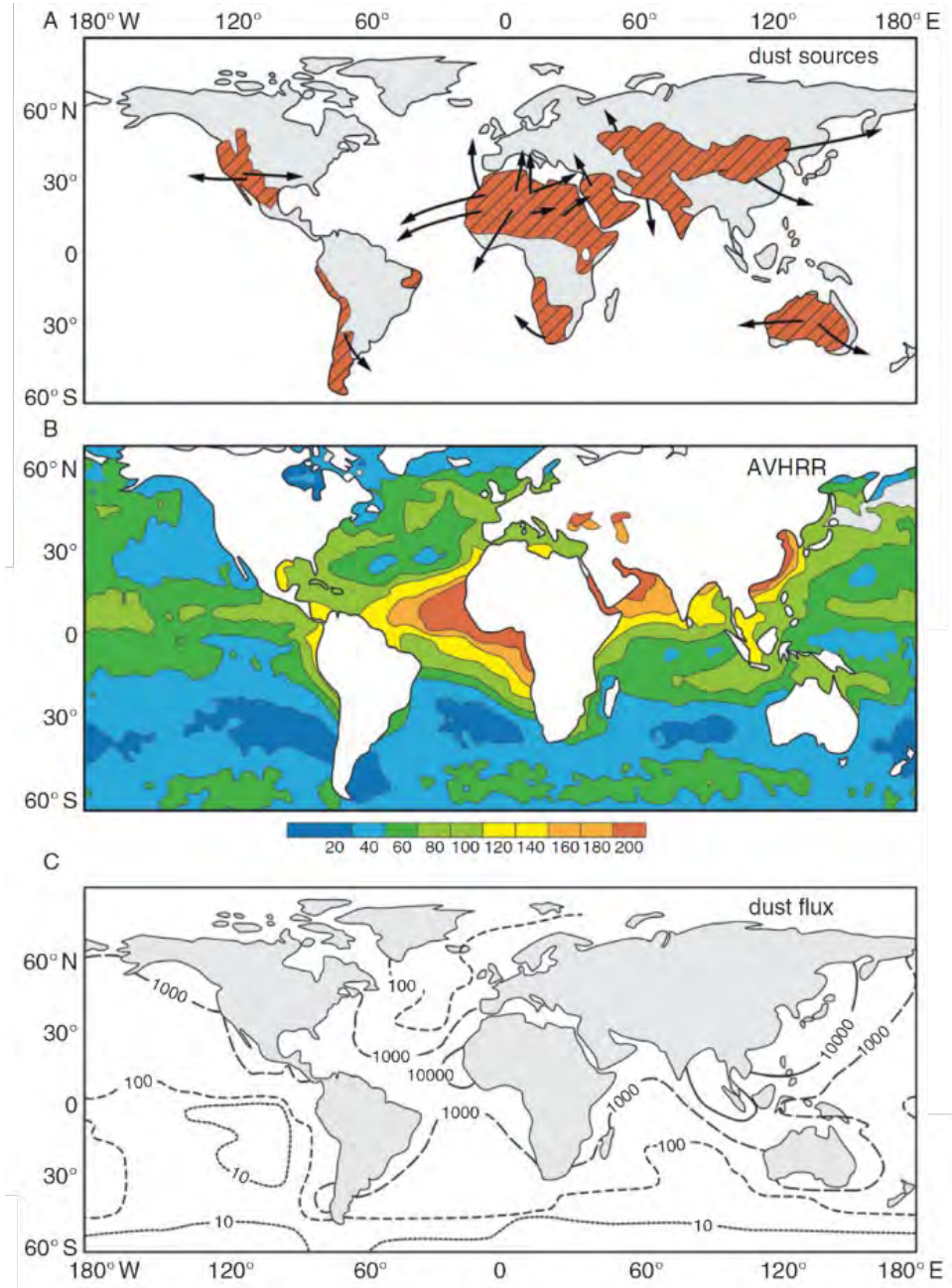

Figure 5.3 Present-day locations of dust sources, transport paths and deposition zones. (A) Present-day dust source regions and wind trajectories reconstructed from observations of dust storms (redrawn and slightly modified after Livingstone and Warren, 1996). (B) Zones of high atmospheric dust concentrations, inferred from the mean annual equivalent aerosol optical depth (×1000) as measured by an Advanced Very High Resolution Radiometer (AVHRR). (C) Global fluxes (mg m^{-2} a^{-1}) of mineral aerosols to the ocean (redrawn and slightly modified after Harrison et al., 2001). (A multi-colour version of this figure is on the included CD-ROM.)

Hüneke, H. (Ed.), 2011. Deep-sea sediments, Developments in sedimentology. Elsevier, Amsterdam.


23.10^6 t.an^{-1} < Débit solide < 130.10^6 t.an^{-1}
Modélisation hydrologique sur la reconstitution topographique du dernier maximum glaciaire
Surface = 1.2 Mkm² (terre) et 3 Mkm² (glace)

Quantification du débit solide du Fleuve Manche entre 24 et 16 ka BP.

Sédiment exporté par un fleuve

part hémipélagique
(sédimentation directe)

part turbiditique
(sédimentation remaniée)

levées

~~***lobes***~~
(pas de données)

Toucanne et al 2010

Estimation de la masse déposée dans les levées turbiditique : Mt

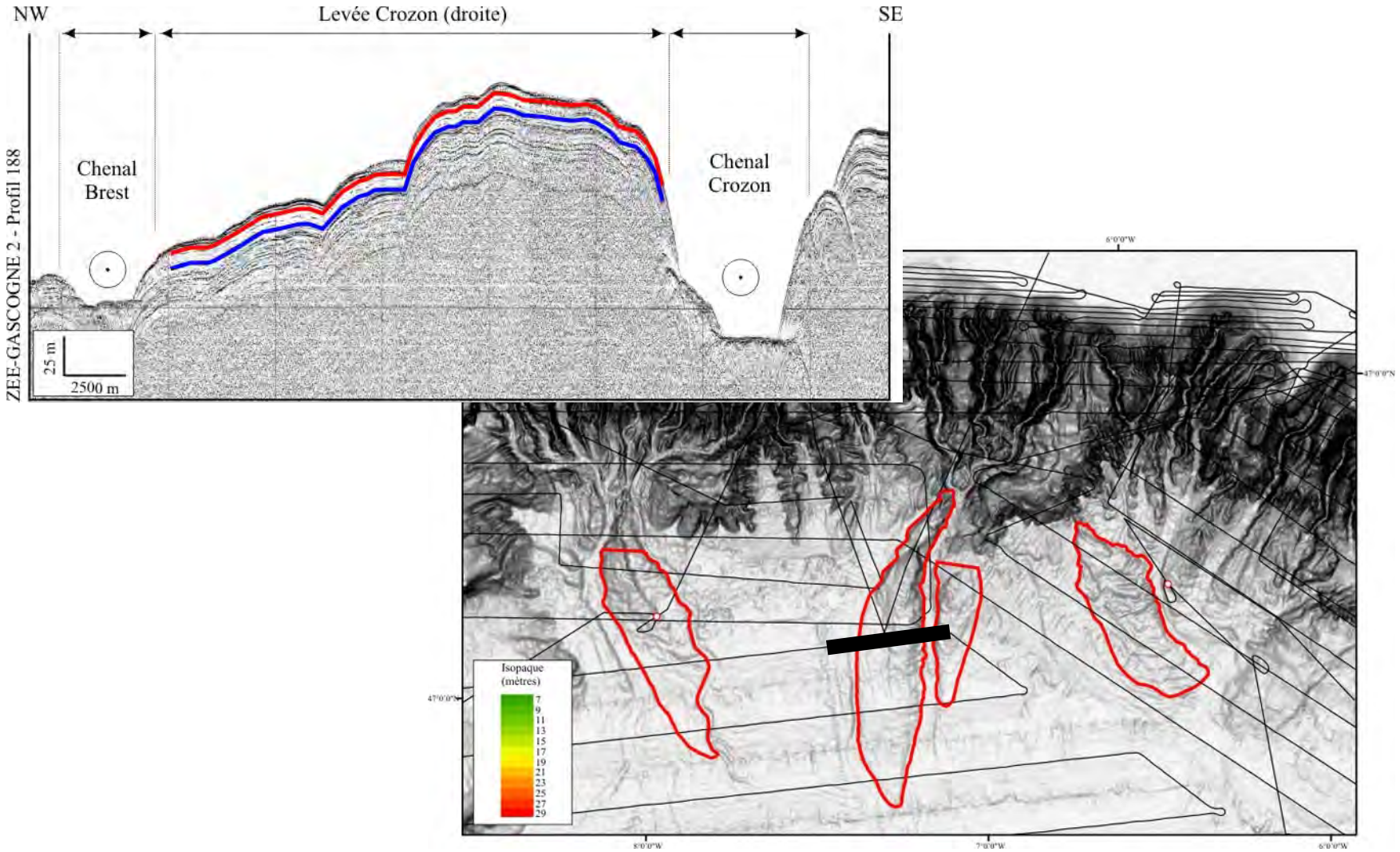

Toucanne et al 2010

Estimation de la masse déposée dans les levées turbiditique : Mt

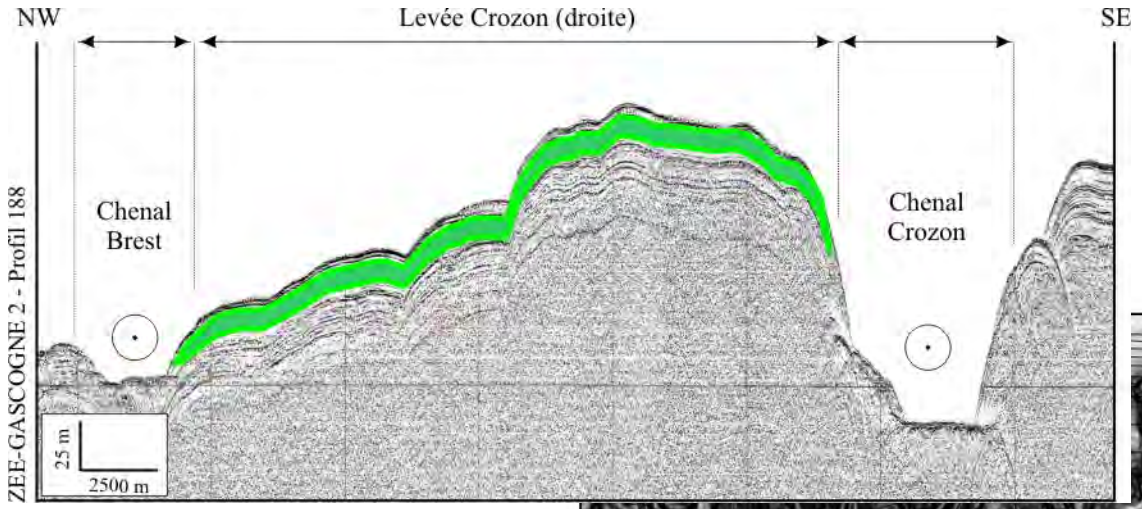

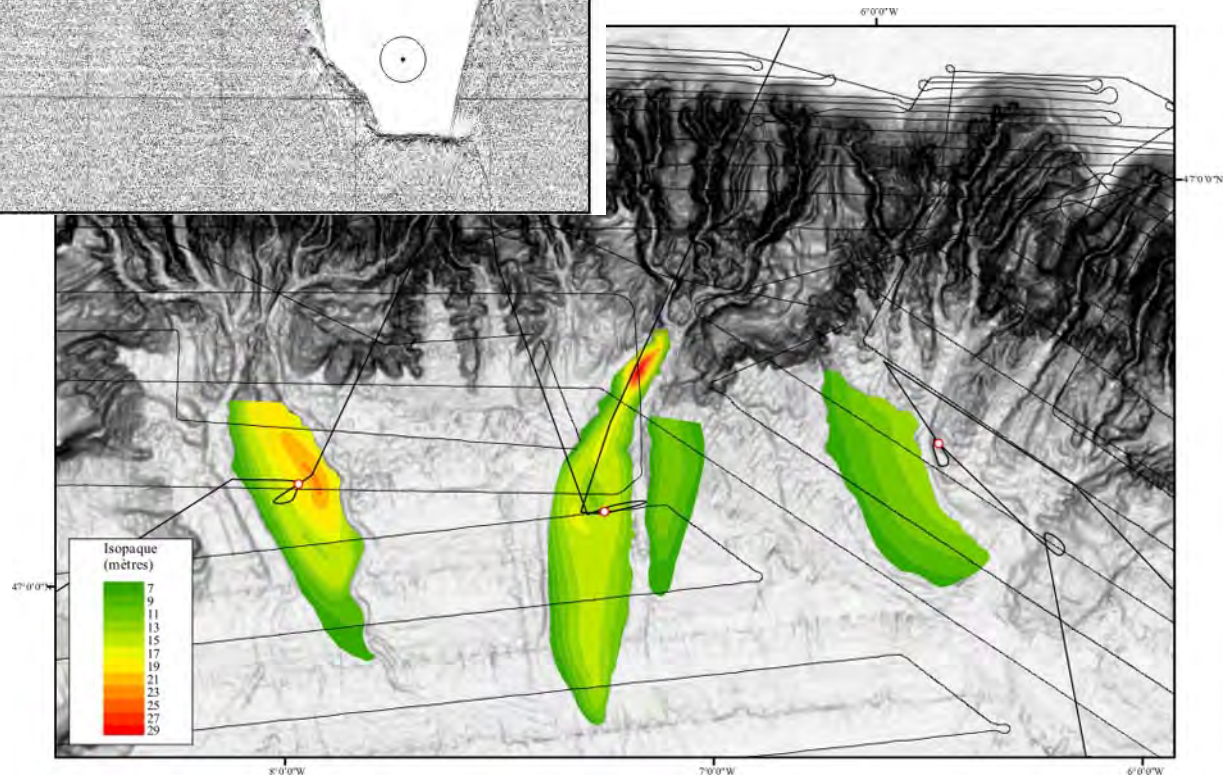

Entre -16 000 et -24 000 ans

$$8\ Gt < Mt_{16\text{-}24} < 14\ Gt$$

Toucanne et al 2010

Estimation de la masse hémipélagique : $Mh_{16\text{-}24}$

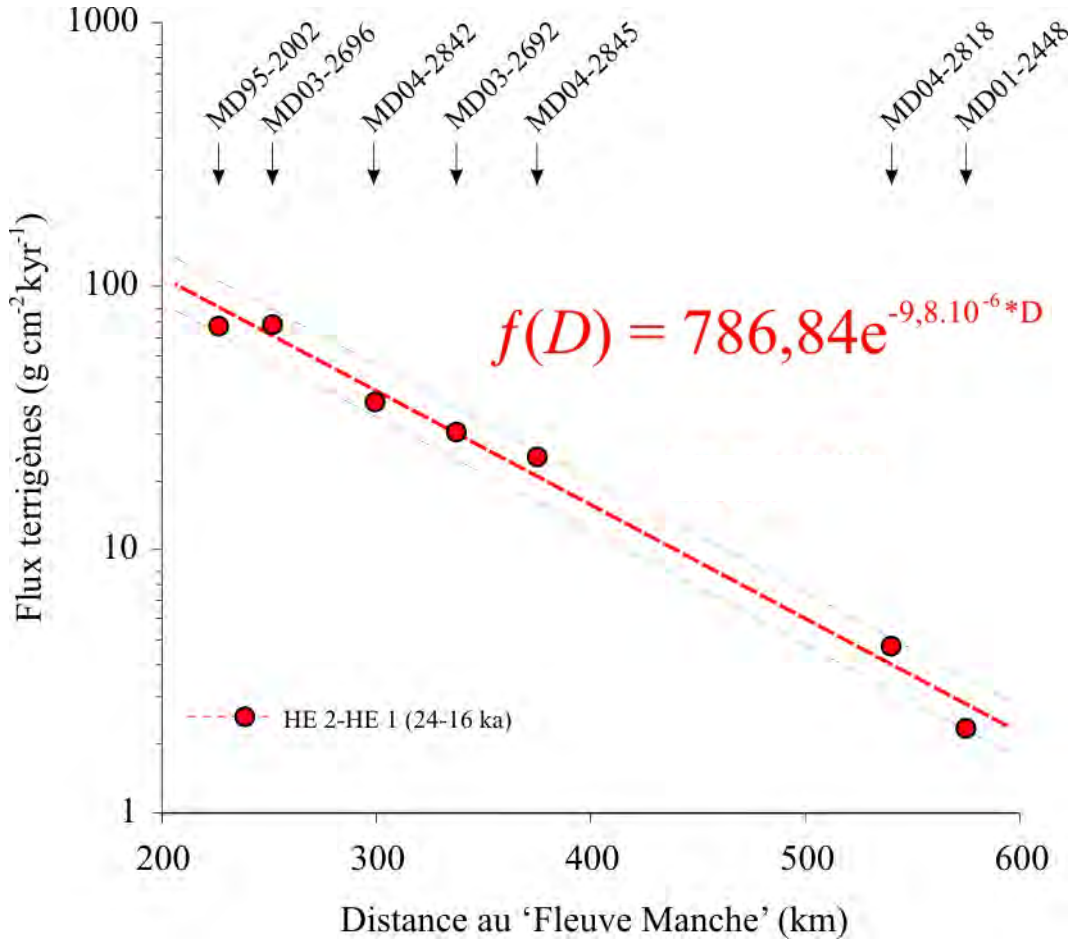

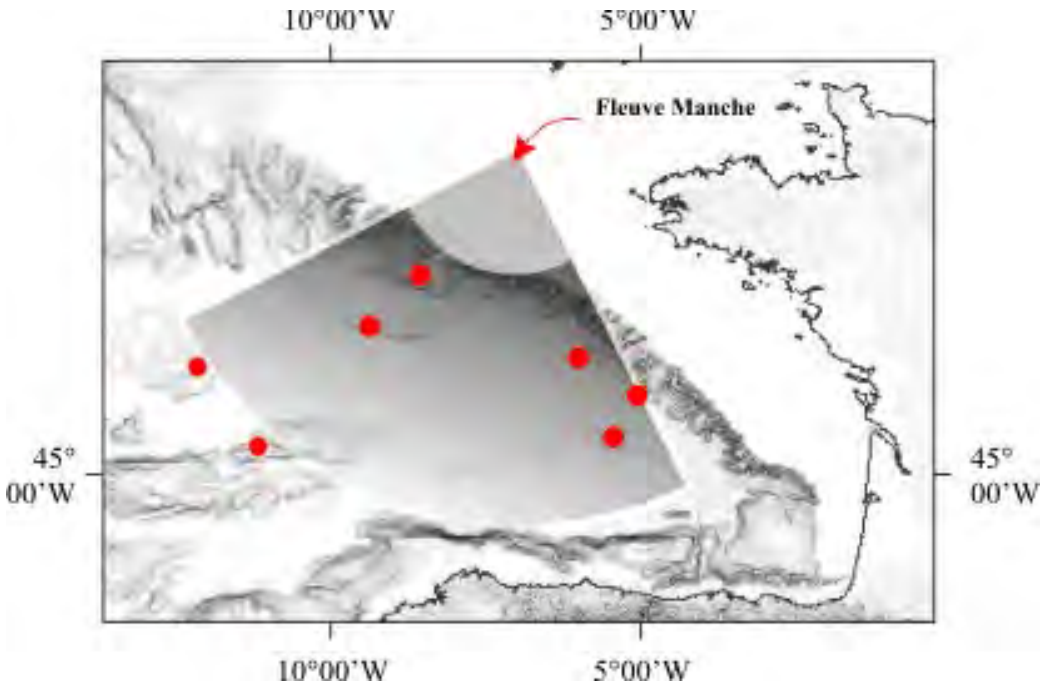

Entre -16 000 et -24 000 ans

414 Gt < $Mh_{16\text{-}24}$ < 504 Gt

Toucanne et al 2010

Estimation globale (Mh + Mt)
entre -24 000 & -16 000 ans

$8\ Gt < Mt_{16\text{-}24} < 14\ Gt$

$414\ Gt < Mh_{16\text{-}24} < 504\ Gt$

$422\ Gt < M_{16\text{-}24} < 528\ Gt$

Décharge solide (Ds)

$56.10^6\ t.an^{-1} < Ds < 67.10^6\ t.an^{-1}$

Actuellement : Loire + Gironde + Vilaine + Charente + Adour = $2.10^6\ t.an^{-1}$ (Jouanneau et al., 1999)

Dépôts turbiditiques$_{16\text{-}24}$ = 2 % de la sédimentation

Dépôts hémipélagiques$_{16\text{-}24}$ = 98 % de la sédimentation

Toucanne et al 2010

1. Sédimentation gravitaire – turbiditique

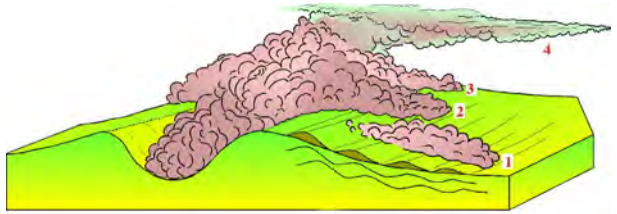

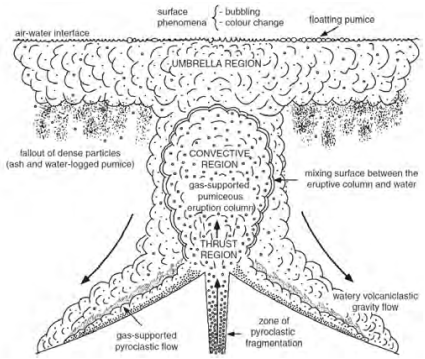

2. Sédimentation volcanoclastique

3. Sédimentation pélagique et hémipélagique

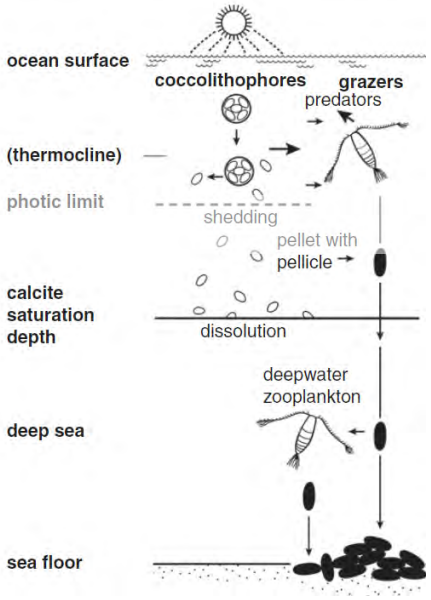

4. Sédimentation glaci-marine

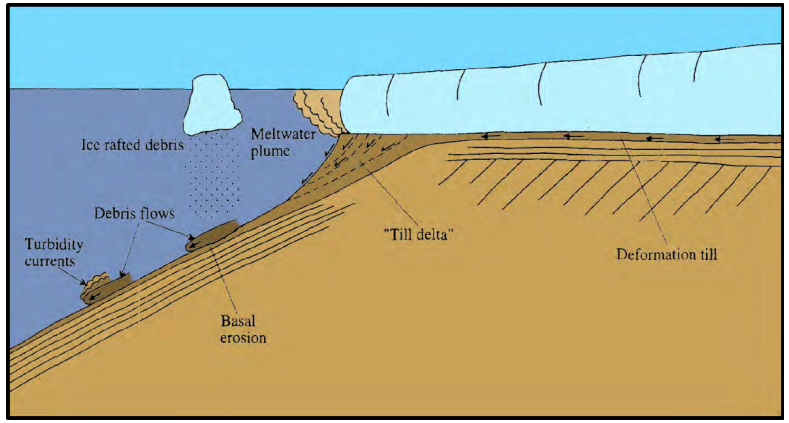

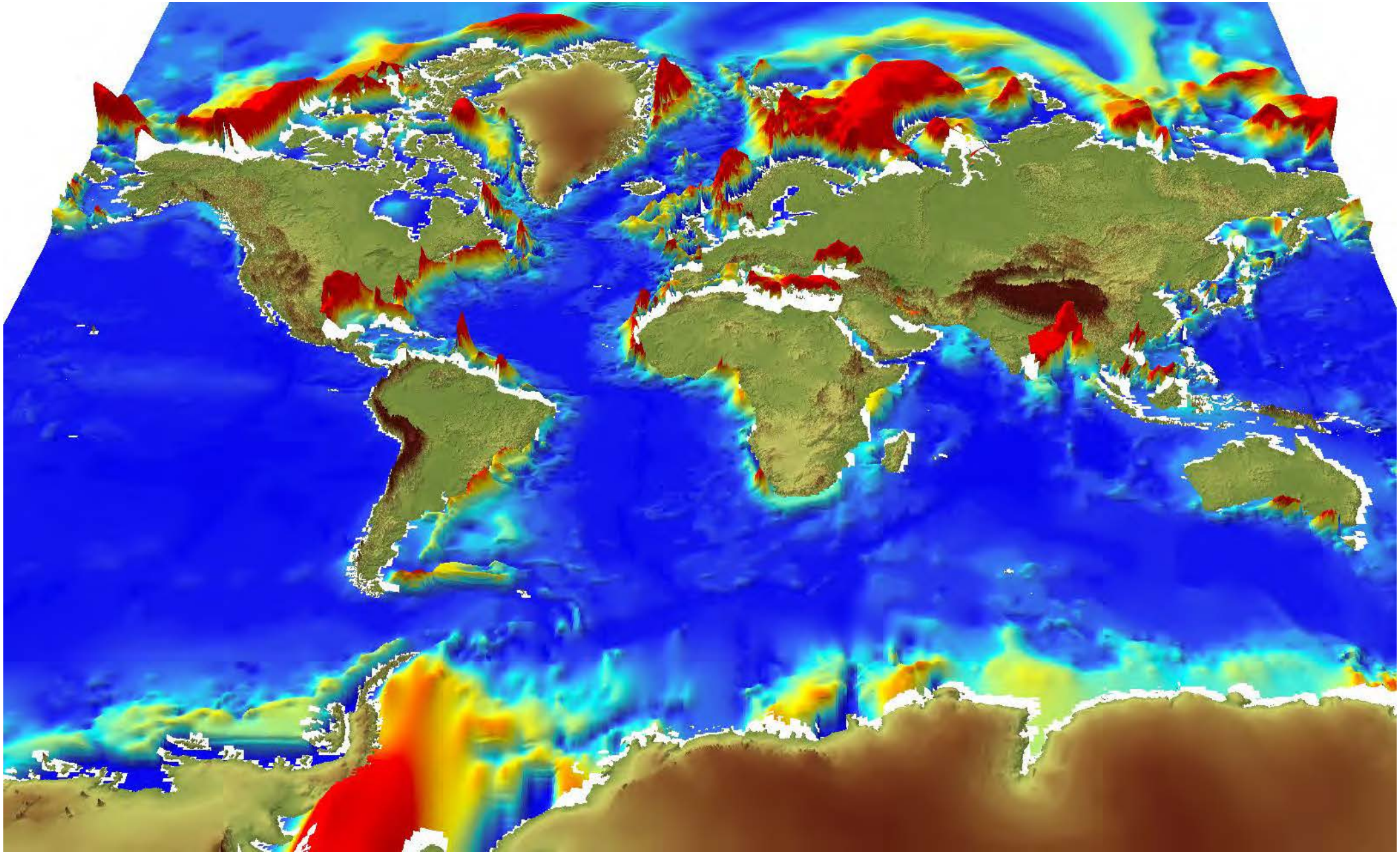

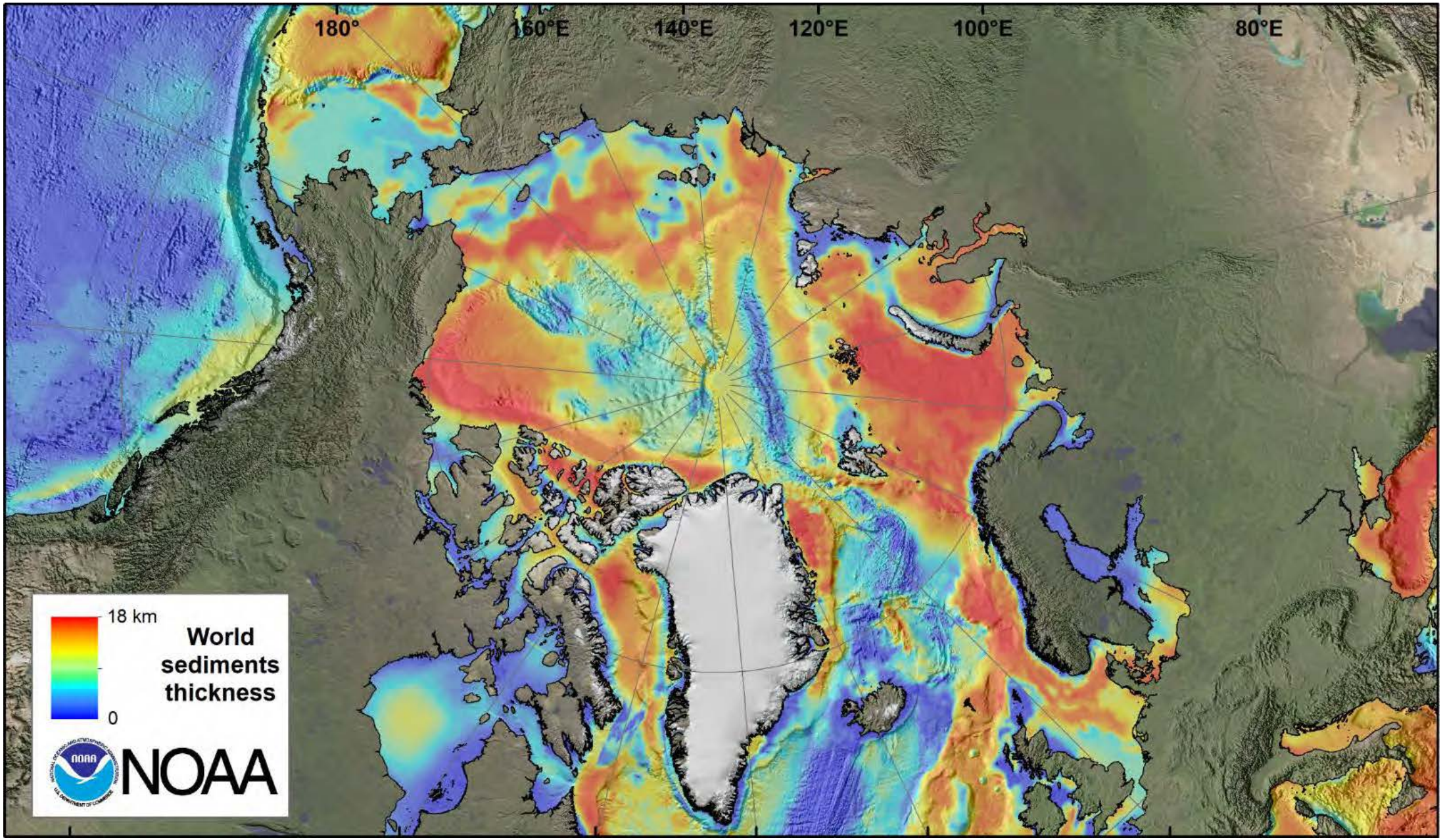
180°
160°E
140°E
120°E
100°E
80°E
18 km
0
World sediments thickness
NOAA

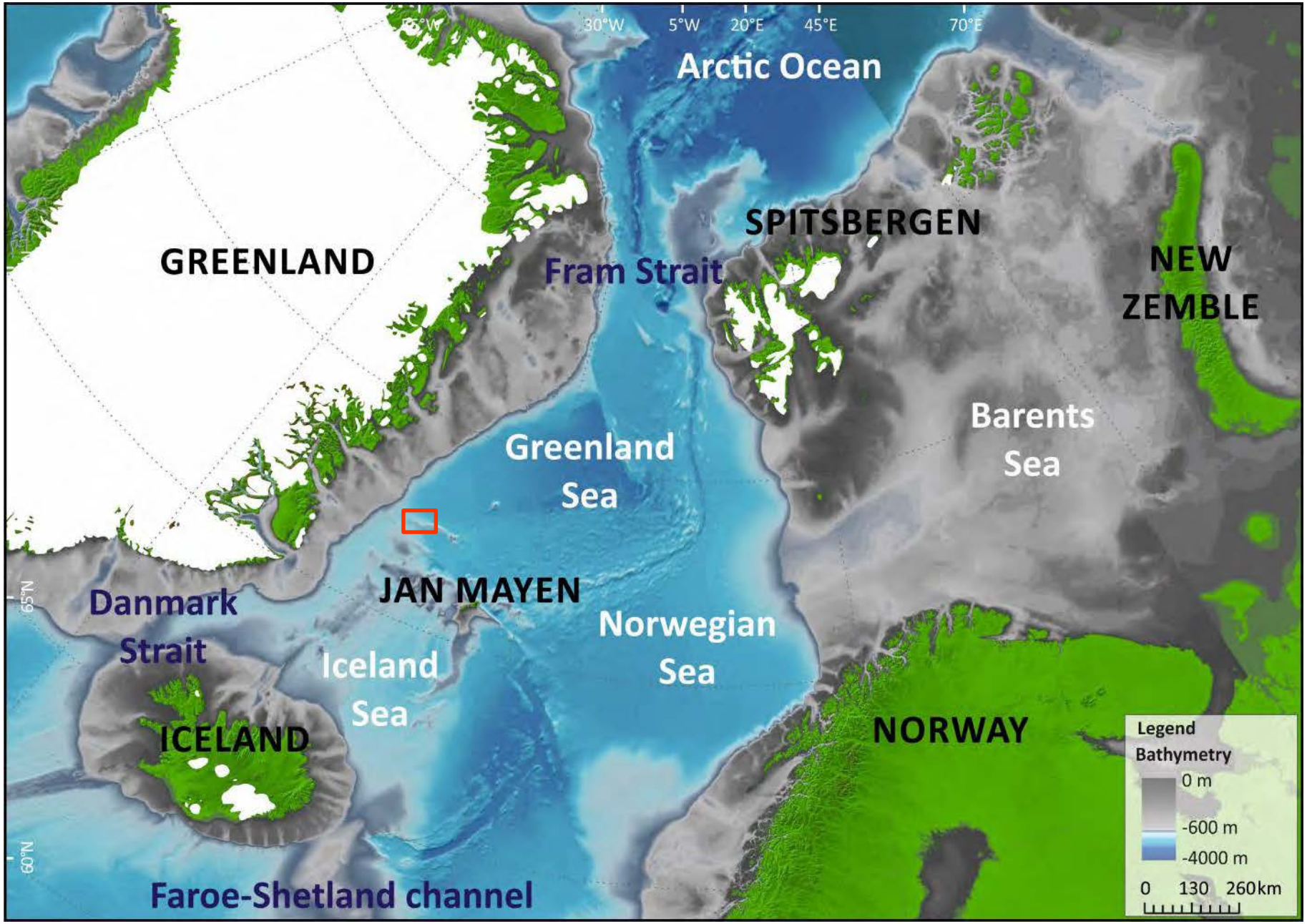

Marjolaine Sabine thèse en cours

4. Sédimentation glaci-marine : la marge est-Groenlandaise

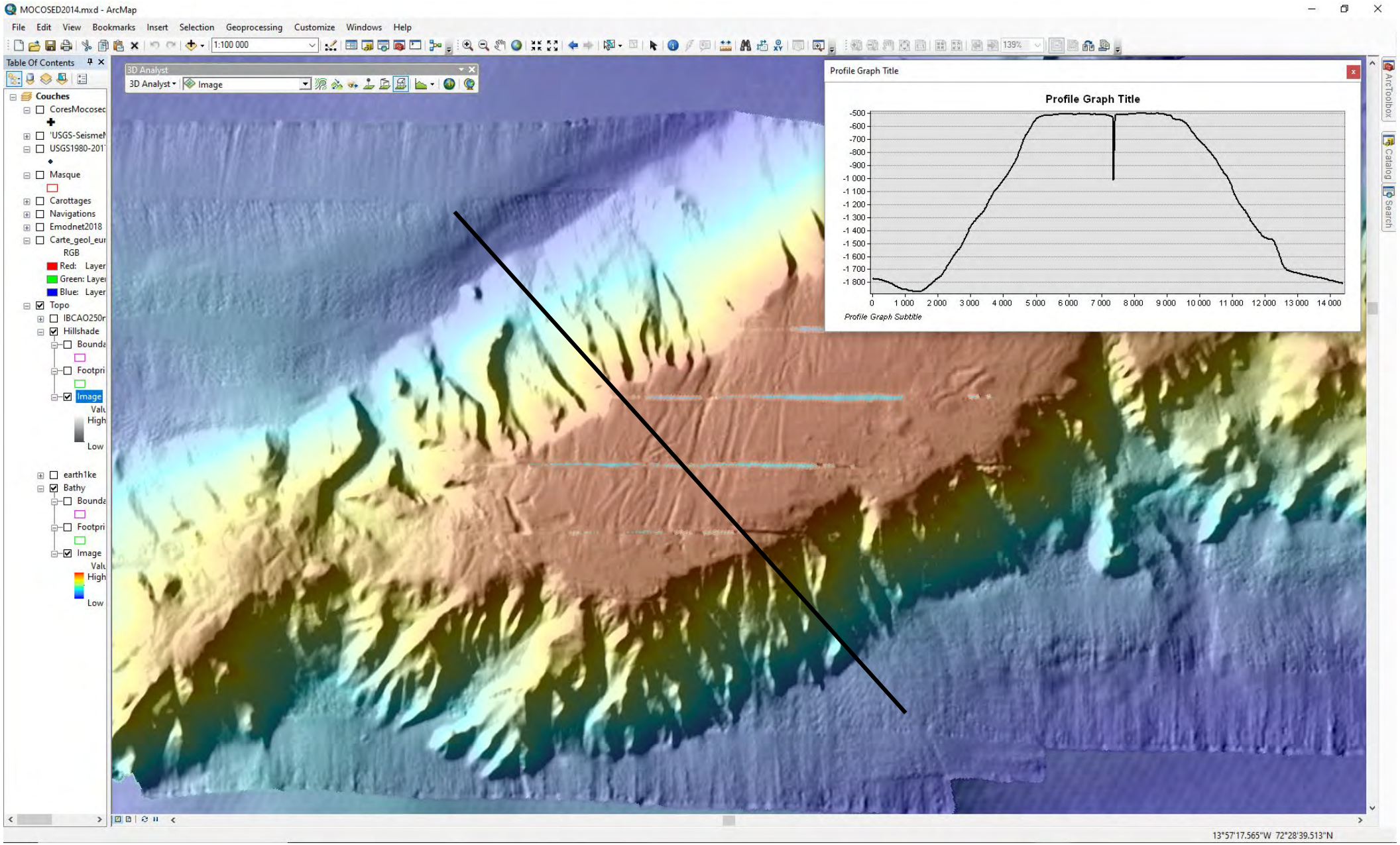

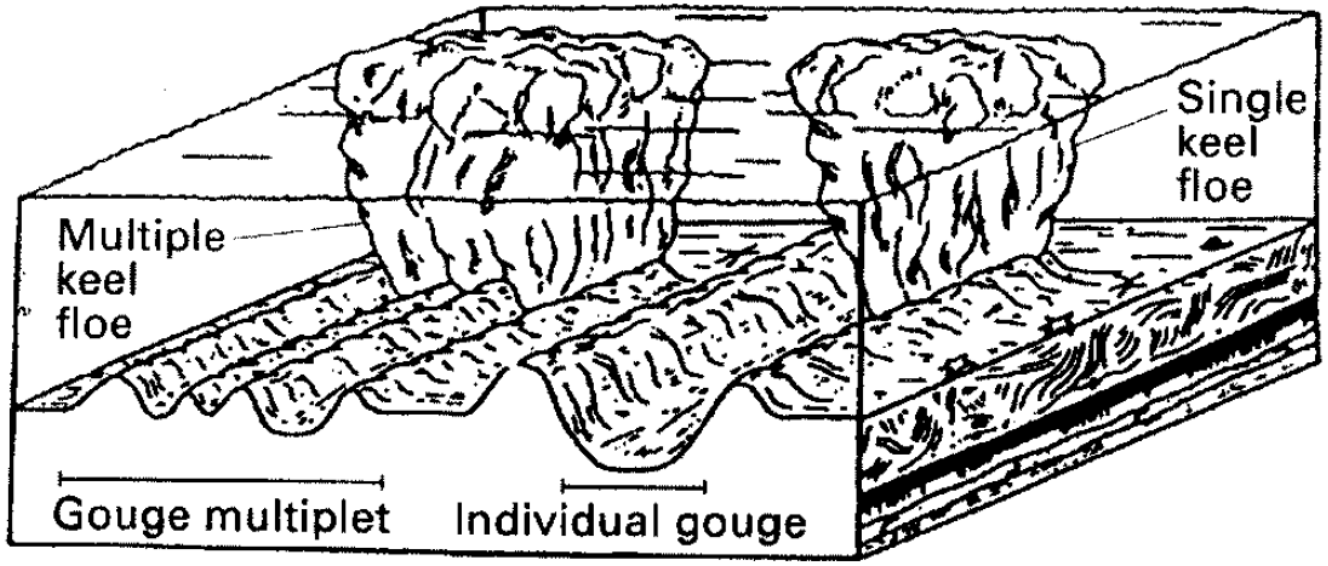

Figure 11.15 Scouring by single and multiple keel icebergs (floes) to produce an idealized ice gouge and gouge multiplet (from Barnes, Rearic & Reimnitz, 1984).

Iceberg plough-marks

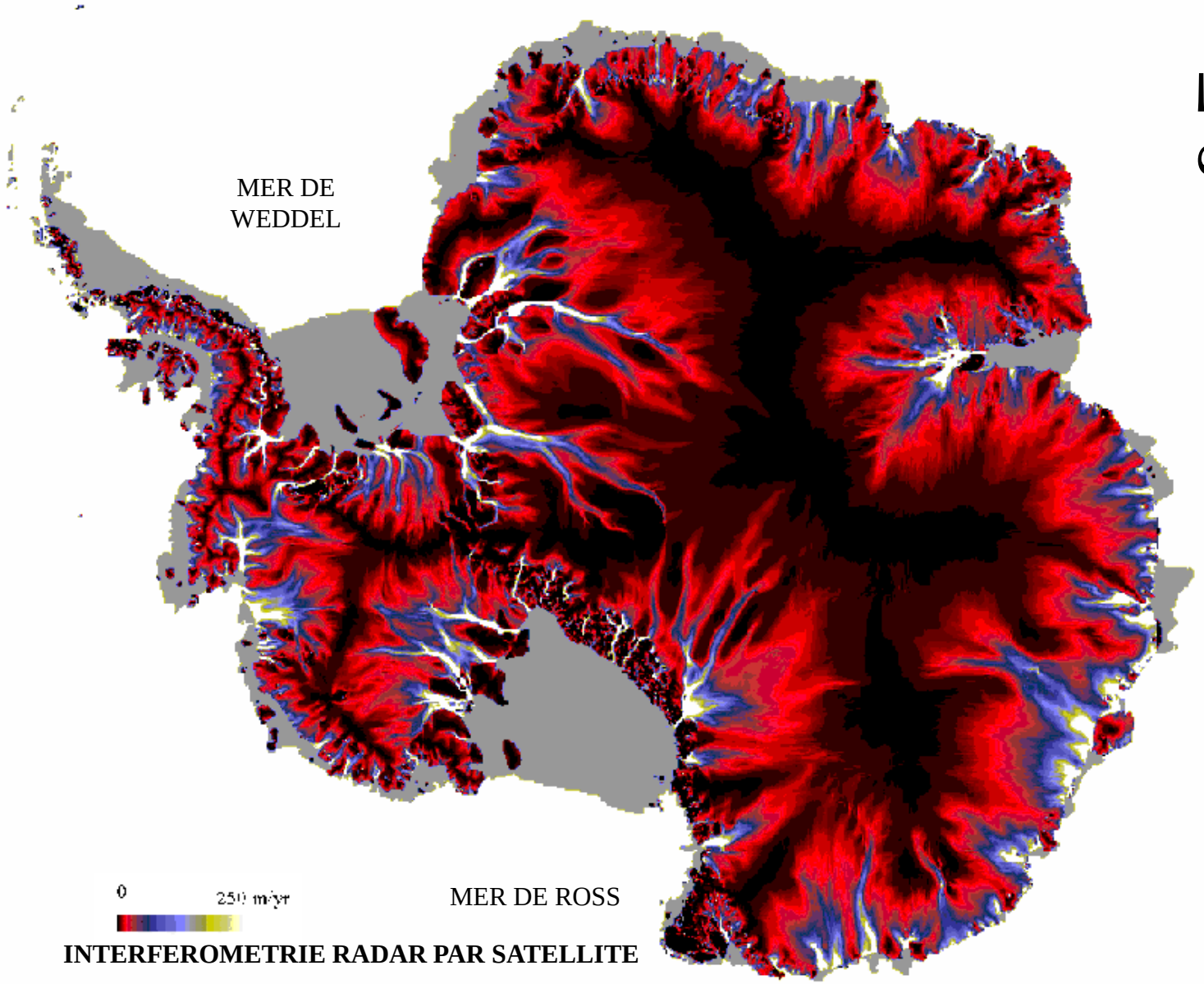

Shepherd et al. 2001

Ice streams : les couloirs d'écoulements glaciaires

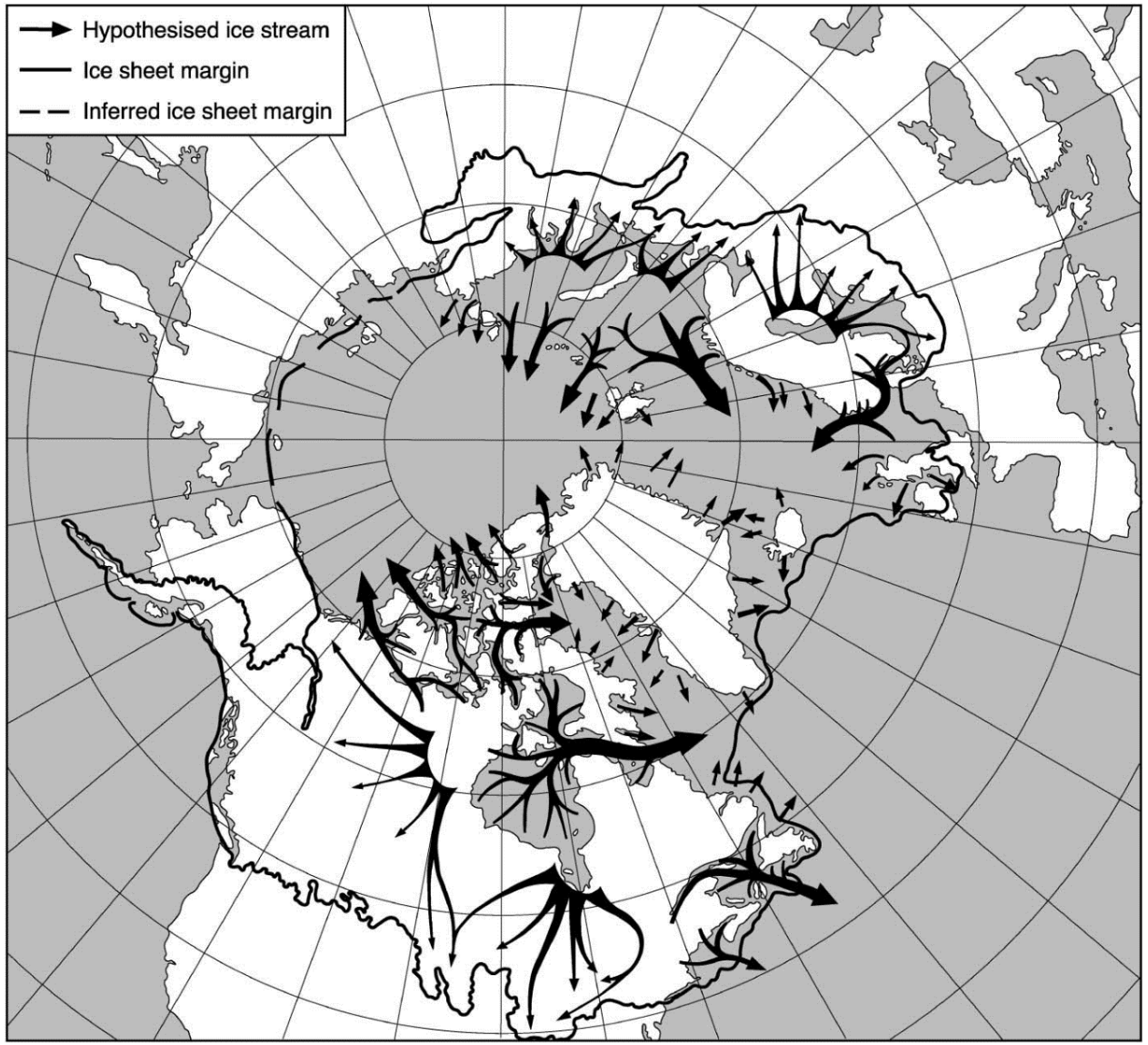

Ice streams au dernier maximum glaciaire

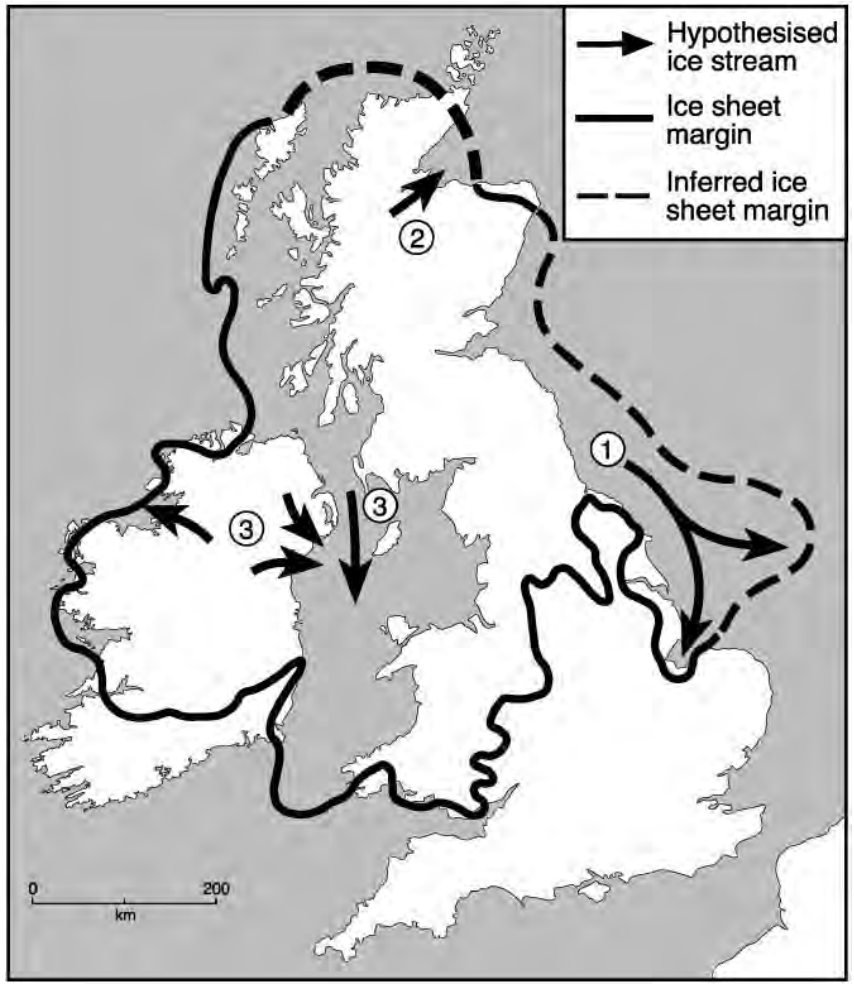

Denton, G. H. and Hughes, T. J. (Eds.): The Last Great Ice Sheets, Wiley, New York, 484 pp., 1981.

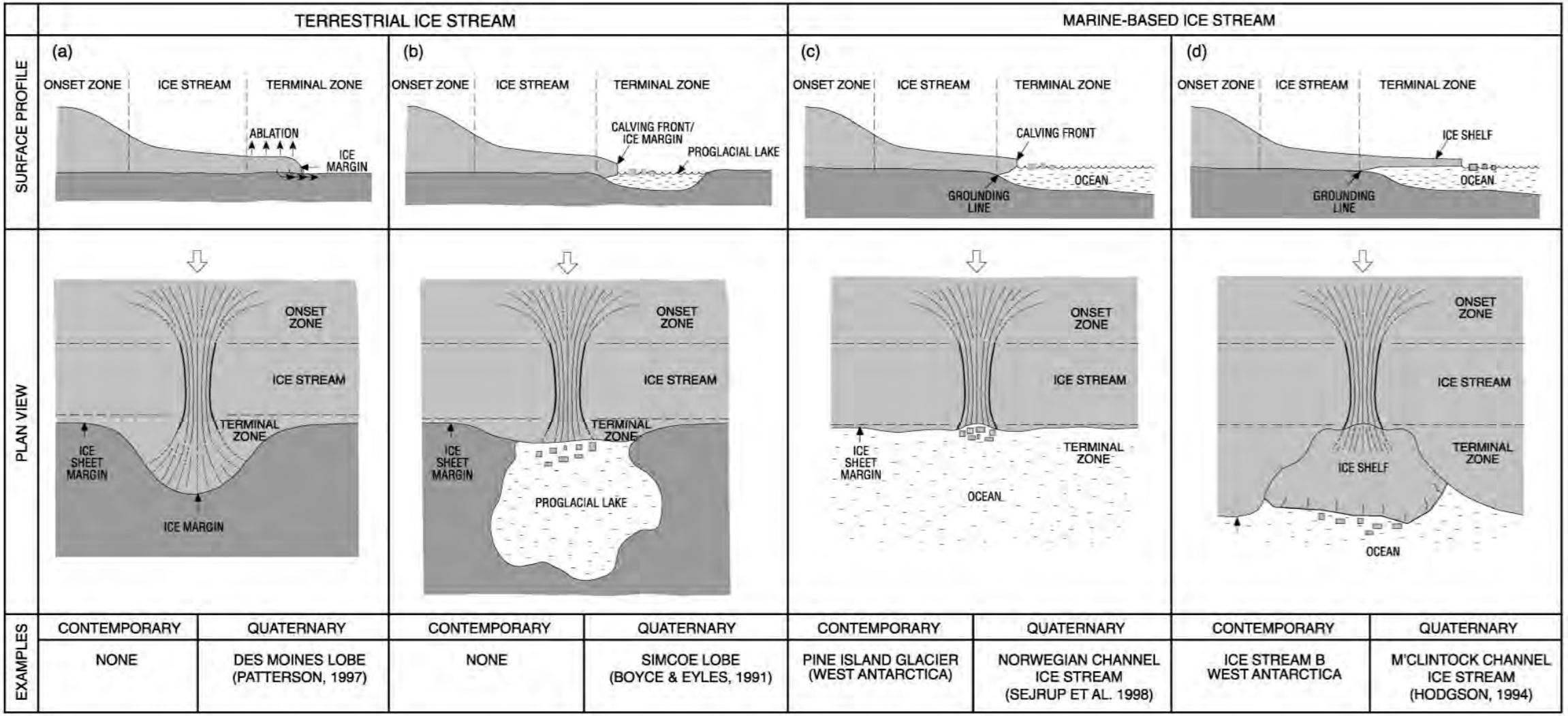

Fig. 7. Conceptual configurations of terrestrial and marine-based ice streams and contemporary and palaeo examples. Some terrestrial ice streams terminate on land and have no way of rapidly removing ice. Margin advance produces splayed lobes which lowers the surface elevation of the ice sheet, enhancing ablation, see (a). Other terrestrial ice streams may drain into proglacial lakes and discharge their huge ice flux in the form of icebergs. This configuration is shown in (b). All contemporary ice streams are marine based and can be broadly classified as those which drain into open water (c) and those which feed ice shelves (d).

Stokes et al , 2001


Hagavatn, Langjökull - Islande

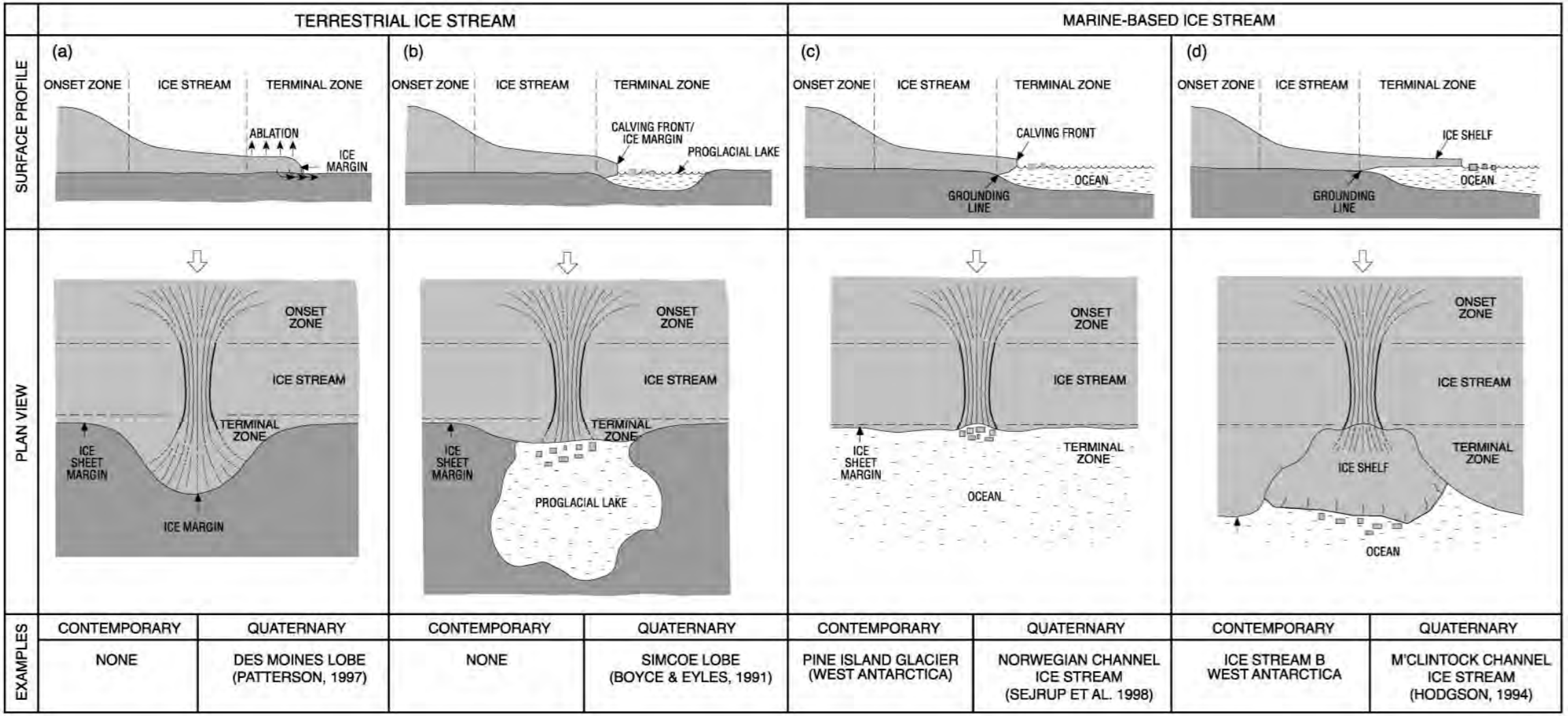

Fig. 7. Conceptual configurations of terrestrial and marine-based ice streams and contemporary and palaeo examples. Some terrestrial ice streams terminate on land and have no way of rapidly removing ice. Margin advance produces splayed lobes which lowers the surface elevation of the ice sheet, enhancing ablation, see (a). Other terrestrial ice streams may drain into proglacial lakes and discharge their huge ice flux in the form of icebergs. This configuration is shown in (b). All contemporary ice streams are marine based and can be broadly classified as those which drain into open water (c) and those which feed ice shelves (d).

Stokes et al , 2001


Jökulsárlón, Vatnajökull - Islande


Jökulsárlón, Vatnajökull - Islande


Jökulsárlón, Vatnajökull - Islande

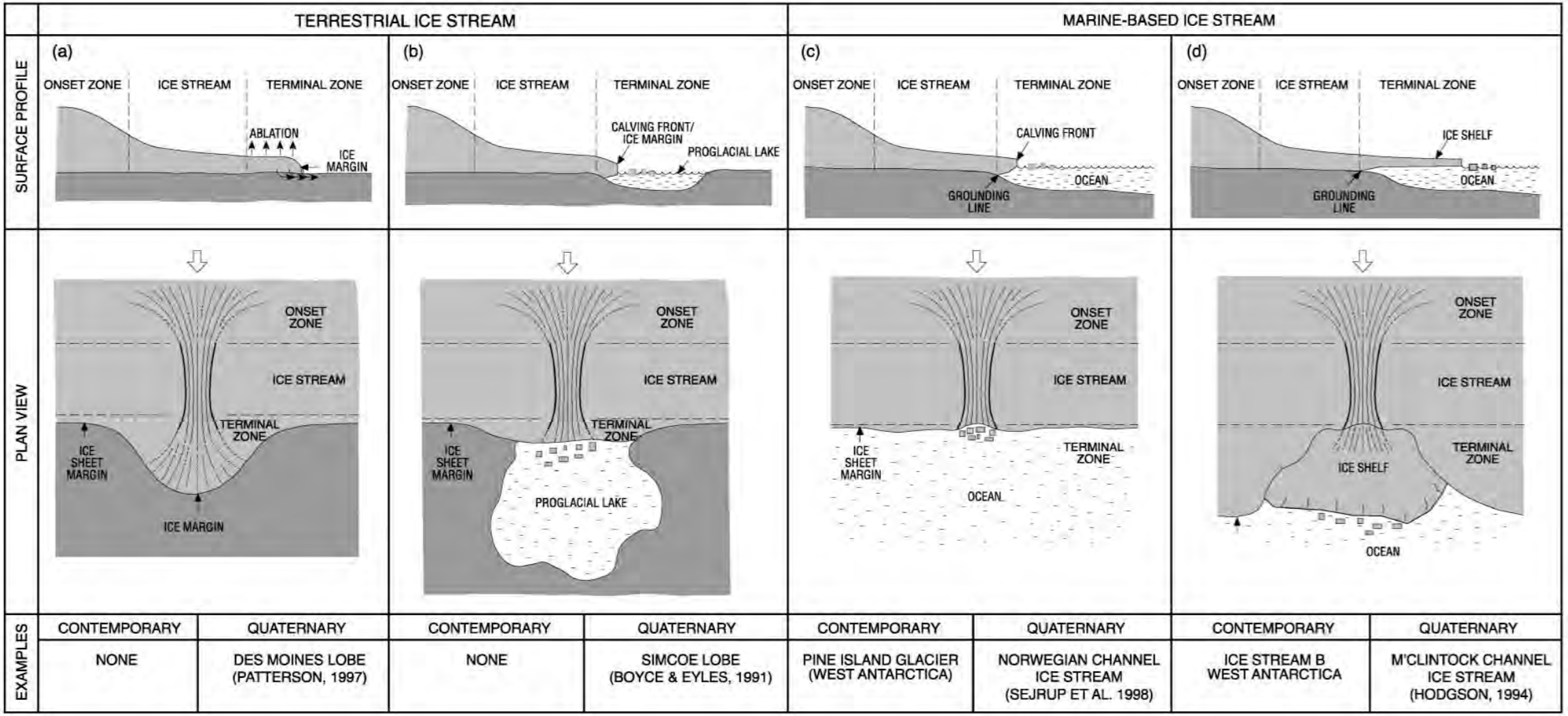

Fig. 7. Conceptual configurations of terrestrial and marine-based ice streams and contemporary and palaeo examples. Some terrestrial ice streams terminate on land and have no way of rapidly removing ice. Margin advance produces splayed lobes which lowers the surface elevation of the ice sheet, enhancing ablation, see (a). Other terrestrial ice streams may drain into proglacial lakes and discharge their huge ice flux in the form of icebergs. This configuration is shown in (b). All contemporary ice streams are marine based and can be broadly classified as those which drain into open water (c) and those which feed ice shelves (d).

Stokes et al , 2001

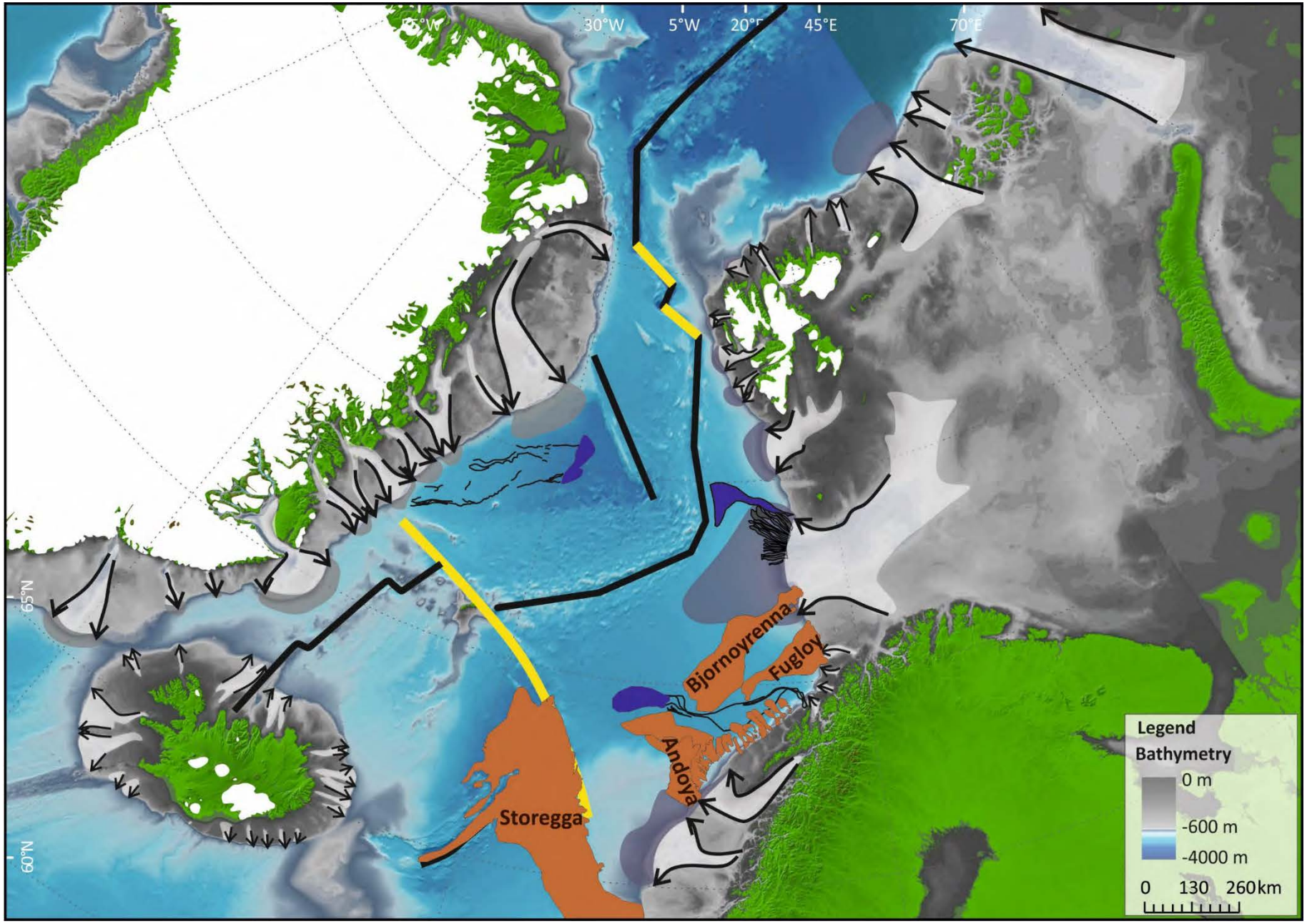

Marjolaine Sabine thèse en cours

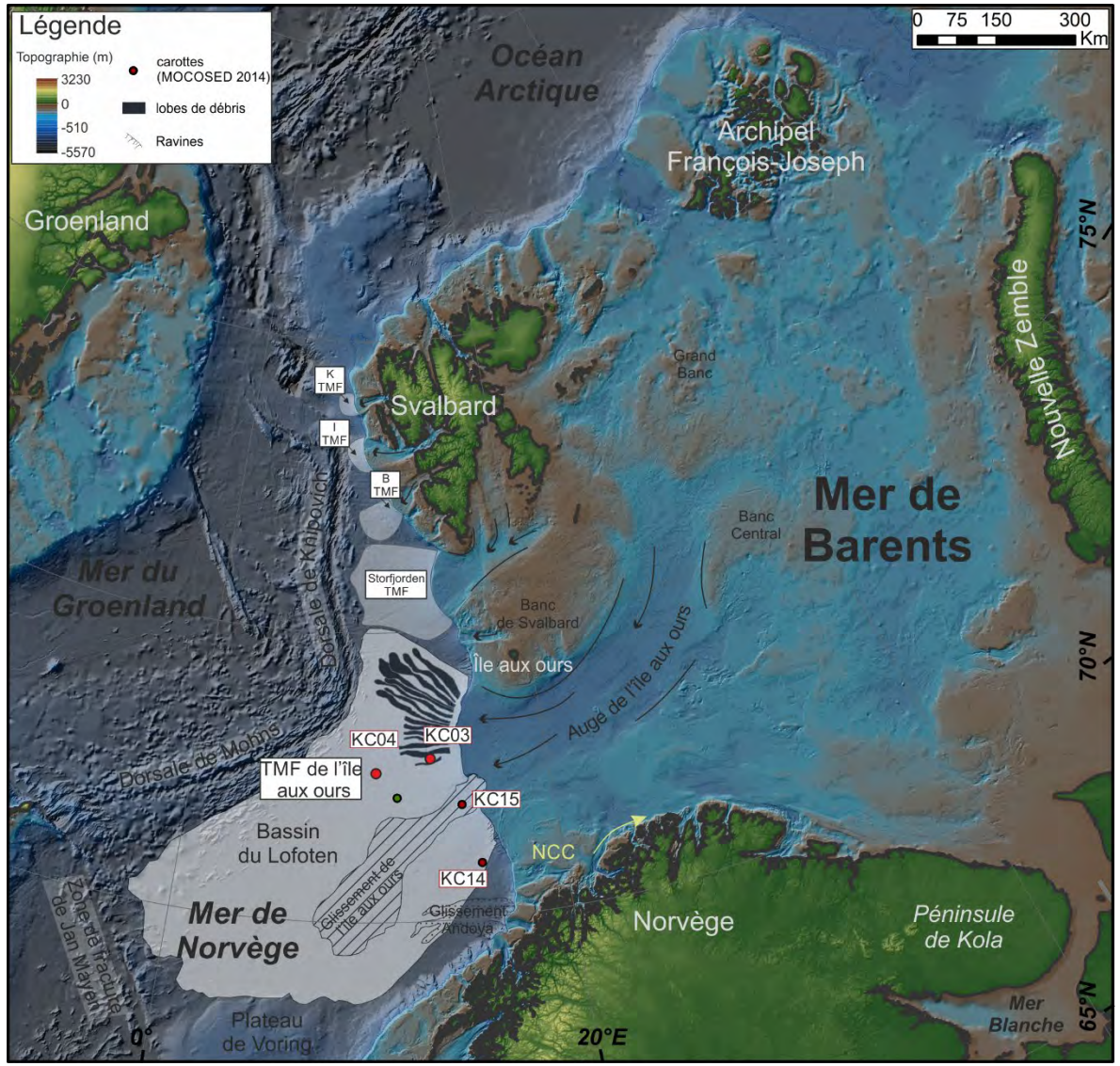

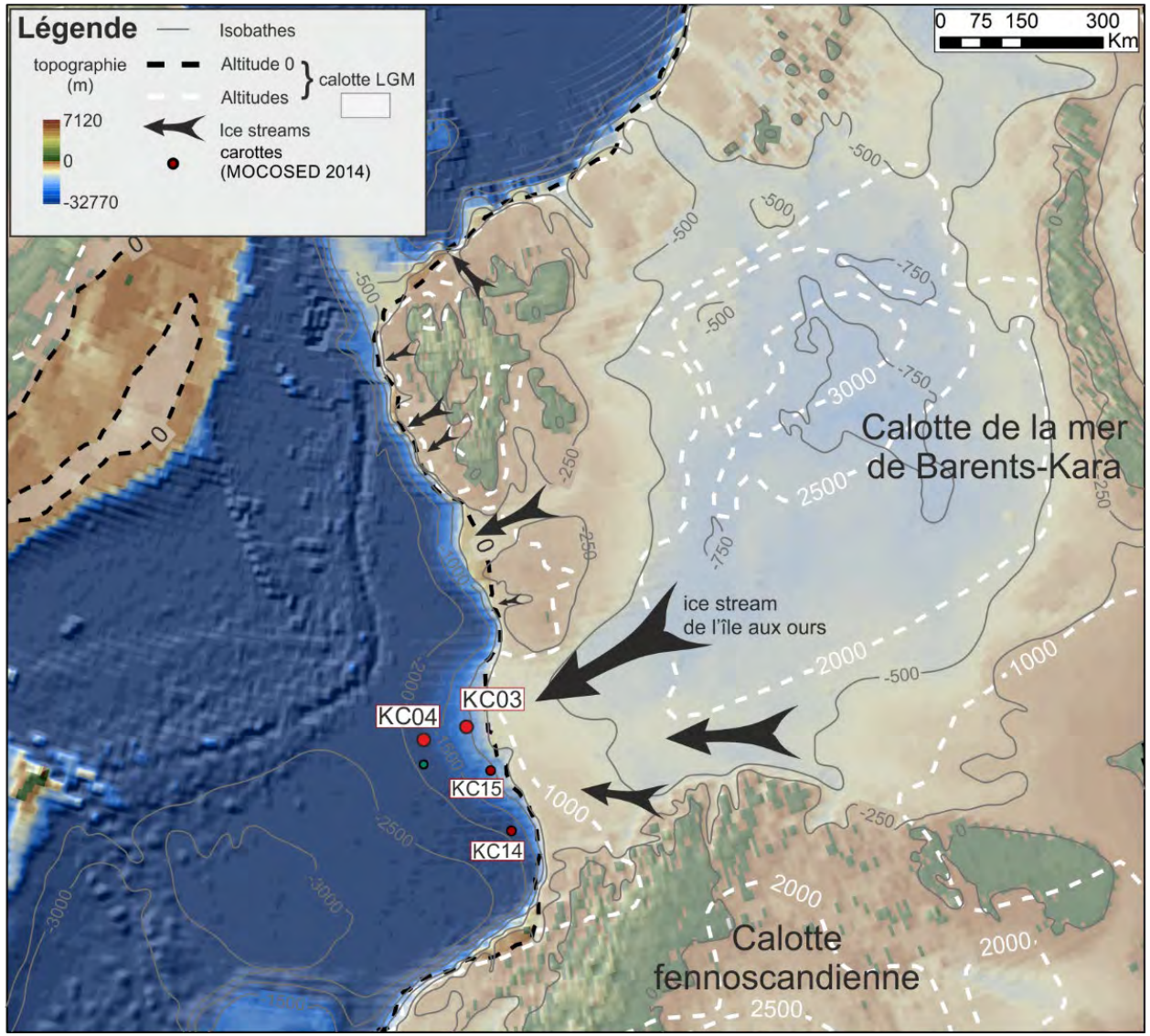

Chloé Siebert, 2015. Histoire sédimentaire du Sud-ouest de la mer de Barents au cours des derniers 40 000 ans. Master 2 Université de Bordeaux.

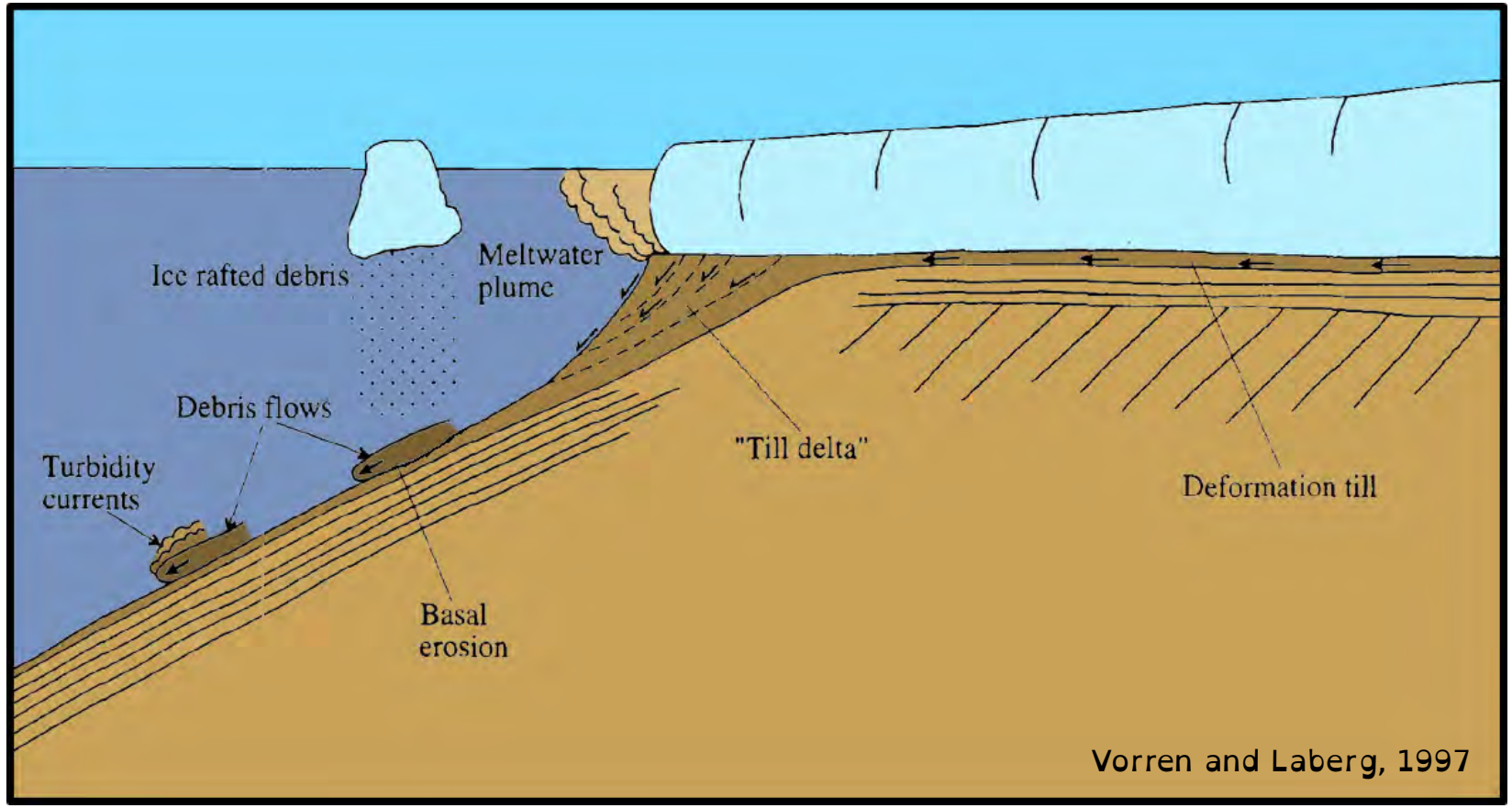

Vorren and Laberg, 1997

Till : Sédiments transportés et déposés par les glaciers.

Diamicton : sédiment constitués de particules grossières (sables à graviers) inclues dans une matrice fine.

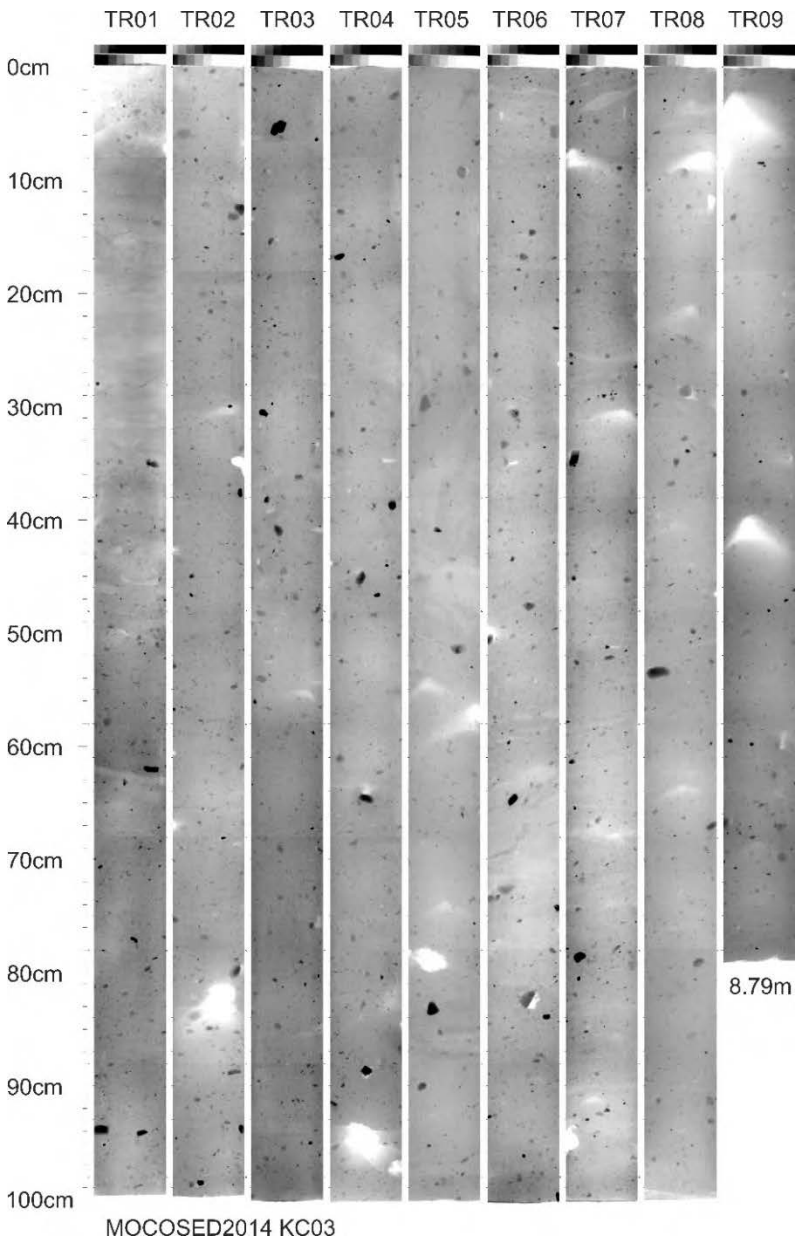

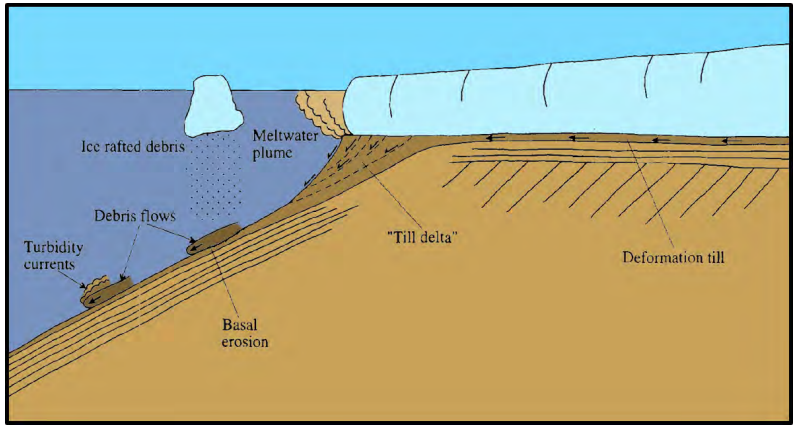

Diamicton d'origine glaciaire :

IRD dans une matrice argileuse

Chloé Siebert, 2015. Histoire sédimentaire du Sud-ouest de la mer de Barents au cours des derniers 40 000 ans. Master 2 Université de Bordeaux.

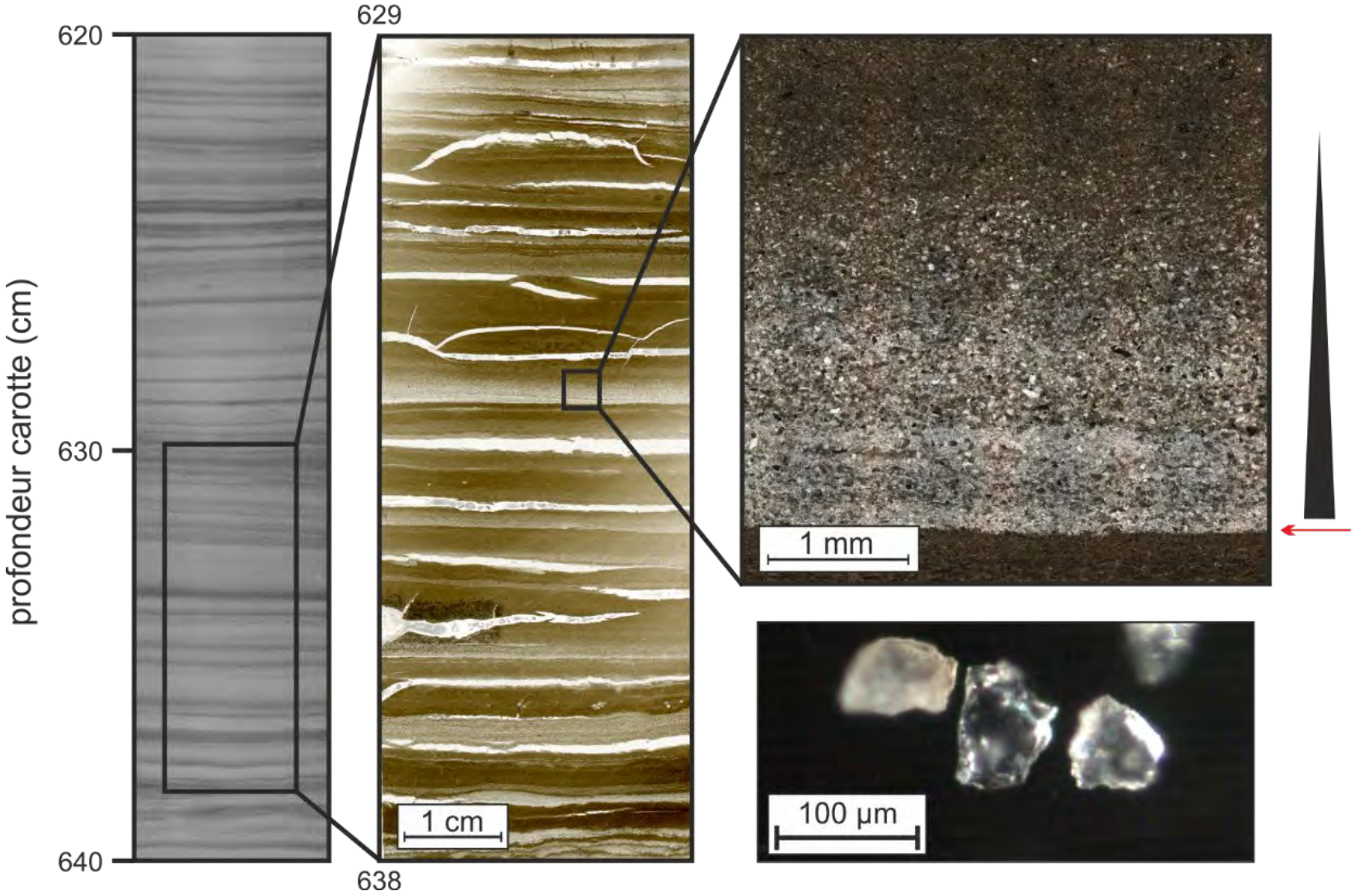

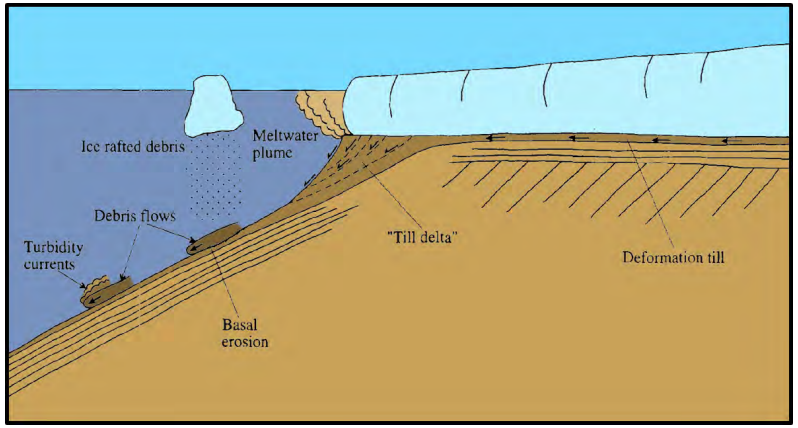

Dépôts turbiditiques

Chloé Siebert, 2015. Histoire sédimentaire du Sud-ouest de la mer de Barents au cours des derniers 40 000 ans. Master 2 Université de Bordeaux.

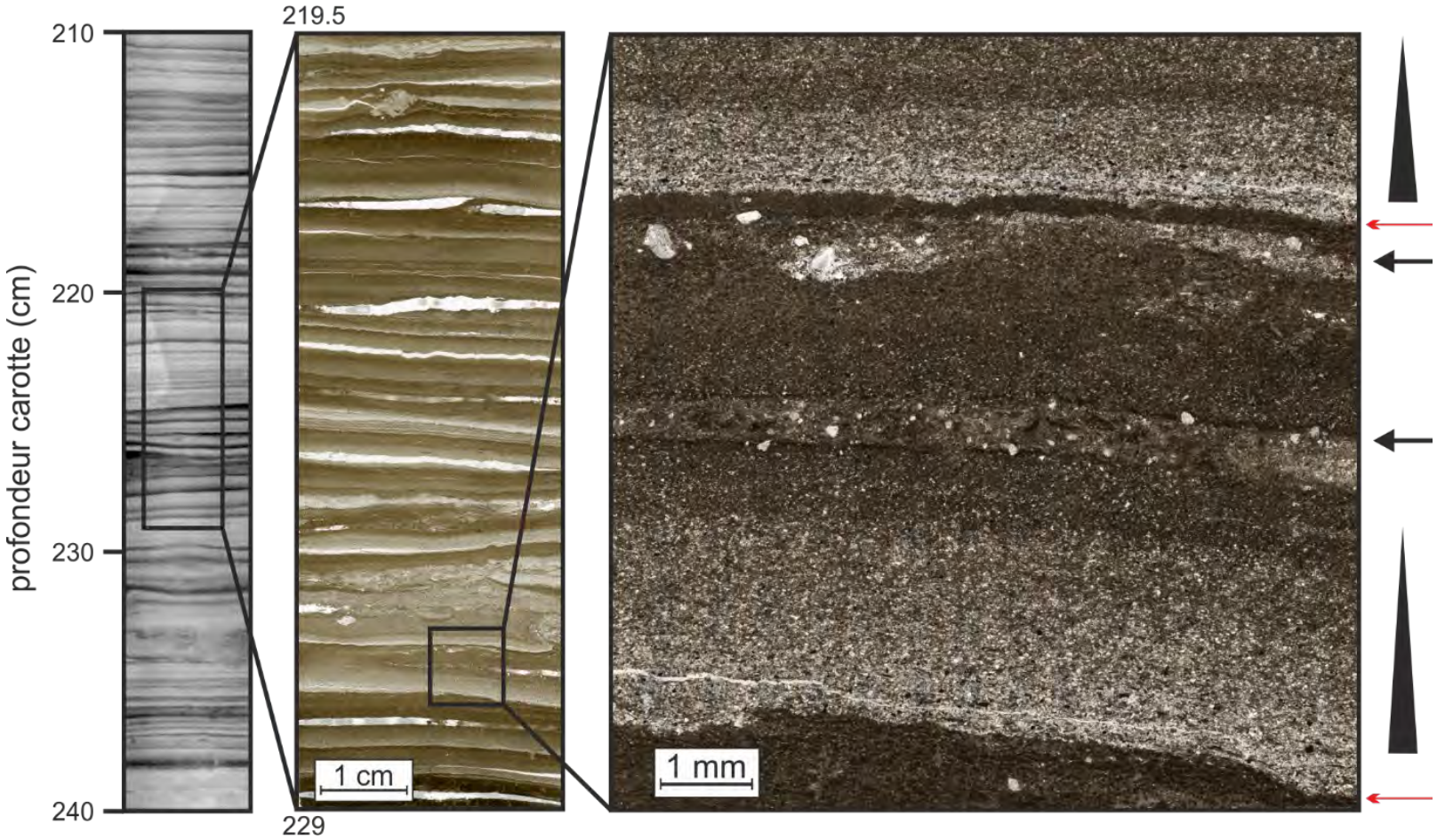

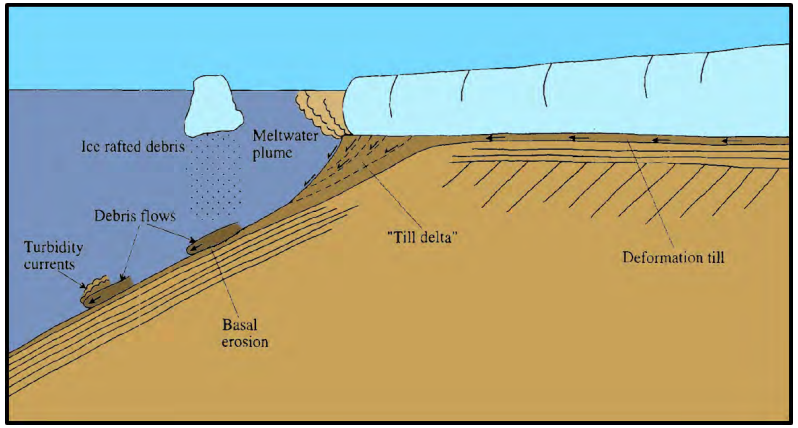

Dépôts turbiditiques & IRD

Chloé Siebert, 2015. Histoire sédimentaire du Sud-ouest de la mer de Barents au cours des derniers 40 000 ans. Master 2 Université de Bordeaux.

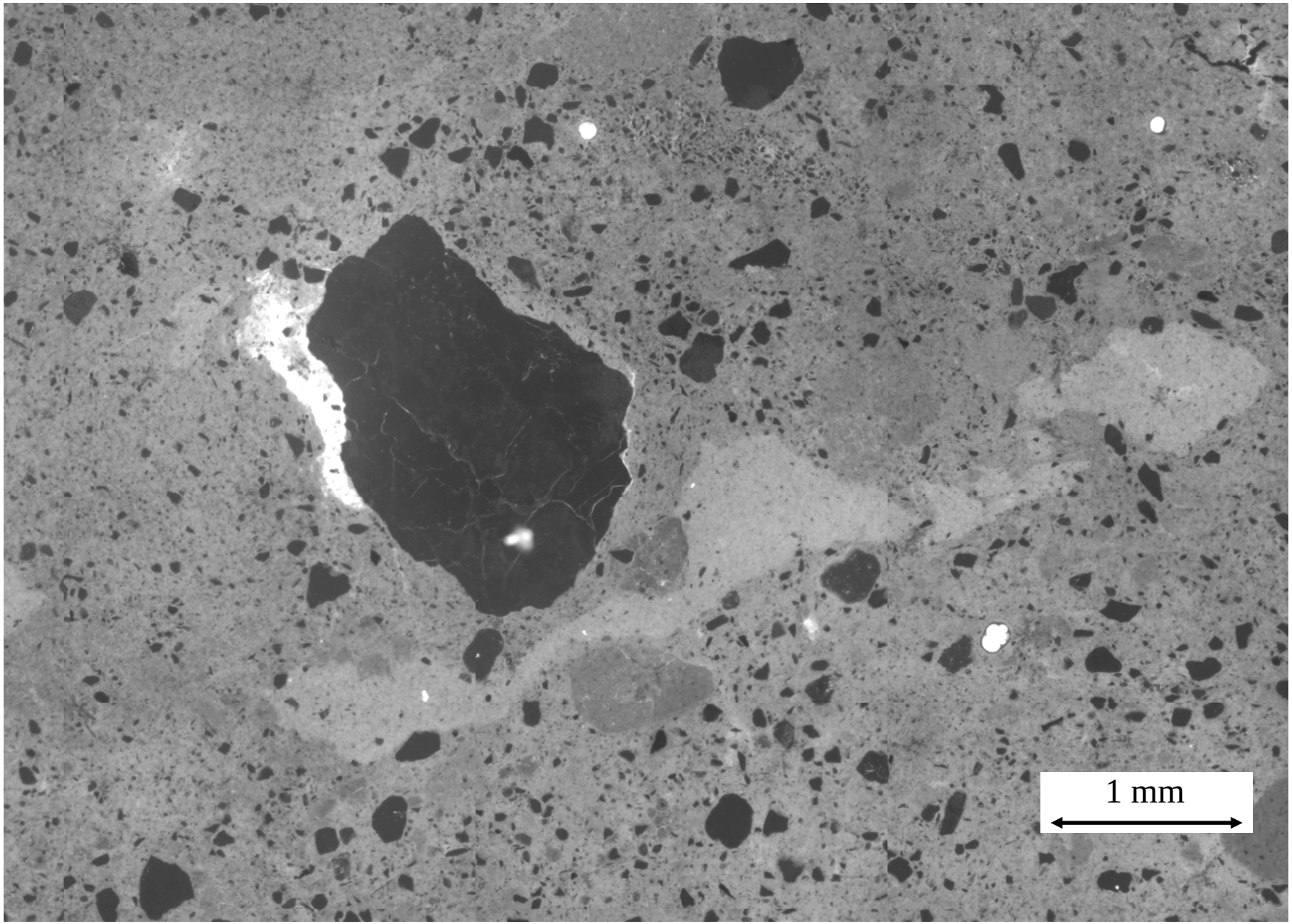
1 mm

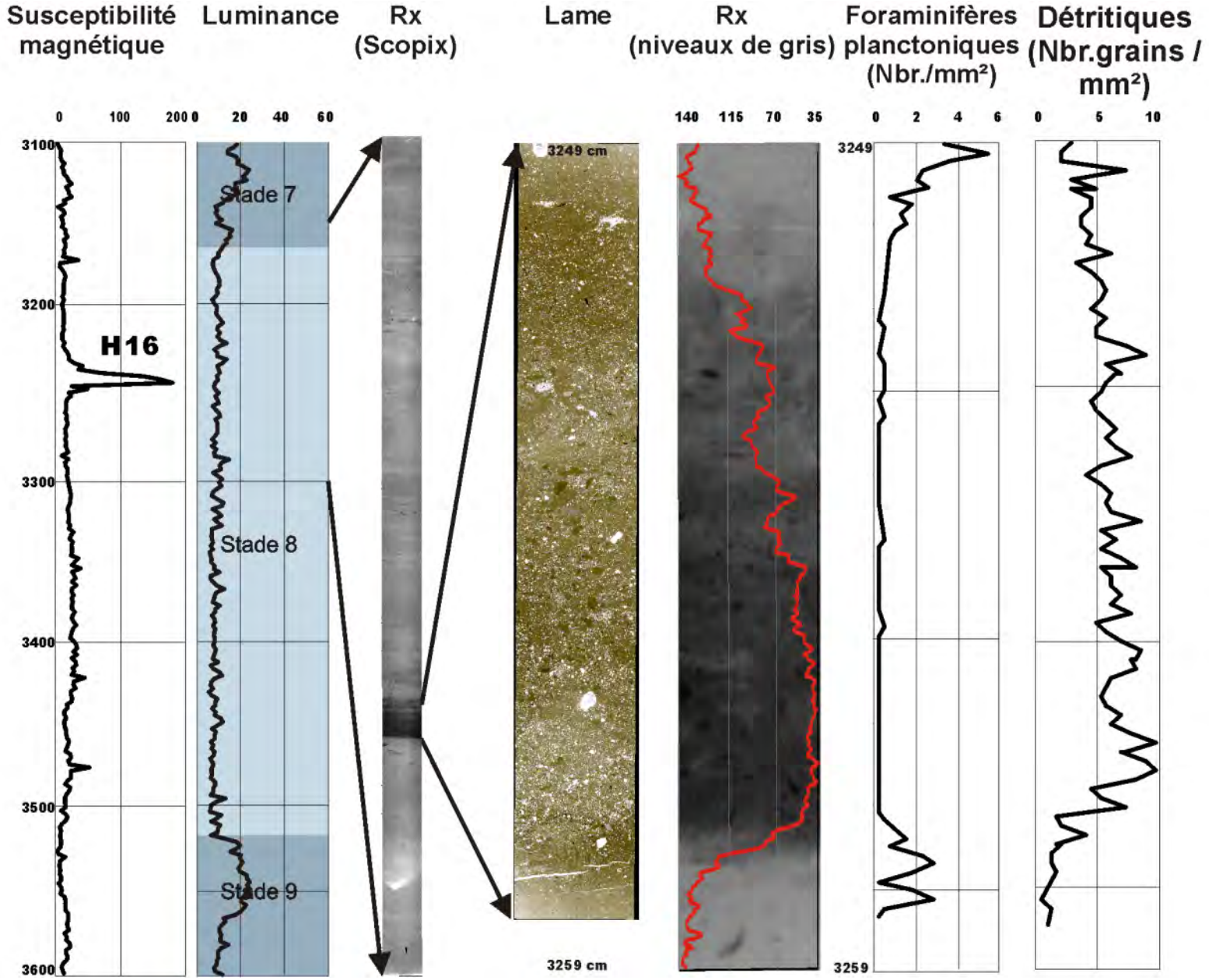

H16 env. 250 000 ans

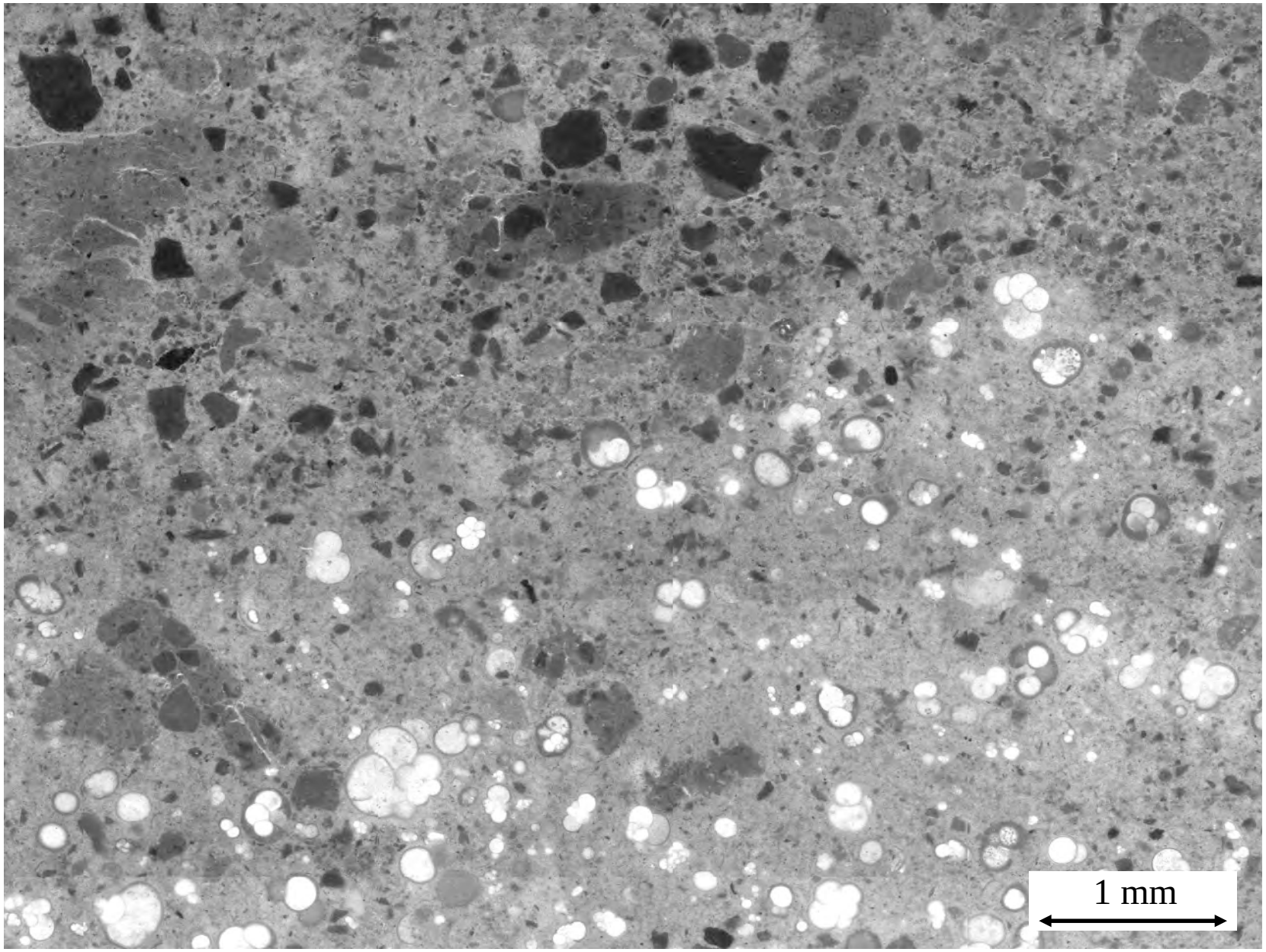

H4 env. 40 000 ans

La ceinture de Ruddiman

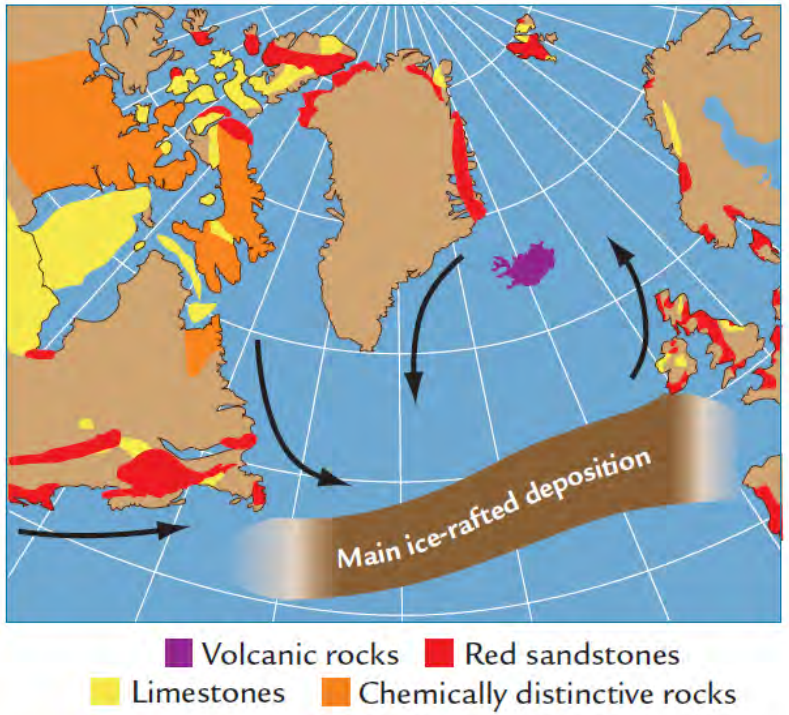

FIGURE 15-3

Sources and deposition of ice-rafted debris

Highest rates of deposition of ice-rafted debris occur in the North Atlantic Ocean between 45° and 50°N. During smaller ice-rafting episodes, sources of debris include volcanic rocks on Iceland and red sandstone rocks on several coastal margins. During large ice-rafting events, massive amounts of material come from eastern North America, including limestone from Hudson Bay and fragments from other regions with distinctive chemical signatures. (ADAPTED FROM G. BOND ET AL., "EVIDENCE OF MASSIVE DISCHARGES OF ICEBERGS INTO THE NORTH ATLANTIC DURING THE LAST GLACIAL PERIOD," *NATURE* 360 [1992]: 245–49.)

Faciès Laminé (18,3-17 ka)

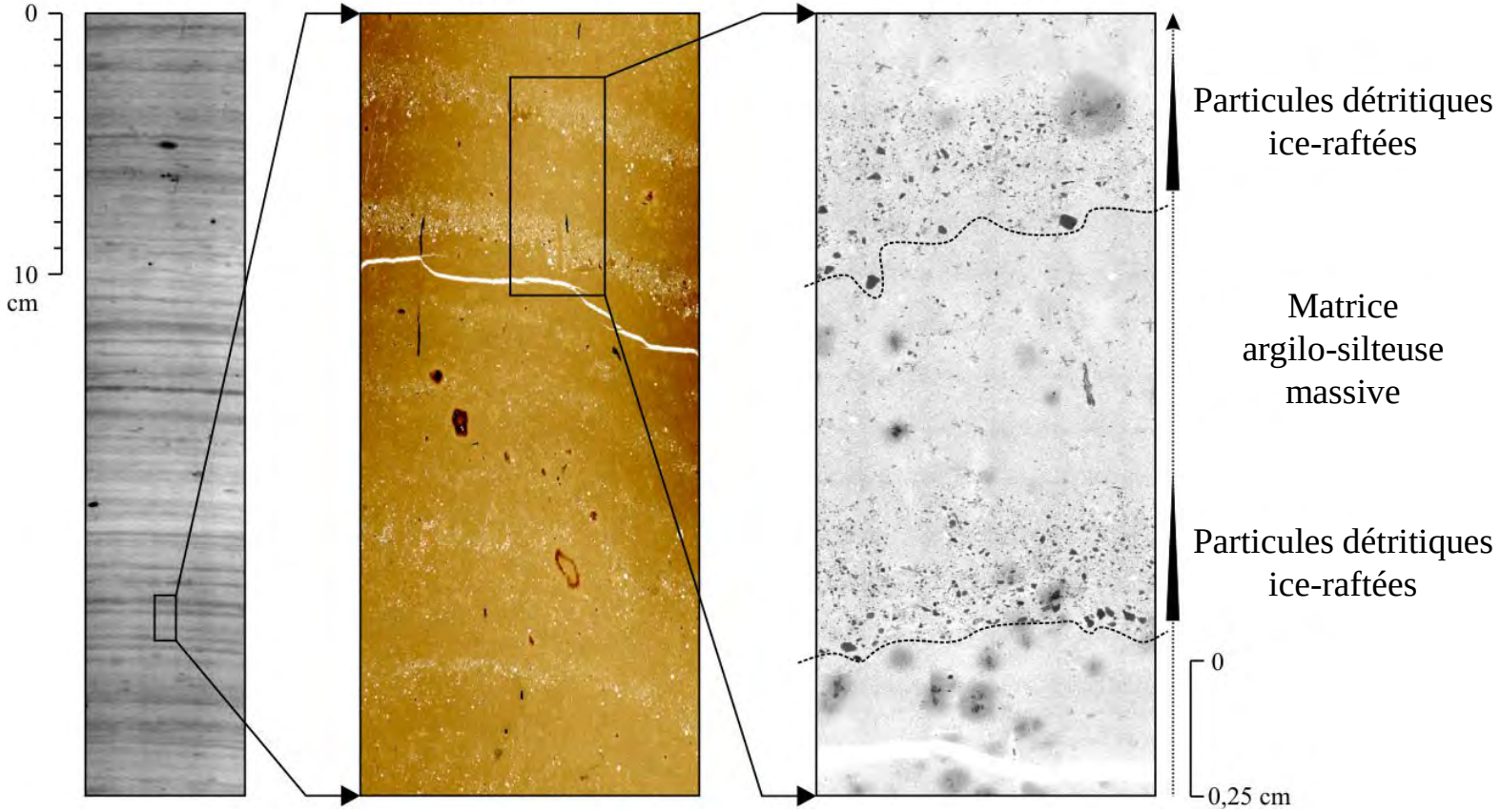

rX *lame mince* *zoom*

Toucanne 2008

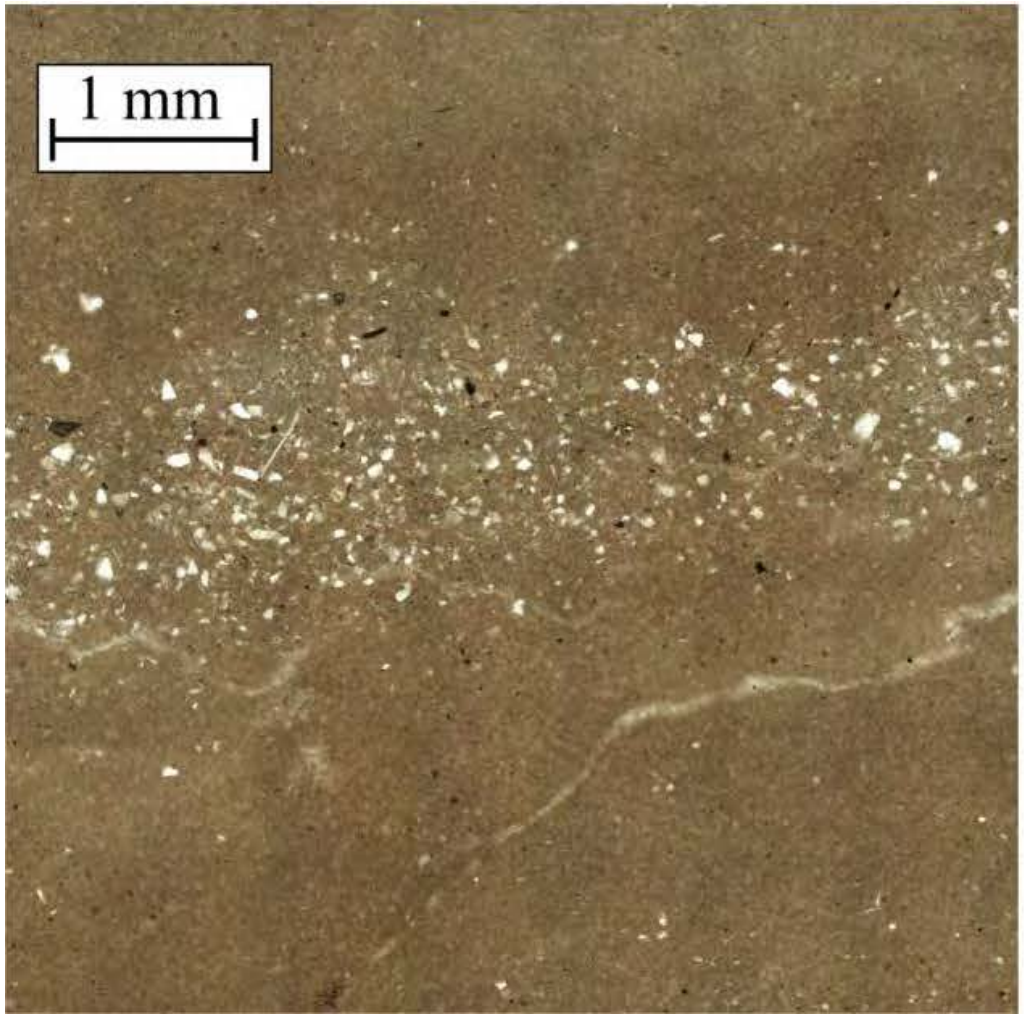

Natural light

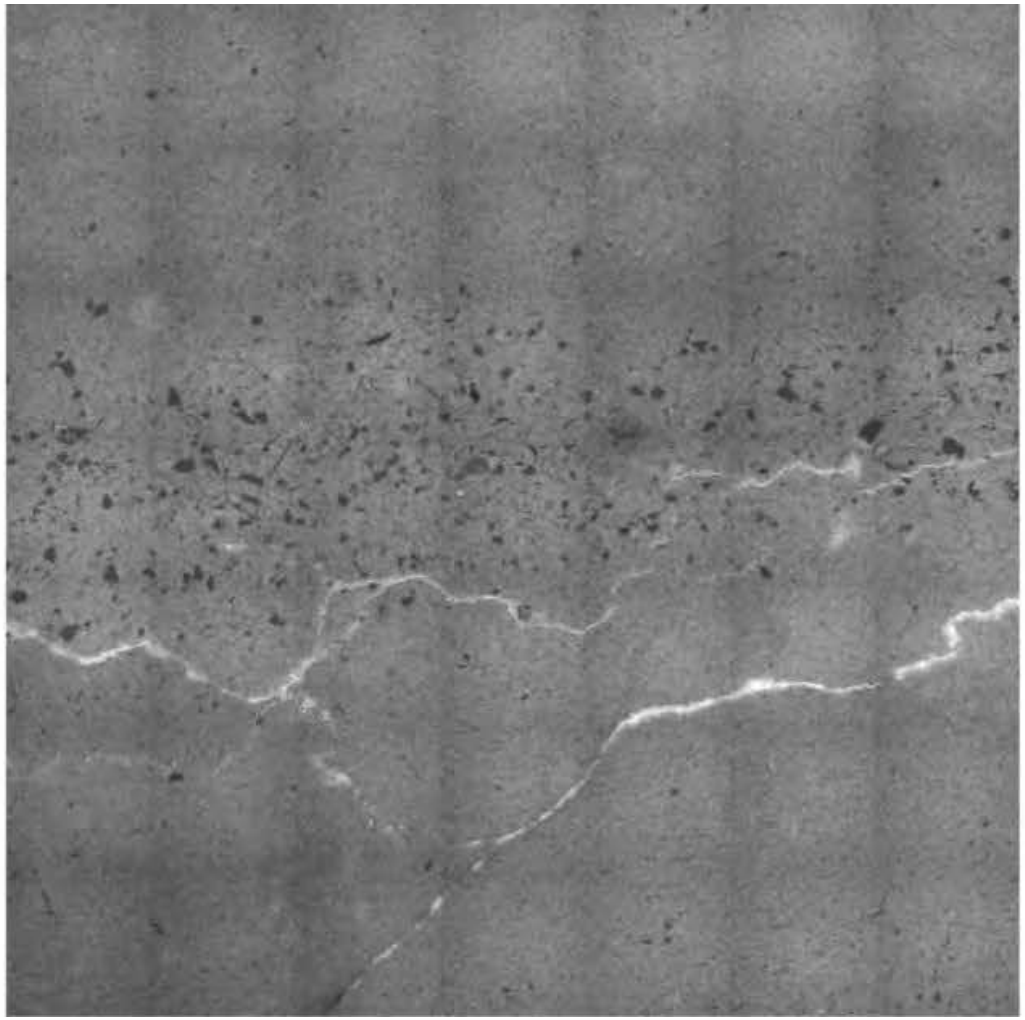

Fluorescent light

MD042790

Débâcle printanière du St Laurent (Canada, mai 2014)

Débâcle printanière du St Laurent (Canada, mai 2014)


Débâcle printanière du Fleuve McKenzie (Canada, mai 2004)
Exportation actuelle conséquente :
5 à 8.10⁶ t.an⁻¹sur le plateau continental de la mer de Beaufort
(Eicken et al., 2007)

1. Sédimentation gravitaire – turbiditique

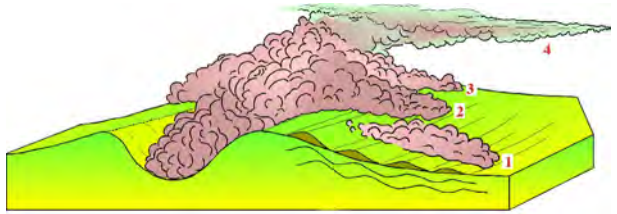

2. Sédimentation volcanoclastique

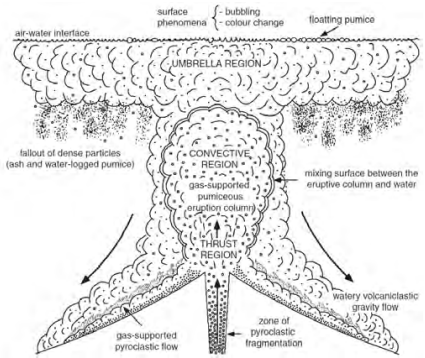

3. Sédimentation pélagique et hémipélagique

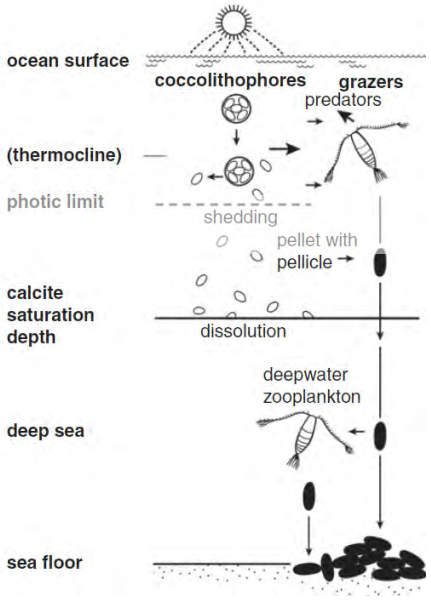

4. Sédimentation glaci-marine